The characterisation and analysis of in-situ and blasted block-size distributions and the blastability of rock masses.

Lu, Ping

THE CHARACTERISATION AND ANALYSIS OF IN-SITU AND BLASTED BLOCK SIZE DISTRIBUTIONS AND THE BLASTABILITY OF ROCK MASSES

Ping LU
B.Sc. (Eng.), M.Sc. (Eng.) (South China Inst. of Metall.)

QUEEN MARY
AND WESTFIELD COLLEGE
UNIVERSITY OF LONDON

A thesis submitted for
the degree of Doctor of Philosophy of the University of London

Dept. of Engineering (Civil), Queen Mary and Westfield College
1997

ABSTRACT

In this thesis, previous research on discontinuity geometry, in-situ block size distribution (IBSD), blasted block size distribution (BBSD), and blastability of rock mass is discussed. The IBSD with special reference to discontinuities with a fractal spacing distribution is investigated using computer simulation, from which a set of empirical equations is derived for predicting the IBSD of a rock mass with discontinuities of fractal spacing distributions. The goodness-of-fit of theoretical as compared with real spacing distributions is discussed and a grey correlation analysis technique is introduced into the goodness-of-fit.

An estimation of mean trace length of discontinuities with lognormal and fractal distributions is derived. A numerical algorithm and associated computer program for estimating the discontinuity size distribution is developed from which empirical equations for estimating the mean size of discontinuities with negative exponential, lognormal and fractal trace length distributions have been derived. A factor which accounts for the discontinuity impersistence is incorporated into the estimation of IBSD.

Combining both Ross-Ram and Schuhmann models, a reasonably accurate and user-friendly "photo-scanline" technique is devised for the estimation of BBSD of the blastpile.

Blasting results, as a function of both the intact rock properties and the discontinuity structures are investigated, and an energy-block-transition model characterising the blastability of rock masses is developed. It is argued that the blastability of rock mass is governed by a comprehensive range of both intact rock properties and discontinuity parameters, and that the fractal dimension of the IBSD of a rock mass could be an indicator of blastability. Taking into account that blastability is a complex property, a methodology of assessing blastability of rock masses is introduced using a Rock Engineering Systems method.

Published data from the literature has been used wherever possible to support the validation of the new techniques of analysis and two case histories in which applications of the developed methodologies and techniques are presented.

ACKNOWLEDGEMENT

I am very grateful to the K C Wong Education Foundation and the British Government for funding the research, via the London University K C Wong Scholarship and ORS Award respectively.

Special thanks to my supervisor, Dr. J.-P. Latham, who initiated the project together with the author. Throughout the research study, he offered invaluable advice and suggestions enabled the project to come to fruition. Stimulating discussions provided a beneficial insight to the problems under investigation. His assistance with my English language was helpful.

Mr. J. Yin is acknowledged for preparing the samples and photographs used in Chapter 5. I wish to convey thanks to Dr. A. B. Poole, the director of the Geomaterials Unit, and to all the other staff and colleagues in the unit for their support and assistance during the research. Suggestions made by Prof. J. White after reading the author's Transfer Research Report - which forms part of this thesis is acknowledged.

I am thankful to Drs. G. Walton and H. Wang of the Geoffery Walton Practice and Mr. G. Pugh at C A Blackwell who provided the opportunity to be involved in the highway cutting improvement case study presented in Chapter 7. Many thanks go to Mr. J. D. Simm at H R Wallingford who provided the opening for the author to carry out the Overseas Quarry case study presented in Chapter 7.

I am indebted to Prof. J. Hudson who encouraged the author to carry out a particular line of research into Rock Engineering Systems, while the author was an Academic Visitor to Imperial College, which has benefited the research presented here.

Last but not least, I would like to express my gratitude to my wife, son and parents for their unstinting support, encouragement, patience, and love.

CONTENTS

NOTATION

A	Rock factor in the Kuznetsov equation; Constant
B	Burden
B_i	Energy-Block-Transition coefficient in Energy-Block-Transition model
BD	Blastability designation
b	Subscript, signifying blastpile
$C_{p,i}$	In-situ block size coefficients
D	Fractal dimension
E_e	Relative weight strength of the explosive
E_c	Bond's work index in the Bond model
E_s	Required energy for fragmentation in the Bond model and the Energy-Block-Transition model
F_{imp}	Relative impersistance factor
i	Subscript, signifying in-situ
l	Discontinuity trace length
l_l, l_u	Lower and upper values of discontinuity trace length
m_s, m_v	Indices of uniformity in Schuhmann equation, v for block volume and s for block sieve size
m_d	Mean discontinuity diameter
m_l	Mean discontinuity trace length
n_s, n_v	Indexes of uniformity in Ros-Ram equation, v for block volume and s for block sieve size
Q	Amount of explosive per blasthole
R	Discontinuity diameter
RQD	Rock quality designation
S	Block sieve size; Discontinuity spacing
S_a	Average block size
$S_c(S_{63.2})$	Characteristic size in Ros-Ram equation

S_e	Specific charge or powder factor
$S_{i,p}$	Blastpile block sieve size
S_{i50}	50% passing of the in-situ block sieve size
S_{i80}	80% passing of the in-situ block sieve size
S_{i100}	100% passing of the in-situ block sieve size
S_{b50}	50% passing of the sieve size of the blastpile
S_{b80}	80% passing of the sieve size of the blastpile
S_{b100}	100% passing of the sieve size of the blastpile
S_l, S_u	Lower and upper values of block sizes
S_m	Mean discontinuity spacing
S_{min}	Lower value of discontinuity spacing
S_{max}	Upper value of discontinuity spacing
S_p	Principal discontinuity spacing
S_{pm}	Principal mean discontinuity spacing
V	Volume of rock mass or rock blocks
W	Weight of rock
W_i	Bond's work index
X_0	Average value of a parameter
ΔA	The transformation area
ρ	Density of the rock mass in t/m^3

LIST OF FIGURES

LIST OF TABLES

1. INTRODUCTION

1.1 BACKGROUND

Maritime defence structures such as breakwaters and seawalls are built to protect shoreline, coastal and other harbour facilities. Quarried rock has been widely used in these coastal defence structures and can be employed in a wide rang of structure types (CIRIA/CUR, UK & The Netherlands, 1991). Rock armour can, in many cases, offer considerable benefits, and is an attractive option in many circumstance, in forming a secure, cost effective and environmentally accepted defence (Thomas, 1992). For example, in the United Kingdom, approximately 750,000 tonnes of armour was used in 1989, and the annual figure in 1994 is believed to have doubled. Combined with the concerns about rising sea level, the increasing market requirement for rock armour will impose considerable demands on the quarry resources around the world (Simm et al., 1992). Until recently, very little expertise in armourstone production had been available and the key research topic was identified to be the in-situ block size distribution (IBSD) (Latham & Wang, 1992).

In mining, the sizes of the rock fragments after blasting exerts a major influence on the downstream processing. Oversize rock has to be reduced to a size which can be handled by excavating, transporting, crushing and milling machinery. The loading rate of a drawpoint is directly governed by block size. Internal mine transport, crushing and milling can be adversely influenced by poor fragmentation. Poor fragmentation with excess fines or oversize blocks in the blasted block size distribution (BBSD) can affect costs by more than twice the cost of the blast itself (Scott et al., 1993). The prediction of IBSD and BBSD has been one of main pursuits of mining operations although it is notoriously difficult.

A considerable amount of research on both the IBSD and the BBSD has been conducted in several fields; the main ones being mining engineering and quarrying. Significant contribution have also come from research into armourstone production and highway cutting. The need for a forum of research on this aspect of excavations helped the initiation of the following international symposia on rock fragmentation: Lulea (Holmberg & Rustan, 1983), Keystone (Fourney & Dick, 1987), Brisbane (AusIMM, 1990), and Vienna (Rossmanith, 1993) and *Advanced Blasting Technology* (Julius Kruttschnitt Mineral Research Centre (JKMRC), Australia, 1991). Research on the use of rock in coastal defence structures that was highlighted in the *Manual on the*

use of rock in coastal and shoreline engineering (CIRIA/CUR, 1991) provides a wealth of geological and scientific background as well as practical engineering guidance on block sizes of armourstone for coast protection.

Amongst the many research teams, the Geomaterials Unit of Queen Mary and Westfield College has made significant contributions (Wang et al. 1990, 1991a; CIRIA/CUR, 1991; Latham, 1992; Latham et al., 1994). Although obvious to some, a valuable observation was made: to ensure the production of sufficient proportions of large blocks for armourstone, the in-situ block size prior to blasting is one of the most important geological factors. Based on this recognition, a computer program was written which sorts out the problem of block sizes and shapes formed by the dissecting discontinuities in the rock mass (Wang, 1992).

A continuous research effort into blasting technology at JKMRC also recognised that it is the in-situ rock mass rather than the rock properties measured in the laboratory that are important in the control of blasting (JKMRC, 1991). They developed an estimation technique for the IBSD based on a three dimensional model of rock structure and a comminution-based model of blast fragmentation for estimation of the BBSD (Kleine & Villaescusa, 1990; JKMRC, 1991). The research effort into highway cutting has also highlighted the significance of in-situ rock mass properties in control of blasting in highway cutting operations (Matheson, 1995).

To build a deeper insight into in-situ block size, a deep understanding of the statistical nature of spacing and trace length data from discontinuity surveying has to be provided. This understanding usually involves describing statistically the probability distribution functions. For example, discontinuity spacing distributions have often been considered to be fitted adequately by negative exponential distributions (Priest & Hudson, 1976, 1981).

A fractal - a special concept for describing the geometric properties of irregular patterns or fragments devised by Mandelbrot (1983) has been increasingly applied in geoscience and geological engineering. Discontinuity spacing, reported from many rock exposures, could be described using a fractal distribution (Gillespie et al., 1993; Boadu & Long 1994); so too could discontinuity trace length (Segall & Pollard, 1983; Ranalli & Hardy, 1989). Take characterisation of the discontinuity pattern as an example. If the pattern is a fractal, the information obtained about the pattern at any scale might be statistically similar to that at another scale (Ghosh & Daemen, 1993). This has great significance as it implies that information about large scale behaviour

can be obtained from small scale observations and vice versa. It has been recognised that the power law distribution often observed in the fragmentation of geomaterials is a consequence of the scale invariance of the fragmentation mechanism. The scale invariance is a basic property possessed by a fractal distribution. These characteristics have encouraged a further examination into whether discontinuity patterns can be better described using fractal concepts on the occasions when using other descriptive distributions prove unsatisfactory. Moreover, it invites the questions, what is the IBSD resulting from a fractal discontinuity pattern, and, what influence will it exert on the BBSD during rock fragmentation by blasting. A particular form of the fractal relation, known as the Schuhmann equation (Schuhmann, 1940), has often provided a good fit to the BBSD assessed directly from blastpiles (Turcotte, 1986; Clarke, 1987). Unfortunately, analyses of block size distributions of rock masses intersected by discontinuities with fractal spacing distribution are not available, although fractal concepts have found their way into increasing numbers of applications in engineering practice and fracture modelling.

Obtaining a functional relationship which closely describes or nearly fits a distribution of discretely observed geometrical or geological data that is quantifying a geometric parameter important in rock engineering (e.g. discontinuity spacing) is helpful to an understanding of the nature and applications arising from the variations of this parameter. In many cases, therefore, the examination of goodness-of-fit is necessary to obtain a better description of a parameter. There have been a few conventional statistical methods for this, but the conventional statistical methods for evaluating goodness-of-fit and selecting a preferable fitted result have some shortcomings (Benjamin & Cornell, 1972). Thanks to the development of grey correlation analysis in Grey Systems Theory (Den, 1985), which concerns the analysis, handling, and interpretation of uncertain or indeterminate information, the author is able to propose the use of grey correlation analysis as an alternative means of examining goodness-of-fit, and, selecting a preferable fitted result.

To date there is little scientific understanding of the ease with which a rock can be fragmented by blasting. Selecting one or more parameters of rock properties reflecting the resistance of the rock mass to being fragmented by blasting has been a major obstacle to the description of the ease of fragmentation. The effect, until recent times, has been that blasting design has relied on rules of thumb (Scott et al., 1993) obtained by precedent practice. The failure to promote blast design tools beyond rules of thumb might have resulted from the fact that the influence of in-situ rock properties, discontinuity structures and their interactions are often too difficult to be quantitatively

isolated and determined. Rock Engineering Systems recently developed by Hudson (1992), aims at providing both a useful checklist for technical factors of rock engineering projects and a logical framework for the complete design procedure. It clearly has potential for coping with complex rock engineering problems (e.g. Lu & Hudson, 1992). By means of this innovative methodology, it is now considered possible to tackle the complexity of rock blasting design systematically and to propose a classification system for the ease of fragmentation of rock by blasting.

1.2 DISCONTINUITIES AND BLOCK SIZE IN QUARRYING AND MINING

The natural i.e. in-situ block size plays an important role in many rock engineering projects. It is examined in mining and quarrying blast operations (Coates, 1970; Cunningham, 1983; Ord & Cheung, 1991; Wang et al., 1991b), in rock mass characterisation (Franklin, 1974, 1986; ISRM, 1978; Hoek et al., 1992), stability analysis of excavations in jointed rock masses (Hoek & Bray, 1981; Goodman & Shi, 1986), and, fracture network flow properties (Rives et al. 1992; Long, 1993).

The formation of different sizes and shapes of individual blocks of intact rock results from the mutual intersection of discontinuity sets with different spacing and orientation. Among all the kinds of discontinuities, joints and bedding planes exert most control on the size and shape of the in-situ block size. Both the spacing and the persistence of discontinuities greatly influence the size of individual blocks of intact rock. The mutual orientation of joints determines the shape of the individual blocks comprising the rock mass. The number of discontinuity sets also influences the appearance of the rock mass. It is common in engineering practice to group joint sets according to the clustering of orientations of discontinuities as seen on a stereographic projection. It is therefore suggested that the in-situ block sizes are mainly affected by the spacing and the persistence of discontinuities, and, the number of discontinuity sets (ISRM 1978).

Several estimation methods of IBSD have been proposed, such as the Block Size Index method (Franklin, 1974; ISRM, 1978), a simulation method (Hudson & Priest, 1979) and a computational method (Da Gama, 1977; Stewart, 1986; Wang & Latham, 1991). Impressive developments in the estimation of IBSD are the work carried out by Wang and his co-workers (Wang et al, 1990, 1991a; Wang & Latham, 1991; Wang 1992), who developed two techniques of predicting the in-situ block size and shape parameters. The first is the so-called the Dissection Method, which uses a computer

program to determine the sizes and shapes of all blocks produced by intersecting discontinuities within a boundary block formed by six planes. The second is the so-called Equation Method, which uses a set of empirical equations to estimate the IBSD.

In his work, Wang investigated discontinuities with uniform, negative exponential, as well as lognormal spacing distributions. In developing the above two prediction methods, an assumption that all discontinuities within the rock mass are persistent was made. This assumption is probably acceptable for a small volume of rock with highly persistent discontinuities, but the errors related to this assumption will inevitably increase with the increase of both the volume of rock mass and the impersistent discontinuities in question.

One of most important aims of any blasting investigation related to quarrying and mining is to predict the degree of fragmentation (Hagan & Just, 1974; Singh & Sastry, 1987). For mining, the degree of fragmentation is one of the basic measures of relative efficiency for different blasting designs (Just, 1979; Scott et al., 1993). For quarries producing armourstone, both the production rate and a sufficient quantity of armourstone or aggregate in a given size range are among the major concerns for which the predicted BBSD is vital information (Latham & Wang, 1992). To assess whether a blasting operation is optimal requires an appraisal of the actual blastpile's block size distribution. Thus, the development of methods of assessing the BBSD has been an important topic in both quarrying and mining, whether measured directly from the blastpile itself or predicted from application of blast design models.

Direct sieving and measuring is the most reliable method to obtain the blastpile size distribution. However, at full scale, it is expensive and tedious, generally being used only in scaled down trial blasts or model studies (Yang & Rustan, 1983; Singh & Sarma, 1983; Singh & Sastry, 1987). Photographic and image analysis techniques (Nie & Rustan, 1987; Franklin & Maerz, 1988; Hunter et al., 1990; Ord & Chueng 1991; Farmer et al., 1991) and prediction methods based on empirical blast design models such as Kuz-Ram (Cunningham, 1983) and Bond-Ram (Da Gama, 1983; Wang et al, 1992) have been proposed to help tailor the explosive and geometric parameters of the blast towards a desired BBSD for full scale production.

An ideal technique for the estimate of BBSD should be reasonably accurate, cost-competitive and user-friendly. The exclusive and expensive methods reported above, appear not to meet all these requirements. The direct photographic and image analysis techniques usually need complex equipment and/or software. The indirect prediction

models do not have their governing parameters determined with sufficient reliability. However, in combining parts of the prediction models with a simple photographic method, a technique which may meet all the above requirements can be developed.

1.3 THE EASE OF FRAGMENTATION OF ROCK MASSES BY BLASTING

Ease with which a rock can be fragmented by blasting should be a kind of intrinsic property of rock. This property is referred to as Blastability. The necessary energy input in a blast and the BBSD are clearly influenced by blastability.

The influence of properties of a rock mass on blasting operations has long been studied. Their influence has been mentioned and incorporated in various ways, such as Bond's work index (Bond, 1952), Hino's Blastability Coefficient (see Just, 1974), Rock Factor (Kuznetsov, 1973), and Blastability index (Lilly, 1986). However, little attempt has been made to develop a quantitative parameter or system to define the ease of fragmentation of rock by blasting, in spite of the fact that this kind of development was suggested long ago by Hagan and Just (1974). The advice to concentrate research effort towards the study of blastability models was given by Scott et al. (1993), and this research study has taken his advice on board.

Turcotte (1986) suggested that in many cases, fragmentation assumes a fractal distribution or power law form. Also a theoretical study (Nagahama, 1993) has indicated that the fractal dimension of fragments can be related to the energy density for the fragmentation. These make the investigation into the possible relationship between blastability of a rock mass and the fractal dimension of IBSD an attractive research topic.

2. REVIEW OF PREVIOUS RESEARCH ON DISCONTINUITY GEOMETRY, IBSD, BBSD AND BLASTABILITY

2.1 DISCONTINUITY GEOMETRY

In the rock engineering fields dealing with excavation and construction on and within rock masses such as quarrying, mining, hydraulic power projects, the term "discontinuity" as a general collective name has become accepted and is now widely used. A discontinuity can be any type of weak plane within a rock mass across which the rock is structurally and/or mechanically discontinuous and has zero or low tensile strength. Discontinuities include all weak planes of geological origin, such as joints, bedding planes, cleavages, planes and faults.

The ISRM (1978) refers to the use of ten parameters for the characterisation of discontinuities and these include three geometric parameters: spacing, persistence, and orientation. Each of these ten parameters can have a significant influence on the rock properties that control the success or otherwise of an engineering project. However, three geometric parameters in particular, and their spatial distributions, are most important in the estimation of both the IBSD and the BBSD: spacing distributions, trace length distributions and orientation distributions (ISRM, 1978; Hudson & Priest, 1979; Priest & Hudson, 1981; CIRIA/CUR, 1991; Wang, 1992; Latham et al., 1994).

2.1.1 Discontinuity Measurement

There are a variety of methods for collecting, analysing and using discontinuity data. In many cases it is only necessary to estimate the most important features of the major discontinuity sets. These might be obtained readily from a simple visual inspection of rock exposures. Other forms of analysis will require detailed information and will take longer time to complete. Measurements and analyses of rock structures could range from rough estimation of the mean spacing of three major discontinuity sets, to complicated modelling of parameters describing the three dimensional discontinuity pattern. The more complex models will take account of the variability of discontinuity shape, size, orientation and clustering.

Discontinuity data acquisition is achieved by mapping. The mapping methods developed can be grouped into two types. One is by direct survey and another is by indirect measurement. The indirect methods are based initially on measurements of physical parameters of the rock mass such as seismic velocity and the discontinuity parameters are then estimated from the physical parameters (e.g. Grainger et al., 1973). The direct methods use visual measurement of each discontinuity. Such measurements of lengths or angles are made directly on rock outcrops, bench faces, boreholes (Piteau, 1970, ISRM, 1978) as well as from photographs of rock exposures (Franklin & Maerz, 1988; Farmer et al., 1991). The direct measurement on rock exposures can be carried out using either area mapping or line mapping techniques.

Area mapping techniques have been adopted by some researchers in collecting the discontinuity trace length as well as spacing information (Mathis, 1987; Kikuchi et al, 1988). The mapping technique uses such measurements as spacing and trace length exposed in a chosen area on an exposure. The exposure should be sufficiently large in area so that the discontinuities measured are representative. This is often limited by the accessibility and availability of rock exposures.

Line mapping, often referred to as the scanline technique, is widely used nowadays. The principles are shown in Fig. 2.1. The line mapping technique was originally proposed by Jennings (1968) and further extended and described by Piteau (1970) and Hudson and Priest (1979). Wang (1992) described the technique in detail and further grouped it into "detailed scanline" and "quick scanline" techniques. These techniques are examined further below.

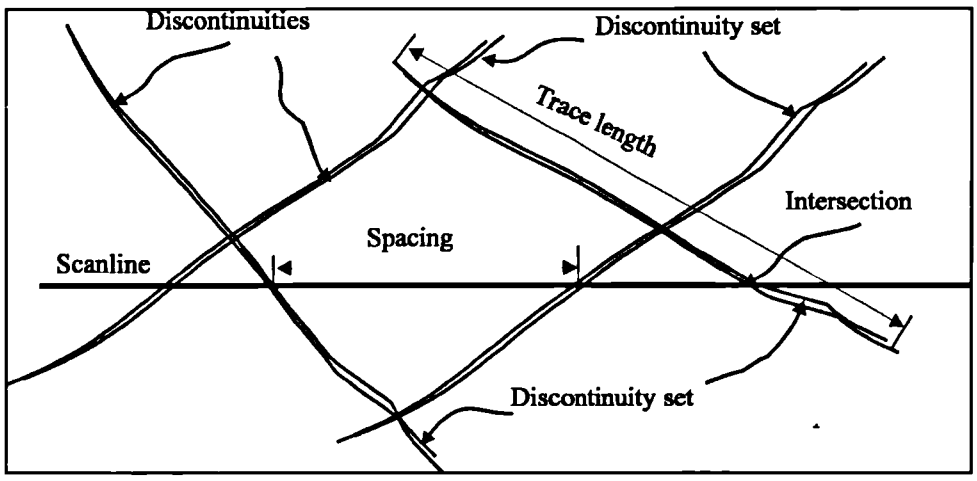

Fig. 2.1 Schematic illustration of scanline mapping of discontinuity characteristics

Detailed scanline technique

The detailed scanline technique measures discontinuity orientation, trace length, position, roughness, and aperture of each discontinuity intersecting the scanline in question. The measurements can be collected from outcrops, excavation walls, boreholes or photographs. Where the objective is the analysis of IBSDs, the measurement can be reduced to orientation, spacing and trace length.

The basic equipment used for the detailed scanline is a compass clinometer, a measuring tape of approximately 30 m length calibrated in centimetre divisions, a customised pro-forma data entry sheet, pencil and notebook. Two chisels may also be useful for setting out the tape where it is difficult to secure the tape ends.

The detailed scanline technique can provide the information needed to yield a detailed discontinuity pattern. However, it is usually time-consuming and may be restricted and unsuitable because of such factors as the inaccessibility of exposed surfaces. Thus, a quick scanline technique has also been proposed.

Quick scanline technique

The quick scanline measures only the intercepts of discontinuities with the tape. However, persistence data is often gathered at the same time. This surveying technique can be conducted on outcrops and tunnel walls, along boreholes or directly on photographs provided care is taken with possible distortion.

Using the quick scanline technique it is possible to obtain the mean spacing value relevant to the scanline orientation and location, but impossible to group discontinuities into sets, which limits its application in practice. A simple development by Karzulovic and Goodman (1985) was put to use by Wang (1992) and has given quick scanline techniques greater potential for exploitation. From this development, it is possible to estimate the principal mean spacings (see section 2.1.2) by combining data from several quick scanline surveys and this is explained below.

Hudson and Priest (1979) have shown that the discontinuity frequency along a scanline is given by

$$\lambda = \sum_{1}^{n} \lambda_i \cos\theta_i, \qquad (2\text{-}1)$$

where λ_i is the frequency of the *ith* discontinuity set along the normal to the *ith* set, i.e. the reciprocal of the *ith* principal mean spacing, θ_i is the acute angle between the scanline and the normal to the *ith* set, and, N is the number of discontinuity sets, which is selected as three in this example.

According to Karzulovic and Goodman (1985), for a group of three sets of discontinuities, there is the following relation if there are n scanlines ($n \geq 3$).

$$\begin{bmatrix} AA & AB & AC \\ AB & BB & BC \\ AC & BC & CC \end{bmatrix} \begin{Bmatrix} S_{pm1} \\ S_{pm2} \\ S_{pm3} \end{Bmatrix} = \begin{Bmatrix} LA \\ LB \\ LC \end{Bmatrix}, \qquad (2\text{-}2)$$

where S_{pm} is the principal mean discontinuity spacing, and,

$$AA = \sum \cos\theta_{1j} \cos\theta_{1j}$$
$$AB = \sum \cos\theta_{1j} \cos\theta_{2j},$$
$$AC = \sum \cos\theta_{1j} \cos\theta_{3j}$$

etc.

$$LA = \sum S_{mj} \cos\theta_{1j}$$
$$LB = \sum S_{mj} \cos\theta_{2j},$$
$$LC = \sum S_{mj} \cos\theta_{3j}$$

$$j=1,...n,$$

where, j represents the number of the scanlines, S_{mj} is the mean spacing value of discontinuity along the *jth* scanline, and, θ_{1j} is the acute angle between the *jth* scanline and the first discontinuity set. It is important to point out that it is critical to know the discontinuity set orientations that enable substitution of the values of θ_{ij}. The discontinuity set orientations can be estimated by reconnaissance mapping, plotting and contouring.

Eqn. 2-2 provides the estimate of the principal mean spacings from the general mean spacing values measured by the quick scanline technique, for the case where the detailed scanline is considered inappropriate. The greater the number of scanlines

measured (the minimum is three), the more reliable are the estimates. This method is of significance in providing estimation of the principal mean spacing values, even though its wide application may be restricted by the uncertainty in the accuracy of the results provided.

2.1.2 Discontinuity Spacing and its Terminology

2.1.2.1 Terminology of Spacing Distributions

ISRM (1981) described discontinuity spacing as the perpendicular distance between adjacent discontinuities. To give more precision, Priest & Hudson (1981) defined discontinuity spacing as the distance between an adjacent pair of discontinuities measured along a straight line of a given orientation within or on the surface of a rock mass. According to this definition, the discontinuity spacing is affected by both orientation and location of the scanline measuring it.

The mean discontinuity spacing (S_m) is the algorithm average value of n discontinuity spacing measurements S_i (i=1,...,n) along a scanline, where n measurements can be generated from n discontinuities.

$$S_m = \frac{1}{n}\sum_{1}^{n} S_i . \qquad (2\text{-}3)$$

In the case of using detailed scanlines, the mean spacing value S_m of each scanline can be obtained using the above definitions, and the distribution of the discontinuity spacings can then be discussed. It is worth pointing out that S_m as well as relevant distributions are usually influenced by all sets of discontinuities in the rock mass and related to the scanline's orientation (Hudson & Priest, 1979). For this reason, it is helpful to follow Wang (1992) and introduce spacing parameters for each set of discontinuities: the principal spacing S_p and the principal mean discontinuity spacing S_{pm} and the principle spacing distribution.

Under the condition of parallel discontinuities, the spacing measured along a scanline will be the shortest when the scanline is perpendicular to discontinuities. For this perpendicular condition, the spacing value is called the principal spacing S_p. The concept can be further extended to include the spacing between two adjacent discontinuities in one set where the scanline is parallel to the pole of mean orientation of the set. The two adjacent discontinuities may be subparallel or parallel. When the

principal spacing S_p of a particular set of discontinuities is used to calculate and generate the mean discontinuity spacing for this set, this mean discontinuity spacing is named the principal mean discontinuity spacing S_{pm} or briefly, the *principal mean spacing* (Wang, 1992) , which is as follows.

$$S_{pm} = \frac{1}{n}\sum_{1}^{n} S_p . \tag{2-4}$$

Methods of obtaining the principal mean spacing

The discontinuity frequency (λ) is defined as the number of discontinuities per unit length of scanline, and is therefore the reciprocal of the discontinuity mean spacing.

$$\lambda = \frac{1}{S_m}. \tag{2-5}$$

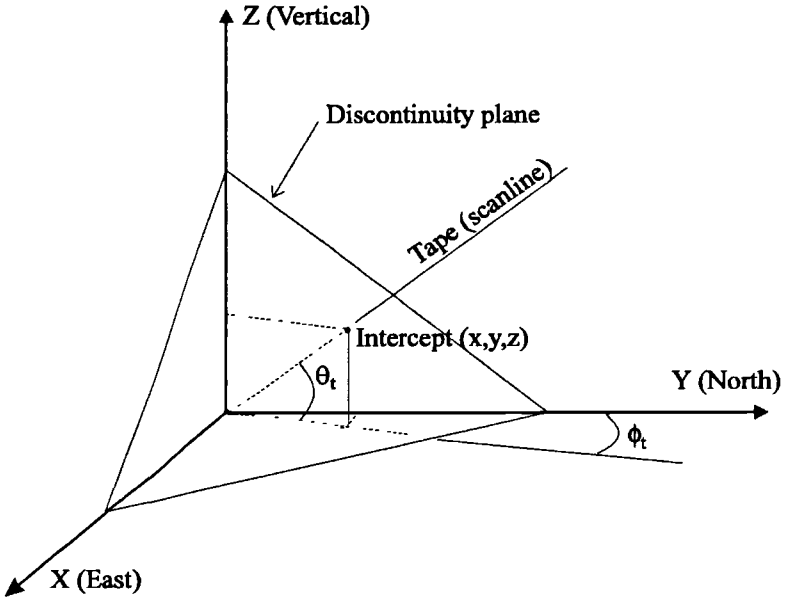

Fig. 2.2 Schematic illustration of the generic relationship between a discontinuity and the tape (scanline) in a reference frame (*X Y Z*)

Using the detailed scanline, both the principal spacings and the principal mean spacings can be obtained. There are two methods, with a little difference, for calculating the principal mean spacing and these are described as follows.

1) First, a plane function describing the spatial position and orientation of each discontinuity is defined. To implement this, the raw survey data: dip angle, dip direction and intercept with the oriented tape, have to be transformed into five parameters: the dip angle and the dip direction of the discontinuities, and the three co-ordinates (*x, y, z*) of any point on the discontinuity plane in an orthogonal Cartesian co-ordinate reference frame as illustrated in Fig. 2.2. The intercept of the first discontinuity with the tape is usually set out to be the origin of this reference frame.

The intercept of the discontinuity with the oriented tape defines a location on the discontinuity plane and this location is therefore used to calculate the required co-ordinate point (*x, y, z*) of that discontinuity plane,

$$\begin{aligned} x &= I_t\, Cos(\theta_t) Sin(\phi_t) \\ y &= I_t\, Cos(\theta_t) Cos(\phi_t), \\ z &= I_t\, Sin(\theta_t) \end{aligned} \qquad (2\text{-}6)$$

where I_t is the intercept of discontinuity, θ_t is the plunge angle of the tape with a positive sign (if the tape is downwards) or negative sign (if the tape is upwards), ϕ_t is the azimuth of the tape.

An artificial scanline can be drawn along the mean orientation of a set of discontinuities (i.e. the mean normal direction of this discontinuity set) determined for example using the stereographic method. All discontinuities within the set will intersect the artificial scanline, and, the intercepts can be determined by their trigonometric relationships between: the orientation of the tape; the orientation of the artificial line; and the orientation and intercept of the discontinuity. The principal spacing between two adjacent discontinuities in the set is the distance between two intersections along this artificial scanline (Fig. 2.3).

The advantage of this method is that it is not necessary that discontinuities in each set are all parallel. However, the principal mean spacing value will be influenced by possible variation in the relative location of the artificial scanline though the effect could be reduced by increasing the numbers of discontinuities in a set.

2) When two adjacent discontinuities in a set are parallel, the principal mean spacing, can be obtained from illustration in Fig. 2.3, as follows:

$$S_p = S \times \cos\alpha = S \times (\cos\theta_l \cos\theta_m \cos(\phi_l - \phi_m) + \sin\theta_l \sin\theta_m), \qquad (2\text{-}7)$$

where S is the spacing value from the original scanline of any orientation and α is the intersection angle between the orientation of the scanline and the artificial scanline (i.e. the mean normal direction of the set of discontinuities). The angles θ and ϕ are the plunge and the azimuth of the oriented lines respectively. Subscript l indicates the scanline and m is the normal direction of the set of discontinuities.

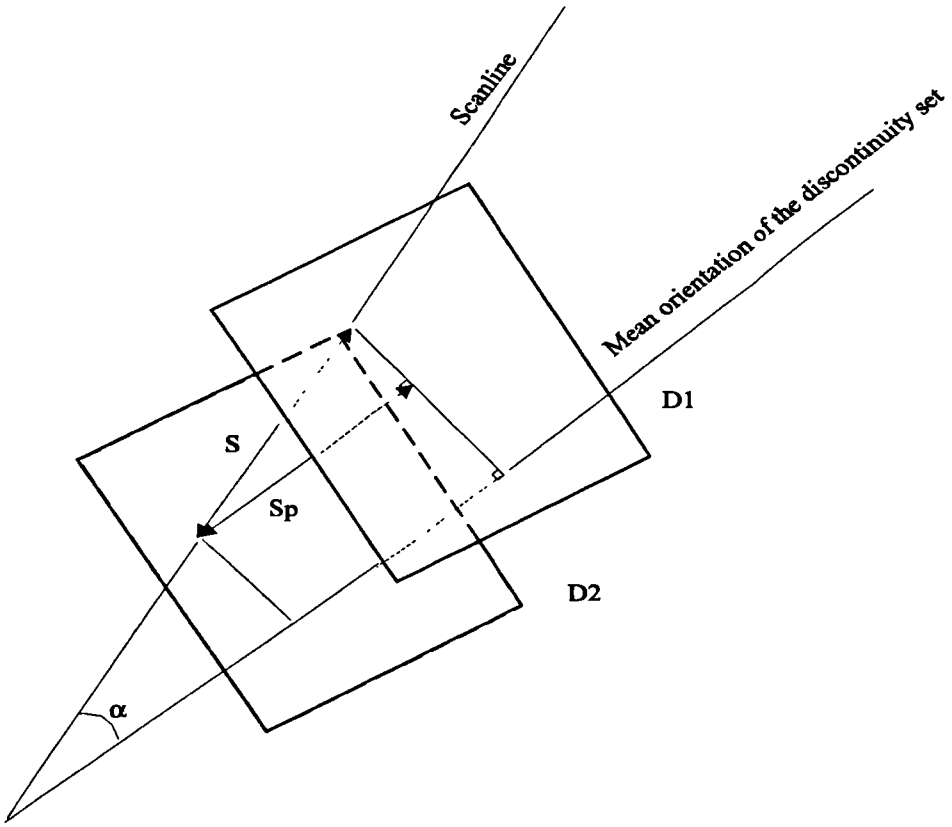

Fig. 2.3 The relationship between the principal mean spacing from the known spacing and orientation of the scanline and the mean orientation of the discontinuity set. (*D1* and *D2* are two adjacent parallel discontinuities)

While the second method is simpler than the first it may introduce errors when discontinuities are not parallel. After the principal spacing value in each set is determined, the principal mean spacing value of each set of discontinuity can be worked out using Eqn. 2-4.

The data for the above two methods of calculating the principal mean spacing is provided by the detailed scanline surveys. When using quick scanline surveys, we can use the techniques proposed by Karzulovic and Goodman (1985) (see Eqn. 2.2) to estimate the principal mean spacings.

2.1.2.2 Characterisation of Discontinuity Spacing

The spacing of discontinuities is one of the most influential parameters for the in-situ block size. Thus, numerous research studies on the characterisation of discontinuity spacing have been conducted.

Priest and Hudson (1976, 1981), Hudson and Priest (1979, 1983), and, Priest (1993a) carried out in-depth studies and discussions which have effectively provided the basis for our correct understanding of discontinuity geometry. They gave a non-mechanical but more mathematical treatment of the tendency to produce negative exponential spacing distributions.

Call et al. (1976) investigated the possibility of deriving reasonable estimates of discontinuity spacing distributions from surface mapping data. Baecher and co-workers (Baecher et al., 1977; Baecher, 1983) discussed and summarised the stochastic description and statistical design of discontinuity spacing surveys. Einstein and Baecher (1983) examined the probable distributions of discontinuity spacings using the Chi-square (χ^2) test. Assuming that visual inspection of the histograms of spacings is not enough to prove whether a proposed theoretical spacing distribution gives the goodness-of-fit to the measurements, Rouleau and Gale (1985) used the Kolmogorov-Smirnov test to examine the goodness-of-fit of spacing distributions to the negative exponential, lognormal and Weibull distributions. They found that the lognormal distribution was the best among them. This type of work has only received a little attention and is a topic to be discussed later in this research study.

Dershowitz and Einstein (1988) discussed possible reasons for different spacing distributions, pointing out that discontinuity location is the results of different mechanical processes, and thus, different discontinuity spacing distributions would be expected in terrain exposed to different deformation histories.

Discontinuity spacing distribution has recently been studied by Harris et al. (1991), Barton and Zoback (1992), Gillespie et al. (1993), and, Boadu and Long (1994) with

the motive in common. Their investigations have been concerned with an interesting possibility that the spacing of discontinuities and discontinuity patterns could be scale invariant in general or in certain aspects, i.e. the spacing distribution of discontinuities could exhibit fractal characteristics. The fractal concept has found an increasing number of applications in geoscience and geological engineering (Allegre et al., 1982; Aviles & Scholz 1987; La Pointe 1988, 1993; Ghosh et al., 1990; Poulton et al., 1990; Genske et al., 1992; Nagahama, 1993; Hobbs, 1993). If the discontinuity pattern generation in a rock mass is self-similar then the information obtained about the pattern at any scale would be statistically similar to that at other scales (Ghosh & Daemen, 1993). The advantage of characterising discontinuity with fractal tools is that in a given rock mass, only one small size interval needs to be measured to determine a much wider range of characteristics. Whereas Hudson and Priest (1976) showed how superposition of separate discontinuity spacing patterns would tend to produce an overall spacing of negative exponential distribution, Hobbs (1993) has suggested that rock masses would show a tendency towards fractal spacing frequency distribution. The fractal spacing distribution has therefore been selected for detailed examination in this research study.

The distribution law of discontinuity spacings along a scanline in line mapping is often represented by an available probability distribution function (PDF). Nowadays, this is usually done in the following way. First, the spacing values are grouped into a certain, say, ten intervals in an order of increasing spacing. Then, the frequency of spacing data within each interval is computed and plotted as a histogram. The most likely theoretical distribution to give a good description of the histogram is assessed visually. To get more reliable results, it is necessary to fit the frequency-spacing data to some theoretical distributions and to examine the goodness-of-fit. Many researchers have looked into the possible spacing distributions practically and theoretically. These are summarised in Table 2.1.

The ability to identify the form of discontinuity spacing distributions is a basic requirement for any study of discontinuity spacing analysis. Gillespie et al. (1993) have shown how synthetic fracture logs can be created for uniform, lognormal, negative exponential and fractal discontinuity spacing distributions by the following processes.

(1) a bisection process, giving a fairly regular distribution with constant spacing;

(2) a Poisson process, or a random point process, giving a negative exponential spacing distribution;

Table 2.1 Summary of discontinuity spacing distributions

Distributions	Sources	Theory/Application/Case study
Negative exponential	Priest & Hudson (1976)	Theoretical approach /Discontinuities in sandstone, limestone, and chalk (UK)
	Call et al. (1976)	Theoretical approach/Joints (USA)
	Baecher et al. (1977)	Joints in shale, siltstone, and igneous rocks(USA)
	Hudson & Priest (1979)	Theoretical approach /Discontinuities in sandstone, limestone, mudstone, and dolerite (UK)
	Priest & Hudson (1981)	Discontinuities in sandstone and mudstone (UK)
	Einstein & Baecher (1983)	Theoretical approach/joints
	Sen (1984)	Theoretical approach
	Sen & Kazi (1984)	Theoretical approach / joints in schists (Saudi Arabia)
	Rouleau & Gale (1985)	Joints in the Stripa granite (Sweden)
	La Pointe & Hudson (1985)	Theoretical approach/Joints in dolomites (USA)
	Kikuchi et al. (1987)	Joints in granite (Japan)
	Villaescusa & Brown (1990)	Joints in rock from different mines (Australia)
	Kulatilake et al. (1990)	Theoretical approach/joints
	Wang (1992)	Theoretical approach/joints in granite gneiss (Norway) and limestone (UK)
	Rives et al. (1992)	Theoretical approach
	Kulatilake et al. (1993)	Theoretical approach/joints (Sweden)
Lognormal	Bridges (1975)	Joints
	Baecher et al. (1977)	Joints in shale, siltstone, and igneous rocks (USA)
	Sen (1984)	Theoretical approach
	Sen & Kazi (1984)	Theoretical approach / joints in schists (Saudi Arabia)
	Rouleau & Gale (1985)	Joints in the Stripa granite (Sweden)
	Wang (1992)	Theoretical approach/joints in granite gneiss (Norway) and limestone (UK)
	Rives et al. (1992)	Theoretical approach
Fractal	Harris et al. (1991)	Theoretical approach
	Barton & Zoback (1992)	Theoretical approach
	Gillespie et al. (1993)	Theoretical approach/Discontinuities in sandstones and shales, UK
	Hobbs (1993)	Theoretical approach / examination of joints in the Stripa granite (Sweden)
	Boadu & Long (1994)	Theoretical approach/Discontinuities in several different locations (UK)
Uniform	Hudson & Priest (1979)	Theoretical approach
	Wang (1992)	Theoretical approach
Normal	Hudson & Priest (1979)	Theoretical approach
	Rives et al. (1992)	Theoretical approach
Weibull	Rouleau & Gale (1985)	Joints in the Stripa granite (Sweden)
	Sen (1993)	Theoretical approach
Gamma	Sen (1984)	Theoretical approach
	Kulatilake et al. (1993)	Theoretical approach/joints (Sweden)

(3) a Kolmogorov process, giving a lognormal frequency distributions of spacing; and,

(4) a fractal clustering i.e. a scale invariant process, resulting in a power-law spacing distribution.

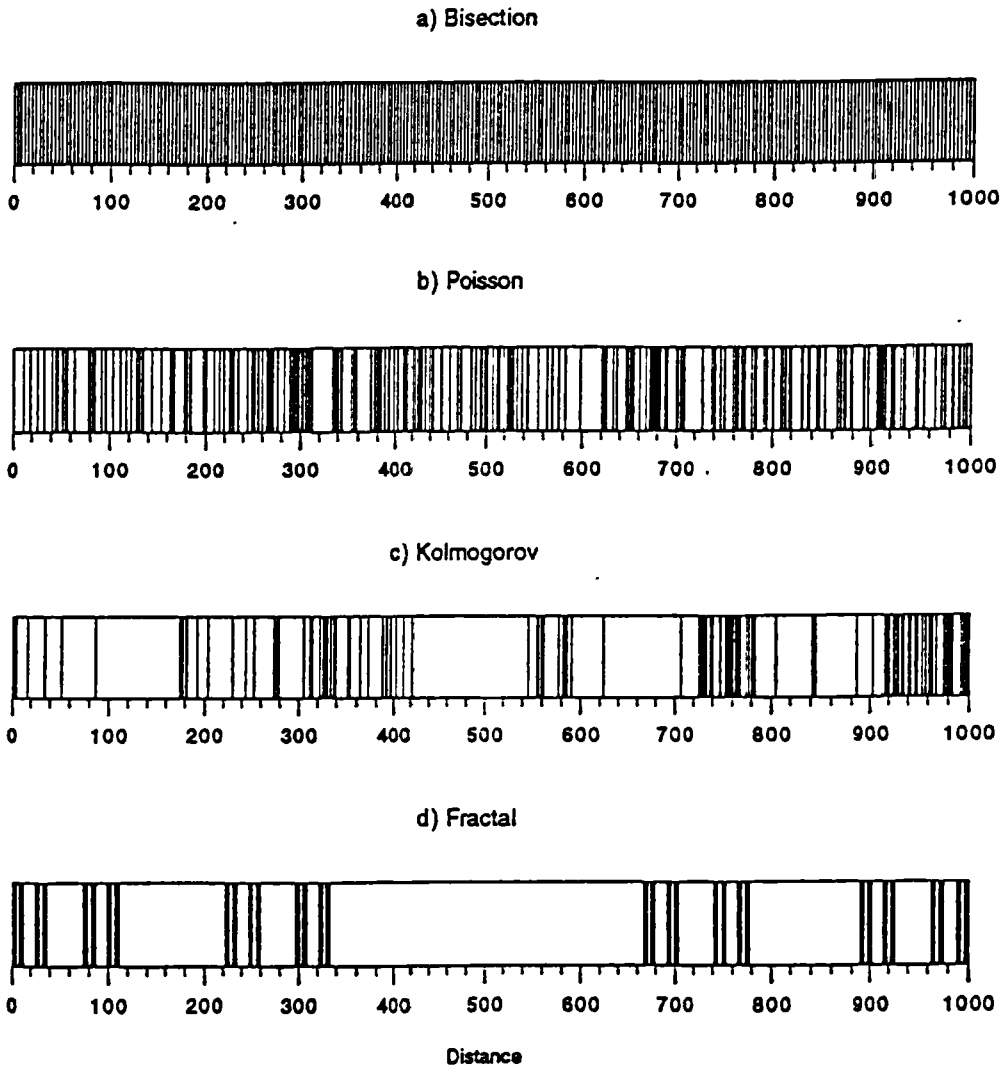

Fig. 2.4 Fracture logs for four kinds of theoretical distributions of discontinuity spacings, each log has a sample line length of 1000 units and 256 fractures (after Gillespie et al., 1993).

The random point distribution is simply generated by randomly distributing fractures along a sample line. A Kolmogorov process is generated by an iterative

process of random bisection, in which each iteration randomly places an additional fracture in every space between adjacent fractures. The Cantor Dust model (Mandelbrot, 1983) can be used to produce the fractal data set. The fracture logs for these four kinds of theoretical distributions of discontinuity spacings are illustrated in Fig. 2.4.

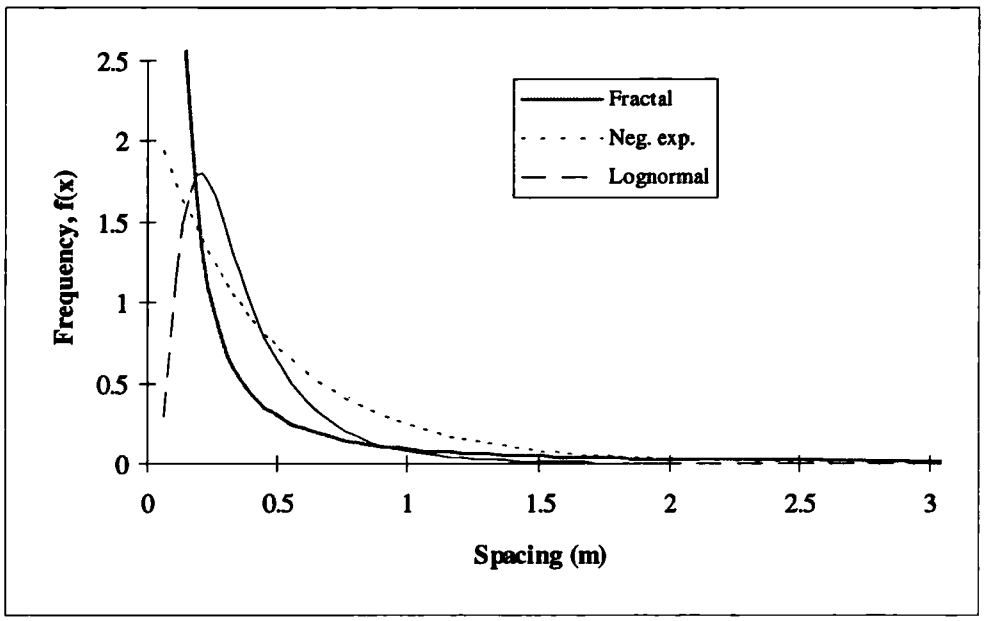

Fig. 2.5 Three theoretical distributions (all three distributions have the same value of mean spacing, 0.45 m)

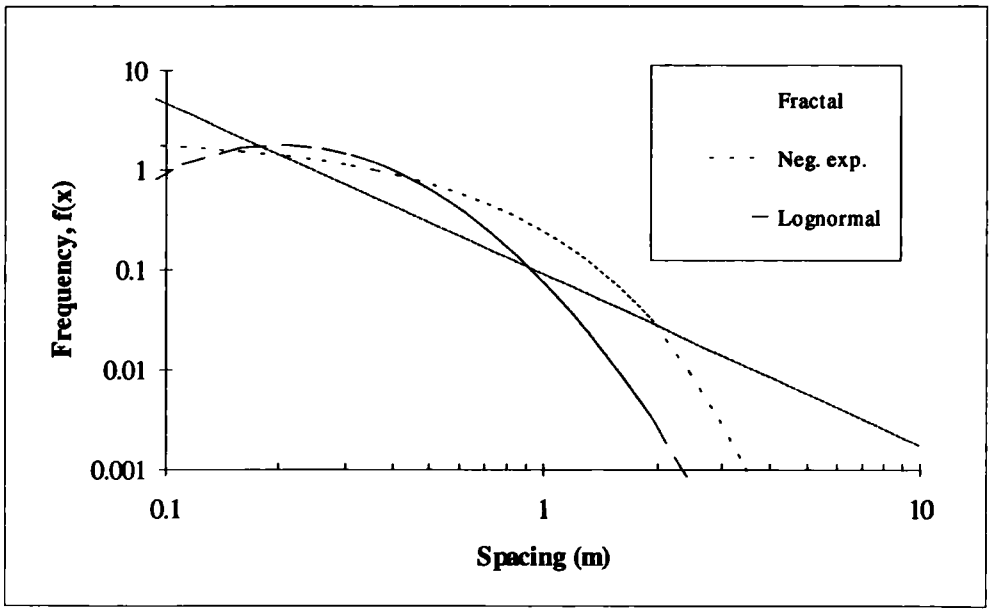

Fig. 2.6 Log-log plot for three distributions (The mean spacing for all three distributions is the same: 0.45 m)

Table 2.2 The probability density functions, the cumulative probability functions, the mean and standard deviations for the four distributions

	Uniform	Negative exponential	Lognormal	Fractal
Probability density function $f(x)$	$f(x)=\frac{1}{b-a}$ $a \le x \le b$	$f(x)=\lambda e^{-\lambda x}$ $0 \le x < \infty$	$f(x)=\frac{1}{\sqrt{2\pi}Bx}e^{\frac{(Ln\,x-A)^2}{2B^2}}$ $A=Ln(\bar{x})-\frac{Ln(1+(\sigma/\bar{x})^2)}{2}$ $B=\sqrt{Ln(1+(\sigma/\bar{x})^2)}$	$f(x)=Ax^{-(1+D)}$ $a \le x \le b,\ 0<D<1$ $A=\frac{D}{a^{-D}-b^{-D}}$ where D is the fractal dimension defined by $N(x) \propto x^{-D}$
Cumulative probability function $F(x)$	$F(x)=\frac{x-a}{b-a}$ $a \le x \le b$	$F(x)=1-e^{-\lambda x}$ $0 \le x < \infty$	$F(x)=\Phi(Ln\,x, A, B^2)$ where, Φ is the normal distribution function with mean A and standard deviation B.	$F(x)=(1-(\frac{a}{x})^D)\Big/(1-(\frac{a}{b})^D)$ $a \le x \le b$
Mean $(\bar{x})$	$\bar{x}=\frac{a+b}{2}$	$\bar{x}=\frac{1}{\lambda}$	$\bar{x}=e^{A+\frac{B^2}{2}}$	$\bar{x}=\frac{A}{1-D}(b^{1-D}-a^{1-D})$
Standard deviation (σ)	$\sigma=\sqrt{\frac{(b-a)^2}{12}}$	$\sigma=\frac{1}{\lambda}$	$\sigma=\sqrt{e^{2A+B^2}(e^{B^2}-1)}$	$\sigma=\sqrt{\frac{A}{2-D}(b^{2-D}-a^{2-D})-\frac{A^2}{(1-D)^2}(b^{1-D}-a^{1-D})^2}$

The frequency distribution of spacing is conveniently represented on a frequency-spacing plot of spacing x vs. frequency $f(x)$. The three types of theoretical distributions of discontinuity spacings are illustrated in Fig 2.5.

For the analysis of fractal spacing distributions, the spacing is usually represented on a double-logarithm plot of spacing, x versus cumulative number $N(x)$, where $N(x)$ is the number of discontinuity spacing values $\geq x$. On the log-log plot of spacing versus cumulative number $N(x)$, a fractal distribution will be a straight line. After obtaining $N(x)$ the related fractal dimension can be determined. On the log-log plot of spacing x vs. $f(x)$, the fractal distribution also plots as a straight line, as illustrated in Fig. 2.6, which is distinct from the curves of the other spacing frequency distributions. Whereas on the log-log plot of $f(x)$-x, a negative exponential frequency distribution will be a distinct convex upwards curve, a log normal frequency distribution forms a gentle curve and can resemble those of fractal distributions for the range representing the large spacing values. The uniform frequency distribution of spacing, with all spacing almost equal, are easily isolated from other types of distributions. This technique is helpful to distinguishing between the four population types, and is specially useful for examining fractal distribution.

The probability density functions, the cumulative probability functions, the mean and standard deviations for four types of theoretical distributions are given in Table 2.2. They can be used in the analysis of both the discontinuity spacing data and the discontinuity trace length data.

2.1.3 Discontinuity Persistence and Size

Discontinuity persistence is defined as the discontinuity trace length as observed in an exposure, and is a measure of the extent to which discontinuities persist before terminating in rock or against other discontinuities (ISRM, 1978; Einstein et al., 1983).

A discontinuity with a given trace length may be treated as persistent by one worker with an objective of, for example, predicting block sizes; whereas another with an objective of predicting the permeability of rock might not consider it to be persistent. Thus, the persistence is related to scale of concern and the study objectives, i.e. it is a relative term.

Table 2.3 Summary of discontinuity trace length distributions

Distributions	Sources	Theory/Application/Case study
Negative	Robertson (1970)	Theoretical approach /joints
exponential	Call et al. (1976)	Theoretical approach/Joints (USA)
	Cruden (1977)	Theoretical approach
	Baecher et al. (1977)	Joints in shale, siltstone, and igneous rocks (USA)
	Priest & Hudson (1981)	Discontinuities in sandstone and mudstone (UK)
	Panek (1985)	Limestone, mudstone, and dolerite (UK)
	La Pointe & Hudson (1985)	Theoretical approach/Joints in dolomite (USA)
	Rouleau & Gale (1985)	Joints in the Stripa granite (Sweden)
	Kikuchi et al. (1987)	Joints in granite (Japan)
	Ranalli & Hardy (1989)	Faults in world-wide, local or region
	Zhang & Liao (1990)	Joints in mudstone and sandstone (China)
	Kulatilake et al. (1993)	Theoretical approach/joints
Lognormal	Piteau (1973)	Joints, openpit, Zambia
	McMahon (1974)	Discontinuity in rock slope
	Bridges (1976)	Joints associated with caving mining
	Baecher et al. (1977)	Joints in shale, siltstone, and igneous rocks (USA)
	Warburton (1980)	Theoretical consideration
	Baecher (1983)	Theoretical approach/joints
	Rouleau & Gale (1985)	Joints in the Stripa granite (Sweden)
	Barton & Larsen (1985)	Theoretical approach
	Ranalli & Hardy (1989)	Faults in world-wide, local or region
	Villaescusa & Brown (1990)	Theoretical approach
	Kulatilake et al. (1993)	Joints in the Stripa granite (Sweden)
Fractal	Stone (1980, cf. Bahat, 1988)	Theoretical approach
	Segall & Pollard (1983)	Joints in granite rocks (USA)
	Barton & Larsen (1985)	Theoretical approach/fractures (USA)
	Ranalli & Hardy (1988)	Faults in world-wide, local or region
	Bahat (1988)	Theoretical consideration
	Davy et al. (1990)	Laboratory simulation/theoretical consideration(France)
	Sornette et al. (1990)	Laboratory simulation/theoretical consideration(France)
Uniform	Hudson & Priest (1979)	Theoretical approach
	La Pointe & Hudson (1985)	Theoretical approach/Joints in Niagaran dolomite
Normal	Baecher et al. (1977)	Joints in shale, siltstone, and igneous rocks (USA)
	Hudson & Priest (1979)	Theoretical approach
	La Pointe & Hudson (1985)	Theoretical approach/Joints in Niagaran dolomite
Gamma	Baecher et al. (1977)	Joints in shale, siltstone, and igneous rocks (USA)
	Kulatilake et al. (1993)	Theoretical approach/joints (Sweden)

While the size of a discontinuity is one of the most important rock mass parameters, it is one of the most difficult to quantify in anything but crude terms (ISRM, 1978; Priest, 1993a). Discontinuity size is generally represented by trace

length on a two-dimensional surface or, the surface area of the individual discontinuity which in practice is rarely observed. Trace length as observed in an exposure is both objective and measurable. Discontinuity trace length may give a crude measure of the area extent or penetration length of a discontinuity. Thus, the persistence or the size of discontinuities can be quantified by measuring the discontinuity trace lengths on the exposures.

Discontinuity trace lengths can range from centimetres to hundreds of meters. Persistence mapping techniques vary with scale and targeted problem. Scanline surveying, which samples the traces intersecting a line drawn on the exposure (see Fig. 2.1), is an ideal procedure from which to sample trace lengths.

In measuring the trace length of discontinuities, measuring errors are inevitably introduced and a measuring bias is usually carried in the measurements. There are essentially four biases: size bias, orientation bias, truncation bias and censoring bias. The biases involved in the surveying of trace lengths have been discussed by Baecher (1983). Among these biases, contributions from truncation bias could be made negligible by selection of a low cut-off (Baecher & Lanney, 1978). Correction of remaining biases has been discussed by Priest and Hudson (1981), Kulatilake and Wu (1984a), and, La Pointe and Hudson (1985).

The statistical characterisation of discontinuity trace lengths is analogous to the characterisation of discontinuity spacing. Einstein and Baecher (1983), for example, believed that the discontinuity trace lengths could be well described by a lognormal distribution.

A number of distributions describing discontinuity trace lengths have been proposed. So far, the existing PDFs used for idealisation of discontinuity trace length distributions are the negative exponential, the lognormal, and, the fractal or power-law distributions, as summarised in Table 2.3. Consideration of which one is applicable is necessary when drawing inferences from discontinuity mapping measurements. The uniform and normal distributions have sometimes been used to investigate the trace length distribution. However, the applicability in practice of these two trace length distributions remains uncertain and is in need of further investigation. The Gamma distribution has its advantage of including the negative exponential distribution as a special case, but is mathematically much more sophisticated than the negative exponential distribution. The fractal or power-law distributions have been reported for several years (Stone, 1980 (cf. Bahat, 1988); Segall & Pollard, 1983). Recently, Davy

et al.(1990), and Sornette et al (1990) in their experiments on the formation of faults in a laboratory observed that the distributions of fault lengths exhibited a fractal dependence over a certain significant range.

Various authors have provided geological evidence for dominance of particular distributions. In most cases these authors collected data and then determined the best of several theoretical distributions. Sometimes, the fitted distributions would be subjected to a goodness-of-fit test (Einstein & Baecher, 1983; Rouleau & Gale, 1985; Villaescusa & Brown, 1990). The variety of observed distributions can be produced from different models describing the mechanical process and the geometric effects owing to the fact that surface traces and not actual discontinuity sizes are observed (Dershowitz & Einstein 1988).

Mean trace length is one of most important parameters to characterise discontinuity persistence and size. Thus, many efforts have been made to estimate the mean trace length.

Cruden (1977) described a method for estimating the mean trace lengths and the potential longest trace length using line sampling while studying slope stability problems. Pahl (1981) proposed a technique of estimating the mean trace length of discontinuities observed in mine drive walls by assuming that the midpoints of traces are uniformly distributed. The method appears, in a sense, distribution-free, since the only parameter required for each discontinuity is whether it is censored (at one or both ends) or not, and no information of the actual lengths of observed traces is needed. The method, however, is limited by the assumption that the traces should be parallel.

The estimation of the mean trace length using scanline mapping was described in detail by Priest and Hudson (1981). They proposed an analytical technique of estimating mean trace length from measurements of semi-trace length of joints on a finite-sized exposure using scanline surveying. Using the analytical technique, the mean trace length, for a large sample, can be estimated by simply counting the number of discontinuities with semi-trace length less than a range of censored levels and the total number in a sample. This technique is of significance in the estimation of mean trace length, and will be used for considering the influence of impersistent discontinuities on the prediction of IBSD in this research study.

Kulatilake and Wu (1984a) described a technique for estimating the mean trace length on infinite vertical sections from the observations made on finite rectangular

vertical exposures. This technique followed the same basic steps as proposed by Pahl to discontinuities whose orientations are described by a probability distribution function. In addition, it was assumed that both trace length and orientation are independent of each other.

After defining the distribution of trace lengths and thereby the mean trace length, discontinuity size cannot be determined unless assumptions about discontinuity shape and the nature of their size distributions have been made. Under special assumptions, the underlying discontinuity size can be estimated from trace length measurements on exposures.

Robertson (1970) has found that the lengths of joints in both the strike and the dip direction are approximately equal, from which circular discs were proposed as models for joints although other models, such as Poisson planes, were proposed for discontinuity models (Baecher et al., 1977; Dershowitz & Einstein, 1988).

On the basis that the sizes of discontinuities have a statistical distribution related to the distribution of trace length, Warburton (1980) derived an analytical relationship between trace length and discontinuity size, using mathematical stereology and geometric probability methods. This would appear to be of great significance for the research objective which is to determine the invisible discontinuity size information from visible and measurable trace lengths. Therefore, further study of its practical applicability would seem important. Based on Warburton's work, Kulatilake et al. (1990) found that diameter distributions for all discontinuity clusters will tend to be gamma type assuming that joints are finite circular discs. In an effort to investigate the influence of non-persistent discontinuities on the IBSD in this research, Warburton's relationship will be used to develop a numerical solution for the determination of discontinuity sizes.

It is seen from Table 2.3 that negative exponential, lognormal, and fractal trace length distributions are often encountered. Thus, the research emphasis will be put on these three trace length distributions. It is worth noting that so far, little study of the persistence of discontinuities with fractal distributions has been done. Characterising persistence and size parameters of discontinuities with fractal distributions will therefore be highlighted in this research study.

The discussion of discontinuity trace length distribution laws and identification techniques is similar to the discussion of discontinuity spacing distributions made in

the last section, and is therefore not described here. Just as with discontinuity spacing distributions, to identify the quantity of fit to ideal lognormal, negative exponential and fractal discontinuity trace length distributions is also important in the study of discontinuity persistent analysis.

2.1.4 Discontinuity Orientation and Sets

For discontinuity geometry, the orientation of the most important discontinuity sets is another of the main factors to be considered. In the modelling of discontinuity geometry, delineation of the discontinuity sets is a first step to creating discontinuity geometry patterns (Dershowitz & Einstein, 1988). Discontinuities in rock masses are not uniformly distributed in all directions, but are often formed in sets (Piteau, 1970; Pollard & Aydin, 1988). There are several analytical functions available to describe the discontinuity orientation distribution, such as the Fisher and the Bingham distributions (Baecher, 1983; Dershowitz & Einstein, 1988; Priest, 1993b).

Grouping discontinuities within rock masses into sets usually consists of three phases: mapping and logging the data, defining the criteria for membership of a set, and assigning individual discontinuities into each of the sets. In practice, the stereographic projection method has traditionally been used for a basic approach to identification and assignment of the discontinuity sets. Poles of discontinuity planes are plotted to produce a scatter plot which can be contoured to give orientation densities. Certain criteria are then applied to the contoured plot which allows the discontinuities to be grouped into several discontinuity sets with a distinct clustering around one particular set. The mean orientation and dispersion of each set are then estimated. With the help of computers, this graphical method may be objectively implemented.

A goodness-of-fit test is often used to examine whether a proposed form of theoretical distribution can reasonably describe the scatter of orientation data from site surveys. For example, Baecher (1983) carried out the goodness-of-fit tests using χ^2 examination.

The discontinuity orientation distribution will be subject to error from sampling bias arising from the mapping. A series of techniques for error reduction have been suggested and used in practice (e.g. Einstein & Baecher, 1983; Kulatilake & Wu, 1984b; La Pointe & Hudson, 1985; Priest, 1993b).

The discontinuity orientations of the dominant sets play a significant role in most rock engineering applications. A detailed survey of discontinuity orientations and a careful grouping of discontinuity orientations into different sets are therefore necessary. However, for certain applications and practical reasons, for example, the prediction of IBSD, some simplifications have often been made.

The IBSD and the shape of the in-situ blocks and similarly their equivalent sizes and shapes after blasting are a function of orientation distribution and nature of the main discontinuity sets. In most cases, the in-situ and blasted block size and shape are greatly influenced by three main sets of discontinuities. The other discontinuity sets and random discontinuities influencing the in-situ and blasted block size could be included, but they have often little effect on the results (ISRM, 1978; Wang et al., 1990).

In fact, according to Costa and Baker (1981) and many other structural geologists, discontinuities are closely associated with both the geological structure and the region deformation history which are dependent upon the stress fields within a rock mass. A region earth stress field is always revealed through three principal stresses. So, it may be reasonable to assume that there will be three main sets of discontinuities for many situations where the principal stresses have not rotated significantly. In addition, to develop a procedure for tackling more than three sets of discontinuities will be much more complex than that for dealing with three sets. Therefore, a simplified assumption that there are three sets of main discontinuities will be sustained in this research study for the prediction of IBSD.

2.2 IN-SITU BLOCK SIZE DISTRIBUTION

Both the Ros-Ram (Rosin & Rammler, 1933) and the Schuhmann equations (Schuhmann, 1940) have been widely used for representing block size distributions.

The Ros-Ram equation is given by

$$P = 1 - e^{-(\frac{S}{S_c})^{n_s}}, \qquad (2\text{-}8a)$$

or

$$P = 1 - e^{-(\frac{V}{V_c})^{n_v}}, \qquad (2\text{-}8b)$$

where, P is the proportion of the blocks smaller than the sieve size S or volume V (%); S_C (V_C) is characteristic sieve size (volume), given by the point on the size distribution curve when 63.2% of blocks have a sieve size (volume) finer than S_C (V_C); n_S (n_V) is the index of uniformity given by the steepness of the curve of the block size distribution. Theoretically, lower values of n_S (n_V) mean more fines, more oversized blocks and less blocks in middle sizes.

The Schuhmann equation is given by

$$P = (\frac{S}{S_{100}})^{m_s}, \qquad (2\text{-}9a)$$

or

$$P = (\frac{V}{V_{100}})^{m_v}, \qquad (2\text{-}9b)$$

where S_{100} or V_{100} is the 100% passing block sieve size S or volume V; m_S or m_V is the index of uniformity in the Schuhmann equation and the rest of the terms are the same as those for the Ros-Ram equation.

2.2.1 Developments in IBSD Prediction

The earliest work related to quantitative description of in-situ block sizes was the development of Rock Quality Designation (RQD) (Deere, 1964). Originally, RQD was the proportion of borehole core that consists of 0.1 m or longer intact length. Priest and Hudson (1976) extended RQD to scanline survey data, based on which an analytical relation between RQD and the discontinuity frequency derived from the scanline survey was proposed (Hudson & Priest 1979). Either a borehole or a scanline is by nature one dimensional so that the RQD value obtained from a borehole or a scanline will be influenced by the direction in which the measurements are taken.

To overcome the disadvantage of dependence of RQD upon direction, Kazi and Sen (1985) suggested the use of the Volumetric Rock Quality Designation (V. RQD) . The

V. RQD is a three-dimensional parameter. It is defined as the proportion of the volume of intact matrix rock blocks equal to or exceeding 0.001 m^3 in size, which can be related to the average volume of a matrix block and the number of matrix blocks per m^3. However, the proposal of V. RQD is limited to the estimation of the average block volume rather than the IBSD.

Apart from RQD, Franklin (1974) proposed a simple "size-strength" classification, in which a fracture spacing index I_f, the diameter of a "typical block" was recommended for the use of description of block size. I_f was estimated by visually selecting typical sizes of core or outcrop material and recording their average dimension. The ISRM (1978) suggested a Block Size Index I_b and the Volumetric Discontinuity Count J_v, which could be an indication of the in-situ block size, where I_b is similar to I_f and estimated by selecting by eye several typical block sizes and taking their average dimensions, and J_v is the sum of the number of discontinuities per meter for each discontinuity set present. Obviously, both I_f and I_b are semi-quantitative and have limited use in practice.

Palmstrom (1985) suggested several empirical equations to link J_v, RQD and linear fracture frequency λ, and proposed a correlation between the in-situ block size and J_v, which was represented in a figure incorporating the influence of block shape. From the figure the block size can be estimated from J_v. This method could only estimate a rough upper and lower range of block sizes and thus has restricted application.

Sen and Eissa (1992) derived analytical expressions relating J_v, RQD, and block volumes of different shapes such as bars, plates, or prisms, the result of which were presented in the form of charts. These charts provided a simple tool for practising rock engineers without the need for recourse to theoretical calculations. Unfortunately, the block volume was also given in terms of average block size, and was thereby of limited use in describing the block size distribution.

Another means of tackling the prediction of IBSD is computer modelling. Using analytical geometry, Da Gama (1977) developed a computer simulation program to implement the IBSD analysis, assuming that the orientations of discontinuities in space have been derived from field measurements of the orientations and positions of discontinuities. A significant contribution to simulation of discontinuity geometry was made by Hudson and Priest (1979) who introduced Monte Carlo simulation procedures into the study of discontinuity spacing distributions which were also related to the rock block lengths. These ideas in the study of discontinuity spacing distributions were

further extended to both studies of block area distributions in a plane and block volume distribution of a particular rock mass. Stewart (1986) reported a simulation of IBSD conducted by the Climax Molybdenum Company. The algorithm and computer programme was considered to give a direct simulation of fractured rock blocks using discontinuity set statistics, Monte Carlo techniques, analytical geometry, and, scanline mapping data and therefore had much in common with Da Gama's work. Xu and Cojean (1990) developed a model which was based on the algorithm developed by Lin et al. (1987) for simulating three-dimensional rock mass granulometry. An important advance in this model is that the connectivity of fractures, which is usually difficult to characterise, was taken into account.

Ghosh et al. (1990) reported one procedure to estimate the IBSD. In the procedure, the core logging, largest block, RQD and the percentage of larger than 25 mm, are collectively used to estimate the IBSD assuming that the length distribution of the core fragments is representative of the IBSD. However the IBSD derived from drill hole data could often be considerably underestimated since the maximum dimensions of the blocks are not often in the vertical direction when cores are taken. Thus the IBSD has to be corrected.

Assuming that intact blocks in a volume of naturally jointed rock occur with the same frequency as simulated discontinuity spacings of that size, a three-dimensional rock model has been developed by Kleine and Villaescusa (1990), which takes into account the finite extension, location and orientation of the discontinuities within a rock mass. The most likely distributions of discontinuity extension, location and orientation were derived from line mapping, which were then used to compute the IBSD. However, an assumption was made whereby intact blocks of a certain size will occur with the same frequency as the measured or calculated discontinuity spacing associated with that size.

Ord and Cheung (1991) described an automatic mapping system in which a video camera was used to record images produced from multiple scans of a rock exposure. The information included in the images was used to establish the complete three dimensional shape of the scanned exposure. Using this system, instantaneous outputs such as the in-situ block size could be obtained in the field. This technique was based on image analysis. Therefore, the relevant equipment and a suitable field working environment have to be provided, which is considered likely that this will limit its application in practice until its accuracy has been proven to be acceptable in many working environment.

Dershowitz (1992) has devised a stochastic simulation procedure based on forward modelling. It repeatedly simulates a three-dimensional fracture system until the trace length statistics for simulated sampling planes, which were the same as the surface on which the original data was collected, match sufficiently with the trace statistics of measured data. It was claimed that this method worked well for complex fracture geometry where analytical methods prove difficult to cope with. This simulation method usually needs large exposures. Small natural exposures are common, which makes it difficult to evaluate fracture size in small exposures reliably. However, it is a substantial advance as it deals with finite size discontinuities.

Only discontinuities with either uniform, negative exponential or lognormal spacing and/or trace length distribution were considered in all the methods or techniques mentioned above. Turcotte (1986) showed that the power-law distribution is equivalent to the fractal distribution and that the distribution of fragment sizes produced by blasting is likely to be related to the distribution of discontinuities in the rock. In addition, he has gone as far as to suggest discontinuity distributions may determine the distributions of fragment sizes by dynamic breakage. Poulton et al. (1990) suggested that both massive and fragmented rock masses have scale invariant behaviour, i.e., the fractal characteristic. They also suggested that fracture spacing and block size might show similar fractal dimensions for a given rock mass if the scale invariance could be applied to in-situ, i.e. geological rock breakage. Genske et al. (1992) stated that fractal geometry may serve as a tool to build models for jointed rock masses, and that complicated structures can be reduced to simple fractal models, thereby accelerating the analytical work, although they acknowledged that most phenomena in geomechanics may not be fractal in terms of strict mathematics. Hobbs (1993) proposed that the distributions of rock discontinuity patterns are not random, but deterministic and as such may be described by a fractal dimension.

2.2.2 Wang's Methods

Wang and his co-workers (Wang et al., 1990, 1991a; Wang & Latham, 1991; Wang, 1992) illustrated the development of two different techniques which use either orientation and location data from individual discontinuities or, only location data of the discontinuities mapped combined with a knowledge of the main discontinuity set orientations. Both of them are incorporated in a computer program and these are called respectively the Dissection Method and the Equation Method.

Dissection Method

The Dissection Method uses a computer program to determine the sizes and shapes of all blocks produced by intersecting discontinuities within a boundary block formed by six persistent planes. The algorithm developed in this computer program takes advantage of the block theory by Goodman and Shi (1985). The data set required to run the program is discontinuity orientation parameters and intercepts with reference to an oriented scanline, all of which can be provided from detailed scanline surveying. Six discontinuities are chosen to form an executable six-sided block called the boundary block for which the IBSD is to be computed. This boundary block is first dissected into two blocks of varying shape by a discontinuity which is read from the discontinuity data file (refer to Fig. 2.2). These two may be further dissected into three or four blocks by another discontinuity. This dissection process is carried out until the last discontinuity in the working data file is executed, yielding an intermediate file of co-ordinates of corners of all natural blocks existing in the boundary block formed by the dissecting discontinuities. The sizes of these blocks are given in terms of volume, maximum length, and nominal diameter. Shape in terms of number of facets, ratio of maximum length over nominal diameter are then defined. Accordingly, the block size distribution is given. The geometrical pattern of discontinuities intersected with the boundary block can be viewed in three dimensions from the computer program.

Equation Method

The Equation Method uses a set of empirical equations to estimate the IBSD. This set of empirical equations relates the IBSD to the principal mean spacings and the mean orientations of the three principal sets of discontinuities defined to best characterise the rock mass. The equations are ones derived from computer modelling results of the block sizes distributions obtained from the dissection method described above. To calibrate the equations, input data was introduced from artificial discontinuities having a given distribution but with a random sequence of generation. Depending upon which specific spacing distribution is chosen, different sets of empirical equations are offered. These equations are all given by the general equation:

$$V_{i,p} = \frac{C_{i\,p} \times (S_{pm1} \times S_{pm2} \times S_{pm3})}{\cos\theta \cos\phi \cos\alpha}, \qquad (2\text{-}10)$$

$i = 10, 20, ..., 100,$

where, $V_{i,p}$ and $C_{i,p}$ ($i=10,20,...100$) are respectively block sizes of percentage passing and empirical coefficients; i are percentages; S_{pm1}, S_{pm2} and S_{pm3} represent the three principal mean spacings; and θ, ϕ and α are the angles between the mean orientations of the three discontinuity sets. The $C_{i,p}$ in Eqn. 2-10 for discontinuity sets with negative exponential and uniform distribution and a certain lognormal distribution spacing law have been given elsewhere (Wang, 1992) as simple look-up tables.

In the dissection method, it is very important to select the six boundary planes carefully in order to form an "executable boundary block" capable of yielding meaningful and reliable block size distributions. In addition, the execution of the computer programme is often very time-consuming owing to problems with the dissection method in terms of user-friendliness and user access. The equation method which evolved from the dissection method, in certain respects, is preferable since it is simpler and more time-saving than the dissection method. But, the equation method is less versatile in the sense that the dissection method can solve precisely the problem posed whatever the number and quantity of discontinuity sets to be included.

Although Wang advanced our knowledge, the prediction of the IBSD of rock with discontinuities described by a fractal spacing distribution was not included in his study. Just as with almost all existing methods to estimate the IBSD, the techniques developed by Wang assume that all discontinuities to be included in the analysis of a rock mass are persistent. Certainly, a rock mass with impersistent discontinuities is the normal, indeed, the universal case. This suggests that incorporation of the influence of impersistence on the IBSD into existing approaches is a much needed research topic.

2.3. BLASTED BLOCK SIZE DISTRIBUTION

To assess whether a blasting operation is optimal requires an appraisal of the BBSD. Thus, assessment of the BBSD has been an important topic in quarrying and mining. The tools used for the assessment include simple prediction using empirical blast design models, image analysis and prediction involving numerical modelling.

The simple prediction approaches are employed to help tailor the explosive and geometric parameters of the blast towards a desired BBSD for full scale production and they use empirical blast design models such as Kuz-Ram (Cunningham, 1983), Bond-Ram (Da Gama, 1983; Wang et al, 1992). These models which are based on the classical Ros-Ram and Schuhmann equations can give a good fit to the BBSD

(Gilvarry, 1966; Just, 1979; Da Gama, 1983; Cunningham, 1983, 1987; Gozen et al, 1986; Turcotte, 1986; Clarke, 1987; Grady & Kipp, 1987; Wang, 1992).

Image analyses are the approaches to determination of the blasted block size distribution by direct measurements from blastpile images, which are often implemented by means of computers (Noren & Porter, 1974; Carlsson & Nyberg, 1983; Van Aswegen & Cunningham, 1986; Cunningham, 1987; Franklin & Maerz, 1988; Hunter et al, 1990; Farmer et al., 1991; Cheung & Ord, 1991; Wang, 1992).

Prediction involving numerical modelling has usually incorporated parameters such as explosive properties, blasting pattern and in-situ rock properties (Harries & Hengst, 1977; Lownds, 1983; JKMRC, 1991; Owen et al., 1992).

Other pragmatic approaches, for example, the "analogous model method" (JKMRC, 1991) and the boulder count (Johansson & Persson, 1974; Rustan & Vutukuri, 1983) have occasionally been used in practice.

Among the above approaches, the prediction approaches and image analyses remain the most promising in the near future while numerical simulation using a computer will be still used as an auxiliary tool of understanding the fracturing mechanism. Thus, the following discussion will focus on both prediction approaches and image analyse.

2.3.1 Prediction Approaches

The Kuz-Ram model

Kuznetsov (1973) studied different materials with widely varying types of blasting scales ranging from normal openpit mining to a nuclear blast. Based on the measurements of fragmentation from the studies, he proposed an empirical equation used to estimate the 50% passing block size of a blastpile, which is given by:

$$S_{b50} = A(\frac{V_b}{Q})^{\frac{4}{5}} Q^{\frac{1}{6}} (\frac{115}{E})^{\frac{19}{30}}, \qquad (2\text{-}11)$$

where S_{b50} represents a sieve size (in cm) through which 50% of the blastpile will pass; Q equals the weight of explosives (in kg), and, V_b is the volume of rock mass per blasthole (in m^3); E is relative weight strength of the explosive, taking E=100 for

ANFO; A is a rock factor which is dependent on the description of the rock mass in terms of discontinuity structure, rock density and rock hardness. Originally, Kuznetsov suggested that A take one of the following values: (i) 7 for medium rocks; (ii) 10 for hard, highly fissured rocks; and (iii) 13 for very hard, weekly fissured rocks.

Combining the Ros-Ram equation (see Eqn. 2-8) with Kuznetsov's equation, Cunningham (1982, 1983) suggested an empirical approach to estimating fragmentation. This approach has been called the "Kuz-Ram" model. In the Kuz-Ram model, the characteristic size in the Ros-Ram equation is derived from S_{b50} obtained by the Kuznetsov equation, the uniformity index n characterising the steepness of the Ros-Ram curve is estimated by

$$n = (2.2 - 14\frac{B}{d})(\frac{1}{2}(1+\frac{S}{B}))^{0.5}(1-\frac{W}{B})(\frac{|BCL-CCL|}{L}+0.1)^{01}\frac{L}{H}, \qquad (2\text{-}12)$$

where d is blasthole diameter (mm), B is burden (m), S is spacing (m), BCL *(m)* and CCL (m) are respectively bottom and column charge length, L is total charge length (m), W is the standard deviation of drilling accuracy (m), and H is bench height (m).

Cunningham (1987) developed an algorithm for the value of A with reference to the research of Lilly (1986). It attempts to improve the values of A originally suggested by Kuznetsov and is given by,

$$A = 0.06\,(RMD + JF + RDI + HF), \qquad (2\text{-}13)$$

$$JF = (JCF \times JPS) + JPA,$$

where RMD is the description of rock mass, JF is the discontinuity factor, RDI is the rock density influence, HF is hardness factor, JCF represents discontinuity condition, JPS is the vertical discontinuity spacing, and JPA is the discontinuity plane angle. The value of A estimated by this algorithm falls in the range from nearly 1 to 13. The new algorithm promoted the application of the Kuz-Ram model in practice.

The Kuz-Ram model is the most widely used published approach for predicting the BBSD. This approach has several particular advantages: familiar parameters, simple calculation and good adaptability to different blasting situation. But, it gives emphasis to the details of the explosives and the blast design geometry and arguably does not take good account of the geological conditions of the in-situ rock mass.

The Bond-Ram Model

Bond (1952, 1959) proposed an equation used to relate the blasted block size, the in-situ block size and energy input, which has been called Bond's third comminution theory. It has the following form:

$$E_s = 10 E_c \left(\frac{1}{\sqrt{S_{b80}}} - \frac{1}{\sqrt{S_{i80}}}\right), \tag{2-14}$$

where, E_S is the required energy for fragmentation in *kwh* per ton of processing rock material; E_C is Bond's work index; S_{b80} and S_{i80} are the blastpile and in-situ block size for this application rather than product and feed sizes that are used in milling. Subscript 80 means that the block size is equivalent to the sieve opening (in microns) through which 80% of the rock materials pass. E_S can be taken as input energy, which is determined from the specific charge and the type of explosive (see Da Gama, 1983; CIRIA/CUR, 1991) as follows.

$$E_s = \frac{0.00365 E_e P_f}{\rho}, \tag{2-15}$$

where E_e is the weight strength of the chosen explosive in weight (%); P_f is the specific charge or powder factor in kg/m^3; and, ρ is the density of the rock mass in t/m^3. E_C can be estimated using an empirical equation suggested by Da Gama (1983) as :

$$E_C = 15.42 + 27.35 \frac{S_{i50}}{B}, \tag{2-16}$$

where S_{i50} is 50% passing in-situ block size and B is the burden used in the blasting.

Combining the Bond's theory, the Ros-Ram model and Eqn. 2-16, Wang et al. (1992) have suggested an approach to the estimation of BBSD, referred to as the Bond-Ram model, which gives greater emphasis to the initial geological controls, by providing a detailed analysis of the discontinuity spacing data and thereby obtaining the IBSD in the rock mass prior to blasting (IBSD). A major but reasonable assumption of the Bond-Ram model is that given an approximately constant blast

design, wide variations in the IBSD from different locations and depths within a rock mass will to a large extent govern the variation in BBSD that will be obtained.

2.3.2 Direct Measurement from Blastpile Images

Image analysis approaches are both safe and thorough, and thereby promise to be a useful tool for measuring rock fragmentation (Franklin & Maerz, 1988).

As an early example, Noren and Porter (1974) used the photographic method to assess blasting results in open pit operations. A series of tests at the operation mine were conducted to assess surface fragment distribution versus blastpile fragment distribution. The cross sectional view of the blastpile was successively evaluated and compared with the results from surface views. The results suggested that surface measurements are a reasonable representation of the blastpile fragmentation, which greatly encouraged the further application of photographic methods.

Carlsson and Nyberg (1983) proposed a method for estimation of fragment size distribution with automatic image processing. This study marked an advance in the analysis of fragmentation by means of computer techniques.

Van Aswegen and Cunningham (1986) proposed a "standard photograph" method. Using some standard fragmentation photographs of blastpiles with known distribution as references, the BBSD of a new blastpile could be estimated by means of the photographs taken of blastpiles. The accuracy of this method, to a great extent, depends upon the subjective judgement of operators, however it is a useful tool.

Nie and Rustan (1987) used the digitising technique and a so-called radial lines sampling procedure for analysing fragmentation. In their study, the validity of assumptions generally used by photographic methods were discussed and the errors in image analysis methods were outlined. Their study also indicated that the accuracy of the proposed technique was reasonable in terms of practical and economical need for accuracy although more detailed work needed to be performed.

Franklin and Maerz (1988) developed a method of measuring fragmentation by digital photo analysis. The photographs of fragmented rock in the backs of dumper trucks were taken as the input of photo analysis. The blocks were traced and the image

analysis was conducted. An important development in this technique was claimed to be that the overlapping is taken into account using a relevant "unfolding function".

Grainger and Paine (1990) described a photographic fragmentation assessment technique and the comparisons of the photographic technique with manual measurements in several mine applications. Two problems encountered were: the scaling of rock fragments on the photographs to actual size and, the overestimate of fragmentation measurements using photographic techniques. These were discussed and possible solutions were suggested.

Cheung and Ord (1991), and, Ord and Cheung (1991) developed an on line, non-contact fragment size monitoring and image analysis system. The system was based on a stereo imaging technique using a laser, a video camera and a computer. It determined the size distribution from rapid sampling of the visible rock fragments on the surface of the burden travelling on a conveyor belt. The technique appears to have considerable quarrying and mining potential, but the general application of this technique might be limited by its specific equipment and operational needs.

Farmer et al. (1991) developed techniques of digital processing to determine the three-dimensional block size distributions from images taken of the surface of a blastpile. A set of tests, deriving the relationship between the surface distribution and the interior volume distribution, were carried out to verify the key assumptions of block shape that must be made in most image processing analyses. A similar technique was also reported by Stephansson et al. (1992).

Singh et al (1991) focused on the development of a photographic technique for assessing fragmentation in an underground environment. Due to the only moderate quality of underground photographs, it is usually difficult to trace small particles. The solution used was to fit the fines portion of the distribution to a Ros-Ram curve. The percentage of fines was determined by measuring the percentage area of the photograph covered by the fines. An associated computer programme for this purpose was developed.

Wang (1992) devised a simple technique to estimate the median sieve size or 50% passing block volume using a photographic method. This technique was combined with the direct measurements of oversized blocks in a quarry giving an estimation of the BBSD and the yields of armourstone sized blocks. However, this technique appears to be oversimplified and is in need of further refinement.

The above discussions have shown that the main concerns in the applicability of results from photographic approaches usually derive from three sources: (1) the sampling representativity, (2) the shape assumption of fragments, and (3) the correction of image analysis. The sampling representativity includes whether the surface fragment distribution is representative of the blastpile, and, whether the random sampling e.g. from dumper trucks is representative of the over-all distribution. The shape assumption is centred on how the three dimension information is derived from the one and/or two dimensional data measured. The correction is to refine the analysis results. The most probable source of error would result from the assumption that the surface fragment distribution is representative of the blastpile, which has been found to be reasonably accurate (Noren & Porter, 1974; Van Aswegen & Cunningham, 1986; Nie & Rustan, 1987; Ord & Cheung, 1991; Hunter et al., 1990; Farmer et al., 1991), thereby permitting it to be applied to the image analysis of the BBSD.

2.4 BLASTABILITY OF ROCK MASSES

In recent years, there has been a series of investigations into diggability, drillability, rippability and excavability of rock materials (e.g. Scoble & Muftuoglu, 1984; Kirstern et al., 1988; Karpuz et al., 1990; Haines, 1993). However, in spite of these, blasting is the most frequently used means for quarrying, mining and other excavating operations, and there remains an insufficient scientific understanding to quantify the ease with which a rock mass can be fragmented by blasting. There appears to be a wide gap between the level of blasting technology in laboratories and the technology applied to quarrying and mining sites. One of the main reasons for this has probably been the failure of existing empirical models to provide satisfactory solutions to blasting operations (Scott et al., 1993).

A blasting operation can be comprehensively described by: rock mass properties, explosive properties, blasting geometry or pattern, and, initiation sequences. A number of studies on how these factors influence a blasting operation for quarrying and mining have been discussed elsewhere (for example, Hagan & Just, 1974; Da Gama, 1983; Atlas Powder Company, 1987; Wang et al., 1991b; Scott et al., 1993). Since this research study mainly concerns the influence of rock properties and discontinuity structures on blasting operations, the wider considerations arising from the explosive design of a blasting operation in a quarry or a mine is beyond the scope of this

research. Thus, the review below focuses attention on the influence of rock mass properties and discontinuity structures on fragmentation.

2.4.1 Previous Attempts

In either the Ros-Ram or the Schuhmann model, there is an index which characterises the steepness of the fragmentation curve (n_S and m_S, see Section 2.2). The index is generally considered to be primarily a function of the "nature" of rock material rather than the blasting design.

Belland, (1966) carried out a series of blasts to examine the influence of rock mass structure on rock fragmentation. He found that the range of patterns of discontinuities exerted a greater influence on fragmentation than the range of practical blast design and explosive. He therefore suggested that a blast design be based on a discontinuity survey to take advantage of their influence. Others recognised the likely importance of rock mass structure. Coates (1970) pointed out that there were indications that in most formations the fragmentation was primarily determined by the geological structure, i.e. the rock blocks had already been created, the blast merely loosened them and threw them into the blastpile. Therefore, an increase in the powder factor was not likely to have a proportional influence on the degree of fragmentation because the basic element, the geologic block, was not affected.

A rather simple description related to rock properties is probably Hino's blastability coefficient (see Just, 1973) which is the ratio of both compression and tensile strength of a rock.

The linking of rock properties to rock fragmentation, as expressed by the Kuznetsov's equation (1973), was a major advance in the study of blasting. The equation made possible the estimation of the mean block size and lead to the development of the Kuz-Ram model. In Kuznetsov's equation, the parameter "Rock Factor" A, which essentially depends on the hardness and jointing of the rock, is required to account comprehensively for the influence of the rock properties on the blast result. However, there are rarely any experimental results available to establish the rock factor in advance of a blast, and this parameter has to be either estimated or determined with time-consuming and expensive trial blasts and block size assessment performed under conditions encountered in actual blasting operations.

Khanukayev (1974) urged that special attention should be paid to the classification of rock mass regarding its fracturing because the degree of fracturing considerably influences the specific consumption of explosives and the fragmentation ability of rocks. Hagan and Just (1974) believed that optimum selection and application of an explosive for a given operation would not be achieved until the influence of rock properties on the nature and extent of fracture mechanisms was fully understood. They therefore advised that a kind of quantitative classification system which defines the ease of fragmentation of rock would be needed. Bellairs (1986) stated that both experiments and practice had indicated that blasting results were influenced by rock properties more than explosive properties. He went on to describe a classification system for blasting, including physical hardness, mineralogical and genetic characteristics of ore for fine-tuning blast pattern design at Mt Whaleback Mine.

Langefors and Kihlstrom (1978) developed an empirical formula to calculate the maximum burden. It incorporated a blastability factor which indicates the explosive needed to break but not throw the rock (see Rustan, 1992; Kou & Rustan, 1992).

Another approach to the modelling of blasting is to consider the process as one of explosive energy input in order to achieve a certain amount of work which is expressed by the reduction from in-situ to blasted block sizes. This is the basis of the Bond-Ram model describes in Section 2.3.1. A significant step towards the establishment of correlation between input energy, the size distribution before and after blasting has arisen from the Bond's third theory of comminution. Considering a compromise between the first theory of comminution (Rittinger, 1867, see Da Gama, 1983) and the second theory of comminution (Kick, 1885, see Da Gama, 1983), Bond (1952) proposed the third theory of comminution (see Eqn. 2-14). In the theory, there is a key parameter, called the work index which is defined as the energy required to crush a solid of infinite size to a product of which 80% will pass a sieve size of 100 microns. The work index reflects the resistance of a rock to crushing, grinding and breaking by blasting (Bond & Whitney, 1959). The remarkable advantage of Bond's theory when applied to blasting is that the estimation of the fragmentation of a blast (i.e. the BBSD) is related to the in-situ block size and the input energy of explosives. Putting Bond's theory into practice, Da Gama (1983) suggested an empirical equation for estimating this index especially suitable for rock bench blasting, which related to the 50% passing in-situ block size V_{b50} and the burden used in blasting (see Eqn. 2-16). Not surprisingly, however, the equation presented by Da Gama suffers the usual limitations of an empirical formula with a relatively low correlation coefficient and a far from comprehensive set of rock masses tested.

Studies by Singh and Sarma (1983), and Yang and Rustan (1983) used a series of small scale physical tests to evaluate the influence of the discontinuities present in a rock mass on the blasting results. According to Yang and Rustan, different blast designs did not change S_{b50} significantly, which suggested to them that S_{b50} was largely governed by S_{i50}. A similar suggestion was also made by Wang (1992).

Lilly (1986) suggested an approach to assessing the blastability of a rock mass which is essentially a procedure linked to the blastability classification system. Taking a pragmatic viewpoint and extending the concepts of empirical rock mass classifications to blasting, Lilly proposed an empirical rating index for blastability of a rock. He selected a few easily obtained rock parameters which contributed significantly to blasting performance and assigned weighted ratings. These parameters included the hardness, the specific gravity, the structural characteristics, and the jointing situation of the rock mass. Lilly claimed the Index to be a measure of the overall blastability of the rock mass.

In 1987, Cunningham produced a review on applications of the Kuz-Ram model in fragmentation estimation. He outlined the three problem areas in any blasting model which were: (1) definition of the relevant rock properties, (2) selection of the appropriate explosives performance indices, (3) determination of the actual blasting fragmentation. Furthermore, he predicted that a meaningful explosive/rock performance index was likely to emerge from further research.

The investigations of influence of the intact rock properties and the rock mass structure on the blast were also reported by other researchers (e.g. Clarke, 1987; Kleine & Villaescusa, 1990; Wang et al., 1991b; Scott et al., 1993). These investigations are similar to the suggestion that the blast results would depend largely on the geological properties of the rock mass. Particularly, Scott et al. suggested that emphasis need to put on the development of a more accurate fragmentation model.

It appears obvious from the foregoing review that there is a fundamental dependence of blasting results on the rock mass properties and that these are significantly governed by the discontinuity structures. A serious effort has been made to uncover the relationships between the rock properties and discontinuity structures and the blasting results but it remains a challenge. Thus, uncovering the relationships through further investigations will be one of main aims of this research study.

2.4.2 Fractal Dimension, Blastability and Fragmentation

The Schuhmann equation has been one of the most widely used models to statistically describe the size distribution that is used to quantify the fragmentation. This equation can be transformed to give the fractal distribution (Turcotte, 1986).

A number of researchers have been devoted to the fractal characterisation of fragmentation (Turcotte, 1986; Poulton et al. 1990; Xie, 1990; Crum, 1990; Ghosh et al., 1990; Turcotte, 1992). The proposition that rock fragmented by an explosion often satisfies a power law size-frequency or fractal distribution over a wide range of scales has been supported by a variety of data (Hartmann, 1968; Turcotte, 1986; Clarke, 1987).

By means of renormalization studies, Turcotte (1986) shown that a more fragile material when subjected to a fragmentation process might be associated with a smaller fractal dimension. Provided that scale invariance (an important characteristic of a fractal) can be applied to rock breakage, Poulton et al. (1990) proposed that the fractal dimension of a rock mass before blasting could be indicative of the BBSD.

It would appear then, that the fractal dimension could be a sensitive parameter to consider in seeking the dependence of the breakage resistance of the rock mass during the process causing fragmentation. The possible role of fractal concepts in developing a description of blastability will therefore be explored in this research study.

2.5 SUMMARY AND CONCLUSIONS

2.5.1 Outstanding Problems

From the foregoing discussion, several outstanding problems can be identified.

First, there has been an impressive development in the prediction of the IBSD. However, as yet there has been no investigation into the IBSD of rock masses with fractal spacing distributions. The fractal spacing distribution has been found to be a distribution potentially encountered in rock masses and is being increasingly recognised in geological engineering. Thus, there is a need to provide insight into the IBSD of a rock with fractal spacing distributions.

Second, discontinuities that are impersistent are to be found in natural rock masses in practice. The consideration of the influence of discontinuity impersistence on the IBSD in existing prediction methods of the IBSD is unsatisfactory. Research should therefore be pursued to consider the contributions of impersistence of discontinuities to the IBSD. Based on this consideration, the existing prediction methods of the IBSD could be updated and founded on a more rigorous basis.

Third, both the Ros-Ram and the Schuhmann equations have had, and will still have their wide applicability in representing the BBSD, and the photographic method promises to be a simply practical tool for measuring rock fragmentation in the blastpile. However, the exclusive and expensive approaches reported above, appear not to meet all possible user requirements which typically include: reasonable accuracy, cost-competitiveness and user-friendliness. The direct photographic and image analysis techniques usually need complex equipment and/or software. The indirect empirical prediction models do not have their governing parameters determined with sufficient reliability to form the basis of assessing the fragmentation in a blastpile. In combining parts of the empirical prediction models with a simple but comprehensively calibrated photographic method, the development of a technique which may meet many user requirements would appear to be an achievable aim for this research study.

Fourth, to date there is neither sufficient understanding of the blastability of rock nor a systematic method to characterise the blastability. The fragmentation achieved is the most fundamental economic variable in a blasting operation. It is governed by the geomechanical and geometric nature of the in-situ rock mass. There is a functional link between the energy input, the IBSD and the resulting fragmentation. Consequently, a research study should set out to attack the problems of adequately characterising the dependence between them. A promising approach would appear to be to introduce a blastability model and a relevant rock mass classification system; one which will relate blasting results to the most relevant rock mass parameters.

Lastly, existing techniques of selecting a theoretical function that best fits the discontinuity distribution parameters have often been found to be unsatisfactory (see Section 3.5). Thus, an attempt to introduce a technique to help obtain a better fitted curve from given measured data is seen as an important step in advancing this field of research which is so dependent upon accurate descriptions of distributions.

2.5.2 Objectives of this Research Study

Faced by the above problems, this research study will focus upon the following objectives.

1. To investigate the IBSD produced by discontinuity networks with fractal spacing distributions using numerical simulations and Wang's dissection method, and to derive a set of empirical relationships for estimating the IBSD of rock masses with discontinuity spacings that have fractal distributions, in order to improve our understanding of the influence of different discontinuity patterns on the IBSD.

2. To introduce an approach to the selection of the best distribution function for the representation of the observed discontinuity spacing and trace length data, using both grey correlation analysis methods and classical goodness-of-fit tests, in order that the characterisation of discontinuity parameters and size distribution laws can be on a more effective footing.

3. To develop a quantitative description of the influence of the impersistence of discontinuities on the IBSD and thereby update and improve the existing prediction methods of the IBSD.

4. To derive a model which will be able to reflect the relationship between the blastability, the energy input, the IBSD and the BBSD and to investigate the potential relationship between the blastability and the fractal dimension characterising the IBSD. Furthermore, in the light of Rock Engineering Systems, to develop a blastability classification system which will embrace the key parameters influencing the blastability of a rock mass, helping to direct a blasting operation towards an optimal result.

5. To develop a pragmatic and reasonably accurate approach to the estimation of the BBSD using photographs of the blastpile and to combine their analysis with both the Ros-Ram and the Schuhmann equations which are the ones often used with predictive methods.

3 IBSD ASSESSMENT WITH SPECIAL REFERENCE TO DISCONTINUITIES WITH FRACTAL SPACING DISTRIBUTIONS

3.1 INTRODUCTION

The spacing of discontinuity greatly dominates the size of individual blocks and is therefore one of the most important parameters concerning in-situ block size. Possibly, the fractal distribution is among the most common distributions of discontinuity spacings (see Table 2.1) and researchers have shown increasing interest in the implications of such distributions (Allegre et al., 1982; La Pointe, 1988, 1993; Hobbs, 1993; Boadu & Long, 1994).

Applying the dissection method developed by Wang (1992) to the discontinuity data surveyed by detailed scanlines, it should be possible to identify all blocks formed by intersections of discontinuities with a fractal spacing distribution. However, as described in Chapter 2, implementation of the dissection method on the computer usually takes a relatively long time, particularly for discontinuities with a fractal spacing distribution (typically, such a single run of the implementation takes more than 2 hours using 80486 IBM-PC with 66 MHz CPU speed, sometimes is up to 10 hours), and execution of the computer procedure of the dissection method needs experience and computer system resources. Moreover, the detailed scanline mapping is often time-consuming, and may be restricted by the availability of rock mass exposures. These factors, including software availability, will discourage the widespread application of the dissection method to the estimation of the IBSD of rock masses, particularly ones with fractal spacing distributions. Therefore, the aim here is to develop a user-friendly technique for estimating the IBSD from discontinuity data, whether it is provided by detailed or quick scanline method, a technique that will embrace discontinuities with fractal spacing distributions. So, for precisely the same reasons that Wang (1992) developed the equation method and calibrated its coefficients for negative exponential and uniform distributions, this chapter reports research leading to coefficients for fractal distributions, also to be used with the equation method.

The basic aim of this chapter is to study the IBSD of rock masses intersected by discontinuities with fractal spacing distributions. Section 3.2 is a description of block size parameters. This section is followed by an introduction to fractal dimension and a

presentation of the evidence of fractal spacing distributions. Section 3.4 briefly presents the technique for deriving the fractal dimension from spacing data. After this, assigning a preferable spacing distribution function to spacing data is discussed in the context of both the goodness-of-fit test and the grey correlation analysis. Section 3.6 consists of a detailed investigation of the estimation of the IBSD with fractal spacing distributions using a combination of random simulation of pre-defined distributions of discontinuity spacings. A comparison between IBSDs arising from different spacing distributions is then given.

3.2 TERMINOLOGY, PARAMETERS AND THEORETICAL BLOCK SIZE DISTRIBUTIONS

Terminology and Parameters

Rock block size can be represented by many parameters such as: equivalent sphere's diameter, nominal diameter or equivalent cube's side length, maximum length, and sieve dimension measured in one dimension; or equivalent spherical volume and apparent volume in three dimensions. In the context of quarrying and mining, the most widely used ones are the sieve dimension and the block volume. The following size parameters have been used in this research study.

(1) Maximum length (l): the distance between two extreme points on the block that are furthest apart;

(2) Thickness or minimum breadth (d): the distance between two parallel bars (strictly speaking, lines) through which the block can just pass;

(3) Sieve size (S): the aperture of a square hole through which a block can just pass;

(4) Maximum, intermediate and minimum dimensions (X, Y, Z): dimensions of a rectanguloid which can just contain a block, where, $X > Y > Z$. When a block is convex, the minimum dimension Z will be equal to the thickness d. They are different when the block is concave:

(5) Apparent volume (V_a): $V_a = X\,Y\,Z$:

(6) Actual volume (V_w): determined by the ratio of the block weight to its density;

(7) Nominal diameter (d_n): $d_n = \sqrt[3]{V_w}$

Theoretical block size distribution

Research on size distributions of comminuted materials has been going on for several decades. In practice, two most widely used distributions are respectively the Ros-Ram distribution and the Schuhmann distribution (see Section 2.2). In addition, a log-linear distribution (CIRIA/CUR, 1991) is also often used to approximate narrow gradings of coastal engineering materials such as armourstone and granular filters.

The log-linear equation may be expressed as follows.

$$P = 1 - \frac{LnV_{100} - LnV}{2(LnV_{100} - LnV_{50})}, \qquad (3\text{-}1)$$

where, P is the proportion of the blocks less than volumes V (%); V_{50} is 50% passing block volume (i.e. the median volume); and V_{100} is 100% passing block volume.

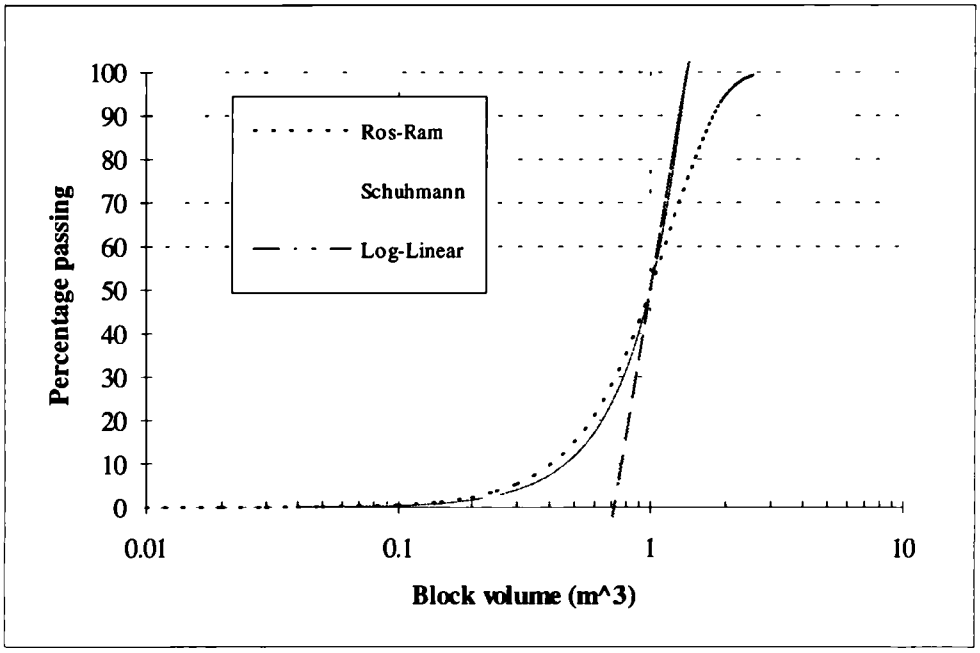

Fig. 3.1 Illustration of comparison of the Ros-Ram, the Schuhmann and the log-linear equations for fragmentation (n_V=m_V=2.1; V_{50}=1.0 m^3, $V_{63.2}$=1.19 m^3 for Ros-Ram, V_{100}=1.40 m^3 for Schuhmann and log-linear)

A comparison between the Ros-Ram distribution, the Schuhmann distribution and the log-linear distribution is illustrated in Fig. 3.1. The overall steepness indicating the

grading width for each distribution is respectively characterised by n_v for the Ros-Ram equation and m_v for the Schuhmann equation. The log-linear distribution is a straight line when presented on the log-linear plot as shown. The Ros-Ram distribution gives an S-shaped curve on the log-linear plot which is often observed for both the IBSD and the BBSD. However, this distribution implies that the largest block can be an unlimited size in the context of mathematics, which is impossible in practice. The Schuhmann distribution produces a one-tail curve and approaches a straight line on the log-linear plot towards the end of the coarse blocks, becoming very similar to the log-linear distribution for the coarse blocks. The Schuhmann distribution is a type of power law. As such, it will reveal self-similarity or fractal features if the distribution is describing geometric relationships, which in this case, it is. It can be considered to be a fractal distribution. The Schuhmann and the Ros-Ram, as well as the log-linear distributions, in due course, will be used in this thesis for describing both the IBSDs and the BBSDs. The subscripts *i* and *b* respectively indicate in-situ and blasted block size distribution and are used hereafter.

3.3 INTRODUCTION TO FRACTAL DIMENSION AND EVIDENCE OF FRACTAL SPACING DISTRIBUTIONS

3.3.1 Introduction to Fractal Concepts

The term "fractal" is perhaps best described as a general concept which is relevant in describing the geometry of irregular objects or patterns. The fractal concept was originally introduced by Mandelbrot (1967). Noting that the length of a coastline increased according to a power law, when the length of measuring rod decreased, Mandelbrot related the power to a real number which he called the fractal dimension.

The length of rocky coastline has served as a classic example to illustrate the fractal concept. If the measured perimeter length of the coastline $P(l)$ and the length of measuring rod l varies as

$$P(l) \propto l^{1-D}, \tag{3-2}$$

then the coastline geometry is said to be self-similar, which describes fractal geometry and D is then the fractal dimension for the coastline. Mandelbrot (1967) showed that the west coast of Britain was a well-defined fractal with D of 1.25. Since then, the fractal concept and its associated mathematical tools have been generalised for

describing the geometric properties of irregular patterns or fragments (Mandelbrot, 1983, 1990).

If examination of geometric features such as cloud or jagged outlines and profiles using different scales of observation shows the same form, the features are said to be "self-similar". This self-similarity is an important property and it is necessary if such a feature is to be termed a fractal and for it to be mathematically described by fractal geometry.

The fractal dimension is another important concept in fractal geometry. The higher the value of a fractal dimension the more irregular a pattern. The introduction of fractal dimensions is a relaxation or generalisation of Euclidean geometry that posits a noninteger dimension for describing irregular and fragmented patterns. Mandelbrot (1986) has offered a rather loose definition of a fractal as follows: a fractal is a shape made of parts similar to the whole in some way. Thus, a fractal which can be a set (say patterns or shapes or objects) looks the same from whatever scale it is observed. That is, a fractal is self-similar at all scales between upper and lower fractal limits, such that any part of this system is a scaled down version of the whole.

The fractal concept is therefore both attractive and important in that an irregular and complex pattern might be simply described using the fractal dimension and that the characteristics of the pattern can be investigated at a convenient scale and then extrapolated to other larger or smaller scales.

For a feature with fractal geometry, the relative number of large and small elements within it remains the same at different scales. The size-frequency distribution of parts or elements is therefore power-law and this scaling relationship is characterised by its fractal dimension, a parameter simply drawn from the power-law exponent.

The fractal concept has been applied to many aspects of nature and has brought together under one umbrella a broad range of pre-existing concepts from pure mathematics to the most empirical aspects of engineering (Mandelbrot, 1983). It is not clear that a single mathematical definition can embrace all these applications, but one can illustrate his quantitative discussion by following Turcotte (1992) and defining

$$N = CS^{-D}, \tag{3-3}$$

where N is the number of objects (e.g. fragments) with a characteristic linear dimension greater than S, C is a proportional constant, and D is the fractal dimension. When objects forming a set, e.g. fragments in a blastpile, can be characterised using Eqn. 3-3, then we say that the objects satisfy a fractal distribution with a fractal dimension D. The fractal dimension D is generally not an integer but a fractional dimension (which is the origin of the term fractal), although it might coincide with an integer value where the D is equal to a Euclidean dimension. It is well known that the Euclidean dimensions of a point, a line, a square, and a cube are respectively zero, one, two, and three.

3.3.2 Fractal Patterns and the Determination of a Fractal Dimension

To discuss fractal patterns, let us review a fundamental feature of the concept of dimension and to illustrate how it can be directed towards the consideration of fractal dimensions, along with the arguments made by Mandelbrot (1967, 1983).

A Euclidean dimension is generally an integer. For every positive integer N, the segment x ($0 \le x \le X$) for a straight line can be divided exactly into N non-overlapping segments with length of form

$$(n-1)\frac{X}{N} \le x < n\frac{X}{N}. \qquad n = 1, 2, \ldots N. \qquad (3\text{-}4)$$

Each of these segments is deduced from the whole by a similarity of ratio with the following form:

$$r(N) = \frac{1}{N}. \qquad (3\text{-}5)$$

Likewise, for every perfect square N, the rectangle Γ (Γ: $0 \le x \le X$, $0 \le y \le Y$) can be also divided into N non-overlapping rectangles of the form:

$$\begin{matrix} (n-1)\dfrac{X}{N^{\frac{1}{2}}} \le x < n\dfrac{X}{N^{\frac{1}{2}}} \\ (m-1)\dfrac{Y}{N^{\frac{1}{2}}} \le y < m\dfrac{Y}{N^{\frac{1}{2}}} \end{matrix}, \qquad n = 1, 2, \ldots N^{1/2},\ m = 1, 2, \ldots N^{1/2}. \qquad (3\text{-}6)$$

Again, each of these rectangles is deducible from the whole by a similarity of ratio,

$$r(N) = \frac{1}{N^{\frac{1}{2}}}. \tag{3-7}$$

For a rectangular parallelepiped, the same argument brings the following similarity of ratio:

$$r(N) = \frac{1}{N^{\frac{1}{3}}}. \tag{3-8}$$

More generally, whenever $N^{1/D}$ is a positive integral, a D-dimensional rectangular parallelepiped can be decomposed into N parallelepipeds deduced from the whole by a similarity of ratio,

$$r(N) = \frac{1}{N^{\frac{1}{D}}}. \tag{3-9}$$

As such the dimension D is characterised by the following relation:

$$D = -\frac{\mathrm{Log}\, N}{\mathrm{Log}\, r(N)} = \frac{\mathrm{Log}\, N}{\mathrm{Log}(1/r)}. \tag{3-10}$$

Now let us move to non-standard shapes, in order for D, the exponent of self-similarity to have a generalised but formal meaning. The only requirement is that the shape is self-similar, i.e. that the whole can be decomposed into N parts, obtainable from it by a similarity ratio r. It is seen that Eqn. 3-9 is equivalent to Eqn. 3-3. Thus, when a pattern or a shape or a figure can be characterised by Eqn. 3-9 or Eqn. 3-10 it can be referred to as a fractal.

In order to illustrate how mathematical relations can be used to generate fractal patterns, let us take two examples which show the construction of fractal shapes.

In Fig. 3.2, at order one (i.e. the first separation) a line segment of unit length is divided into an integer number of equal-sized smaller segments. A fraction of these segments is retained. The construction is repeated at higher orders. The first two orders are illustrated. For (a), a line segment is separated into two divisions and one is

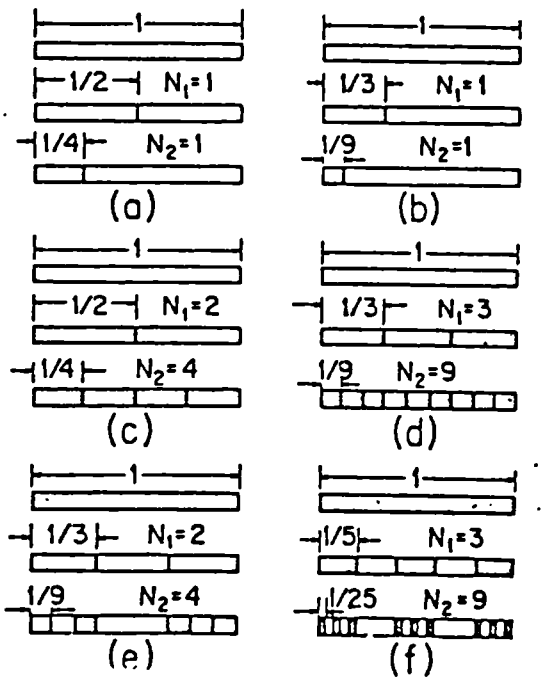

Fig. 3.2 Illustration of fractal pattern construction (from Turcotte, 1992)

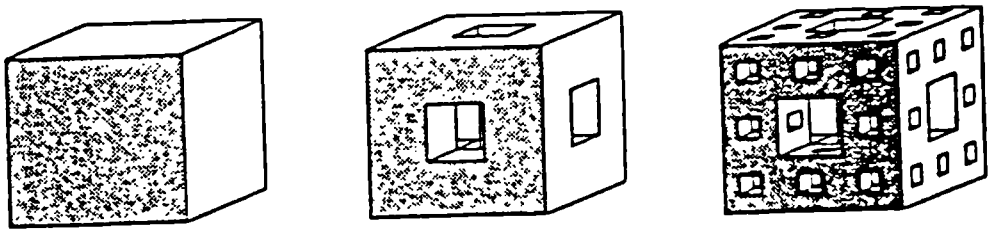

Fig. 3.3 The construction of a Menger Sponge, D= 2.727 (from Turcotte, 1992)

retained, $N=1$, and the similarity ratio $r=1/2$; according to Eqn. 3-10, $D = Log1/Log2 = 0$, which is the fractal dimension of a point. For (b), a line segment is separated into three divisions and one is retained, $N=1$, and the similarity ratio $r=1/3$; $D = Log1/Log3 = 0$, which is the fractal dimension of a point, too. For (c), a line segment is separated into two divisions and both are retained, $N=2$, and $r=1/2$; $D = Log2/Log2 = 1$, which is the fractal dimension of a line. For (d), a line segment is separated into three divisions and all three are retained, $N=3$, and $r=1/3$; $D = Log3/Log3 = 1$, which is the fractal dimension of a line. Note that both (c) and (d) suggest that a simple distribution will have a fractal dimension D of ~ 1.0. For (e), a line segment is

separated into three divisions and two are retained, $N=2$, and $r=1/3$; $D = Log2/Log3 = 0.6309$, which is a non-integer fractal dimension and is known as a Cantor set (Mandelbrot, 1983). For (f), a line segment is separated into five divisions and three are retained, $N=3$, and $r=1/5$; $D = Log3/Log5 = 0.6826$, which is also a non-integer fractal dimension. Both (e) and (f) have fractal dimensions between the limiting cases of zero and one. In the sense described above they therefore have fractional dimensions.

In Fig. 3.3, a solid cube of unit dimension has square passages with dimensions r=1/3 cut through the centres of the six sides. The six cubes in the centre of each side are removed as well as the centre cube, i.e. the unit cube is divided into 27 equal-sized smaller cubes with r=1/3, 20 cubes are retained. $N=20$, $r=1/3$, $D= Log20/Log3=2.727$. This construction is known as the Menger Sponge (Turcotte, 1992).

Since self-similarity in nature is often found to apply within a range of scales of observation defined by upper and lower bounds, one might expect practical application of fractal tools within certain limits. However, a statistically satisfactory form of self-similarity is often encountered, and the assigning of fractal dimensions to data or patterns that are not perfectly fractal is a popular new development in natural sciences. Thus it is not surprising that many geological and geophysical data sets are considered to be fractals. A variety of quantitative observations can be rapidly reduced to enable empirical correlation to be investigated and in this respect the fractal concept is undoubtedly of great significance (Turcotte, 1992).

3.3.3 Evidence of Fractal Spacing Distributions

The fractal concept and its analysis techniques are quite new, but the empirical applicability of power law dependence on the size was recognised long before the concept of fractal was conceived (Turcotte, 1992). For example, the power law size distribution - named the Schuhmann distribution when observed in the fragment size distribution of geomaterials is a consequence of the scale invariance of the fragmentation mechanism, and the pre-existing weak zones or planes where breakage happens which exist on all scales (Allegre et al., 1982; Turcotte, 1986; Korvin, 1989).

Discontinuities with fractal spacing distributions tend to give clustered patterns (see Fig. 2.4). Clustered discontinuities were treated as one type of distribution and discussed together with a fairly evenly spaced distribution (normal distribution) and a

random distribution (negative exponential distribution) by Priest and Hudson (1976). Clustering, it was suggested, could either result from spalling near a free face or around joints due to stress or weathering effects, or from cyclic variation in lithology, say alternating layers of sandstone and highly fractured siltstone.

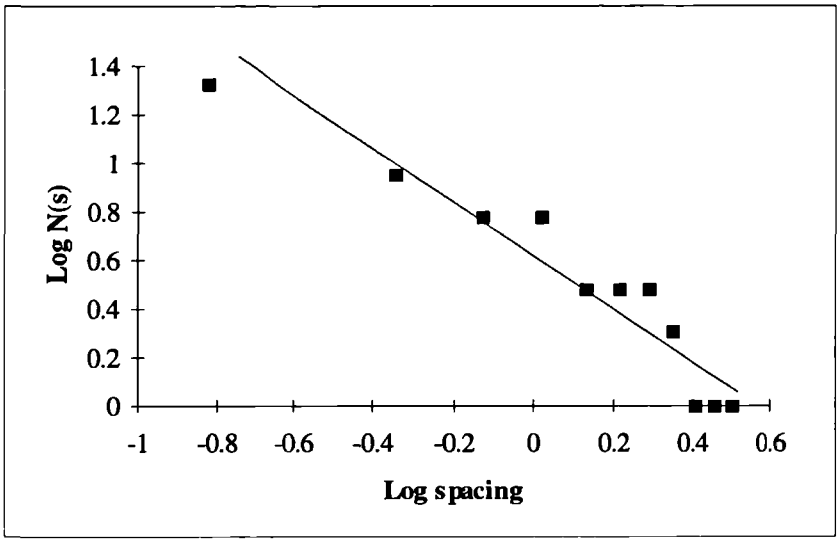

(a)

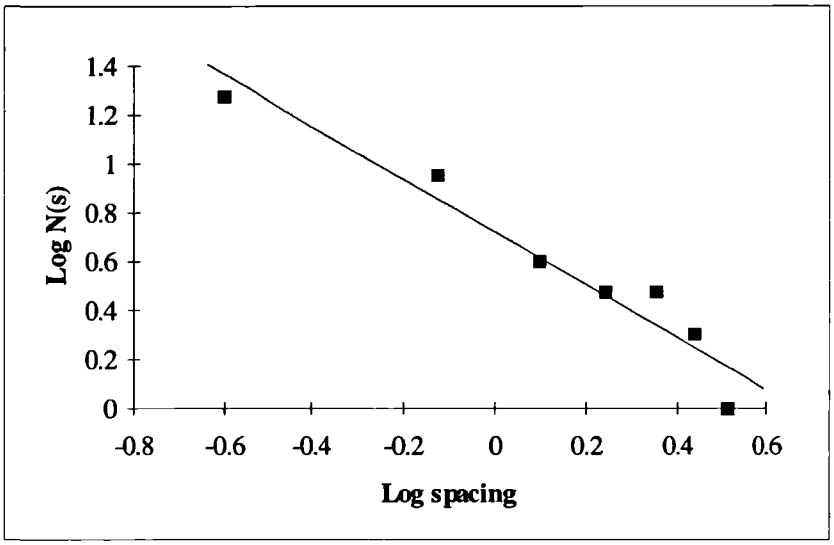

(b)

Fig. 3.4 Spacing distributions of discontinuities within a rock mass at a highway cutting site. (a) D=0.11 (SL-3); (b) D=0.10 (SL-5).

It is sometimes the case that the negative exponential or lognormal distributions fail to fit field data adequately enough to characterise discontinuity occurrence, particularly if there are clusters of discontinuities along a scanline (Sen, 1993). As for discontinuities with a fractal spacing distribution, many discontinuities with low

spacing values will tend to occur within clusters while high spacing values will occur sparsely between clusters. The fractal spacing distributions would seem ideal for describing this clustered appearance often seen.

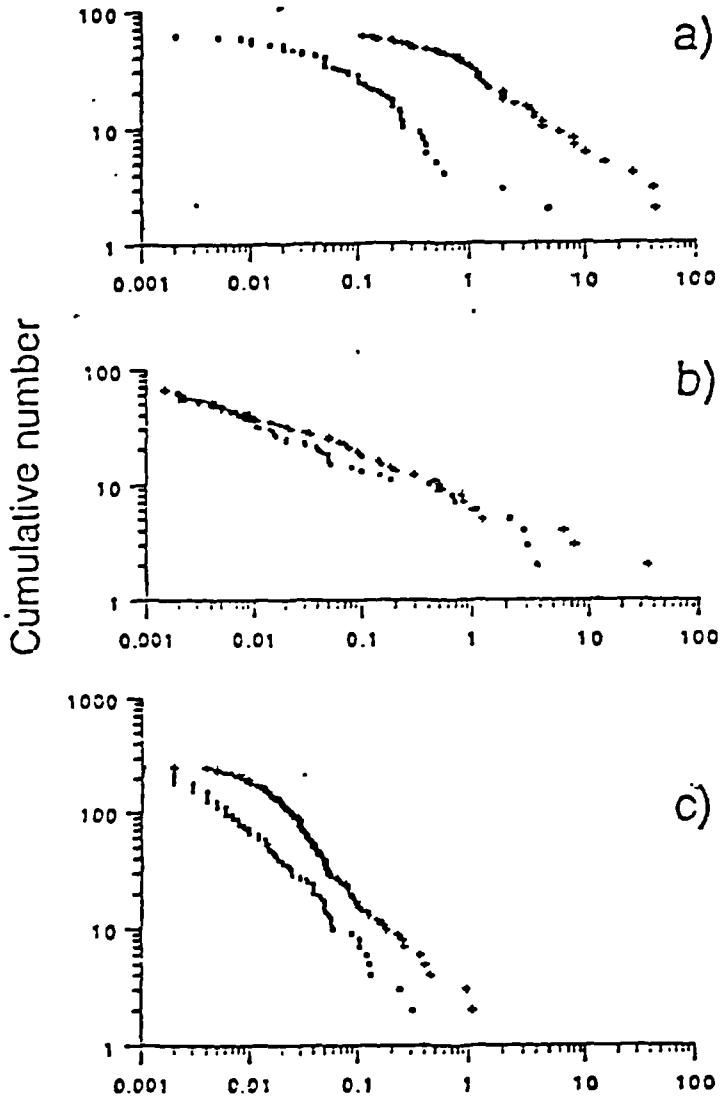

Fig 3.5 Population curves for line sample data set for fault/joint systems (from Gillespie et al., 1993) (■: throw; +: spacing); (a) the Whitworth Quarry, Lancashire (b) the Round O Quarry, Lancashire, (c) the Star Crossing Quarry, Clywd.

In a recent investigation into the discontinuity structure of a rock mass at a highway cutting site carried out by the author, six locations along the cutting faces were surveyed using detailed scanline mapping. For each of the six, one out of the three sets of discontinuities clearly exhibits the fractal characteristic of linearity on a log-log plot, as shown in Fig. 3.4 (fitting discontinuity spacing data to a proposed distribution will be discussed in Section 3.5). The fractal dimensions for the spacings of these discontinuity sets in the six locations varied from 0.05 to 0.6.

Gillespie et al. (1993) used a variety of mapped data sets of faults and joints to investigate the spatial distribution of fractures and to test the techniques of fractal analysis. The results indicated that tectonic faults and/or joints frequently exhibited power law spacing populations with fractal dimensions of between 0.4 and 1.0. Fig. 3.5 shows the population curves for line mapping data sets for discontinuity systems from three field areas. The cumulative number $N(r)$ vs. the characteristic value r of spacing or throw on a fault is presented on a log-log plot.

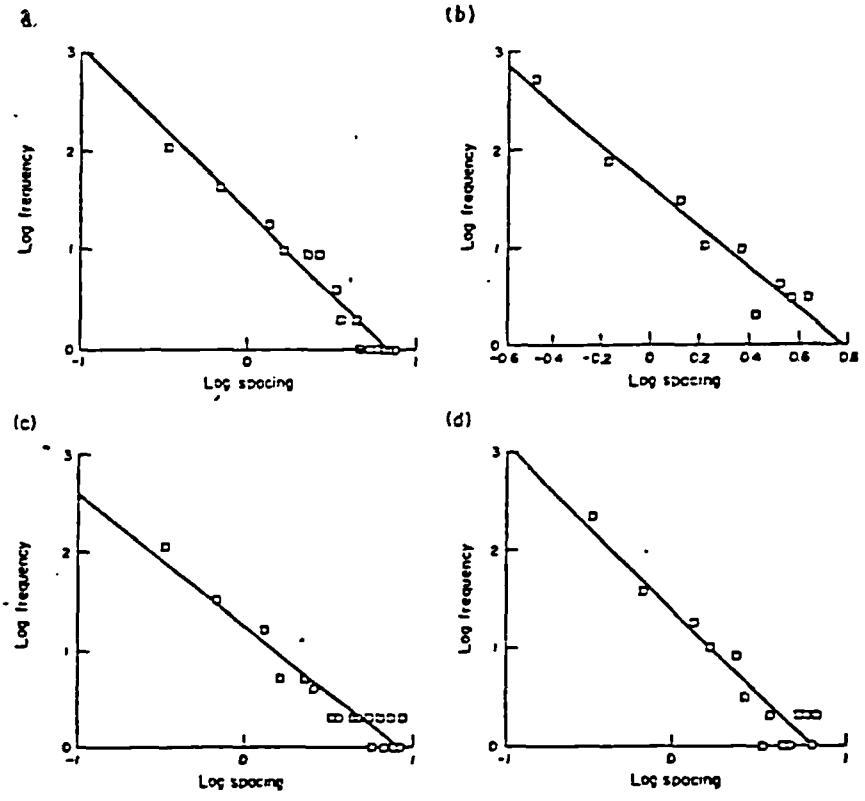

Fig 3.6 Power law fitting to joint sets 1-2, Stripa Granite, Sweden (from Hobbs, 1993) (a)-(d) Power law fit for Joint Sets 1-4

Fig. 3.5 shows that the fractal distributions can be satisfied within the range of from 0.001 m to 100 m, indicating the prevalence of fractal geometry over several orders of magnitude. Fig. 3.6 (from Hobbs, 1993) is the illustration of power law fitting to joint set data, based on some of the results of Rouleau and Gale (1985) for joint spacings in the Stripa Granite. Rouleau and Gale (1985) claimed that a log-normal distribution was a good fit for the data. However, Hobbs used the figure to suggest that a fractal distribution could be considered just as well. The suggestion made by Hobbs has been supported by the study conducted in Section 3.5.

Boadu and Long (1994) investigated the fractal nature of discontinuity spacings for several sites of exposed fractured rock in a 50 km study area located in the crystalline Piedmont of Georgia and South Carolina. Their studies indicated that the discontinuity spacings exhibited fractal characteristics with a fractal dimension of 0.55-0.63.

Harries et al.(1991) investigated a fractal fracture pattern consisting of two sets of perpendicular fracture sets, with fractal dimensions of 0.75 and 0.25, using a spacing population technique.

It is seen from the above that the contention that discontinuity spacing distributions can often been described with satisfactory accuracy by a fractal relationship is supported by field data from a number of researchers. In fact, Hobbs (1993) suggested that any geometrical model of discontinuities in real rocks will show a tendency towards fractal or log-normal frequency distributions for joint spacing, although particular joint sets may show a tendency towards a negative exponential distribution over a limited range. Therefore, we might see more evidence of discontinuities with fractal characteristics reported with the increasing understanding of fractal dimension and its application to practical engineering. This is one important motive for this part of the research which is the investigation of IBSD with special reference to discontinuities with fractal characteristics.

3.4 ANALYSIS TECHNIQUES FOR FRACTAL SPACING

To identify discontinuity spacing distributions is a basic requirement for a study of discontinuity spacing analysis. It is of special relevance to this study since as shown by Wang (1992) the IBSD can be given by a prediction that is a sensitive function of mean spacings. We have learned that using the log-log plot of spacing vs. the cumulative numbers of spacings greater than a given spacing value, the fractal

distribution will be plotted as a straight line, a negative exponential frequency distribution will be a distinct convex upwards curve, and a log normal frequency distribution forms a gentle curve (see Fig. 2.6). Thus, by using the log-log plot, the different frequency distributions of spacing, in particular fractal ones, might be distinguished.

Harries et al. (1991) has suggested a simple technique for determining the fractal dimension of discontinuity spacings which is similar to the scanline technique used in geological surveying. This technique was used in the investigations into measurement and characterisation of spatial distributions of discontinuities carried out by Gillespie et al. (1993) who referred to this technique as the Spacing Population Technique. Boadu and Long (1994) also used the technique to investigate the fractal characteristics of discontinuity spacing and RQD.

The spacing population technique is a one-dimension fractal analysis technique. The fracture pattern is first broken down into its constituent orientation sets by grouping the discontinuities into sets according to their orientation clustering. Then measurements are made on each set individually. The measurements refer to a scanline which is perpendicular to the mean orientation of the set in question. The distance between neighbouring points, i.e. the spacing is preferably measured to the highest resolution in order to obtain satisfactory results. If a set of discontinuity spacings has a fractal distribution, then the distribution will plot as a straight line on the log-log plot of spacing S, vs. cumulative number, $N(s)$. Thus a fractal distribution is described by the relation:

$$N(s) \propto S^{-D}, \tag{3-11}$$

where $N(s)$ is the number of discontinuity spacing values $\geq S$, and D is the fractal dimension which provides a measure of the degree of clustering of discontinuity structure on a line sample. Lower fractal dimensions indicate larger gaps and tighter clusters. Note that for this method, each individual spacing measured can be represented by one data point.

In any study examining fractal or other spacing (or trace length) distributions, the following conventional method can also be used which groups spacing data before it is plotted. First the spacing values are grouped into certain intervals in an order of increasing spacing. Then the frequency of spacing (or trace length) data within each interval is computed and plotted as a histogram. The frequency-spacing (or frequency-

trace length) shown in the histogram is then fitted to a theoretical distribution either visually or mathematically using regression. This is the so called Regression Fitting Technique which was used by Segall and Pollard (1983) to obtain the fractal distribution of trace lengths in granitic rock of the Sierra Nevada.

The spacing population and the regression fitting techniques described above will be used as tools for the analysis of fractal distributions in this research, although other analysis techniques, such as the interval counting and the fracture number box-counting techniques, (La Pointe, 1988; Turcotte, 1989; Davy et al., 1990; Harris et al., 1991; Gillespie et al., 1993) have been used to study the spatial distributions of discontinuities.

3.5 ASSIGNING SPACING DISTRIBUTION FUNCTIONS TO DATA USING BOTH GREY CORRELATION ANALYSIS AND GOODNESS-OF-FIT CRITERIA

Prior to an assessment of IBSD, particularly one based on Wang's equation method (see Section 2.2.2), it is necessary to determine observed spacing data using a mathematical function and to quantify how acceptable this selected characterisation is. Furthermore, which theoretical distribution should be selected from among several contending distributions when no single one is preferred on the basis of the physical characteristics of the phenomena, must be correctly answered.

Visually inspecting the histograms of observed spacings is often not good enough to assign confidently the most representative distribution to the data of spacing distribution. When using either the population spacing or the regression fitting technique in practice, the results obtained are not often so straightward that we can choose one distribution among several presumed theoretical distributions. Frequently, a classical goodness-of-fit analysis is therefore used to obtain a solution to this sort of problem (Baecher et al., 1977; Einstein & Baecher, 1983; Rouleau & Gale, 1985; Villaescusa & Brown, 1990)

3.5.1 Classical Goodness-of-fit Analysis

Goodness-of-fit analyses are designed to examine whether there is a significant difference between the observed distribution (frequency or cumulative frequency) and

the specific presumed distribution we would expect. Both Chi-squared (χ^2) and Kolmogorov-Smirnov goodness-of-fit tests are two classic tests that are most often used for this purpose (Siegel, 1956; Benjamin & Cornell, 1972).

Chi-squared test

The χ^2 technique is related to the deviation of the frequency histogram from the predicted vales. It tests whether the observed frequency is sufficiently close to the expected one to be likely to have occurred under a null hypothesis H_0, say, discontinuity spacing is of a specific distribution.

The hypothesis may be tested by χ^2 statistics

$$\chi^2 = \sum_{i=1}^{k} \frac{(O_i - E_i)^2}{E_i}, \tag{3-12}$$

where O_i is the observed number of cases categorised in the *ith* category and E_i is the expected number of cases in the *ith* category under H_0. Eqn. 3-12 leads one to sum over k categories the squared differences between each observed and expected frequency divided by the corresponding expected frequency. If the agreement between the observed and expected frequencies is close, χ^2 will be small.

We can determine critical values $\chi^2_{\alpha,k-1}$ associated with any desired significance level α for any value of *k-1* such that

$$P[\chi^2 \geq \chi^2_{\alpha,k-1}] = \alpha. \tag{3-13}$$

After observing a sample of a variable, say discontinuity spacing, we can compute the observed value of the χ^2 statistics and compare it to the critical values $\chi^2_{\alpha,k-1}$, reporting the conclusion to accept or reject the presumed distribution according to the following operating rule:

$$\begin{aligned} &\text{Accept } H_0 \quad \text{if } \chi^2 \leq \chi^2_{\alpha,k-1}, \\ &\text{Reject } H_0 \quad \text{if } \chi^2 > \chi^2_{\alpha,k-1}. \end{aligned} \tag{3-14}$$

For a continuous distribution hypothesised, it can be seen that χ^2 test compares the degree of fitness between an observed histogram and a density function lumped into a

corresponding bar-form PDF. Since the χ^2 test is based on the proposition that a sample is large enough to be approximated by χ^2 statistics, the χ^2 test should not be used if more than 20% of the expected frequencies are smaller than 5 when k>2 (Siegel, 1956). It is commonly recommended for a valid goodness-of-fit test that the smallest number of expected frequency is 5 (Benjamin & Cornell, 1972). Expected frequencies may be increased by combining adjacent categories if the combinations can be meaningfully made.

There are several limitations on using the χ^2 test. The first lies in that quite a large sample is needed, which is not always the case. The second is that classifying data into discrete categories may cause the loss of information in a continuous distribution, since lumping data may introduce artificial errors in the numbers actually observed in each interval used in the test. The last is its sensitivity to the choice of intervals. Adjacent categories may sometimes have to be combined in order to increase the frequencies in each category to the recommended smallest number 5, which will decrease the number of categories. The choice of intervals may be important in the χ^2 test since different divisions of intervals for the same data might lead to contradictory conclusions. An example of this has been illustrated by Benjamin and Cornell (1972).

Kolmogorov-Smirnov test

The Kolmogorov-Smirnov test is also concerned with the degree of agreement between the distribution of a set of sample values and some specified theoretical distribution. The test uses the deviations between the observed cumulative frequency histogram and the hypothesised cumulative frequency distribution. This involves specifying the cumulative frequency distribution which would occur under the hypothesised theoretical distribution and comparing that with the observed cumulative frequency distribution. The theoretical distribution represents what would be expected by the hypothesis H_0. The point at which both theoretical and observed distributions shows the greatest divergence is determined. The sampling distribution indicates whether the deviation of magnitude observed would probably occur when the observations are really a random sample taken from a population given by the theoretical distribution.

Let $F_0(X)$ be a specified cumulative frequency distribution function under H_0, and $S_n(X)$ ($S_n(X)=k/N$) the observed cumulative frequency distribution of a sample of N observations. Where X is any possible score, k is the number of observations $\leq X$. The Kolmogorov-Smirnov test focuses on the largest of the deviations represented by DS.

$$DS = \max_{i=1}^{N} \left| \frac{k}{N} - F_0(X) \right|. \qquad (3\text{-}15)$$

The sampling distribution of DS under H_0 is known. From tables of this distribution we can determine critical values. After observing a sample of a variable, we can compute the observed value of the DS and compare it to the critical values in the associated table (e.g. Siegel, 1956). As before, we may accept or reject the hypothesised distribution through the following operating rule:

$$\begin{aligned} &\text{Accept } H_0 \quad \text{if } DS \le V_c, \\ &\text{Reject } H_0 \quad \text{if } DS > V_c, \end{aligned} \qquad (3\text{-}16)$$

where V_c is the associated critical value.

The Kolmogorov-Smirnov test has an advantage over the Chi-square test in that it dose not compare and cast the data into discrete categories, but compares all the data in an unaltered form. However, the Kolmogorov-Smirnov test is strictly valid only for a continuous distribution and only when the model is hypothesised completely independent of the data (Benjamin and Cornell, 1972). In addition, a perfect table for practical use including a comprehensive range of critical values seems to be difficult to obtain. These may limit its application.

It can therefore be seen that the classical goodness-of-fit tests have certain limitations of their own. However, keeping their limits in mind and using proper judgements, there is value and convenience in the conventional application of these tests to substantiate the model choice.

When using either the χ^2 or the Kolmogorov-Smirnov test, a particular suggested distribution for discontinuous spacings can therefore be tested by comparing the observed spacing data with the predictions under the presumed distribution. It is important to realise, however, that if one sets up a hypothesis that a variable is, say gamma-distributed, or lognormally distributed, or any one of many other choices, the conclusion might very well be the same for various different theoretical distributions: that one should accept (or reject) the hypothesis (see Benjamin & Cornell, 1972). This situation is also likely to be encountered in determining the discontinuity spacing distribution.

For example, using the Kolmogorov-Smirnov goodness-of-fit test, Rouleau and Gale (1985) reported that both the lognormal and the Weibull distributions can be accepted for the first set of data of joint spacings in the Stripa Granite, Sweden at the same significance level. Let us now use the Kolmogorov-Smirnov goodness-of-fit test to examine whether or not a fractal distribution can be accepted for the same spacing data observed by Rouleau and Gale (see Table 3.1).

Table 3.1 indicates that the maximum value of *DS* is 0.073 which is emboldened in the table. From the Table of critical values of the Kolmogorov-Smirnov test (Siegel, 1956), the corresponding critical value is 0.079 at the level of significance 0.15, the same level set by Rouleau and Gale (1985). Therefore the hypothesis of fractal spacing distribution could also be accepted, which is in agreement with the suggestion, made by Hobbs (1993), that a fractal spacing distribution should not be ruled out.

Table 3.1 Kolmogorov-Smirnov test for the fractal spacing distribution*

Spacing $\leq X$ *(m)*	*Observed Number*	$S_N(X)$	$F_0(X)$	$DS=\lvert F_0(X)-S_N(X)\rvert$
0.25	108	0.5192	0.4597	0.0595
0.25-0.5	42	0.7212	0.6586	0.0626
0.5-1.25	17	0.8029	0.7431	0.0597
1.25-1.75	10	0.851	0.7963	0.0547
1.75-2.25	9	0.8942	0.8347	0.0596
2.25-2.75	9	0.9375	0.8646	***0.0730***
2.75-3.25	4	0.9567	0.889	0.0678
3.25-3.75	2	0.9663	0.9095	0.0569
3.75-4.25	2	0.976	0.9272	0.0488
4.25-4.75	1	0.9808	0.9427	0.0381
4.75-5.25	1	0.9856	0.9565	0.0291
5.25-5.75	1	0.9904	0.9689	0.0215
5.75-6.75	1	0.9952	0.9905	0.0047
6.75-7.25	1	1	1	0

*The minimum and maximum spacing value are set as 0.03 m and 7.5 m.

In this case, the lognormal, the fractal, and the Weibull theoretical distributions can all be accepted at the same significance level. The reason for this might be because goodness-of-fit tests are not designed to discriminate among two or more models or to

help one select from among a number of contending distributions but rather to suggest that a particularly proposed distribution should or should not be retained.

In engineering practice, we are not only to answer whether or not a proposed distribution can be accepted but also to select a distribution from among a number of contending distributions when no single one is preferred on the basis of the physical characteristics of the phenomena. Statistical theory may not provide much quantitative help for such a selection (Benjamin & Cornell, 1972).

It is therefore worthwhile to pursue a technique for choosing the most preferable fitted distribution among several contending distributions since the classical statistical approaches are not the only approaches available. The grey correlation analysis in Grey Theory Systems (Den, 1985), used in conjunction with the classical goodness-of-fit tests appears to offer an improved approach to the problem: to what extent a proposed distribution is acceptable; and how to select a distribution from among several contending distributions.

3.5.2 Introduction to Grey Systems Theory

The Grey Systems Theory (Den, 1982, 1985) is a new system methodology developed recently. Early application of this systems theory were in the solution of abstract system and non-technology systems. With its increasing development and applications, it has been proposed for solving technological or engineering problems (Cai 1991, Lu & Latham, 1994).

The darkness and lightness of colour is used to describe the quantity of information in control theory. A system whose parameters, structure and characteristics are fully known is described as a "white" system and a system whose parameters, structure and characteristics are entirely unknown is described as a "black" system. However, most systems are indeed neither completely unknown nor known. Therefore, "a system containing knowns and unknowns is called a grey system" (Den, 1982). The basic contents of Grey Systems Theory include: the systems analysis; the development of systems models; the grey predicting or forecasting; the grey decision-making; and the grey control. The grey correlation analysis is one of devices in the systems analysis. An evaluation of the goodness-of-fit of discontinuity spacings to a proposed theoretical distribution, using the grey correlation analysis is given in the following section.

3.5.3 Grey Correlation Analysis

The grey correlation analysis is the analysis of correlation between various relationships influencing a system and the identification of which relationship will be a dominate one. The technique and algorithm of grey correlation analysis is outlined as follows:

Let the main data set of interest be the parent array X_0, and the influencing data sets be sub-arrays, X_i, $i=1,2,..,n$, n is the number of influencing data sets, then

$$X_0=\{X_0(1), X_0(2), ..., X_0(K)\},$$
$$X_i=\{X_i(1), X_i(2), ..., X_i(K)\}. \tag{3-17}$$

The Correlation Coefficient of sub-array X_i to the parent array X_0 at time k, $r_i(k)$, is defined by the formula (Den, 1985, 1987) below:

$$r_i(k)=\frac{\delta_{\min}+\eta\delta_{\max}}{|X_0(k)-X_i(k)|+\eta\delta_{\max}}, \tag{3-18}$$

where η is the recognition coefficient of the range between 0 and 1, and usually takes on the value of 0.5; δ_{min} and δ_{max} are given by

$$\delta_{\min}=\min_i(\min_k|X_0(k)-X_i(k)|)$$
$$\delta_{\max}=\max_i(\max_k|X_0(k)-X_i(k)|) \tag{3-19}$$

The above correlation coefficient $r_i(k)$, characterises the deviation degree between X_i and X_0 at time k. Summarising the deviation degrees between X_i and X_0 at all times, given the correlation degree between X_i and X_0 as

$$R_i=\frac{1}{K}\sum_{k=1}^{K}r_i(k). \tag{3-20}$$

Den (1985) referred to R_i as the Correlation Measure. Clearly, the correlation coefficient of $r_i(k)$ and the correlation measure R_i satisfy the following relations:

$$0 \leq r_i(k) \leq 1 \qquad \text{and} \qquad 0 \leq R_i \leq 1. \tag{3-21}$$

The closer the relationship between X_i and X_0, or the more similar X_i is to X_0, the greater will be the associated grey correlation measure; only when X_i and X_0 are completely superimposed will the correlation measure be equal to 1. When the bivariate data are expressed in a linearised form, the grey correlation measure appears, to a great extent, as a measure similar to the traditional r^2 correlation coefficient.

For arrays with different units and/or different original values, the original data can be normalised through a process of original value transformation in which all the data in an array are divided by the first datum of the array.

The main feature of grey correlation analysis is a comparative analysis between several curves or relationships. In a simple case, this analysis may be visually made. Situations in the real world are often complicated. For example, there are a large number of data points, and the curve shapes are similar in some intervals but different in other intervals. In the case where the situation is a complex one, the quantitative grey correlation analysis provides a potential tool to obtain solutions to problems.

Compared to classical regression in which a correlation coefficient, typically r^2, is obtained after linearisation, grey correlation analysis has the following characteristics: (1) there is no need for a large population, or a lot of sample data; (2) sample data need not satisfy an explicit functional relation; and (3) calculation is simple and convenient (particularly once the appropriate computer code is implemented, see Appendix A.1).

Returning to the selection of a preferable distribution from among several contending distributions. If we let the observed data of discontinuity spacings be represented by the parent array X_0 mentioned above, and let the values at corresponding observing points for the *ith* contending distributions be represented by X_i, it is possible to use grey correlation analysis to compare and select a theoretical spacing distribution from among several contending distributions.

3.5.4 Selecting a Theoretical Spacing Distribution Using Grey Correlation Analysis

In order to assess the blastability of rock materials at a highway cutting site, a research study was carried out by the author (see Chapter 7). The prediction of the IBSD of the rock mass at the site is one of the important topics in the study. Prior to

the prediction, identification of the distribution of discontinuity spacing has to be made. Detailed discontinuity mapping at 6 different exposures along the cutting faces has been carried out. A best-fit the fractal, the negative exponential and the Weibull distributions, compared with the actual measurements is illustrated in Fig. 3.7 (see Fig. 3.4a for the Log-Log plot of $N(s)$~S of the first set of discontinuities from SL-3 mapping result).

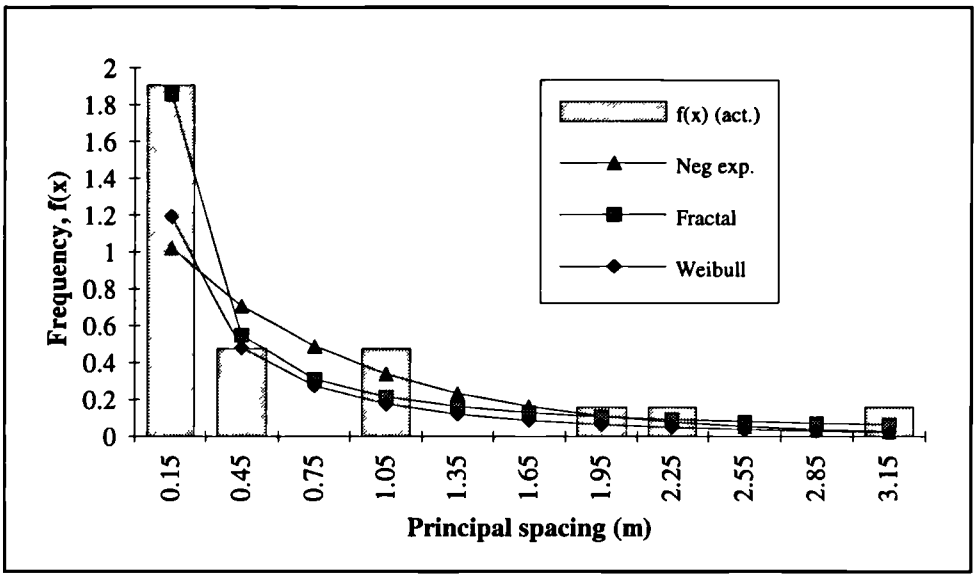

Fig. 3.7 Comparison between the actual measurement and three proposed distributions

The following expressions fitted to the discontinuity spacing data are obtained using a non-linear regression method (Press et al., 1986).

(i) fractal distribution:

$$f(x) = 0.2263x^{-1.110}, \tag{3-22}$$

(ii) negative exponential distribution:

$$f(x) = 1.229e^{-1.229x}, \tag{3-23}$$

(iii) Weibull distribution:

$$f(x)=\frac{0.618}{0.445}(\frac{x}{0.445})^{0.618-1}e^{-(\frac{x}{0.445})^{0.618}} \quad . \tag{3-24}$$

It seems not easy to isolate a preferred distribution among these three proposed distributions (shown in Fig. 3.7). Applying the grey correlation analysis to this case, we obtain the grey correlation measures of these three theoretical distributions to the observed spacing data, which are respectively 0.810 for the fractal distribution, 0.782 for the Weibull distribution, and, 0.718 for the negative exponential distribution. This suggests that the fractal distribution is the most correlated with the observed data. Using the Kolmogorov-Smirnov test, both the fractal and Weibull distributions can be accepted at the level of significance of 0.15 while at this level the negative exponential distribution should be rejected. As a result, the fractal distribution is arguably the best choice for the spacing distribution of this set of discontinuities.

The following is another example, this time taken from the literature: the data is again the joint spacings in the Stripa Granite, Sweden (Rouleau & Gale, 1985). At the level of significance of 0.15, Rouleau and Gale (1985) showed that both the lognormal and the Weibull distributions can be accepted whereas the negative exponential distribution should be ruled out. At the same level of significance and using the same Kolmogorov-Smirnov test, a reworking of the data presented in Section 3.5 showed that the fractal spacing distribution can be accepted (see Table 3.1).

We use the grey correlation analysis to help make the selection of a preferable spacing distribution. Nonlinear regression gives the following best-fit function for the original data set:

(i) the fractal distribution:

$$f(x)=0.2261x^{-1.111}, \tag{3-25}$$

(ii) the lognormal distribution:

$$f(x)=\frac{1}{\sqrt{2\pi}\times 1.317x}e^{-\frac{(Ln(x)+0.658)^2}{2\times 1.317^2}}, \tag{3-26}$$

(iii) the Weibull distribution:

$$f(x)=\frac{0.964}{0.785}(\frac{x}{0.785})^{0.964-1}e^{-(\frac{x}{0.785})^{0.964}} \quad . \qquad (3\text{-}27)$$

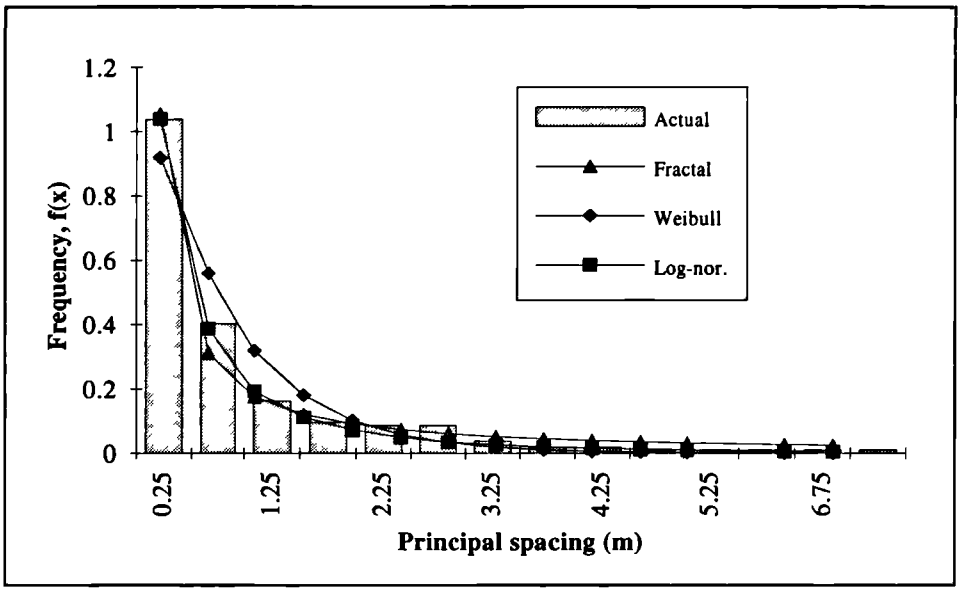

Fig. 3.8 Comparison between the measured and best-fit curves for three distributions

It is quite difficult to say from Fig. 3.8 which one among fractal, lognormal and Weibull distributions is better than another.

Using grey correlation analysis, we obtain the grey correlation measures for these three theoretical distributions when compared to the observed spacing data as follows: 0.90 for the lognormal distribution, 0.84 for the fractal distribution, and 0.81 for Weibull distribution. This suggests that the lognormal distribution is the most correlated with the observed data. We might choose to rule out the Weibull distribution due to both the relatively smaller value of the grey correlation measure and its complicated expression. However, the choice between both the lognormal and the fractal distributions may be finely balanced when finally selecting the representative distribution of the observed spacing data, if it is permitted to take into account the simplicity of the fractal distribution and that the grey correlation measures for the fractal distribution is not far from that for the lognormal. This particular data set happens to be the one discussed by Hobbs (1993) from which he argued that a fractal distribution should be considered in addition to the lognormal distribution selected by Rouleau and Gale (1985).

It is reasonable to conclude from the above discussion that the grey correlation analysis can be used for selecting a preferred distribution from several contending theoretical ones and that the selection will be more effective if the grey correlation analysis is combined with the classical goodness-of-fit tests.

A computer programme for the grey correlation analysis, written in FORTRAN and named GCA, has been developed and presented in Appendix A.1. Later in the thesis the grey correlation analysis will be used together with classical goodness-of-fit test for choosing a distribution from a number of proposed distributions, when analysing spacing and trace length distributions.

3.6 DERIVATION OF IBSD OF DISCONTINUITIES WITH FRACTAL SPACING DISTRIBUTIONS USING BOTH RANDOM SIMULATION AND THE DISSECTION METHOD

Assuming that all the discontinuities are persistent and planar, the individual blocks formed by these discontinuities can be determined analytically using computer algorithms of the types developed by Da Gama (1977), Stewart (1986) and Wang (1992). Wang (Wang & Latham, 1991; Wang, 1992) has applied his algorithm to the development of the Equation Method for the prediction of IBSD of rock mass with discontinuities with a uniform and/or negative exponential spacing distribution. A brief description of how the simulation can be implemented is given in Section 2.2.2 and a detail description is presented in Wang's work (Wang & Latham, 1991; Wang, 1992). In this thesis, the algorithm and the associated computer program developed by Wang (1992) will be used for the investigation of IBSD with fractal spacing distributions. The investigation is based on the same simulation approach as that carried out in the development of the equation method. The difference lies in that the artificial discontinuities in this investigation are given a fractal rather than a negative exponential spacing distribution. The simulation includes :

(1) Generation of three groups of artificial discontinuities governed by particular spatial orientation distributions and fractal spacing distributions with known mean orientations and principal mean spacings or fractal dimensions;

(2) Determination of the IBSD of the simulated groups of discontinuities using the dissection method for 50 different combinations of input parameters (see Table 3.2);

(3) Derivations of the relationships between the known fractal dimension and/or principal mean spacing with the parameters of the IBSDs obtained in the 50 simulations.

In the simulation the assumptions and simplifications are similar to those made by Wang (Wang & Latham, 1991; Wang 1992) in their simulation.

(1) Discontinuity spacing in each set has a fractal distribution defined with reference to a specific fractal dimension and a specific range of spacing values. Note, the principal mean spacing is fixed whenever both the fractal dimension and the range is set;

(2) Discontinuities are persistent (the influence of impersistence of discontinuity on the IBSD will be separately discussed in Chapter 4);

(3) Each group of data always consists of three orthogonal sets of discontinuities;

(4) Each discontinuity in a given set is constructed to be approximately evenly but randomly distributed around the mean orientation of the set within a range of ±10 degrees both in dip angle and dip direction;

(5) Each set usually contains 20 discontinuities, so there are usually 60 discontinuities in one group which are included in the boundary block. Outside of this block, however, there may exist more discontinuities belonging to each set. When for a particular simulation the volume of the boundary block is relatively small, which often occurs for large fractal dimensions or small principal mean spacings, the number of discontinuities chosen for the simulation in one or two or three sets may be more than 20. The actual number of discontinuities may therefore be more than 60 in one boundary block.

For detailed information about the dissection computer procedure and its use for the purpose of simulation, refer to Wang's thesis (1992).

3.6.1 Range of Parameters Examined

It is important to identify the range of spacings and fractal dimensions likely to be of interest before running the simulation.

When taking field measurements, discontinuity spacing values below a known threshold, say, the resolution on a measuring tape, will not be recorded. As such there exists a lower cutoff associated with the effect of resolution of the human eye. On other hand, both actual exposures and discontinuities are of finite size and spacing, and scanlines are of limited length. Discontinuity spacings in an actual engineering project will therefore have an upper cutoff. Thus, the spacing value measured will fall within a range defined by the lower cutoff, S_{min} and upper cutoff, S_{max}. The resolution of measurement and the typical scale at which a rock engineering problem is to be investigated will contribute to the definition of both the lower cutoff and upper cutoff of discontinuity spacings. These consideration were also made elsewhere (e.g. Wang, 1992). However, there are special reasons why setting S_{min} and S_{max} is particular important for fractal simulation.

The range of fractal dimension to be examined is governed by two considerations. The first is the theoretically possible range. The second is the range of fractal dimension values or discontinuity principal mean spacing values encountered in practice.

According to Mandelbrot (1983), the theoretically possible fractal dimension D defined by equation $N=CS^{-D}$ is between 0 and 1. In the author's site investigation on the highway cutting project, the fractal dimension of discontinuity spacing was between 0.05 and 0.6. In the research conducted by Harris et al. (1991), the fractal dimension was between 0.25 and 0.75. Gillespie et al. (1993) showed that the discontinuities were frequently with fractal dimension of between 0.4 and 1.0, and the fractal dimensions derived from the measured data represented by Gillespie et al.(1993) are between 0.4 and 0.7. The range of fractal dimensions of discontinuity spacing measured by Boadu and Long (1994) was around 0.55-0.63.

The lower cutoffs are usually set out around 0.01 - 0.05 m. For example, Priest and Hudson (1976) set it as low as 0.01 m. Wang (1992) suggested that the measuring tape for scanline measurement be calibrated in cm divisions. Boadu and Long (1994) set out the lower cutoff as 5 cm. The upper cutoff typical for quarrying and mining, can be defined as 10 m. Since the scale of mining and quarrying operation is usually in the range of one or several decades of metres, the discontinuity spacing values recorded in practice will be less than this value. For example, most spacing values recorded by Priest and Hudson (1976) were less than 5 m in several field sites. The greatest values from six different field sites recorded by Gillespie et al. (1993) usually remained

below 10 m. The discontinuity spacing values from two different quarry field sites recorded by Wang (1992) were all below 10 m.

It may be recalled from Chapter 2 that if discontinuity spacings are defined by the number-size relationship according to

$$N = C S^{-D}, \tag{3-28}$$

i.e. the discontinuity spacings are of a fractal distribution, then the probability density function $f(s)$ which introduces another coefficient, A, becomes

$$f(S) = A\, S^{-(D+1)}, \qquad S_{min} < S < S_{max} \tag{3-29}$$

The following expression was obtained for the mean spacing in terms of the cutoffs and the fractal dimension:

$$S_m = \frac{D}{1-D} \frac{S_{\max} - S_{\min}(\frac{S_{\max}}{S_{\min}})^D}{(\frac{S_{\max}}{S_{\min}})^D - 1} \tag{3-30}$$

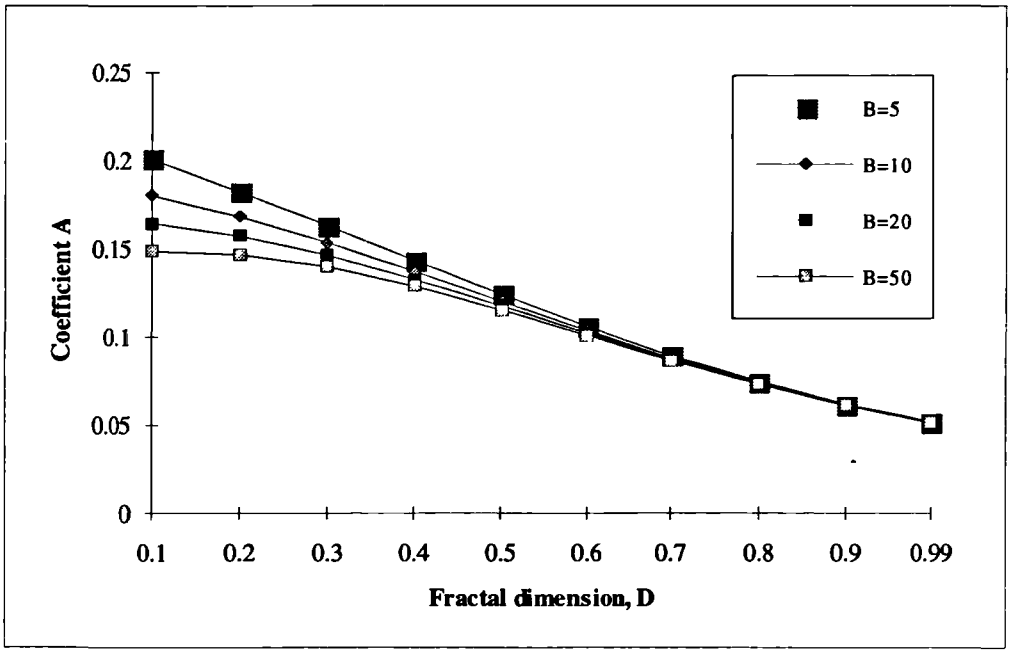

Fig. 3.9 Relation between the coefficient A and fractal dimension with different upper cutoffs (Lower cutoff =0.05 m; B - upper cutoff, in m)

In order to understand the influence of both lower and upper cutoffs and different fractal dimensions on the characteristic parameters, such as the mean spacing and the coefficient A of Eqn. 3-29, a sensitivity analysis has been carried out as given below.

Relationship between coefficient A, fractal dimension D and mean spacing S_m

The influence of the upper cutoff on the coefficient A is shown in Fig. 3.9, which indicates that its influence is not very strong, when fractal dimension D is a large value. The expression for A (see Table 2.2) might therefore be simplified from $A = D/(a^{-D} - b^{-D})$ to $A = Da^{D}$.

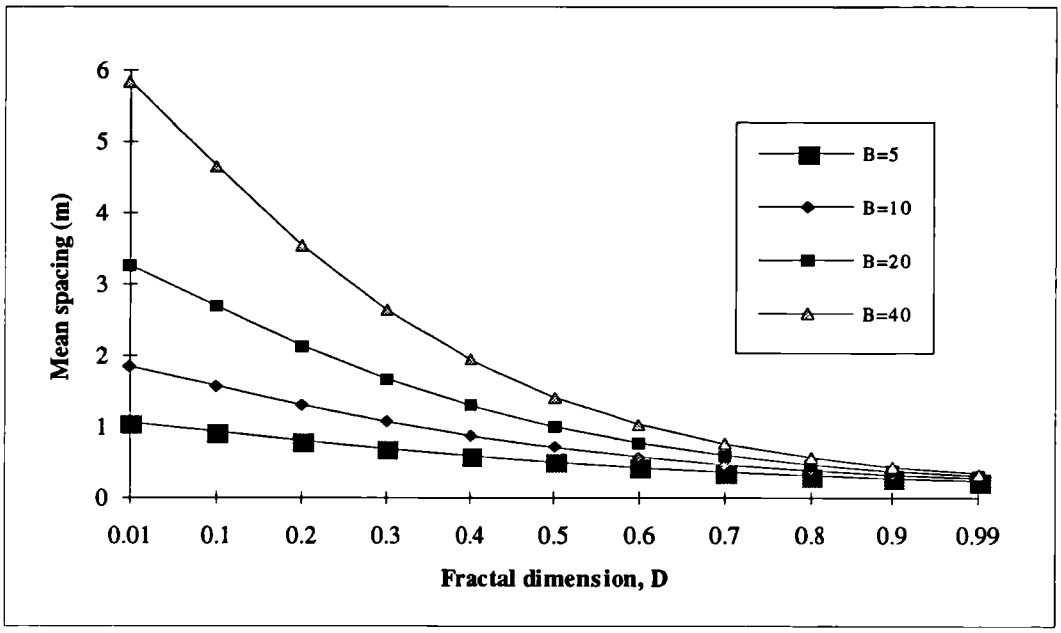

Fig. 3.10 Relation between the mean spacing S_m and fractal dimension with different upper cutoffs (Lower cutoff =0.05 m; B - upper cutoff, in m)

Fig 3.10 illustrates the influence of the upper cutoff on mean spacing. It can be seen that different upper cutoff values can cause significant difference in the values of mean spacing, indicating that the upper cutoff should be defined with caution in the study of discontinuities with fractal characteristics. The influence of the lower cutoff on the coefficient A is illustrated in Fig. 3.11, which shows that this influence is not very significant.

It can be seen from Fig. 3.12 that the mean spacing is sensitive to both fractal dimension and lower cutoff. However, the influence of lower cutoff on mean spacing is not as significant as that of the upper cutoff (see Fig. 3.10).

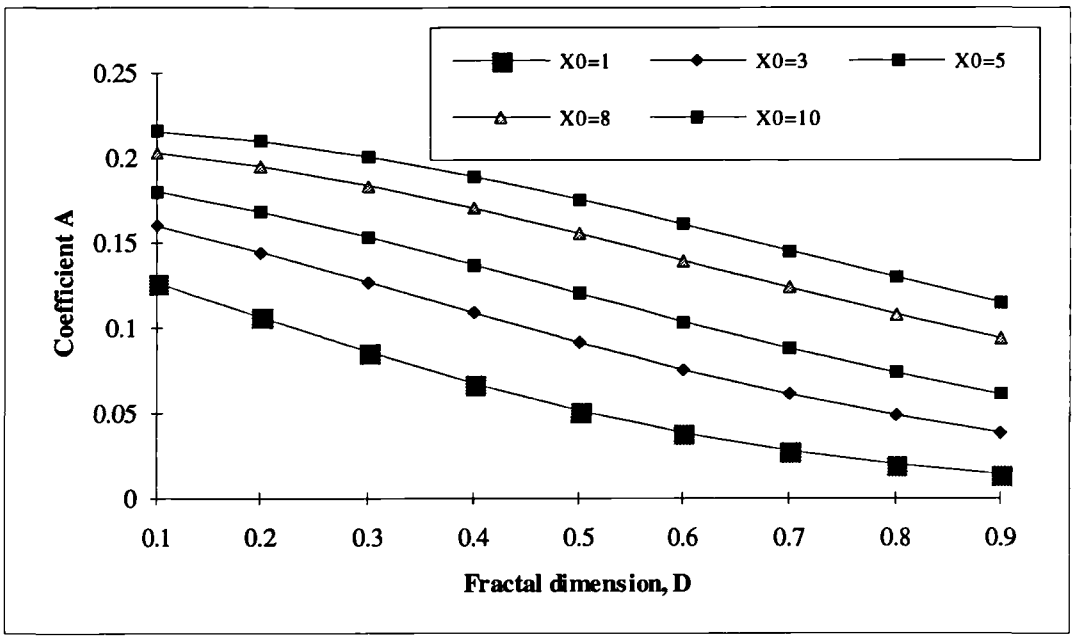

Fig. 3.11 Relation between the coefficient *A* and fractal dimension with different lower cutoffs (upper cutoff=10 m, *X0* - lower cutoff, in cm)

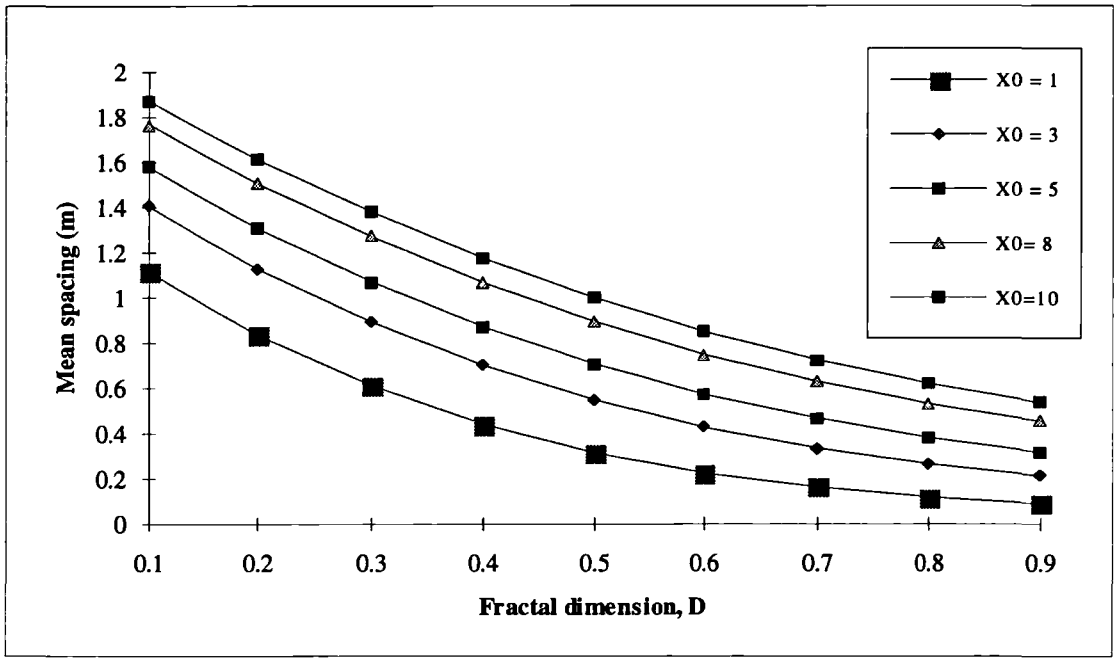

Fig. 3.12 Relation between the mean spacing S_m and fractal dimension with different lower cutoffs (upper cutoff=10 m, X0 - lower cutoff, in cm)

The PDF curves for different fractal dimensions are illustrated in Fig. 3.13, which is used to help understand the trend of the fractal spacing distribution varying with fractal dimensions.

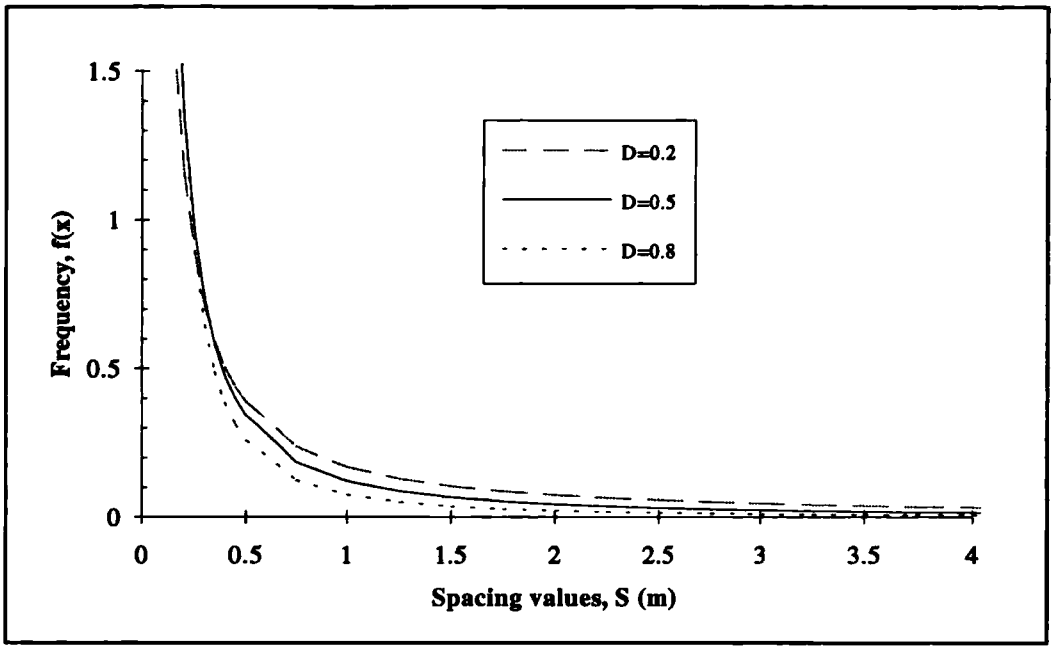

Fig. 3.13 PDF curves with different fractal dimensions (lower cutoff S_{min}= 0.05 m; upper cutoff S_{max}= 10 m)

Consequently, the range of fractal dimensions in the simulation was set between 0.12 and 0.84, and the lower and upper cutoffs were defined as 0.05 m and 10 m in the simulations.

3.6.2 Generation of Artificial Discontinuities with Fractal Spacings

Usually, computer generation of artificial discontinuities that have a prescribed distribution of spacings involves a randomisation process. Since the concept of fractal dimension and its analysis are relatively new, there is no algorithm and associated computer programme available to directly obtain the necessary artificial discontinuities with a fractal distribution.

The transformation method (Press et al, 1986) has been used here to derive the generating algorithm for random numbers with a fractal probability distribution. Based on the derivation of the algorithm a FORTRAN programme named RUNFRA for generating the pseudo-random real number with fractal distribution has been developed, which is described in Appendix B.2. By running the program RUNFRA, we are able to produce artificial discontinuities that have a prescribed fractal distribution of spacings.

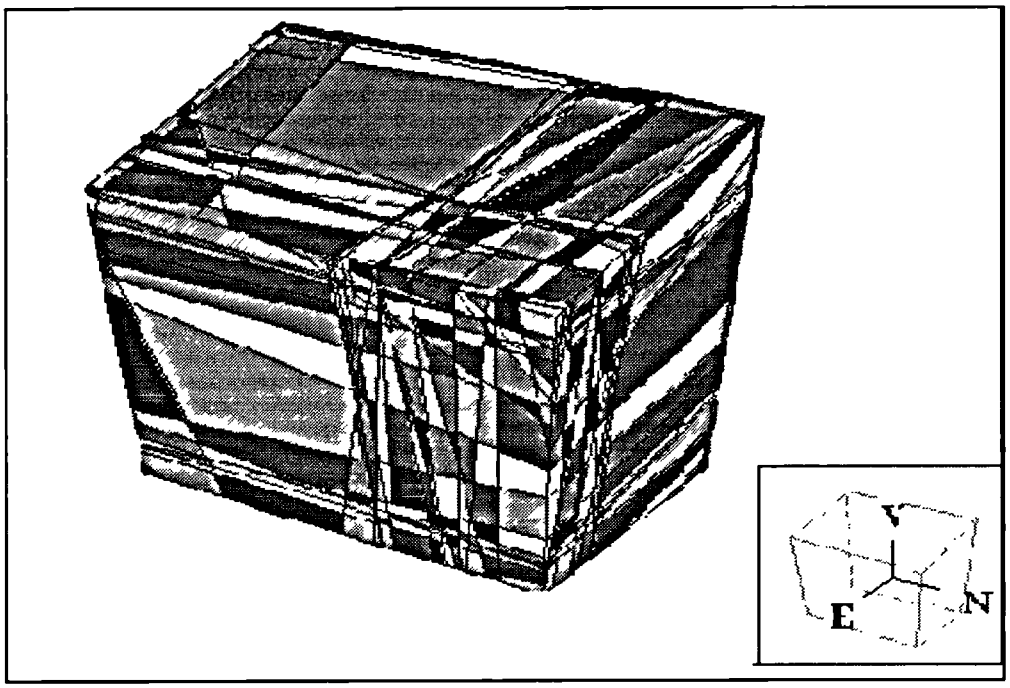

Fig. 3.14 Three-dimensional view of a simulated rock mass consisting of discontinuities with fractal spacing distributions (D=0.36, the whole block volume V=2163 m^3; lower cutoff S_{min}= 5 cm; upper cutoff S_{max}= 10 m)

Fig. 3.14 is an example of a three-dimensional view of the blocks produced by intersection of 3 sets of discontinuities with fractal spacing distributions that were generated artificially using the transforming method described above. The three principal discontinuity sets have an orientation dispersion of ±10°. It has been plotted using the program 'BLOCKS' (Wang, 1992).

3.6.3 Simulation Results of Block Size Distributions

In accordance with the parameters set out in Table 3.2, a total of 60 groups of separate simulations of the type illustrated in Fig. 3.14, were run using the programme BLOCKS. For each simulation, referred to as having a run, the programme calculates the IBSD, an example of which is shown in Fig. 3.15.

A typical simulation result of the IBSD for a group of discontinuities is illustrated in Fig. 3.16. For this group discontinuities the fractal dimensions for three sets are respectively 0.68, 0.36 and 0.44.

Table 3.2 The parameters of the simulation of IBSD with fractal spacing distribution*

	Fractal dimension			Principal mean spacing (m)		
No.	Set 1	Set 2	Set 3	Set 1	Set 2	Set 3
N1-1	0.12	0.12	0.12	1.52	1.52	1.52
-2	0.24	0.24	0.24	1.208	1.208	1.208
-3	0.36	0.36	0.36	0.948	0.948	0.948
-4	0.44	0.44	0.44	0.802	0.802	0.802
-5	0.5	0.5	0.5	0.707	0.707	0.707
-8	0.56	0.56	0.56	0.623	0.623	0.623
-7	0.6	0.6	0.6	0.573	0.573	0.573
-8	0.68	0.68	0.68	0.528	0.528	0.528
-9	0.76	0.76	0.76	0.414	0.414	0.414
-10	0.84	0.84	0.84	0.354	0.354	0.354
N2-1	0.12	0.12	0.24	1.52	1.52	1.208
-2	0.12	0.36	0.44	1.52	0.948	0.802
-3	0.12	0.5	0.56	1.52	0.707	0.623
-4	0.12	0.6	0.68	1.52	0.573	0.528
-5	0.12	0.76	0.84	1.52	0.414	0.354
N3-1	0.24	0.12	0.24	1.208	1.52	1.208
-2	0.24	0.36	0.44	1.208	0.948	0.802
-3	0.24	0.5	0.56	1.208	0.707	0.623
-4	0.24	0.6	0.68	1.208	0.573	0.528
-5	0.24	0.76	0.84	1.208	0.414	0.354
N4-1	0.36	0.12	0.24	0.948	1.52	1.208
-2	0.36	0.36	0.44	0.948	0.948	0.802
-3	0.36	0.5	0.56	0.948	0.707	0.623
-4	0.36	0.6	0.68	0.948	0.573	0.528
-5	0.36	0.76	0.84	0.948	0.414	0.354
N5-1	0.5	0.12	0.24	0.707	1.52	1.208
-2	0.5	0.36	0.44	0.707	0.948	0.802
-3	0.5	0.5	0.56	0.707	0.707	0.623
-4	0.5	0.6	0.68	0.707	0.573	0.528
-5	0.5	0.76	0.84	0.707	0.414	0.354
N6-1	0.6	0.12	0.24	0.573	1.52	1.208
-2	0.6	0.36	0.44	0.573	0.948	0.802
-3	0.6	0.5	0.56	0.573	0.707	0.623
-4	0.6	0.6	0.68	0.573	0.573	0.528
-5	0.6	0.76	0.84	0.573	0.414	0.354
N7-1	0.68	0.12	0.24	0.528	1.52	1.208
-2	0.68	0.36	0.44	0.528	0.948	0.802
-3	0.68	0.5	0.56	0.528	0.707	0.623
-4	0.68	0.6	0.68	0.528	0.573	0.528
-5	0.68	0.76	0.84	0.528	0.414	0.354
N8-1	0.76	0.12	0.24	0.414	1.52	1.208
-2	0.76	0.36	0.44	0.414	0.948	0.802
-3	0.76	0.5	0.56	0.414	0.707	0.623
-4	0.76	0.6	0.68	0.414	0.573	0.528
-5	0.76	0.76	0.84	0.414	0.414	0.354
N9-1	0.84	0.12	0.24	0.354	1.52	1.208
-2	0.84	0.36	0.44	0.354	0.948	0.802
-3	0.84	0.5	0.56	0.354	0.707	0.623
-4	0.84	0.6	0.68	0.354	0.573	0.528
-5	0.84	0.76	0.84	0.354	0.414	0.354

*the lower and upper cutoffs were defined as 0.05 m and 10 m

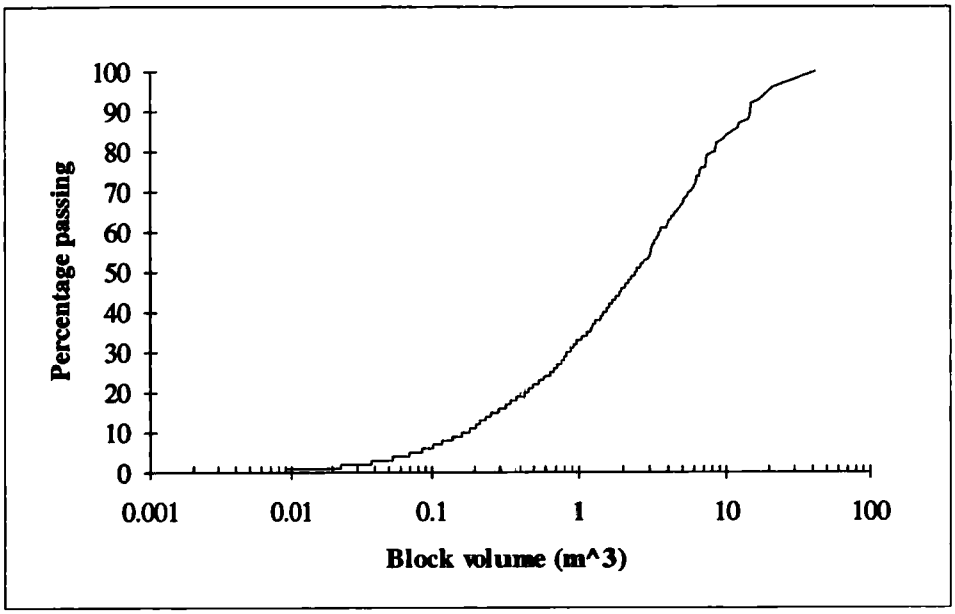

Fig. 3.15 The simulation result of the IBSD for fractal spacings (the whole block volume = 950 m^3; lower cutoff S_{min}= 5 cm; upper cutoff S_{max}= 10 m)

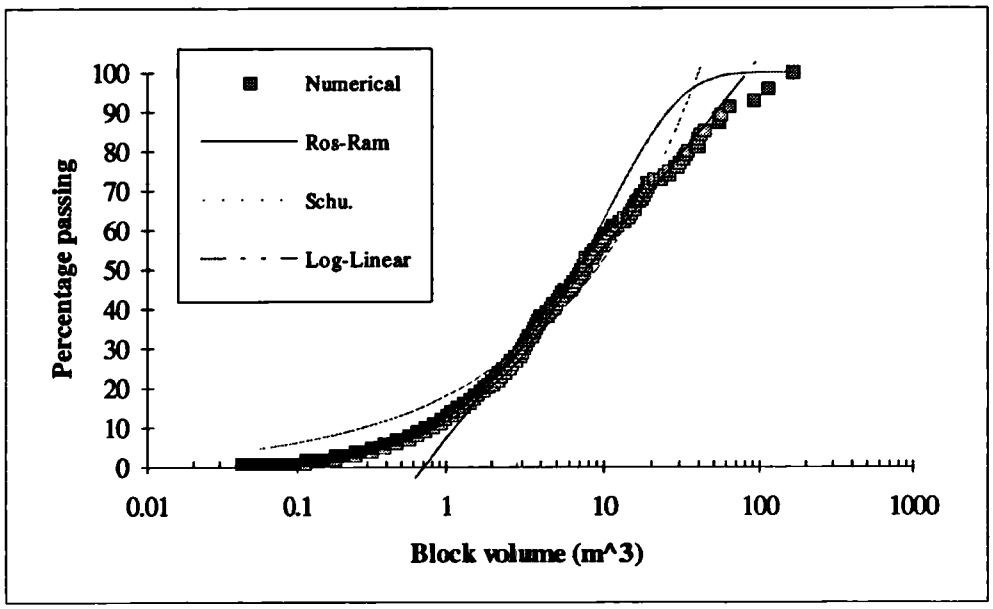

Fig. 3.16 Fitting the theoretical distributions to the IBSD (D=0.24, the whole block volume = 4125 m^3; lower cutoff S_{min}= 5 cm; upper cutoff S_{max}= 10 m)

The Ros-Ram, Schuhmann and log-linear equations have all been considered as a means of describing simulation results of the IBSD. Visual examination of Fig. 3.16 suggests from that the Schuhmann equation may fit as well as the Ros-Ram equation, and that the log-linear equation is basically unsuitable for the typical curvature with the fine part of the IBSD. It is therefore proposed that both the Ros-Ram and the

Schuhmann equations are the two most ideal to be used for representing the IBSD of a rock mass with discontinuities with fractal spacing distributions.

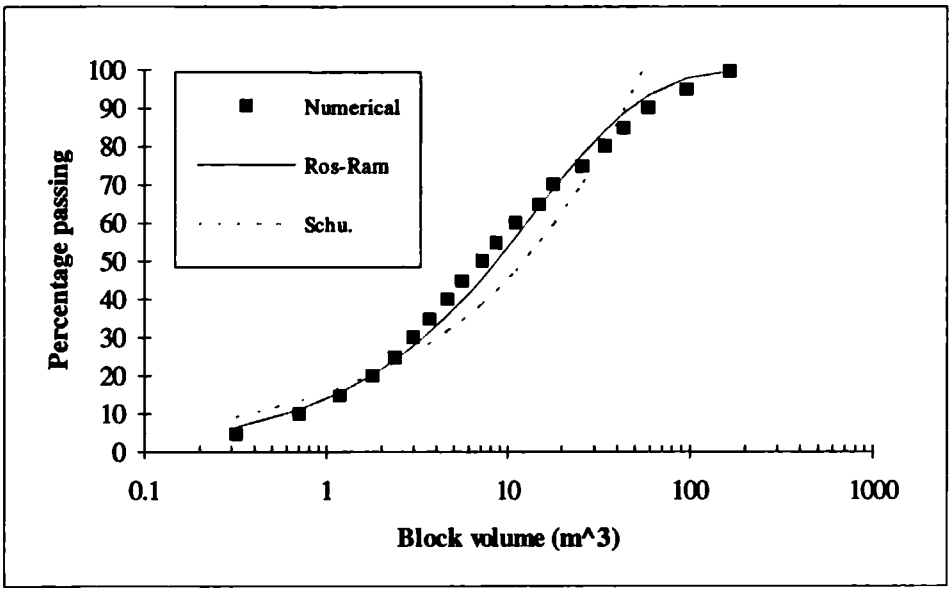

Fig. 3.17 Comparison between simulation and Ros-Ram and Schuhmann distribution fitting for "typical data" (D=0.24, the whole block volume = 4125 m^3; lower cutoff S_{min}= 5 cm; upper cutoff S_{max}= 10 m).

The method of curve fitting to obtain best fits using given equations, when summarising IBSD or BBSD, is not straight forward. With spacing data, considered in Section 3.5, the raw data gives an appropriate weighting for each data point, but this need not be the case for block size. The consideration of whether to and how to weight the data prior to curve fitting should be made after taking into account practical consideration. For example, the most economically significant part of the IBSD or BBSD curve could be he fine end, the middle or the coarse end. An accurate fit at the coarse end was more important in the Overseas Quarry case study concerned with armourstone described in Chapter 7.

In the analysis of IBSD, the most reasonable approach and the one adopted here appears to be by reassignment of the weighted simulated data to an unweighted idealised set of data which in this case, is given at 5% intervals from 5% to 100% passing size. This choice, a removal of the weighting of fines and replacement by 20 evenly weighted data points, is appropriate since the main purpose for the mathematical summary of the IBSD is to give accurate input to the modelling of BBSD.

The influence of weighting is closely shown by a comparison of the best-fit curves in Figs. 3.16 and 3.17 (the "typical data" refers to regularly picking up the point at 5%, 10%, ..., 100% passing). Whereas in Fig. 3.16, some 2000 of the data points alone, account for less than 1% of the whole simulated volume, in Fig. 3.17, the first of 20 data points enters at 5% passing. The effect of removing the fines weighting is to allow a much better Ros-Ram fit for the coarse sizes.

3.6.4 Relationships between Fractal Spacing Parameters and IBSD Parameters

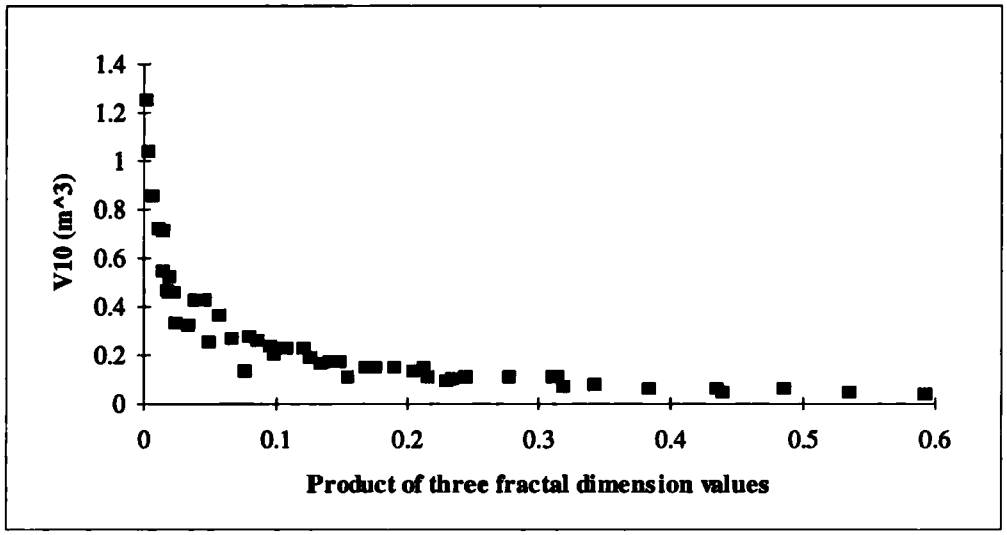

(a)

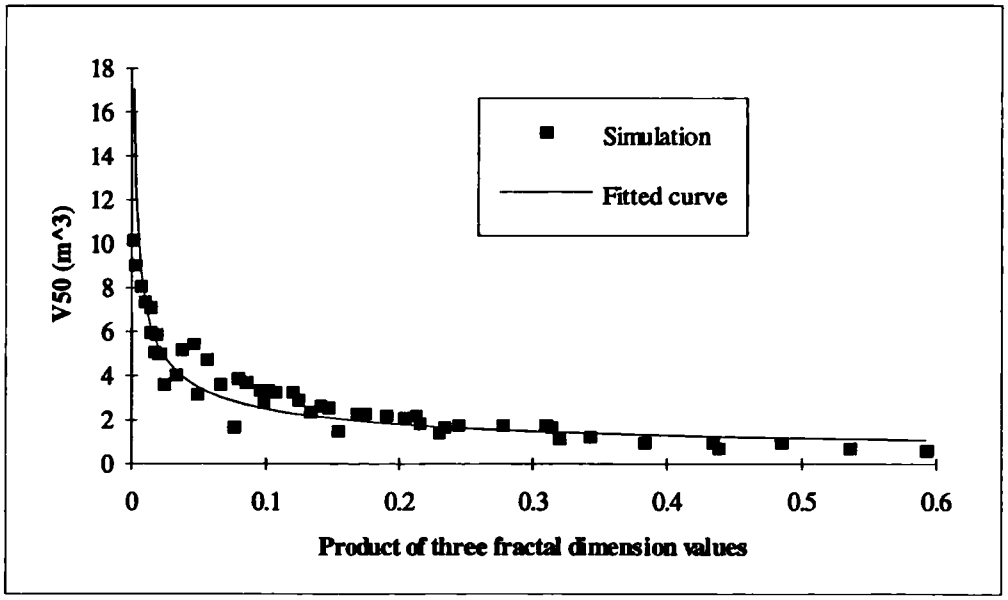

(b)

Fig. 3.18 Relationship between V_{10} and V_{50} and $D_1*D_2*D_3$

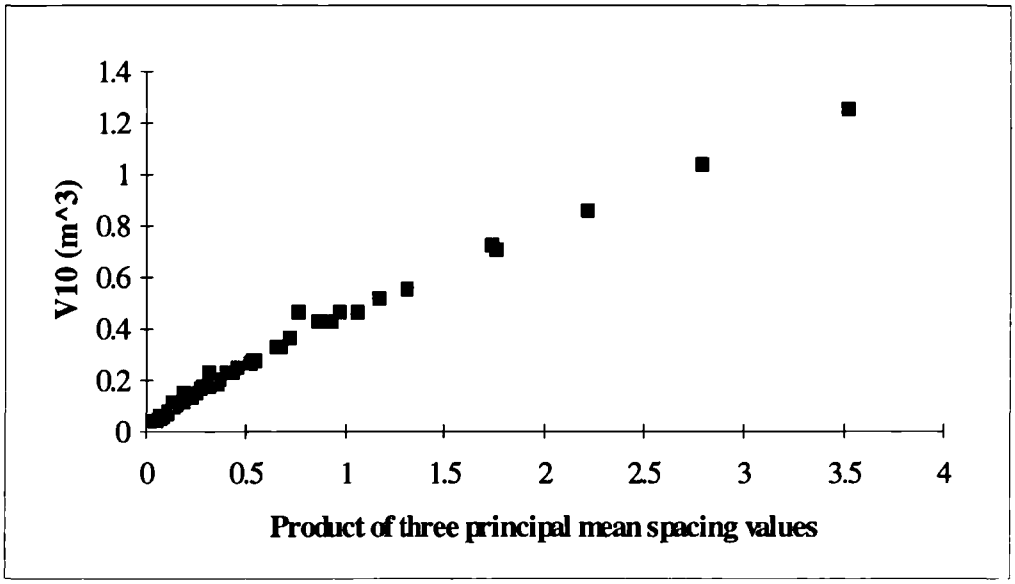

(a)

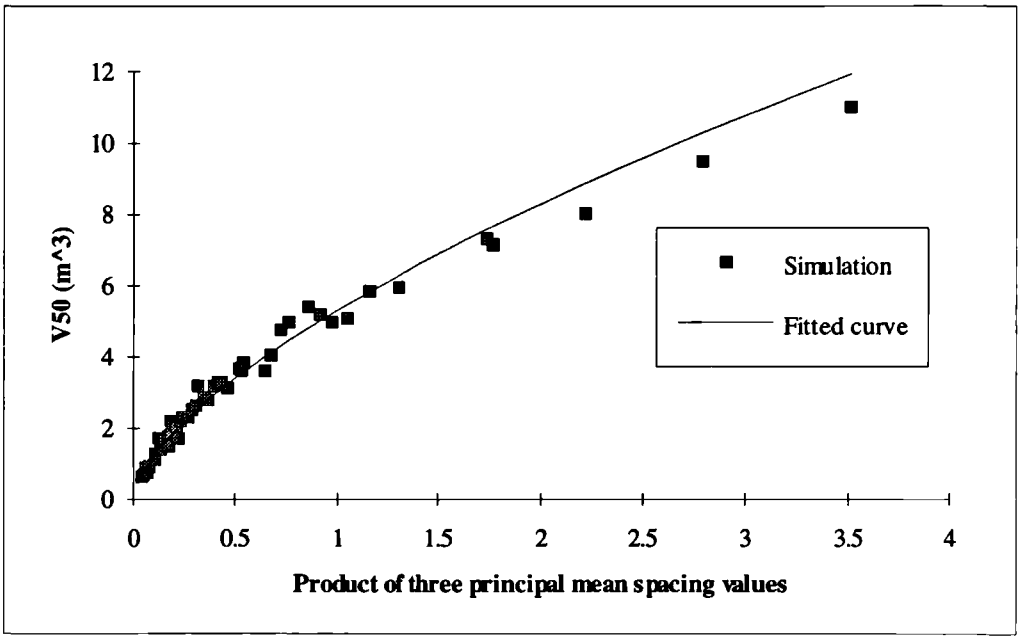

(b)

Fig. 3.19 Relationship between V_{10} and V_{50} and the $S_{pm1}*S_{pm2}*S_{pm3}$

Before proceeding with a compilation of coefficients that enable the reader to apply an equation method to fractal spacing data, there is one major difference between these research results and those of Wang. Wang (1992) referred to a "proportional property" which results in a linear relationship between the IBSD and the products of the three principal mean spacings applicable to the uniformly and negative exponentially distributed spacings. For the case of fractal spacing distribution, this property will not hold, as verified by the simulation results shown in Figs 3.18 and

3.19. The reason that it no longer holds is that there is no longer a proportional property for the generator which produces data with a fractal spacing distribution (see Appendix B.2).

Fig. 3.18 is the relationship between typical (10% and 50%) volume percentage passing values and the product of the three fractal dimensions, and Fig. 3.19 is the relationship between these typical percentage passing values and the product of the three principal mean spacing values. It can be seen from these two figures that there are, indeed, some non-linear relationships between the volume percentage passing values and the products.

Table 3.3 Coefficients $C_{i,p}$ and $b_{i,p}$ for the relationship between $V_{i,p}$ and the product of fractal dimensions of discontinuities with fractal distributions (Eqn. 3-31)

Passing	Coefficient	Standard	90% confidence level			
	$C_{i,p}$	Error	Lower	Upper	Range	Error *(%)
10	0.0468	0.0033	0.0417	0.0526	0.0055	11.66
20	0.1440	0.0099	0.1284	0.1614	0.0165	11.47
30	0.3098	0.0218	0.2755	0.3485	0.0365	11.78
40	0.5642	0.0460	0.4926	0.6462	0.0768	13.62
50	0.8453	0.0660	0.7422	0.9628	0.1103	13.04
60	1.4447	0.1121	1.2695	1.644	0.1872	12.96
70	2.5625	0.2379	2.1959	2.9904	0.3973	15.5
80	4.4490	0.5492	3.6254	5.4598	0.9172	20.62
90	9.2825	1.2878	7.3777	11.6790	2.1507	23.17
100	31.3330	3.5021	26.025	37.7220	5.8485	18.67
	$b_{i,p}$					
10	0.5949	0.0250	0.5529	0.6368	0.0418	7.03
20	0.5423	0.0246	0.5010	0.5836	0.0411	7.59
30	0.5012	0.0253	0.4588	0.5436	0.0422	8.42
40	0.4711	0.0292	0.4220	0.5201	0.0488	10.36
50	0.4712	0.0280	0.4242	0.5181	0.0467	9.92
60	0.4404	0.0278	0.3938	0.4871	0.0465	10.55
70	0.4199	0.0332	0.3642	0.4756	0.0555	13.22
80	0.4072	0.0441	0.3333	0.4811	0.0736	18.07
90	0.3609	0.0494	0.2780	0.4438	0.0825	22.87
100	0.3054	0.0399	0.2384	0.3724	0.0667	21.84

*Error is the ratio of the range over the corresponding coefficient expressed in %;

Table 3.4 Coefficients $C_{i,p}$ and $b_{i,p}$ for the relationship of $V_{i,p}$ and the product of principal mean spacing values of discontinuities with fractal distributions (Eqn. 3-32)

Passing	Coefficient	Standard	90% confidence level			
	$C_{i,p}$	Error	Lower	Upper	Range	Error (%)
10	0.4649	0.0077	0.4523	0.4779	0.0128	2.75
20	1.1685	0.0245	1.1283	1.2101	0.0409	3.50
30	2.1606	0.0448	2.0871	2.2367	0.0748	3.46
40	3.5458	0.0965	3.3882	3.7107	0.1612	4.55
50	5.3165	0.1150	5.1280	5.5120	0.1920	3.61
60	8.0903	0.1855	7.7864	8.4061	0.3098	3.83
70	13.3920	0.5029	12.5780	14.2580	0.8398	6.27
80	22.6070	1.3562	20.4550	24.9850	2.2649	10.02
90	39.6660	3.0117	34.9540	45.0130	5.0295	12.68
100	108.9700	5.7909	99.7240	119.0700	9.6708	8.88
	$b_{i,p}$					
10	0.7882	0.0109	0.7700	0.8060	0.0180	2.30
20	0.7200	0.0140	0.6970	0.7430	0.0230	3.21
30	0.6719	0.0137	0.6489	0.6950	0.0228	3.40
40	0.6433	0.0179	0.6132	0.6730	0.0300	4.66
50	0.6440	0.0140	0.6200	0.6680	0.0240	3.70
60	0.6053	0.0151	0.5800	0.6310	0.0252	4.17
70	0.5874	0.0247	0.5459	0.6290	0.0413	7.03
80	0.5900	0.0395	0.5237	0.6560	0.0659	11.18
90	0.5335	0.0499	0.4497	0.6170	0.0830	15.63
100	0.4675	0.0350	0.4088	0.5260	0.0580	12.50

For discontinuities with a fractal spacing distribution, the fractal dimension is an important characteristic parameter, having significance for the IBSD. However, the mean spacing value within the major discontinuity sets has traditionally been used to give an average dimension of typical in-situ blocks (ISRM, 1978). Therefore, an attempt has been made to present both the relationship between the IBSD and the three principal mean spacing values and the relationship between the IBSD and the three fractal dimensions.

With a careful examination of all of the simulation results using statistical analysis and grey correlation analysis, a negative power law was found to be most suitable to

describe the relationship between the IBSD and the product of three fractal dimensions. It is given by

$$V_{i,p} = C_{i,p} \times (D_1 \times D_2 \times D_3)^{-b_{i,p}}, \qquad (3\text{-}31)$$

where $V_{i,p}$ (i=10, 20,...,100) are block volumes of percentage passing (in m^3), and $C_{i,p}$ and $b_{i,p}$ are empirical coefficients; i are percentages; D_1, D_2 and D_3 are the fractal dimensions of the three sets of discontinuity spacing values. The coefficients $C_{i,p}$ and $b_{i,p}$ together with the 90% confidence intervals are given in Table 3.3.

By analogy with the derivation of Eqn. 3-31, the power law is found suitable to characterise the relationship between the IBSD and the three principal mean spacing values, and is given by

$$V_{i,p} = C_{i,p} \times (S_{pm1} \times S_{pm2} \times S_{pm3})^{b_{i,p}}, \qquad (3\text{-}32)$$

where, S_{pmi} (i=1,2,3) are the principal mean spacing values of three set discontinuities, $C_{i,p}$ and $b_{i,p}$ are the same as the above denotations. $V_{i,p}$, $C_{i,p}$ and $b_{i,p}$ in Eqn. 3-32 together with the 90% confidence intervals are illustrated in Table 3.4.

It seems reasonable to assume that the estimates of coefficients in Eqns. 3-31 and 3-32 have approximately normal distributions. Thus The goodness-of-fit examination for Eqns. 3-31 and 3-32 has been carried out using the classical t test. Also, a grey correlation analysis was used. The results are listed in Table 3.5. The t test indicates a significant dependence of the $V_{i,p}$ on the mean principal spacing or the fractal dimension. That is, the proposed empirical equations for relating the coefficients $C_{i,p}$ and $b_{i,p}$ to the mean principal spacing or fractal dimension obtained from simulations works well. This has been supported by the grey correlation analysis, since almost all the values of the grey correlation coefficients are large. The visual comparison between simulation results and the predictions from Eqns. 3-31 and 3-32 for V_{50} (see Figs. 3.18b and 3-19b) indicates that the two equations fit reasonably well.

From the discussion above, it is found that the fractal dimension, which is the most important spatial parameter of discontinuities with a fractal spacing distribution, is also a measure of in-situ block sizes.

An important point to bear in mind is that both Eqn. 3-31 and Eqn. 3-32 have been developed from simulation data based on a certain range of values of mean spacing or

fractal dimension. It is therefore advised that one should use caution when extrapolating the IBSD of a rock mass with the values of mean spacing or the fractal dimension from outside the range examined by this study.

Table 3.5 Goodness-of-fit examination of Eqns. 3-31 and 3-32

Eqn.	$V_{i,p} = C_{i,p} \times (D_1 \times D_2 \times D_3)^{-b_{i,p}}$				$V_{i,p} = C_{i,p} \times (S_{pm1} \times S_{pm2} \times S_{pm3})^{b_{i,p}}$			
$V_{i,p}$	Grey correlation measure	*t* test*			Grey correlation measure	*t* test		
		t statistics	*t* at Confidence level			*t* statistics	*t* at Confidence level	
			90%	95%			90%	95%
10	0.9781	72.507	1.677	2.01	0.9043	-23.770	1.677	2.01
20	0.9567	52.101			0.8932	-22.010		
30	0.9478	49.185			0.8739	-19.820		
40	0.9237	35.844			0.8552	-16.120		
50	0.9335	45.153			0.8574	-16.830		
60	0.9260	40.045			0.8561	-15.830		
70	0.8835	23.741			0.8228	-12.640		
80	0.8459	14.940			0.8080	-9.242		
90	0.7890	10.684			0.7627	-7.303		
100	0.8179	13.360			0.7782	-7.647		

*where *t* test proceeds as if the data were linearly related, so the transformed and not the raw data have been used throughout this significance test.

3.7 BLOCK SIZE DISTRIBUTIONS WITH FRACTAL COMPARED OTHER SPACING DISTRIBUTIONS

Having discussed the block size distribution arising from rock masses with discontinuities with fractal spacings, it is interesting to compare these results with those for other spacing distributions and to probe into how much difference exists in the IBSDs produced from different spacing distributions.

In comparing Eqn. 3-32 with Eqn. 2-10, it can be found that the nonlinear form is noted for the fractal spacing distribution whereas a linear form was found (Wang , 1992) for the rock mass with negative exponential, lognormal and uniform spacing distributions. Fig. 3.20 gives a comparison of IBSD curves for the special case that the principal mean spacing value of each discontinuity set has been given the value 1.0 m and that appropriate cutoffs have been drawn for the fractal curve.

Clearly, there is a significant difference between the IBSD of discontinuities with a fractal spacing distribution and those with the other three spacing distributions. The IBSD of a rock mass with discontinuities that have a fractal spacing distribution is much larger than that with the other three spacing distributions at corresponding percentage passing points. The fractal IBSD curve is less steep given blocks that are more widely distributed. That is, more fine and more "mammoth" blocks will be produced from the rock mass with discontinuities with fractal distributions. Among the four different spacing distributions, the IBSD intersected by discontinuities with a uniform spacing distribution will form the lower boundary IBSD curve (see. Fig. 3.20).

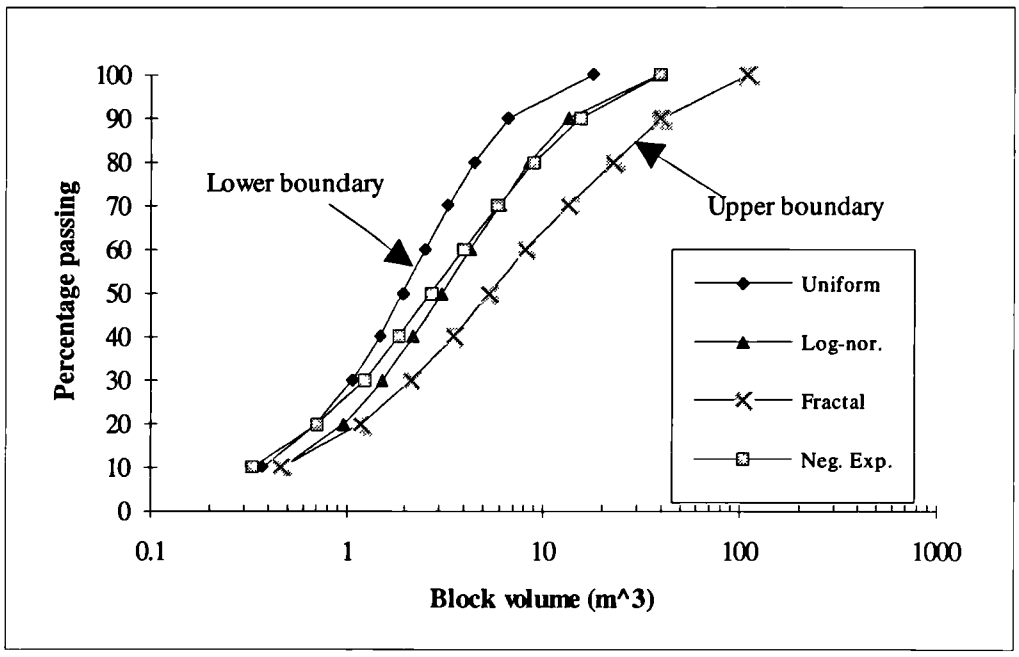

Fig 3.20 Comparison among IBSDs with different spacing distributions, based on the equation methods (all the mean spacings are 1.0 m)

3.8 DISCUSSION

Fig. 3.15 illustrates the case of the three dimension view for a discontinuity network with a fractal distribution where all three sets of discontinuities have the same fractal dimension of 0.36, corresponding to an approximate mean spacing value of 0.95 m. The three dimensional views for both negative exponential and uniform spacing distribution with principal mean spacing values of 1.0 m are presented in Figs. 3.21 and 3.22 respectively. In the case of the fractal spacing distribution, the whole block volume is up to 2160 m^3, and some discontinuities are sparsely distributed

while others are closely clustered. In contrast, we can find from visual examination of both Figs. 3.21 and 3.22 that both the negative exponential and the uniform spacing distribution discontinuities are fairly evenly distributed. The same features can be characterised by fracture logs illustrated in Fig. 2.4.

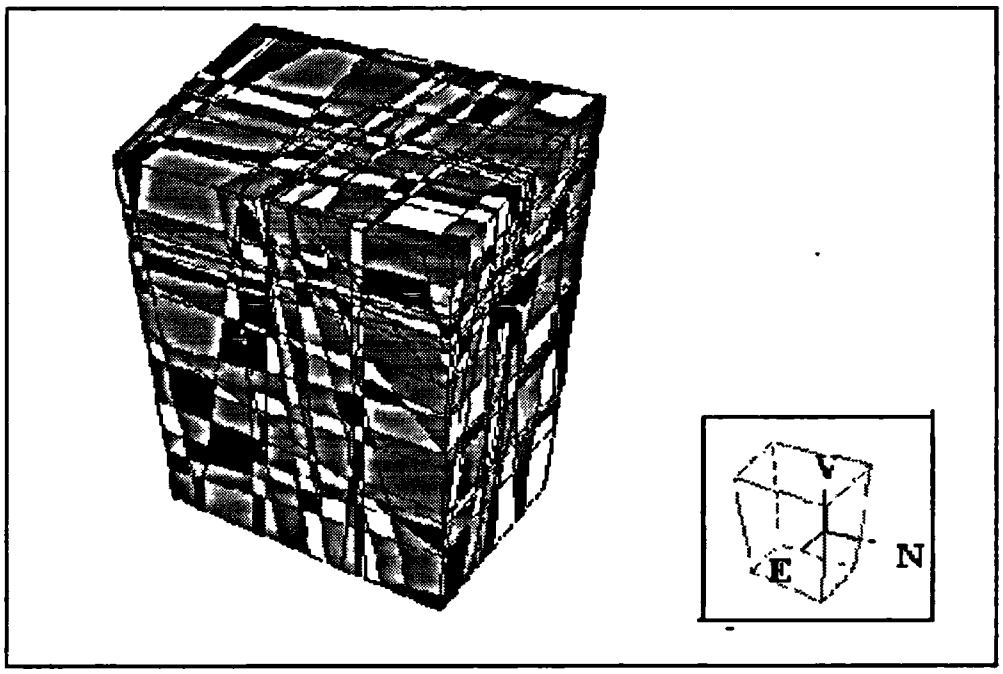

Fig 3.21 Three-dimensional view of blocks consisting of discontinuity sets with negative exponential distributions (the principal mean spacing is 1.0 m; the whole block volume is 6686 m^3)

It is therefore significant to distinguish whether the type of spacing distribution of discontinuities is clearly of a fractal form when the in-situ block size distribution is of practical significance. This will certainly be the case in quarrying for armourstone, aggregates and building stone, especially for operations of quarrying in which the proportion of big blocks is essentially critical.

The IBSD of rock with discontinuities with fractal spacing distribution has been investigated using a combination of random simulation and the dissection method. A comparison of the IBSD with fractal spacing distribution with the IBSDs for negative exponential, lognormal and uniform distributions has also been given. The results have indicated that there is a significant difference between the IBSD with fractal spacing distributions and the IBSDs with the other three spacing distributions. The two sets of empirical equations developed and expressed in Eqn. 3-31 or Eqn. 3-32 can be used to estimate the IBSD when the discontinuities exhibit a statistically good fit to a fractal spacing distribution.

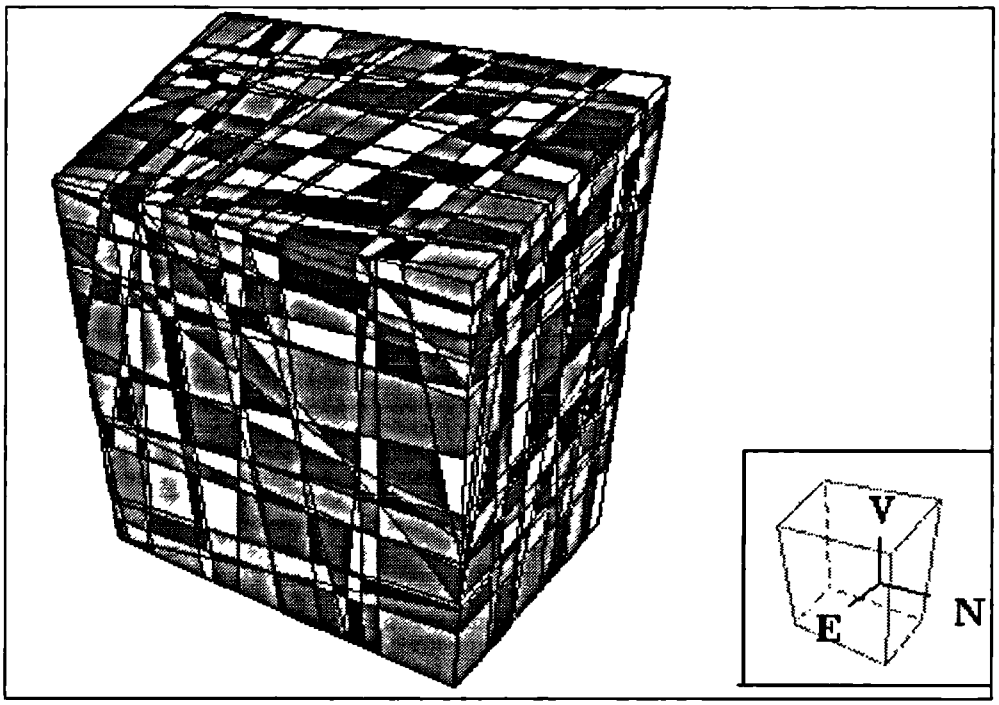

Fig. 3.22 Three-dimensional view of blocks consisting of discontinuity sets with uniform distribution (the mean spacing is 1.0 m; and the block volume is 3900 m^3)

The above investigations of IBSD are based on the assumption that all three sets of discontinuities are with a fractal distribution. In practice, this assumption may seldom be satisfied and the more typical situation is that between the various sets there are two or more kinds of best-fit descriptions for the discontinuity spacing distributions. In such cases we can reasonably predicate that the IBSD will fall in the range formed by a lower boundary IBSD curve from discontinuities with a uniform spacing distribution and an upper boundary IBSD curve from discontinuities with a fractal spacing distribution (see Fig. 3.20), although further investigation should be made to reveal the IBSD of rock with two or more kinds of discontinuity spacing distribution laws. A preliminary examination of the prediction for a mixture of distribution laws has been made in the case study presented in Section 7.1, in which one out of three sets of discontinuities is with a fractal spacing distribution, the other two having either negative exponential or uniform spacing distributions.

In the above simulation and analysis, a supposition that discontinuities are persistent is imposed. As discussed in Chapter 2, this supposition may often not hold. In the next chapter, the influence of impersistent discontinuities on the prediction of IBSD will be investigated.

4. INFLUENCE OF IMPERSISTENCE OF DISCONTINUITIES ON THE IBSD OF ROCK MASSES

4.1 RATIONALE FOR THE CONSIDERATION OF DISCONTINUITY IMPERSISTENCE IN THE PREDICTION OF IBSD

Whether or not a discontinuity can be regarded as persistent is to some extent subjective. It will depend on the scale or resolution used to observe the discontinuities, the area or volume of the rock mass of interest, and the nature of engineering problems for which discontinuity survey data is sought. Of particular interest in this research is the determination of the IBSD in bench blasting in a quarry. For this application, one approach has been to regard discontinuities with traces on the bench face longer than a given cutoff value as persistent and the rest as impersistent. For example, Wang (1992) used a criterion of ≥ 3 m for the trace length of discontinuities that were to be coded as persistent. By treating the dissection of discontinuities that are coded as impersistent together with those are coded as persistent, as if they all extend infinitely he made an estimation of the lower bound for the BBSD, while the dissection of only the persistent ones, he argued, would provide an upper bound estimation for the IBSD. Obviously, the above cutoff criterion is inherently subjective, in spite of its applicability for providing bounds for the IBSD.

A rock mass where all discontinuities extend to the margins of the rock volume of interest is rarely found. However, most existing techniques of predicting the in situ block size, including the techniques developed by Wang (1992) and in Chapter 3 of this thesis, assume that all discontinuities within the rock mass are persistent (this will be referred to as "all-persistent discontinuities" assumption). This assumption is probably acceptable for a small volume of a rock mass or for a rock mass with discontinuities having a large mean discontinuity size, but with the increase of the rock mass in question the errors related to this assumption will increase.

The following case studies described by Wang (Wang et al., 1991a; Wang, 1992) both give an insight into the extent to which impersistence affects the prediction of IBSD (see Table 4.1 and Fig. 4.1). In the first case, V_{50} for the lower bound curve was 4.95 m^3, whereas V_{50} for upper bound curve was 7.69 m^3 (Fig. 4.1). The two different considerations on persistence resulted in a 50% volume increase. In the second case, V_{50} for the lower bound curve was 0.477 m^3, whereas V_{50} for upper bound curve was 1.305 m^3 which is nearly a three fold increase. On describing the

above two cases, Wang argued that the IBSD could be considered to fall between both lower and upper bounds. However, since the difference between these two bounds is often large (see Table 4.1 and Fig. 4.1), it has been recognised that in cases where trace length distribution data can be obtained, it may be possible to further constrain the estimated IBSD.

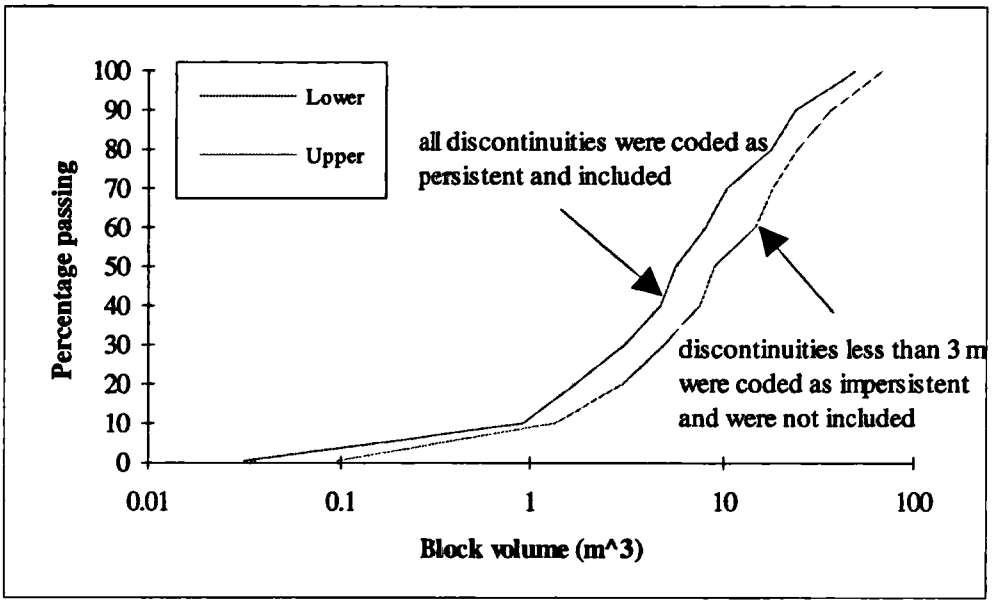

Fig. 4.1 Illustration of influence of persistence of discontinuities on prediction of IBSD (Data from Wang, 1992)

Table 4.1 The influence of impersistence of discontinuities on the prediction of IBSD (50% passing block size, V_{50}, m^3)

	Including all discontinuities	Only including persistent discontinuities
Case 1	4.95	7.69
Case 2	0.477	1.305

The analytical treatment of discontinuities with impersistence is highly complex. This might be one of main reasons that most existing techniques of prediction the IBSD have assumed that discontinuities are all persistent. For the purpose of obtaining estimation of IBSD, an indirect technique is therefore proposed for considering the influence of impersistent discontinuities on the prediction of IBSD. Firstly, an IBSD estimation is obtained using the assumption of all-persistent discontinuities, then the estimate is corrected by introducing a factor reflecting the influence of the degree of persistence of discontinuities.

Persistence can be roughly quantified by measuring the discontinuity trace lengths on the exposures. Furthermore, the underlying discontinuity size may be generated from the measured trace lengths under certain assumptions about the nature and shape of the discontinuities.

It is helpful to begin by revising the two definitions of persistence in current usage.

(1) The first is suggested by the ISRM (1978) where persistence is defined as "the percentage of total area of a plane through the rock mass which is formed by discontinuities co-planar with this reference plane", so that the persistence P_l is given by:

$$P_l = \frac{\sum_i a_{D_i}}{A_D}, \tag{4-1}$$

where A_D is the area of a region of the plane and a_{Di} is the area of the *ith* discontinuity in the A_D, the summation is over all discontinuity in the area, as shown in Fig. 4.2.

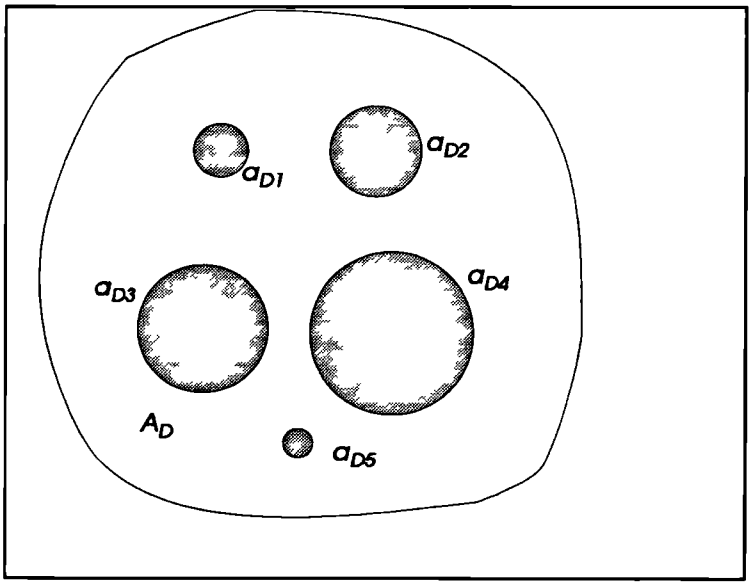

Fig. 4.2 Schematic illustration of discontinuity persistence

(2) The second was given by Einstein et al. (1983) where persistence is defined as the limit of the ratio expressed by Eqn. 4-1 as the size of the plane approaches infinity:

$$P_I = \lim_{A_D \to -} \frac{\sum_i a_{D_i}}{A_D}, \tag{4-2}$$

or the limit of the length ratio along a given line on a joint plane, as given by:

$$P_I = \lim_{L_S \to -} \frac{\sum_i l_{S_i}}{L_S}, \tag{4-3}$$

where L_S is the length of a straight line segment S and l_{Si} is the length of the *ith* discontinuity segment in S, the summation is over all joints in S.

It can be seen from the above equations that these definitions will lead to a scale-dependent persistence value. In other words, the impersistence will depend on the dimensions of the rock mass concerned. As a result, whether the assumption of all-persistent discontinuities is good approximation or not is critically dependent upon two factors: the first is the scale of the in-situ rock mass of interest, and the second is the mean size of discontinuities. The greater the scale of the rock mass, the worse the approximation; the larger the mean discontinuity size, the better the approximation.

Provided that an estimation of mean discontinuity size can be made, it is possible that the influence of impersistence on in-situ block size can be elucidated by comparing the mean discontinuity size to the scale of in-situ rock mass of interest. It therefore seems probable that the determination of the mean size of discontinuities (or an estimate of mean size) could provide a suitable means of accounting for the influence of impersistent discontinuities with particular reference to the prediction of IBSD. In the following sections, this has been shown to be so and the relationships have been derived so as to incorporate the impersistent discontinuities into the prediction of IBSD.

4.2 DISTRIBUTIONS OF TRACE LENGTH AND EVIDENCE OF FRACTAL TRACE LENGTH DISTRIBUTIONS

4.2.1 Distributions of Trace Length and Identification of Distributions

A survey of discontinuities is often made on a small exposure comprising a small sample from which one infers the jointing in a much larger rock volume. Mathematical techniques are usually applied to the survey measurements in order to adjust the trace length distribution to be more representative. As described in Chapter 2, a number of different distributions describing the joint trace lengths have been proposed to help draw inferences from discontinuity survey measurements. To date the main probability density functions for expressing discontinuity trace lengths include the negative exponential, the lognormal and the fractal distributions, as shown in Table 2.3.

When there is a need for selecting a preferable distribution among several contending theoretical distributions, the analysis technique described in Section 3.5 can be used.

The existence of both the negative exponential and the lognormal has been frequently reported. However, the fractal distribution is quite a new one and, therefore further discussion of the evidence supporting its existence follows.

4.2.2 Evidence of Fractal Trace Length Distributions

In the investigation made by Stone (1980, (see Bahat, 1988)) into the length distribution of fractures in the coarse-grained granite of Atilokan, Ontario, he found that joint lengths appeared to have fractal distribution.

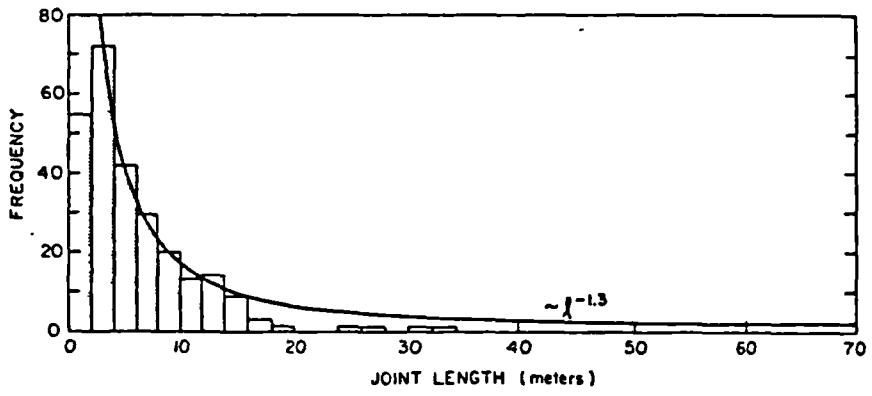

Fig. 4.3 Power law trace length distributions (from Segall & Pollard, 1983)

Segall and Pollard (1983), in their study of joint formation in the granitic rock of the Sierra Nevada, found that the length l of mapped joints from 1 or 2 m to approximately 70 m has the fractal form

$$f(l) \propto l^{-(1+D)}, \tag{4-4}$$

where $f(l)$ is the probability density function of joint length and D is the fractal dimension range from 0.2 to 0.8. The results from a mapped area has been shown in Fig. 4.3. It can be seen that the fractal distribution fits the mapped data reasonably well.

Barton and Larsen (1985), Ranalli and Hardy (1989), Sornette et al. (1990) and Davy et al. (1990) have reportedly presented the fractal trace length distributions with the range of fractal dimension from 0.1 to 0.75 respectively in their individual study of trace length distributions of fracture networks.

Power law distributions seem to overpredict the number of joints having small trace length or spacing values, which might be due to incomplete sampling of joints. Segall and Pollard (1983) believed that there may be more joints having low values of trace lengths present in the rock but that they were not able to map them on the outcrops because of mapping resolution or inadequate sampling of joints, and, that one might expect a continuous distribution of crack lengths ranging from the longest joints to very small microcracks. Ranalli and Hardy (1989) suggested that a lognormal distribution might be the result of superposition of fractal subpopulations with size cutoffs. From the above cited literature a greater confidence has been obtained for the validity of the fractal trace length distributions.

If the assumption is made that the measured distribution is indeed truncated and that the shorter trace lengths are under-represented in the data due, for example, to resolution problems, it might be possible to extrapolate the expected untruncated trace lengths using a number of methods, such as the grey prediction approach (Den, 1985).

4.3 DISCONTINUITY SIZE ESTIMATION

Smaller sizes of discontinuities means less persistence and less persistent discontinuities will lead to fewer intersections and thus larger in-situ blocks. Thus

when considering the influence of discontinuity persistence on the estimation of IBSD, the problem becomes one of finding the mean size of discontinuities in an opaque rock mass. However, it is necessary to use distributions of trace lengths derived from measurements of the trace lengths produced by their intersections with exposures. Fortunately, it will be shown below that discontinuity sizes will have a statistical distribution that is related to the distribution of their trace lengths. If the geometry and spatial arrangement of the discontinuities is known or assumed, one is able, in principle at least, to derive the relationship between discontinuity size and trace length distribution by statistical analysis. In turn, this relationship can then be used for the estimation of discontinuity size distribution from the trace length distribution sampled, as shown by Warburton (1980).

4.3.1 The Relationship between Discontinuity Size and Trace Length

It is usually impossible to specify the size of a discontinuity because only by thoroughly dismantling the rock mass can one find and measure its size. Therefore, techniques for the estimation of discontinuity sizes have to be based upon both the measurement of the trace lengths and certain assumptions about the shape of discontinuities. Much impetus in this field of research has arisen through the need to predict fluid flow through fractured rock masses and the assessment of potential sliding planes with the largest size in rock slope stability problem. The site investigation into igneous rock of de Beer Mine made by Robertson (1970) indicated that the trace lengths in both strike and dip directions are approximately equal. Since then, a simplifying assumption that discontinuities are circular discs has been widely adopted (Baecher et al., 1977; Warburton, 1980; Kulatilake & Wu, 1986; Villaescusa & Brown, 1992). Under this assumption, the sizes of discontinuities are completely defined by their diameters. Determination of discontinuity size is therefore simplified to a problem of defining the diameter distribution.

Assuming that discontinuities are circular discs of negligible thickness and the centres of discontinuities hold a three-dimensional Possion process, Warburton (1980) has made a valuable derivation of the distribution of trace lengths formed by the intersections of parallel circular planar discs, which is given by

$$f(l) = \frac{1}{m_d} \int_l^{\infty} \frac{l\, g(R) dR}{\sqrt{R^2 - l^2}}, \qquad (4\text{-}6a)$$

or

$$f(l) = \frac{l}{m_d} \int_l^{\infty} \frac{g(R)dR}{\sqrt{R^2 - l^2}}, \tag{4-6b}$$

where l represents the trace length of a discontinuity, R is the diameter of the discontinuity with the circular disc shape, m_d represents the mean diameter of discontinuities, $f(l)$ is the probability density distribution of the discontinuity trace lengths, and $g(R)$ represents the probability density distribution of the discontinuity diameters.

This is the functional stereological relationship between trace length and diameter distribution for line sampling of discontinuities. Theoretically, the distribution of discontinuity diameter can be estimated for any continuous form of $g(R)$ by applying Warburton's derivation. However, difficulties in both mathematics and practical sampling make it virtually impossible to determine $g(R)$ and its control parameters directly. Therefore, alternative methods of determining the discontinuity diameter distribution and its governing parameters have to be sought, such as the techniques described by Warburton (1980) and Villaescusa and Brown (1992). These two attempts to relate trace length and diameter distribution will now be discussed.

Assuming that discontinuity diameters obey a lognormal distribution, Warburton has examined, by means of a numerical scheme, the relationship between the average discontinuity diameters and the average trace length. For lognormally distributed trace lengths, he obtained the relationship for m_{ll} and m_{la} below :

$$m_d = e^{(\mu_d + \frac{1}{2}\sigma_d^2)}, \tag{4-7}$$

and

$$m_{ll} = \frac{8}{3\pi} e^{(\mu_d + \frac{5}{2}\sigma_d^2)}, \tag{4-8}$$

as well as

$$m_{la} = \frac{\pi}{4} e^{(\mu_d + \frac{3}{2}\sigma_d^2)}. \tag{4-9}$$

Hence

$$m_{ll}:m_{la}:m_d = \frac{8}{3\pi}e^{2\sigma_d^2}:\frac{\pi}{4}e^{\sigma_d^2}:1, \qquad (4\text{-}10)$$

where, μ_d and σ_d are the parameters characterising the log-normal distribution of discontinuity diameters; m_{ll} and m_{la} are respectively the means of trace lengths from line sampling and area sampling. In the numerical technique used by Warburton (1980), the determination of the diameter distribution was implemented by varying μ_d and σ_d systematically to find the combination that produced the best fit of sample data of trace lengths to the corresponding theoretical distribution expected from the model.

Villaescusa and Brown (1992) proposed a method to estimate the mean diameter of discontinuities based upon Warburton's work. The method, outlined below, helps to illustrate difficulties so far encountered in linking trace lengths to diameters.

Under the assumption of discontinuity convexity and circularity, the expected values of the observed joint trace length l and the discontinuity areas are related through Crofton's theorem (see Villaescusa & Brown, 1992) by:

$$\frac{E(\mu^2)}{E(\mu)} = \frac{\pi}{3}\frac{E(l^3)}{E(l)}, \qquad (4\text{-}11)$$

where $E(\mu^n)$ represents the *n-th* moment of the parameter, μ, of interest, for example, discontinuity area, such that $E(\mu^2)$ is the second moment of the discontinuity area and is given by:

$$E(\mu^2) = \int_0^\infty (\frac{\pi}{4}R^2)^2 g(R)\,dR. \qquad (4\text{-}12)$$

Using standard statistics it yields

$$\frac{\theta_g(R^4)}{\theta_g(R^2)} = \frac{4}{3}\frac{E(l^3)}{E(l)}, \qquad (4\text{-}13)$$

where $\theta_g(R^n)$ is the *n-th* moment of the underlying discontinuity diameter distribution, the right hand term, $\frac{4}{3}\frac{E(l^3)}{E(l)}$, is named the Crofton ratio. The method firstly evaluated Eqn. 4-13 and then selected a theoretical discontinuity diameter distribution, which best fitted the field data, from certain distributions which are often adopted in practice.

If, discontinuity diameter, *g(R)*, is assumed to have a negative exponential distribution, substitution of the necessary parameters into Eqn. 4-13 yields:

$$12m_d^2 = \frac{4}{3}\frac{E(l^3)}{E(l)}. \tag{4-14}$$

Whereas, if *g(R)* has a log-normal distribution, developing Eqn. 4-13 yields

$$e^2(\mu_d + 3\sigma_d^2) = \frac{4}{3}\frac{E(l^3)}{E(l)}. \tag{4-15}$$

Comparing the two Crofton ratios of observed trace lengths, *f(l)*, calculated using both Eqn. 4-14 and Eqn. 4-15, the nature of discontinuity diameter, i.e. either negative exponential or lognormal distribution, can be determined. After determination of the distribution, the mean diameter can be found using the equations below.

If *g(R)* is assumed to have a negative exponential distribution,

$$m_d = \frac{\pi}{8} m_l, \tag{4-16}$$

If *g(R)* has a log-normal distribution

$$m_d = E(R) = \frac{(\frac{3\pi m_l}{8})^5}{(\frac{4}{3}(m_l^2 + \sigma_l^2))^2}, \tag{4-17a}$$

$$E(R^2) = \frac{(\frac{3\pi m_l}{8})^8}{(\frac{4}{3}(m_l^2 + \sigma_l^2))^3}, \tag{4-17b}$$

where m_l and $(\sigma_l)^2$ are respectively the mean and the variance of trace length, and both μ_d and σ_d are related to m_d and $E(R^2)$ by

$$\mu_d = 2Ln(m_d) - \frac{1}{2} Ln(E(R^2)), \tag{4-18}$$

$$\sigma_d^2 = Ln(E(R^2)) - 2Ln(m_d). \tag{4-19}$$

It can be seen from the above discussion that there is a prerequisite that an analytical form of discontinuity diameter distribution has to be set up in advance when utilising the techniques used by Warburton (1980) and Villaescusa and Brown (1992). It might be reasonable to assume that the diameters of discontinuities would be a negative exponential, or lognormal or fractal form, etc. The impossibility of dismantling a rock mass and difficulties raised in sampling have, however, so far made it impossible to prove these assumptions. By contrast, it is possible and easy to confirm assumptions about the distribution forms of trace lengths produced by discontinuities. Consequently, imposing a distribution form of trace lengths is more reasonable than doing that for discontinuity diameters. In the next section, an algorithm for determination of discontinuity diameter distribution which is not based on the assumption of the distribution of discontinuity diameters but on that of trace lengths will be represented.

4.3.2 Derivation of a Numerical Approach to the Determination of the Distribution of Discontinuity Diameters

It follows from Eqn. 4-6a that the probability that trace length l is in the range of l and l+dl can be given by

$$\int_{l_{i-1}}^{l_i} f(l)dl = \int_{l_{i-1}}^{l_i} \left(\frac{1}{m_d}\int_{l}^{\infty} \frac{l\,g(R)dR}{\sqrt{R^2 - l^2}}\right)dl. \tag{4-20}$$

On the same lines as the numerical scheme reported by Kulatilake and Wu (1986), based upon Eqn. 4-20, the following approach to the determination of the distribution of discontinuity diameters has been developed using a numerical technique.

Knowing the corrected (without truncation) distribution of trace lengths and supposing $F(l)$ represents the cumulative probability distribution function of trace lengths, it is apparent from Eqn. 4-20 that the left hand side can be written as

$$P(l_{i-1}, l_i) = \int_{l_{i-1}}^{l_i} f(l)dl = F(l_i) - F(l_{i-1}), \tag{4-21}$$

where $P(l_{i-1}, l_i)$ represents the probability that trace length l is in the range of l and l+dl. The Eqn. 4-20 can therefore be expressed as

$$P(l_{i-1}, l_i) = \frac{1}{m_d} \int_{l_{i-1}}^{l_i} \left(\int_{l}^{\infty} \frac{l\, g(R)}{\sqrt{R^2 - l^2}} dR \right) dl. \tag{4-22}$$

Reversing the order of integration in Eqn. 4-22, with the help of Fig. 4.4, we obtain the following expression which transforms the right side of Eqn. 4-22 into two terms as follows

$$P(l_{i-1}, l_i) = \frac{1}{m_d} \int_{l_{i-1}}^{l_i} \left(\int_{l_{i-1}}^{R} \frac{l\, dl}{\sqrt{R^2 - l^2}} \right) g(R) dR + \frac{1}{m_d} \int_{l_i}^{\infty} \left(\int_{l_{i-1}}^{l_i} \frac{l\, dl}{\sqrt{R^2 - l^2}} \right) g(R) dR. \tag{4-23}$$

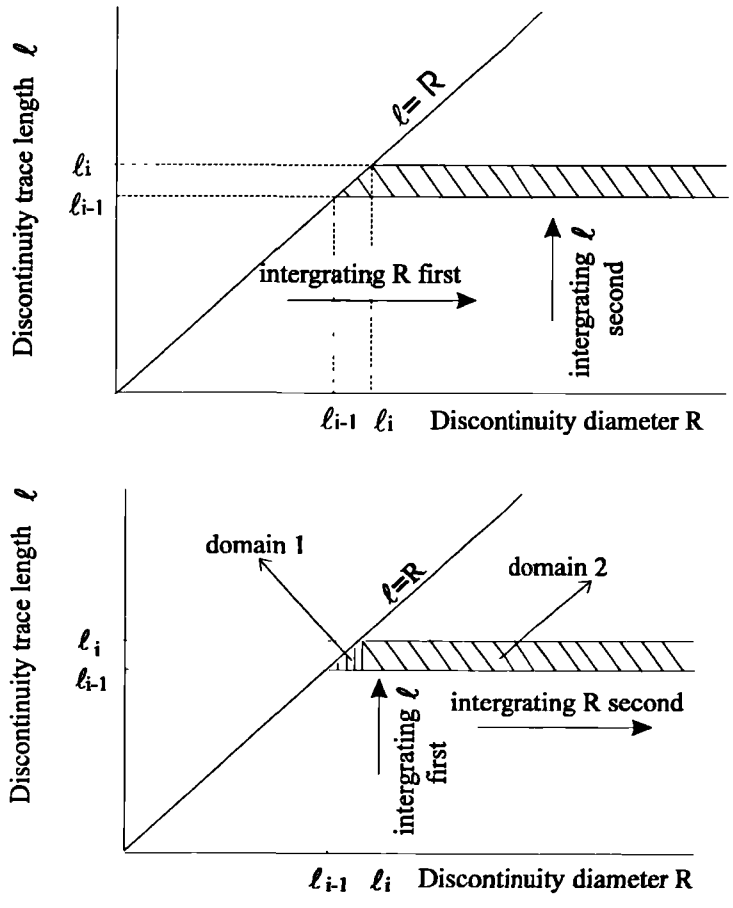

Fig. 4.4 Exchanging the integration orders: (a) the order before exchanging; (b) the order after exchanging

The Eqn. 4.23 can be further developed as

$$P(l_{i-1},l_i)=\frac{1}{m_d}\int_{l_{i-1}}^{l_i}\left(\left[-\sqrt{R^2-l^2}\right]_{l_{i-1}}^{R}\right)g(R)dR+\frac{1}{m_d}\int_{l_i}^{\infty}\left(\left[-\sqrt{R^2-l^2}\right]_{l_{i-1}}^{l_i}\right)g(R)dR, \quad (4\text{-}24)$$

i.e.

$$P(l_{i-1},l_i)=\frac{1}{m_d}\left(\int_{l_{i-1}}^{l_i}\left(\sqrt{R^2-l_{i-1}^2}\right)g(R)dR+\int_{l_i}^{\infty}\left(\sqrt{R^2-l_{i-1}^2}-\sqrt{R^2-l_i^2}\right)g(R)dR\right). \quad (4\text{-}25)$$

The second term of the right hand side of Eqn. 4-25 can be written according to the definition of integration as

$$\begin{aligned}
&\frac{1}{m_d}\int_{l_i}^{\infty}\left(\sqrt{R^2-l_{i-1}^2}-\sqrt{R^2-l_i^2}\right)g(R)dR\\
&\approx\frac{1}{m_d}\int_{l_i}^{l_{i+1}}\left(\sqrt{R^2-l_{i-1}^2}-\sqrt{R^2-l_i^2}\right)g(R)dR\\
&\quad+\frac{1}{m_d}\int_{l_{i+1}}^{l_{i+2}}\left(\sqrt{R^2-l_{i-1}^2}-\sqrt{R^2-l_i^2}\right)g(R)dR\\
&\quad\cdots\\
&\quad+\frac{1}{m_d}\int_{l_k}^{l_{k+1}}\left(\sqrt{R^2-l_{i-1}^2}-\sqrt{R^2-l_i^2}\right)g(R)dR \qquad (4\text{-}26)\\
&\quad\cdots\\
&\quad+\frac{1}{m_d}\int_{l_n}^{l_{n+1}}\left(\sqrt{R^2-l_i^2}_{1}-\sqrt{R^2-l_i^2}\right)g(R)dR\cdot
\end{aligned}$$

According to the mean-value theorem in integration (Korn & Korn, 1968), it follows that

$$\frac{1}{m_d}\int_{l_{i-1}}^{l_i}\left(\sqrt{R^2-l_{i-1}^2}\right)g(R)dR=\frac{1}{m_d}\sqrt{R_i^2-l_{i-1}^2}\int_{l_{i-1}}^{l_i}g(R)dR, \quad (4\text{-}27)$$

where R_i is a value in (l_{i-1}, l_i), here we choose the intermediate value of $[\,l_{i-1}, l_i\,]$, i.e.

$$R_i = \frac{l_{i-1} + l_i}{2}. \tag{4-28}$$

Similarly,

$$\begin{aligned} &\frac{1}{m_d}\int_{l_k}^{l_{k+1}} (\sqrt{R^2 - l_{i-1}^2} - \sqrt{R^2 - l_{i-1}^2})\, g(R)dR \\ &= \frac{1}{m_d}(\sqrt{R_{k+1}^2 - l_{i-1}^2} - \sqrt{R_{k+1}^2 - l_{i-1}^2})\int_{l_k}^{l_{k+1}} g(R)dR \end{aligned}, \tag{4-29}$$

where, R_{k+1} has a similar form to Eqn. 4-28

$$R_{k+1} = \frac{l_k + l_{k+1}}{2}, \tag{4-30}$$

Now the expression $\int_{l_{i-1}}^{l_i} g(R)dR$ in Eqn. 4-27 represents the probability $G(R_i)$ that discontinuity diameter, R, lies between $[l_{i-1}, l_i]$

$$G(R_i) = \int_{l_{i-1}}^{l_i} g(R)dR, \tag{4-31}$$

and the expression $\int_{l_k}^{l_{k+1}} g(R)dR$ in Eqn. 4-29 represents the probability $G(R_{k+1})$ that discontinuity diameter, R, lies between $[l_k, l_{k+1}]$

$$G(R_{k+1}) = \int_{l_k}^{l_{k+1}} g(R)dR. \tag{4-32}$$

Substituting Eqns. 4-27, 4-29, 4-31 and 4-32 into Eqn. 4-25 yields

$$P(l_{i-1}, l_i) \approx \frac{1}{m_d}(\sqrt{R_i^2 - l_{i-1}^2})G(R_i) + \sum_{j=i+1}^{n} \frac{1}{m_d}(\sqrt{R_j^2 - l_{i-1}^2} - \sqrt{R_j^2 - l_i^2})G(R_j). \tag{4-33}$$

$$i = 1, 2, \ldots, n$$

Eqn. 4-33 is a set of simultaneous equations including $G(R_i)$ $(i=1,2...,n)$, totally n unknown numbers. It can be solved using a standard numerical algorithm for solving sets of simultaneous equations. Different value of m_d would produce a different set of $G(R_i)$, but only the combination of $G(R_i)$ $(i=1,2,...,n)$ that holds the following constraints is the correct solution to Eqn. 4-33.

$$\sum_{i=1}^{n} G(R_i) = 1 \qquad \text{and} \qquad G(R_i) \geq 0. \tag{4-34}$$

The different values of mean diameter, therefore, have to be tried to obtain the correct solution.

4.4 IMPLEMENTATION OF NUMERICAL APPROACH

It can be seen that the implementation of the algorithm described in the last section involves solving the following simultaneous linear equations.

$$A \bullet X = B, \tag{4-35}$$

where A is a square matrix, X and B are column vectors.

$$A=[a_{ij}]_{n\times n}, \quad a_{ij} = \begin{cases} 0 & i > j \\ \dfrac{1}{m_d}\left(\sqrt{(R_{i+1})^2 - l_{i-1}^2} - \sqrt{(R_{i+1})^2 - l_i^2}\right) & i < j, \\ \dfrac{1}{m_d}\left(\sqrt{(R_i)^2 - l_{i-1}^2}\right) & i = j \end{cases} \tag{4-36}$$

$$X = (x_i), \qquad x_i = G(R_i), \tag{4-37}$$

$$\mathrm{B} = (b_i), \qquad b_i = P(l_{i-1}, l_i). \tag{4-38}$$

The task for numerical calculation here is to assign a value of m_d and solve Eqn. 4-35 to obtain a set $G(R_i)$. The calculating routines are repeated for different m_d until a particular combination of $G(R_i)$ holds the constraint conditions described by Eqn. 4.34.

The implementation of the algorithm is illustrated in Fig. 4.5. A computer procedure named DIATRACE for the implementation of the determination of the discontinuity diameter distribution and its mean diameter, written in FORTRAN language, is listed in Appendix A.2.

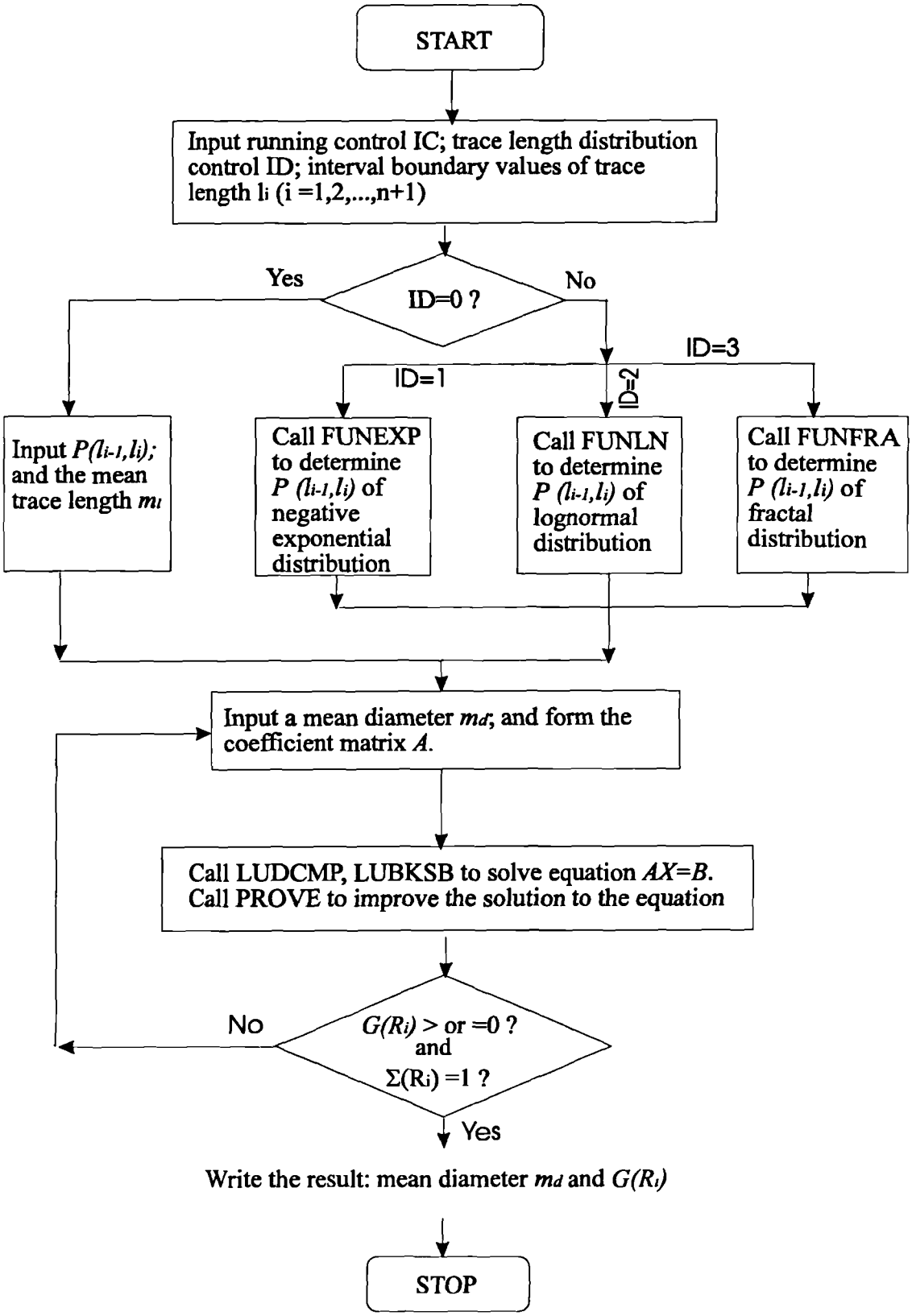

Fig. 4.5 The flowchart of DIATRACE outlining the procedure for the determination of the discontinuity diameter distribution

As described previously, the potential distribution for trace lengths can often be one of three forms: negative exponential, lognormal and fractal. Hence these three forms of trace length distributions are considered in the procedure. It can be noted from the algorithm derived that the diameter distribution can be also established. If a discrete distribution of trace length has been obtained, the procedure can still generate the diameter distribution. Applying the program DIATRACE to Warburton's trace length data (1980) yields results for the corresponding distribution of discontinuity diameters and an estimation of its mean diameter. The results are compared with Warburton's prediction, as shown in Fig. 4.6.

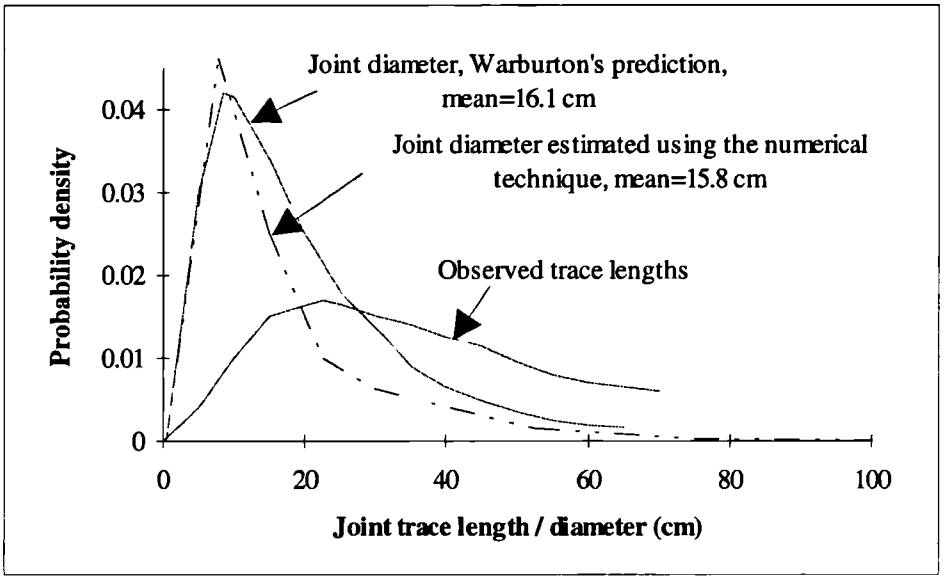

Fig. 4.6 Comparison of Probability density of joint diameter using the numerical method to Warburton's prediction

Based on Warburton's derivation (see Eqn. 4.6) it is now possible using the numerical algorithm in DIATRACE to relate discontinuity diameter distribution to the distribution of measured trace lengths. This makes it possible to estimate the mean diameter of a population of discontinuities. The method to estimate the discontinuity size is still subject to the commonly applied constraint that discontinuities are presumed to be circular discs. Nevertheless, it provides a tool to make an approximation of the discontinuity size, which is of great significance for considering the influence of impersistent discontinuities on the prediction of IBSD.

4.5 ESTIMATION OF THE MEAN SIZE FROM THE MEAN TRACE LENGTH

In the procedure for determining the mean diameter presented above, the distribution of trace lengths needs to be obtained from a detailed survey of trace length measurements on exposures of rock masses. Unfortunately, direct and complete measurements of discontinuity trace lengths on site are usually time-consuming and painstaking jobs.

Recall that the mean diameter of a population of discontinuities is important when considering the influence of impersistent discontinuities on the prediction of IBSD. A number of techniques (Baecher et al., 1977; Cruden, 1977; Pahl, 1981; Priest & Hudson, 1981; Kulatilake & Wu, 1984; Zhang & Liao, 1990; Priest, 1993) are available for making estimations of the mean trace length. If a practical relationship between both mean discontinuity size and mean trace length can be established, it will provide a valuable tool for estimating mean discontinuity diameter from mean trace length. So far there has been no such an analytical relationship available. Therefore a numerical simulation approach to this solution has been proposed here, to explore an empirical relationship between both mean discontinuity size and mean trace length using the algorithm and procedure developed in the last section. The numerical simulation stages using the computer program DIATRACE include:

(1) Assume a population of discontinuities defined only by trace lengths governed by a known distribution law, therefore having a known mean trace length;

(2) Determine the mean diameter of this population of discontinuities by execution of the program DIATRACE;

(3) Repeat (1) and (2) for a series of (c. 20) populations of discontinuities with different mean values of trace lengths but the same trace length distribution law;

(4) Establish the numerically simulated relationship between mean discontinuity size and mean trace length.

It is worth noting that the method for establishing the simulated relations are subject to two assumptions. The first is that discontinuities are presumed to be circular discs, the second is that the mean trace length is the corrected (without truncation) estimate.

Three continuous distributions of discontinuity trace lengths: the negative exponential, the lognormal and the fractal distribution of discontinuity trace lengths have been investigated.

For the negative exponential distribution of trace lengths, the simulated relationship between mean discontinuity size and mean trace lengths yields

$$m_d = 0.779\, m_l. \tag{4-39}$$

For the lognormal trace length distribution, the empirical relationship is given by

$$m_d = 0.737\, m_l. \tag{4-40}$$

For the fractal distribution of trace lengths, the empirical relationship is

$$m_d = 0.503\, m_l. \tag{4-41}$$

The goodness-of-fit of the three simulated equations to the corresponding numerical simulation results is illustrated in Fig. 4.7 to Fig. 4.9.

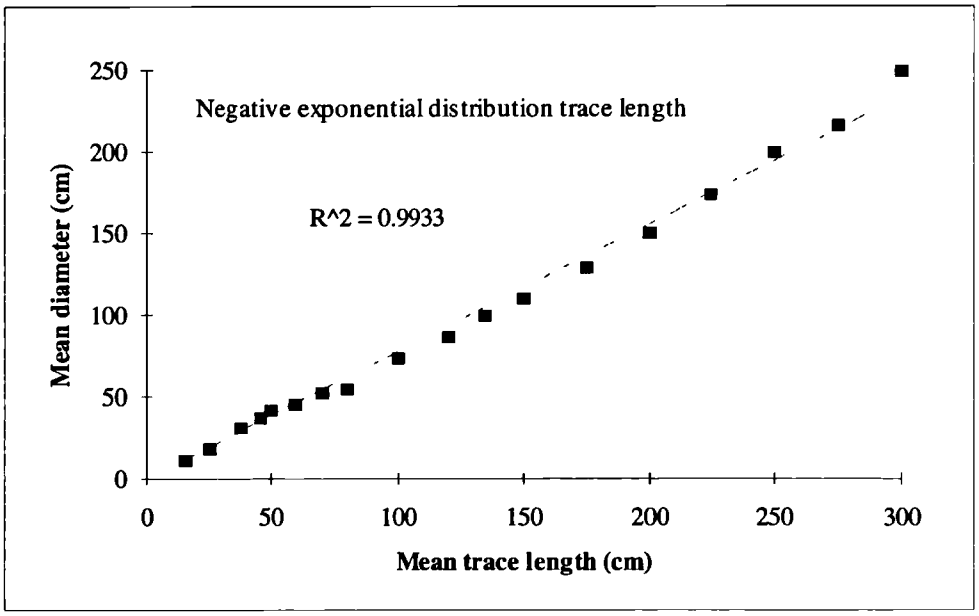

Fig. 4.7 Relationship between means of discontinuity diameter and trace length for a negative exponential trace length distribution

It can be seen that the mean sizes of discontinuities for the above three trace length distributions are all less than the corresponding mean trace lengths, which is in accordance with the results reported by Warburton (1980), Villaescusa and Brown (1992). This may at first seem a surprising result since the diameter must be the maximum trace length possible. However the result is strongly influenced by all the discontinuities that are present but not intersected at all by the sample plane of section upon which the traces are seen.

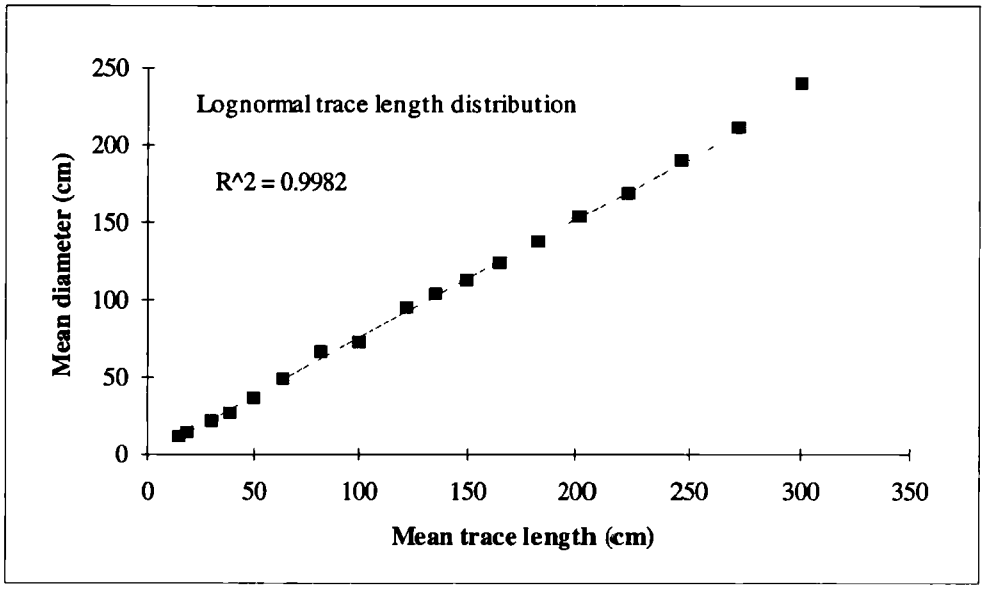

Fig. 4.8 Relationship between means of discontinuity diameter and trace length for a lognormal trace length distribution

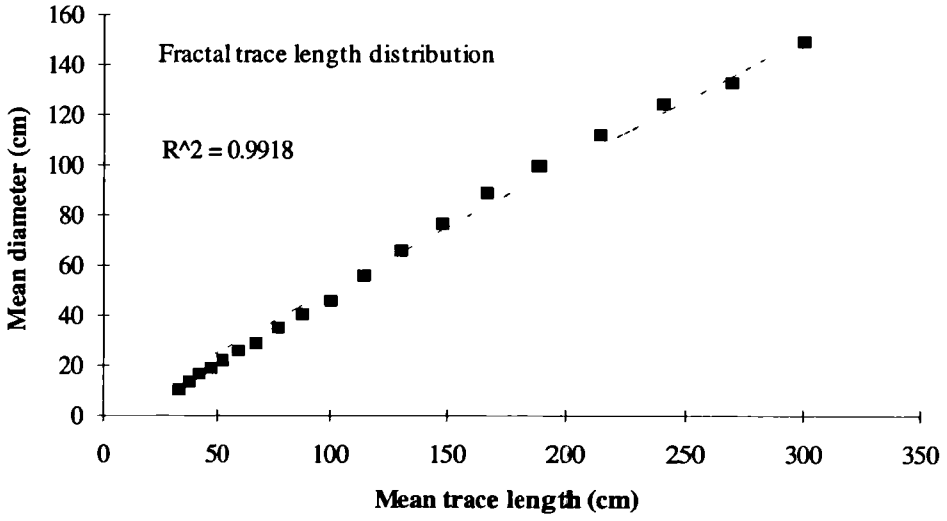

Fig. 4.9 Relationship between means of discontinuity diameter and trace length for a fractal trace length distribution)

Baecher et al. (1977) reported an example in which they used an approximate second-moment analysis statistical method to estimate the mean diameter. For their case the mean trace length was 399.3 cm and the mean joint radius was estimated to be as 163.7 cm for a data set where the trace lengths were lognormally distributed. Using Eqn. 4-40, the mean trace length of 399.3 cm yields a mean radius of 147.2 cm, which differs from the authors' prediction by 10.08%.

Having obtained the simulated relationship between the means of both diameter and trace length, it is now appropriate to see how much difference in discontinuity diameter there is between the three commonly assumed trace length distributions.

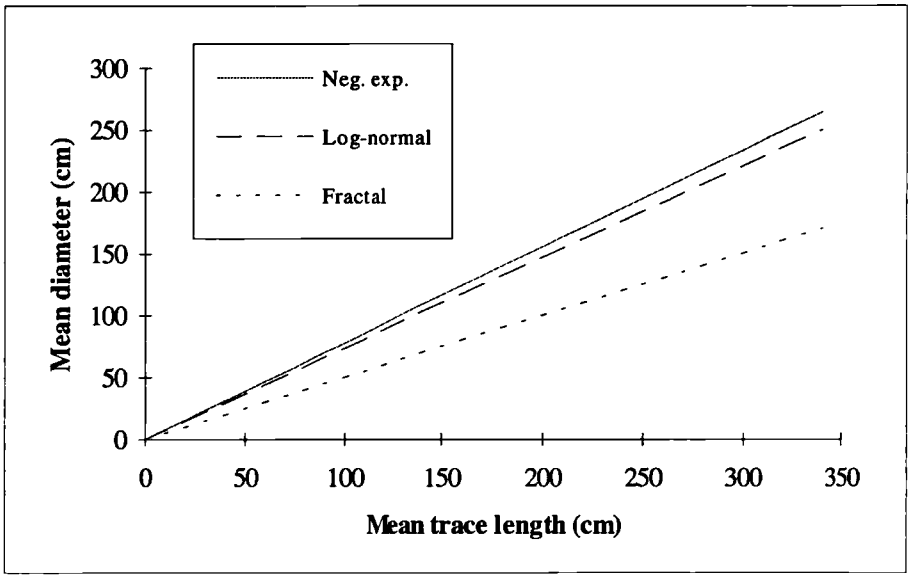

Fig. 4.10 Comparison between discontinuity diameter from three empirical trace length distributions

Under the same mean trace length (Fig. 4.10), the discontinuity diameter with a negative exponential trace length distribution appears the largest, the diameter with a lognormal trace length distribution is slight smaller, and the diameter with a fractal trace length distribution is clearly the shortest. It can be found, by comparing the three theoretical distribution curves with the same mean trace length (see Fig. 4.11), that for the discontinuities with longer trace lengths, both the negative exponential and lognormal distribution curves have greater probability density values than the fractal distribution curve, and that both the negative exponential and lognormal distributions are quite close.

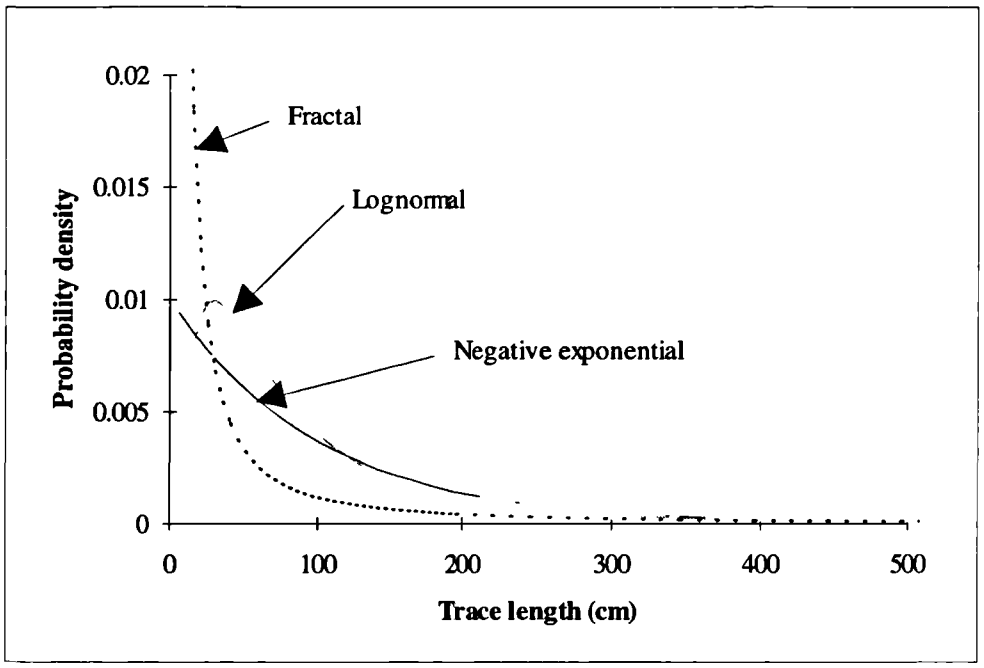

Fig. 4.11 Graphical comparison of three trace length distributions (mean trace length =100 cm; the parameters (see Table 2.2) for lognormal: *A=4.2, B=0.9*; for fractal: $D=0.5,\ 5 \leq l \leq 1000\ cm$),

Before the simulated relationships shown in Fig. 4.10 can be used to give mean diameter, it is necessary to obtain the mean trace length and the trace length distribution itself - various techniques have been proposed, for example, those of techniques proposed by Cruden (1977), or Pahl (1981), or Priest and Hudson (1981), or Kulatilake and Wu (1984). Most of these techniques use directly surveyed measurements of discontinuity trace lengths. It is interesting to note that the estimation of the mean value of trace lengths can also be made from indirect measurements of trace lengths, where truncation due to limited exposure is common place. Such an indirect approach will be explored in the following section.

4.6 ESTIMATION OF THE MEAN TRACE LENGTH OF DISCONTINUITIES

Priest and Hudson (1981) proposed a technique for rapidly estimating the mean trace length by simply counting n and r at a given exposure with censored trace length at some censoring level c. Here, r represents the number of discontinuities with a semi-trace length less than a censoring level c, n is the total number in the sample.

Suppose $f(l)$ represents the probability density distribution of discontinuity trace lengths, $h(l)$ is the probability density distribution of discontinuity semi-trace lengths, $F(l)$ and $H(l)$ are the corresponding cumulative probability functions, then $h(l)$ is given by

$$h(l) = \mu \int_l^{\infty} f(x)dx, \tag{4-42}$$

or

$$h(l) = \mu(1-F(l)), \tag{4-43}$$

where μ is the mean trace termination frequency for the population, i.e. $1/\mu$ represents the mean trace length.

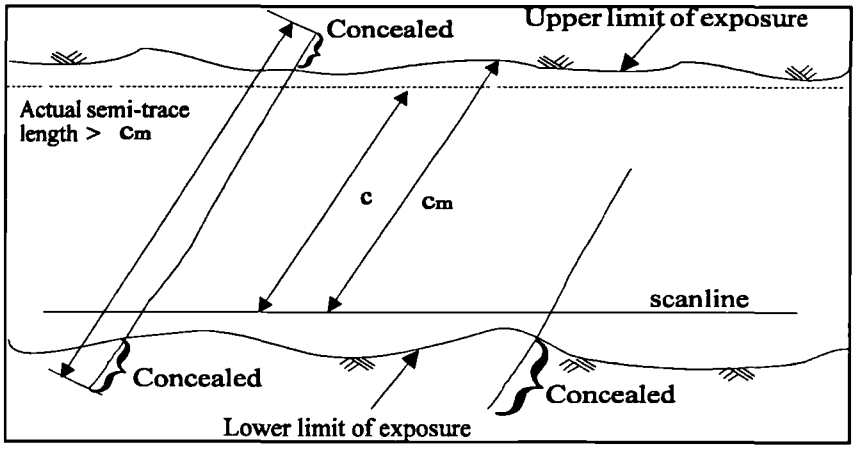

Fig. 4.12 Diagrammatic illustration of discontinuity traces intersecting a scanline on a planar exposure of limited extent (after Priest & Hudson, 1981)

When on site, it is often found that the extent of the exposures and the orientation of discontinuities limits the maximum observed semi-trace length to some censoring level c_m (see Fig. 4.12). The c_m is unlikely to be a whole number and may vary from one end of the exposure to another. It is usually desirable to set up one or more censored semi-trace length levels c, which are less than c_m. The distribution $i(l)$, of the censored semi-trace lengths is directly proportion to the distribution $h(l)$, of semi-trace lengths. The mean trace length m_{li}, estimated from a population of discontinuities censored at some level c, according to Priest and Hudson (1981), is given by

$$m_{l_i} = \frac{\int_0^c l h(l) dl}{H(c)}, \tag{4-44}$$

where $H(c)$ is the numerical proportion of intersected discontinuities with trace lengths less than c, which is given by

$$H(c) = \int_0^c h(l) dl = \int_0^c \mu(1 - F(l)) dl. \tag{4-45}$$

Eqn. 4-44 indicates that m_{li} will significantly depend upon the probability density distribution of discontinuity trace lengths, for a given value of mean trace length m_l for the entire population.

According to Priest and Hudson (1981), for a large sample of semi-trace lengths, $H(c)$ can be approximately expressed as

$$H(c) = \frac{r}{n}, \tag{4-46}$$

where r is the number of discontinuities with a semi-trace length less than c and n is the total number in the sample.

The appropriate form $f(l)$ of the probability density distribution of trace length for a given field or geological domain may be assumed, or a preliminary survey or a detailed local measurement on a quarry or a mine allows a first estimation of the $f(l)$ to be made. After defining or assuming the form of $f(l)$, an estimation of m_l by counting n and r at a given exposure which censored semi-trace lengths at some censoring level c, can be made based upon both Eqn. 4-45 and Eqn. 4-46.

Negative exponential distribution

When the probability density obeys a negative exponential distribution, i.e.

$$f(l) = \mu e^{-\mu l}, \qquad \text{and} \qquad F(l) = 1 - e^{-\mu l}, \tag{4-47}$$

hence

$$H(c) = \int_0^c \mu\,(1 - (1 - e^{-\mu l}))dl, \tag{4-48}$$

and by integration

$$H(c) = 1 - e^{-\mu c}. \tag{4-49}$$

Substituting for Eqn. 4-49 into Eqn. 4-46 yields

$$1 - e^{-\mu c} = \frac{r}{n}. \tag{4-50}$$

This gives the mean trace length, m_l, of the entire population of discontinuities as

$$m_l = \frac{1}{\mu} = \frac{c}{Ln(\frac{n}{n-r})}. \tag{4-51}$$

This is an alternative of the result obtained in Equation 13 of Priest and Hudson (1981). Priest and Hudson (1981) suggested that the method used for obtaining Eqn. 4-51 could be applied to any suitable *f(l)* to yield similar expression for rapidly estimating m_l, though they have not apparently done so. Expressions for both lognormal and fractal distributions may be useful and are thereby derived below. However, some considerable effort is necessary to simplify the mathematics to a more useful form as shown below.

Lognormal distribution

In the case where *f(l)* is a lognormal distribution

$$f(l) = \frac{1}{\sqrt{2\pi}Bl} e^{-\frac{(Lnl-A)^2}{2B^2}}. \tag{4-52}$$

The mean trace length, m_l, of the entire population of discontinuities, and the standard deviation σ are relate to the distribution parameters A and B as

$$m_l = e^{A+\frac{B^2}{2}}, \tag{4-53}$$

$$\sigma = \sqrt{e^{2A+B^2}(e^{B^2}-1)}. \tag{4-54}$$

Because of the difficulty in direct mathematical derivation of *H(c)* for a lognormal distribution, an attempt to avoid the complex integration involved for a lognormal trace length distribution has been made. It is found that a lognormal distribution may be approximated by the following simpler function expressed as

$$f(l) = \frac{20k^4 l}{(k+l)^6}, \tag{4-55}$$

where k is a parameter. The mean m_l and the standard deviation σ of the approximate probability distribution are given by

$$m_l = E(l) = \frac{2}{3}k, \tag{4-56}$$

and

$$\sigma^2 = E(l^2) - (E(l))^2 = \frac{5}{9}k^2. \tag{4-57}$$

The distribution parameters A and B of a lognormal distribution are related to the parameter k of the approximate probability distribution through two conditions. Firstly, both distributions have the same means, which yields

$$\frac{2}{3}k = e^{A+\frac{B^2}{2}}. \tag{4-58}$$

Having the same means may be the most important feature for determining the mean trace length using an approximating function for lognormal distributions. For the second condition, it may be possible to impose that both distributions take their maximum function values at the same value of trace length, or that both distributions have the same standard deviations, etc. That both distributions take their maximum function values at the same trace length yields

$$\frac{k}{5} = e^{A-B^2}. \tag{4-59}$$

Hence, the parameters A and B of the lognormal distribution can be found by solving jointly Eqn. 4-58 and Eqn. 4-59.

In order to examine whether a function expressed by Eqn. 4-55 approximates well to a perfect lognormal distribution, a comparison between the approximate probability

distribution function expressed as Eqn. 4-55 and the lognormal distribution has been made, and is illustrated in Fig. 4.13. In the figure, the discrepancy between the distribution parameters for the perfect lognormal distribution and the approximate probability distribution can be seen by plotting Eqns. 4-52 and 4-55 using Eqns. 4-58 and 4-59.

Fig. 4.13 suggests that the distribution expressed as Eqn. 4-55 approximates well to the lognormal distribution. Using the approximate distribution, it allows an estimate of mean trace length to be made more easily.

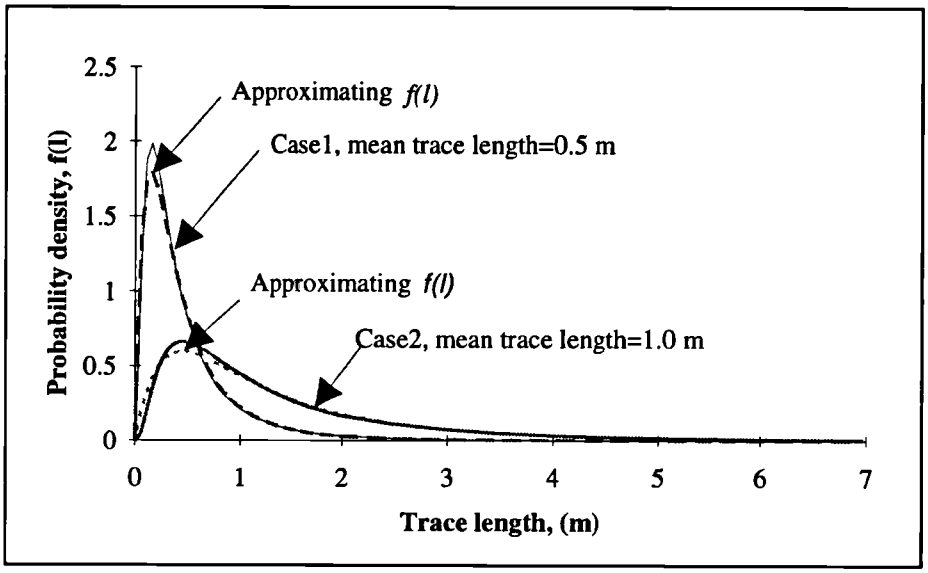

Fig. 4.13 Graphical comparison of the approximate lognormal probability distribution and the lognormal distribution. (Case 1, Lognormal distribution: A=-1.0945, B=0.9; parameter for the approximating distribution, k=0.75. Case 2, Lognormal distribution: A=0.0041, B=0.896; parameter for the approximating distribution, k=2.25.)

Now, since $f(l)$ of a lognormal distribution is approximately given by Eqn. 4-55, it follows that $h(l)$ will be given by

$$h(l) = \mu\int_l^\infty \frac{20k^4 x}{(k+x)^6}\,dx = \mu\frac{k^4(k+5l)}{(k+l)^5}, \qquad (4\text{-}60)$$

hence

$$H(c) = \int_0^c h(l)dl = \int_0^c \mu\frac{k^4(k+5l)}{(k+l)^5}dl = 1-\frac{5}{2}\left(\frac{k}{k+c}\right)^3+\frac{3}{2}\left(\frac{k}{k+c}\right)^4. \qquad (4\text{-}61)$$

Substituting for Eqn. 4-61 into Eqn. 4-46 yields

$$1-\frac{5}{2}(\frac{k}{k+c})^3+\frac{3}{2}(\frac{k}{k+c})^4=\frac{r}{n}. \qquad (4\text{-}62)$$

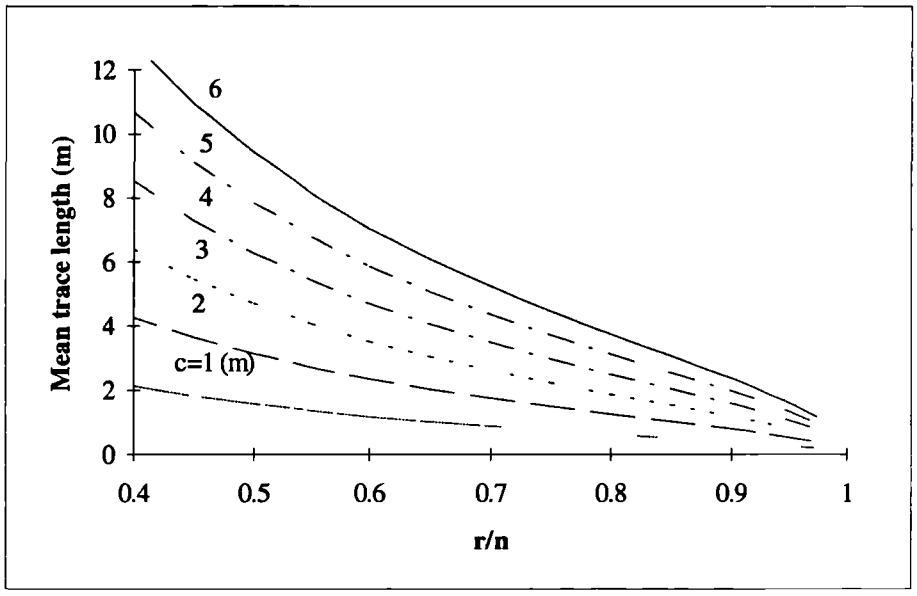

(a)

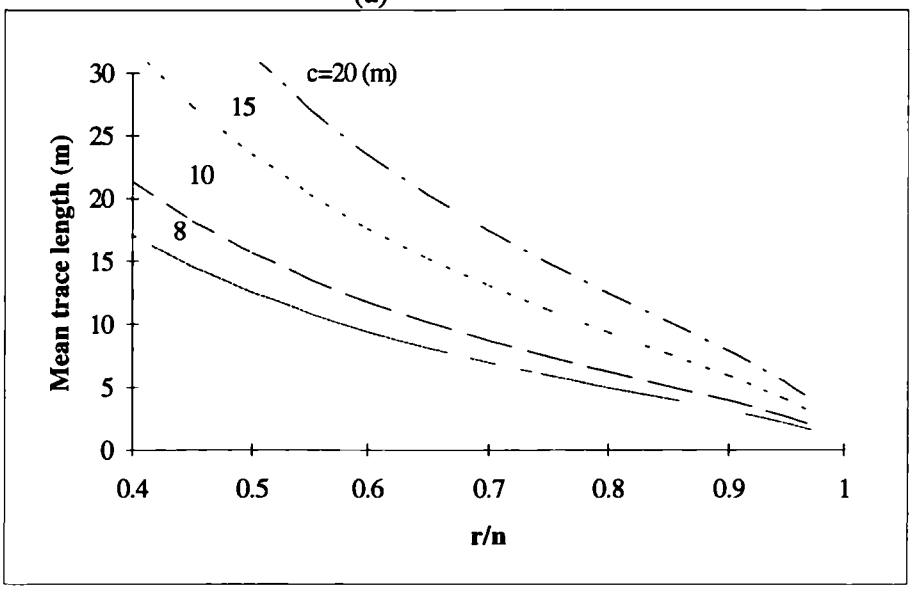

(b)

Fig. 4.14 Relationship between mean trace length and *r/n* with different censored level *c*

Eqn. 4-62 has been used to construct the curves illustrated in Fig. 4.14 which allows us to make a rapid estimate of mean trace length for a large sample by counting

r and n at a given rock face which censors at some level c. These figures, together with Eqn. 4-58 and Eqn. 4-59, provide a tool for estimating the mean trace length as well as the parameters of a lognormal distribution.

Fractal distribution

In the case where $f(l)$ is a fractal distribution

$$f(l) = Al^{-(1+D)}, \qquad (l_l \le l \le l_u) \tag{4-63}$$

where l_l and l_u are the lower cutoff and upper cutoff, and A is a constant and given by

$$A = \frac{D}{(l_l^{-D} - l_u^{-D})}, \tag{4-64}$$

The mean trace length, m_l, of the entire population of discontinuities is as follows

$$m_l \approx \frac{D}{1-D} l_u^{1-D} l_l^{D}. \tag{4-65}$$

Now $h(l)$ is given by

$$h(l) = \mu \int_l^{\infty} f(x)dx = \mu \int_l^{\infty} Ax^{-(1+D)}dx = \mu \frac{A}{D} l^{-D}, \tag{4-66}$$

hence

$$H(c) = \int_0^c h(l)dl = \int_{l_l}^c \mu \frac{A}{D} l^{-D} dl = \frac{\mu A}{D(1-D)} (c^{1-D} - l_l^{1-D}). \tag{4-67}$$

Substituting Eqn. 4-64 into Eqn. 4-67 yields

$$H(c) \approx \frac{\mu}{1-D} c^{1-D} l_l^{D}. \tag{4-68}$$

Substituting $\mu = 1/m_l$ from Eqn. 4-65 into Eqn. 4-68 gives

$$H(c) = \frac{1}{D} \left(\frac{c}{l_u}\right)^{1-D}. \tag{4-69}$$

and hence it follows that

$$\frac{1}{D}(\frac{c}{l_u})^{1-D} = \frac{r}{n}. \tag{4-70}$$

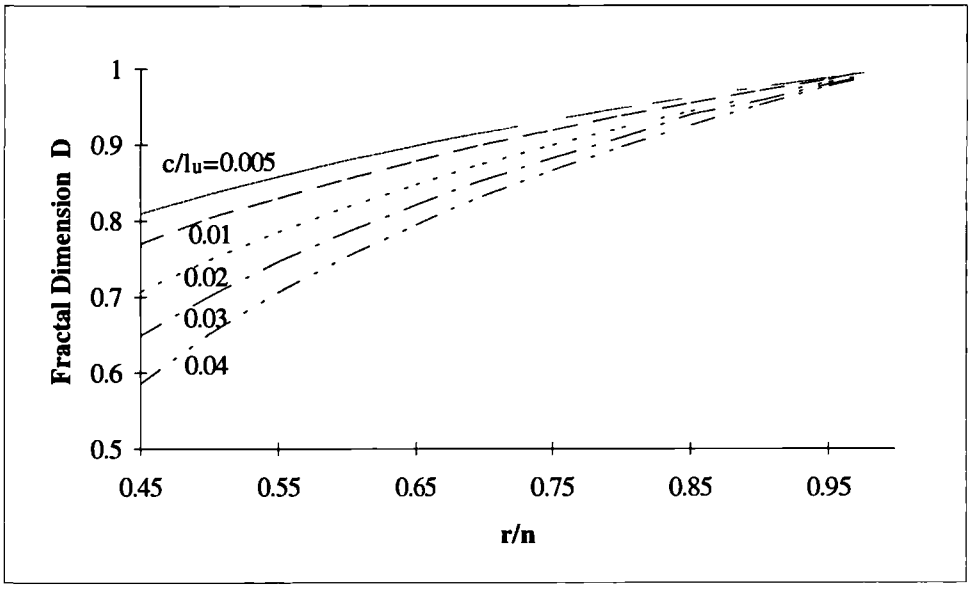

(a)

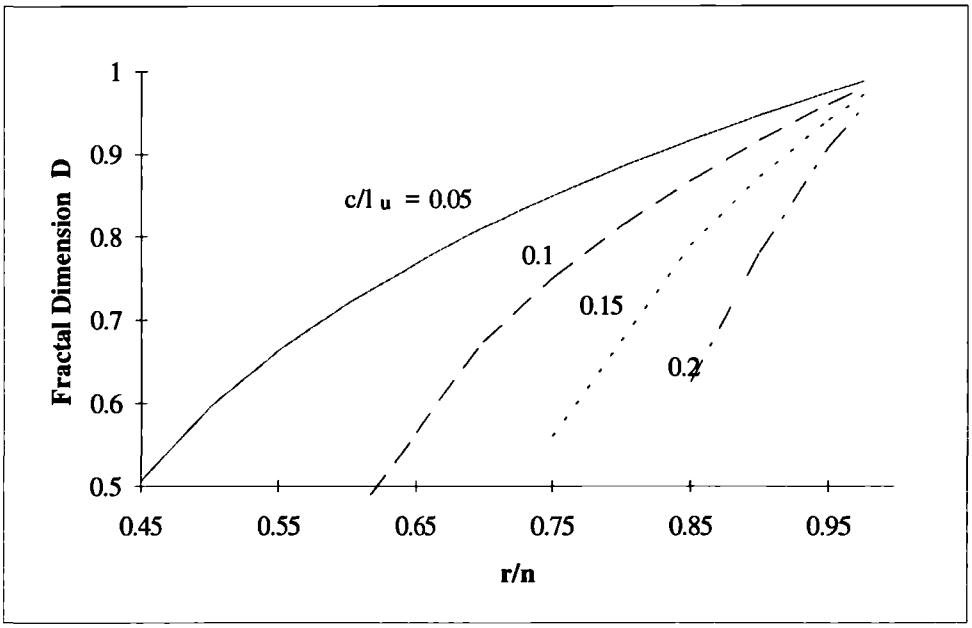

(b)

Fig. 4.15 Relationship between fractal dimension D and r/n with different c/l_u

Eqn. 4-70 has been used for constructing the curves illustrated in Fig. 4.15 which provides us with a tool to estimate the fractal dimension of trace lengths for a large sample by counting r and n at a given rock face and a given censored level c.

The fractal dimension D may also be approximately estimated using the following expression when the value of D is small (say less than 0.5)

$$D=\frac{1+\sqrt{(1-4\frac{n}{r}\frac{c}{l_u}Ln\frac{l_u}{c})}}{2Ln\frac{l_u}{c}}, \qquad (4\text{-}71)$$

where the condition $1 \le 4\frac{n}{r}\frac{c}{l_u}Ln\frac{l_u}{c}$ must be held.

After determination of the fractal dimension, the mean trace length can then be obtained by substituting the value of D into Eqn. 4-65.

A worked example is described as follows. Suppose that after carrying out a measurement of trace lengths on an exposure, we obtain: the lower cutoff trace length l_l =0.05 (m), the assumed upper cutoff trace length l_u=50 (m), when the censored level c=2 (m) the ratio r/n=0.6. Hence c/l_u=0.04, which from Fig. 4.15 yields D=0.75, and therefore the estimate of mean trace length m_l=0.83 (m).

4.7 UPDATING OF THE IBSD PREDICTION

After examining discontinuity size, it is possible to incorporate the degree of persistence of discontinuities into the prediction of IBSD.

As described at the beginning of this chapter, whether the prediction of IBSD based upon the assumption of infinitely extending discontinuities is good or not is critically dependent upon both the dimension of the in-situ rock mass of interest and the mean size of the discontinuities. As such, it may be appropriate to introduce a factor to characterise these properties. The factor is referred to as the "relative impersistence factor". In other words, relative impersistence will include both the information about discontinuity size and the dimension of observed discontinuities or the dimension of the rock mass of interest. It is proposed that the relative impersistence factor F_{imp} can be described as

$$F_{imp} = \begin{cases} \frac{S_D}{S_r} & S_D < S_r \\ 1 & S_D \geq S_r \end{cases}, \qquad (4\text{-}72)$$

where S_D is mean discontinuity size which can be estimated using the techniques developed in the foregoing sections, and S_r represents the characteristic size of the rock mass of interest (say, the cube root of the volume of the rock mass of interest), as illustrated in Fig. 4.16.

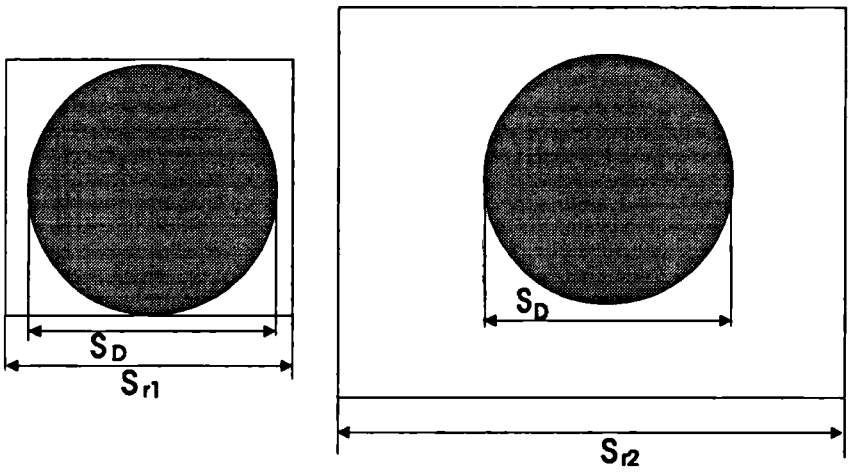

Fig. 4.16 Schematic illustration of the relative impersistence factor

Consider now the influence of F_{imp} on the IBSD predictions developed in previous chapters. Assuming that we obtain a result for IBSD for field data using the techniques based on the all-persistent assumption, and that S_D and S_r are those graphically illustrated in Fig. 4.16a, we can accept this prediction of IBSD because the mean discontinuity size is quite close to the dimensions of the rock mass of interest and the all-persistent assumption is valid. However, if S_D and S_r are as graphically illustrated in Fig. 4.16b, the all-persistent assumption will be clearly violated and the impersistence of discontinuities has to be considered. The IBSD prediction result based on the all-persistent assumption will form the end member with smaller block sizes, and the real IBSD is always larger than this prediction result.

Introducing the above relative impersistence factor F_{imp}, a prediction of IBSD which incorporates the influence of impersistent discontinuities can be made such that existing techniques for the prediction of IBSD, including those developed in Chapter 3 and by Wang (1992), can be employed.

Suppose $(V_{i,p})_0$ represents the prediction result of IBSD using the all-persistent assumption and $V_{i,p}$ is the corrected result incorporating the influence of impersistent discontinuities on the result, then relationship proposed for $V_{i,p}$ is as follows

$$V_{i,p} = \frac{1}{(F_{imp})^q}(V_{i,p})_0, \tag{4-73}$$

in which F_{imp} is the relative persistence factor of the discontinuity population, and q is a constant less than 1. A sensitivity analysis of Eqn. 4-73 suggests that q will take a value of between 1/5 and 1/2, based on the authors experience and the analysis of the data illustrated in Fig. 4.1.

Now the empirical equation, Eqn. 2-10 for predicting IBSD of discontinuities with either a negative exponential or a uniform spacing distribution can be updated to give

$$V_{i,p} = \frac{C_{i,p}}{(F_{imp})^q}\frac{S_{pm1} \times S_{pm2} \times S_{pm3}}{\cos\theta \cos\phi \cos\alpha}, \tag{4-74}$$

$i=10, 20, ..., 100$

The empirical equations, Eqns. 3-31 and 3-32 for predicting IBSD of discontinuities with fractal spacing distributions can be updated to give

$$V_{i,p} = \frac{C_{i,p}}{(F_{imp})^q}(D_1 \times D_2 \times D_3)^{-b_{i,p}} \tag{4-75}$$

$$V_{i,p} = \frac{C_{i,p}}{(F_{imp})^q}(S_{pm1} \times S_{pm2} \times S_{pm3})^{b_{i,p}} \tag{4-76}$$

A worked example

The above updated techniques are now applied to the case study reported by Wang (Wang et al., 1991a; Wang, 1992).

The rock mass in the field was a massive sparsely jointed homogeneous "granite gneiss" on the south west coast of Norway. On an exposure of nearly 2000 m^2, 51 joints were mapped. Of these, 8 joints were considered to be impersistent. The censoring level c=3 m was used in defining whether or not a joint was persistent. In

the first instance, all 51 joints were assumed to be persistent, which formed the lower bound with smaller blocks. Using only 43 persistent discontinuities gave the upper bound with larger blocks (see Fig. 4.1).

Suppose that the characteristic size of the rock mass of interest, S_r = 5 m, and q takes the value of 1/4, using the above updating technique for this example, the results as listed in Table 4.2 are obtained.

Table 4.2 Comparison of the IBSD results updated to include the trace length data correction for impersistence, e.g. from Norwegian rock mass

	All persistent	Neg. exp. T. L. Distribution	Lognormal T. L. Distribution	Fractal T. L. Distribution*	Excluding impersistent
Mean trace length m_l (m)		1.619	1.625	0.735	
Mean size S_D (m)		1.261	1.198	0.370	
F_{imp}		0.252	0.240	0.074	
$1/(F_{imp})^{1/4}$		1.411	1.429	1.918	
V_{50} (m^3)	4.950	6.985	7.076	9.493	7.690

*For fractal trace length distribution, l_u and l_l are respectively 30 m and 0.05 m

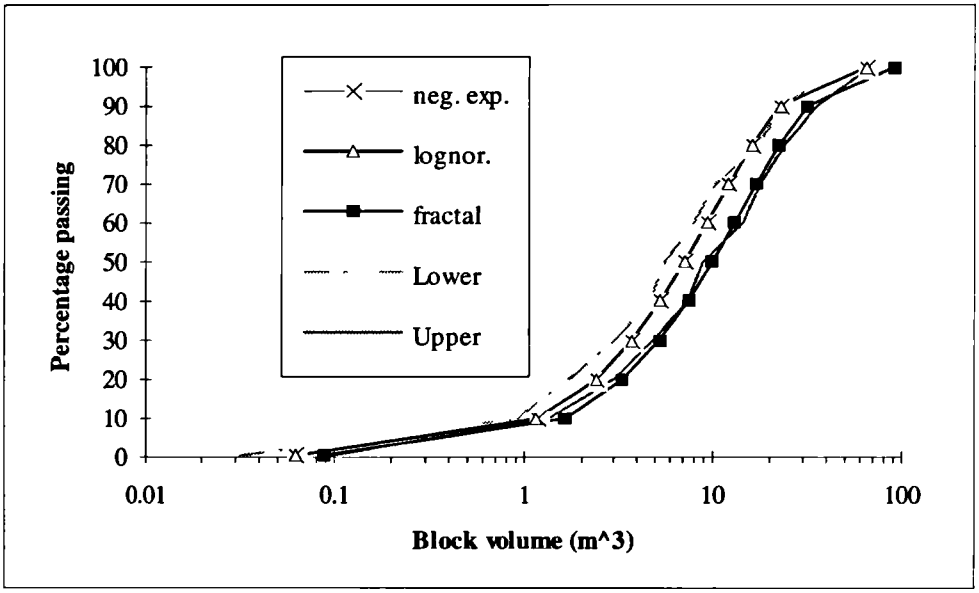

Fig. 4.17 Comparison between the updated IBSD using trace length censored data (with $q=1/4$) to account for impersistence and the original IBSD results using the all-persistent assumption for 51 (lower) and 43 (upper) discontinuities

The corrected IBSDs have been compared to the upper and the lower IBSD bounds resulting from the dissection method using raw data for the two different considerations of discontinuity persistence (see Fig. 4.1) and are illustrated in Fig. 4.17. It can be seen that the corrected results using the equation method for the cases of negative exponential and lognormal trace length distributions, as expected, fall within the zone defined by these upper and lower bounds. By contrast, the corrected result for fractal trace length distribution is partly beyond the zone. This could be for a number of reasons but the most likely is that field data for the discontinuity trace lengths are not in fact well described by a fractal trace length distribution.

It is shown from the above example that using the information about trace lengths (including: n, the total number of discontinuities; r, the number of discontinuities less than c, a given censored level; and S_r, the characteristic size of rock mass of interest), a reasoned estimation of the mean size of discontinuities and thus the F_{imp} can be determined. In turn, a prediction of IBSD accounting for the discontinuity impersistence can be made by applying a correction to the existing techniques that are based on the all-persistent assumption. Such a prediction is obviously an advantage over one in which only lower and upper bounds are given. The technique devised above will be applied to the practical IBSD prediction in a case study described in Chapter 7, although it is acknowledged that the errors associated with the technique are in need of further study.

5. ESTIMATING THE BLOCK SIZE DISTRIBUTION OF A BLASTPILE USING PHOTOGRAPHIC TECHNIQUES

Previous chapters have focused on the development and updating of techniques which can be used to predict the IBSD. The most promising approaches for predicting fragmentation in blasting will tend to use the IBSD as input data. However, as discussed in Chapter 2, to assess whether a blasting operation is optimal or whether a blast design model is working, requires an appraisal of the actual BBSD. Thus, the methods of assessment of BBSD have been an important topic in quarrying and mining. To some extent, advances in predicting the results of a given blast design in a particular rock mass have been hampered by the poor accuracy and scarcity of BBSD estimation methods. An ideal technique for the assessment of BBSD should be reasonably accurate, cost-competitive and user-friendly. The exclusive and expensive methods discussed in Chapter 2, appear not to meet all these requirements. The direct photographic and image analysis techniques usually need complex equipment and software. The indirect prediction approaches based on theoretical models do not have their governing parameters determined with sufficient reliability. However, in combining parts of the prediction models that give the general forms of the most typical BBSDs with a simple photographic method, a technique which may meet all the above requirements will be made in this chapter.

5.1 THE RATIONALE

It is recognised that surface measurements can give a reasonably representative estimation of the blasting fragmentation (Noren & Porter, 1974, Nie & Rustan, 1987; Franklin & Maerz, 1988). Assuming perfect mixing occurs, the information of block size distribution exhibited on a blastpile surface, will reflect the underlying block size distribution of the complete blastpile. Statistically, there exists a relationship between the volumes of blocks in a blastpile and the one- or two-dimensional projecting information (cf. Santalo, 1976; King, 1984), for instance, projecting length or area represented on the blastpile. In other words, the greater is the value of the projecting length of a block, the larger is its volume. That means there should be a relationship between the underlying distribution and the surface distribution. This is the basis of all existing photographic or image analysis methods of block size distribution. Once the relationship between the distribution of block size on the surface of a blastpile and the

underlying distribution is established, the underlying distribution can be derived from the photographs taken of the blastpile surface. Taking this into consideration, a technique of assessing the BBSD based on the surface information of a blastpile can be developed.

5.2 PHOTO-SCANLINE TECHNIQUE

As discussed in Chapter 2, a great number of theoretical and experimental studies, and, practical operations of quarrying and mining indicate that both the Rosin-Rammler and the Schuhmann equations (see Eqns. 2-8 and 2-9) can often effectively characterise the block size distribution of a blastpile.

It can be seen that both the Ros-Ram and the Schuhmann equations are characterised by their two governing coefficients, one locating its position, another characterising its slope on the accumulative plot. Once these two coefficients are obtained, the corresponding equation giving the percentages of all fragment sizes is determined. Based on the assumption that the BBSD will statistically be distributed according to either the Ros-Ram or the Schuhmann equation, it is possible to estimate the governing coefficients of either the Ros-Ram or the Schuhmann equation using the geometric information obtained from a photograph taken of a blastpile. The information needed is the distribution of surface sizes and as shown below, this can be obtained from scanline block intersection lengths. What is interesting is that the intersection length are found to also have a Ros-Ram or a Schuhmann form. It is therefore logical that the underlying block size distribution can be estimated if the following relationships can be established:

$$Z_{ai} = f(Z_{pi}), \tag{5-1}$$

where Z_{ai} and Z_{pi} are the coefficients for the actual distribution and for the photographic measured distribution respectively. For example, Z_{ai} and Z_{pi} could be S_c (or n) in the Ros-Ram equation.

A technique referred to here as the "photo-scanline technique" is developed below to enable the BBSD information of a blastpile to be assessed. This is a method similar to the scanline technique used when mapping discontinuities on an exposure. As illustrated in Fig. 5.1, on a properly scaled photograph of a blastpile (in the laboratory, this blastpile is replaced by an artificial blastpile), several parallel straight lines (i.e.

scanlines) are aligned along representative directions and these intersect a sample of exposed blocks. For each scanline aligned, the lengths of visible blocks exposed on the surface and intersected by the line are recorded. All records from these scanlines are combined into one record of block intersection lengths. It is assumed that the three principal axes of each block lie with random orientation with respect to other blocks on the surface so that the accumulated block length records represent the one-dimension surface information of the BBSD of the blastpile. The parameters, S_c and n (or S_{100} and m for the Schuhmann equation) for the blastpile can then be determined using a relationship derived by comparing the length distribution information of the one-dimensional surface intersection to the BBSD information determined by directly sieving artificial blastpiles.

Fig. 5.1 Schematic illustration of the photo-scanline technique (the scale rod in the centre of the photograph has a 50 cm division).

For an actual blastpile, several representative photographs are taken of the blastpile, and the values of S_c and n (or S_{100} and m) are determined using the above technique. Taking the average of all photographic results for the blastpile, the governing parameters S_c and n (or S_{100} and m) are obtained. The method is considered likely to be more accurate if it can be extended into a field scanline technique. However, this will usually interrupt normal production.

The success of the technique is largely due to the suspected and confirmed observations that the length information of one-dimensional surface intersection tends to have a Ros-Ram form and can thus be fitted by a Ros-Ram equation and that these Ros-Ram coefficients are found to be closely related to the Ros-Ram coefficients of the whole blastpile.

5.3 ERRORS IN USING PHOTOGRAPHIC TECHNIQUES

Ideally, the photographs should be taken perpendicular to the blastpile surface. However, practical factors make this seldom possible. Even when a photograph is taken perpendicular to the blastpile surface, wide-angle lens distortions can occur and the blastpile surface may not be planar. As a result, a projecting error will be introduced into the information of block sizes represented by a photograph and the use of specialist or long focal length lenses will help decrease the source of error. In addition, use of square frames or correction grids on the blastpile surface is to be encouraged.

The influence of block overlap becomes more significant as the viewing angle moves away from perpendicular to the surface. There are also two types of cut-off errors: (i) the edge of photographs causes artificial effects on a scanline since block termination are unknown; (ii) the photograph will only resolve down to a certain size of fragment so that blocks of maybe < 5 cm trace length will remain undetected even though these fines could be 20% or so. In fact, the new technique which uses the well established Ros-Ram and Schuhmann equations will tend to compensate reasonably well for the problem of unknown fines in the blastpile because they would have been equally unresolved but accounted for in the calibration procedure.

The above error sources will reduce the accuracy of the photo-scanline technique. Keeping these in mind and reducing these errors as much as possible, it is possible to obtain reasonably accurate BBSD results.

5.4 DERIVING 3-D INFORMATION FROM 1-D MEASUREMENTS

Without going into detail, it is interesting to consider briefly the significance of the one dimensional size parameter that is being sampled by the lengths intersected on the

surface scanline, hereafter referred to as nominal length. Because blocks tend to lie with their minimum axes vertically, they will tend to present a maximum rather than a random (i.e. average) projection area upwards, thus tending to give longer line segments than is representative of average projection or sieve diameters. However, the overlap effect and segmenting effect of different faces appearing as separate particle will both tend to reduce the nominal length below those of sieve diameters. The overall value of nominal length being sampled may therefore be quite close to the nominal diameter d_n which is the cubic root of the actual volume of a block and is somewhat smaller than the sieve diameter (see below):

$$d_n = k\,S, \tag{5-2}$$

where, S is the sieve size (the aperture of a squared hole through which a block can just pass); k is a shape factor. For 'prismatic' aggregate-sized natural rock fragments k=0.847 was used (Wang, 1992). For rounded blocks, Wang suggested k=0.913. For a generally applicable value for larger and different shape blocks, k=0.84 is recommended (CIRIA/CUR, 1991). The volume of a block can then be given by

$$V = d_n^3. \tag{5-3}$$

5.5 RELATIONSHIP BETWEEN ACTUAL AND ESTIMATED PARAMETERS

As discussed above, the photo-scanline technique will yield, say for the Ros-Ram equation, $S_c(p)$ and $n(p)$. Here (p) represents the estimates of parameters from the distribution of nominal lengths using the photo-scanline technique. Of course, sieving blocks of a blastpile or a truckload will yield its actual block size distribution, but this is not practical. A laboratory experiment using a set of artificial blastpiles with different known block size distributions, which are characterised by their S_c and n for the Ros-Ram equation (or S_{100} and m for the Schuhmann equation), was therefore conducted with appropriate surface photographs being taken.

The experiment was prepared and carried out in the following steps:

(1) Approximately 100 kg of crushed limestone aggregate with sizes up to 150 mm was collected. Coarse sand fractions were also obtained.

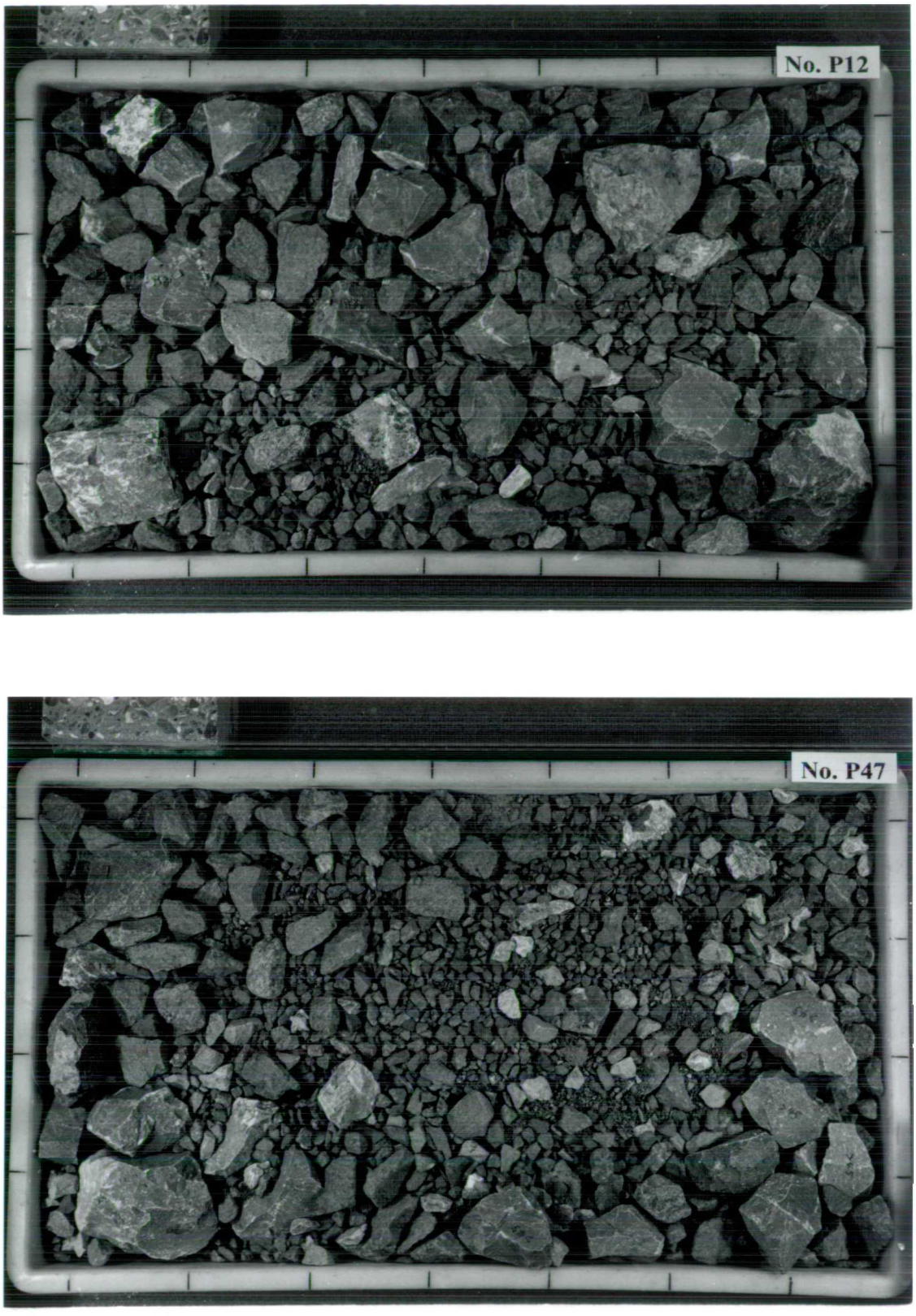

Fig 5.2 The photographs of two artificial blastpiles consisting of aggregates used in the experiment (No. P12: n=1.35, S_c=55 mm; No. P47: n =0.9, S_c=25 mm)

(2) The aggregates were then screened into 12 fractions using a series of sieves from 1 mm to 125 mm. Each aggregate fraction was weighed and its median sieve size was calculated (except for the first and last fractions).

(3) A range of pre-set values of S_C and n were chosen to cover a wide range of prototype distributions. The required fractions of each size range were calculated for a specified (S_C, n) artificial blastpile. Then all fractions were prepared, weighed out, mixed together and dumped onto a flat pan 71.5 by 41.5 cm, giving the required artificial blastpile (S_C, n), as shown in Figure 5.2.

(4) A photograph was taken of the surface of the pile keeping the camera lens perpendicular to the surface.

(5) The above photo-scanline technique was applied to the photographs to obtain the nominal length distribution and the corresponding parameters, $S_C(p)$ and $n(p)$ were determined using a statistical analytical technique.

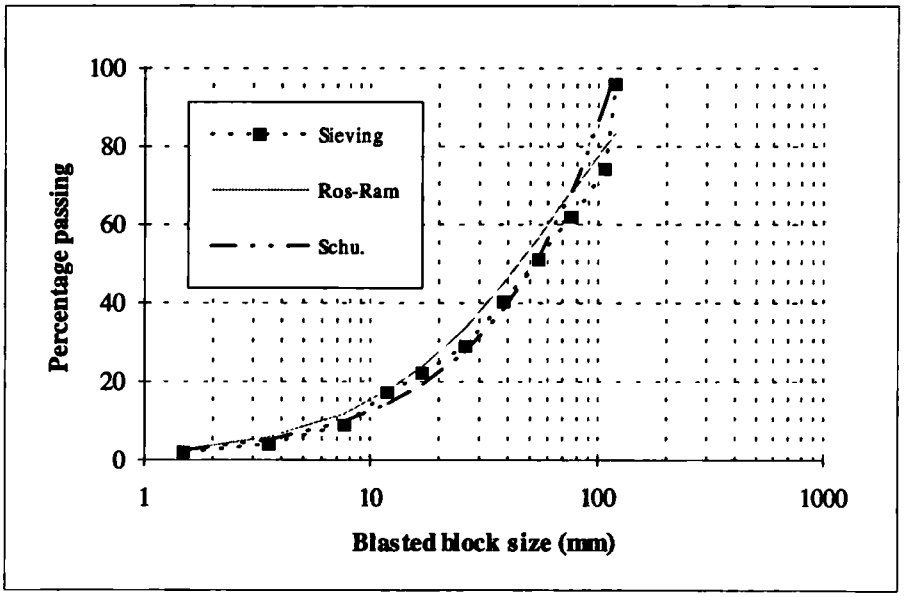

Fig. 5.3 The block size distribution for an artificial-blastpile with fitted Ros-Ram and Schuhmann equations (n=0.96, S_C=65 mm, m=0.84, S_{100}=120 mm).

In total, 30 artificial blastpiles were prepared, each one weighed about 35 kg. The photographs of two artificial blastpiles are illustrated in Fig. 5.2. Each pile was designated by a particular combination of S_C and n. One of typical block size distribution for the artificial blastpile is illustrated in Fig. 5.3. The 30 combinations can be divided into 3 groups. The first group (of 12) had a constant n of 1.75 with S_C

varying from 10 mm to 80 mm. The second group (of 6) had a constant S_C of 80 mm with n varying from 0.5 to 1.75. The third group (of 12) included a range of S_C from 10 mm to 80 mm and a range of n from 0.5 to 1.75.

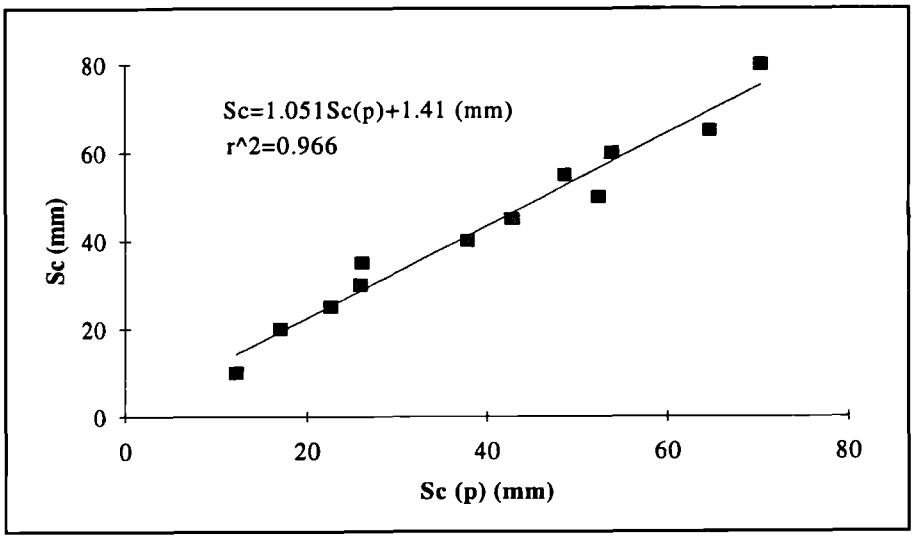

Fig. 5.4 Relationship between the values of S_C from the sieving and the photo-scanline technique (n=1.75, S_C=10-80 mm) using the first group.

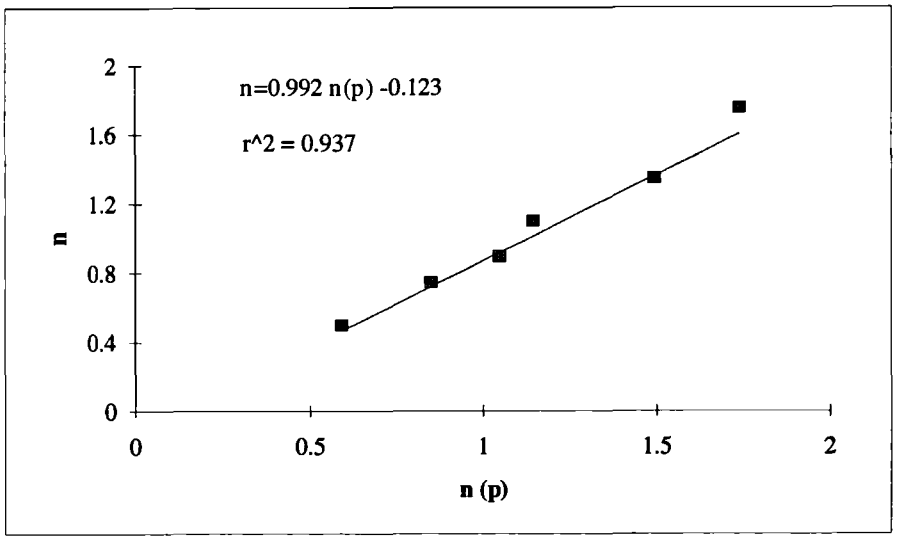

Fig. 5.5 Relationship between the values of n from the sieving and the photo-scanline technique (S_C=80 mm, n=0.5-1.75) using the second group.

For the first group, the relationship between the values of S_C and $S_C(p)$ is illustrated in Fig. 5.4. For the second group, the relationship between the values of n and $n(p)$ is illustrated in Fig. 5.5. For the third group, the relationships between the values of S_C and $S_C(p)$, and between n and $n(p)$ were examined and shown in Figs. 5.6 and 5.7.

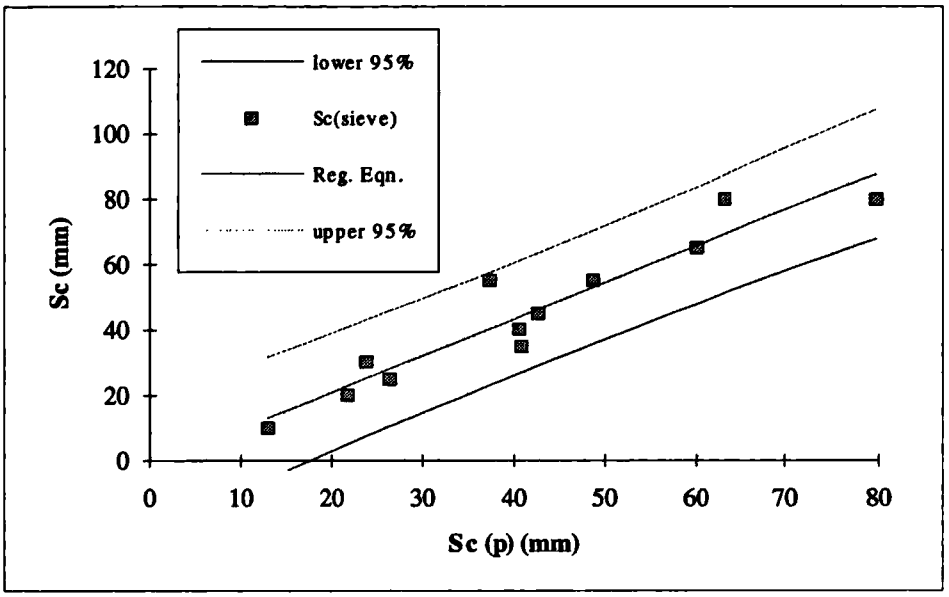

Fig. 5.6 Relationship between the values of S_C from the sieving and the photo-scanline technique with ±95% significance levels (S_C=10-80 mm, n=0.5-1.75)

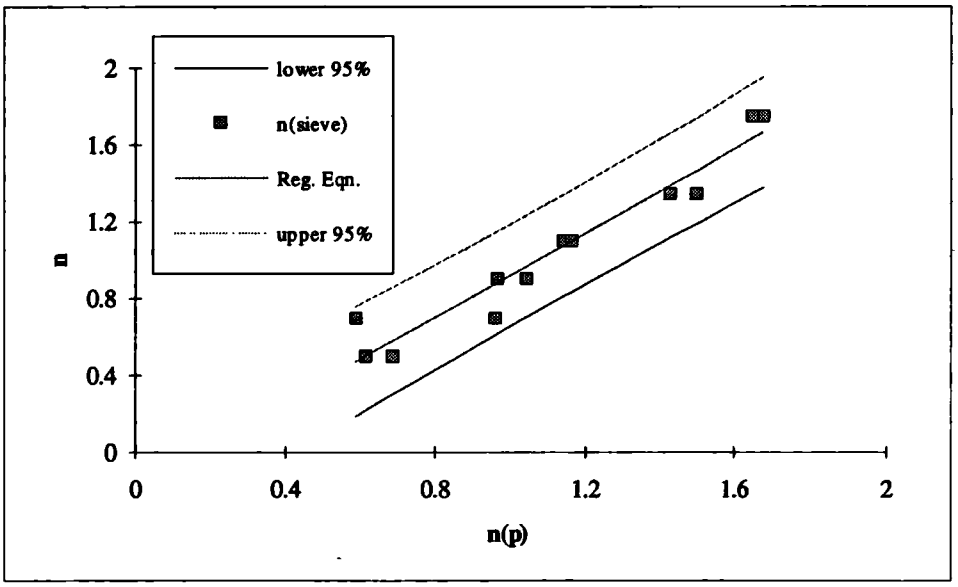

Fig. 5.7 Relationship between the values of n from the sieving and the photo-scanline technique with ±95% significance levels (S_C=10-80 mm, n=0.5-1.75)

It can be seen from Fig. 5.4 to Fig. 5.7 that all the results show good linear relationships between the actual parameters obtained from sieving and those estimated from the intersection lengths using the photo-scanline technique. Finally, the results from the third group are utilised to derive the relationship between the actual parameters and those obtained using the photo-scanline technique, since the variation in both S_C and n in the third group was included. The results are as follows.

$$S_c = 1.119 S_c(p), \tag{5-4}$$

$$n = 1.096 n(p) - 0.175, \tag{5-5}$$

where S_C and n are the actual parameters in the Ros-Ram equation, and $S_C(p)$ and $n(p)$ are those estimated by the photo-scanline technique. The Pearson r-squared correlation coefficients are 0.9503 for Eqn. 5-4 and 0.9680 for Eqn. 5-5 respectively.

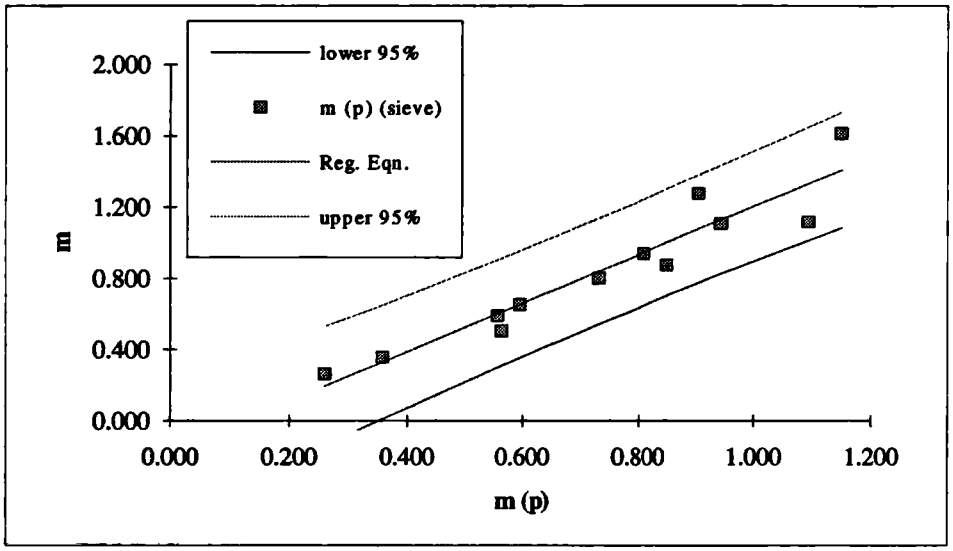

Fig. 5.8 Relationship between the values of m from the sieving and the photo-scanline technique with ±95% significance levels (S_{100}=59-152 mm, m=0.26-1.62)

When using the Schuhmann equation, the following relationships are obtained:

$$S_{100} = 0.964 S_{100}(p), \tag{5-6}$$

$$m = 1.360 m(p) - 0.156, \tag{5-7}$$

where S_{100} and m are the actual parameters in the Schuhmann equation fitted from the sieving results, and $S_{100}(p)$ and $m(p)$ are those estimated by the photo-scanline technique. The values of S_{100} varied between 59 and 152 mm, and the values of m between 0.26 to 1.62. The correlation coefficients are 0.9252 for the Eqn. 5-6 and 0.9752 for Eqn. 5-7 respectively (see Figs. 5.8 and 5.9).

From consideration of estimated parameters within the 95% significance levels, the above results suggest that the photo-scanline technique for assessing the block size

distribution of a well-mixed blastpile could have a reasonable accuracy. This is encouraging for the application of this technique to the practical assessment of blastpiles and to help calibrate better prediction methods for BBSD.

When applying the technique to prototype blastpile photographs, the distribution of surface intersection lengths is presented as a percentage shorter passing plot and the best fitted $S_C(p)$ and $n(p)$ parameters are found and then substituted into Eqns 5.4 and 5.5 to find the S_C and n for the blastpile.

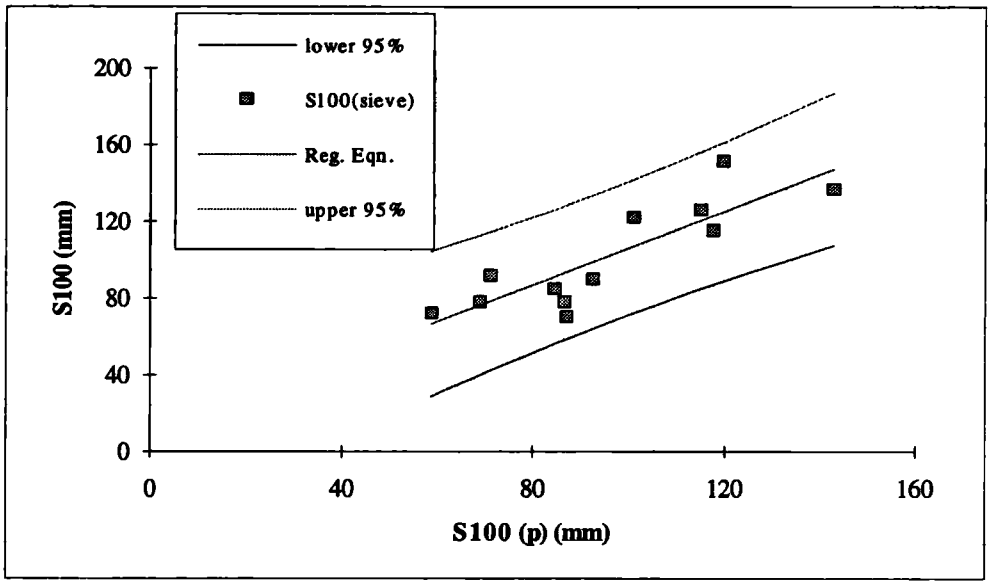

Fig. 5.9 Relationship between the values of S_{100} from the sieving and the photo-scanline technique with ±95% significance levels (S_{100}=59-152 mm, m=0.26-1.62)

After obtaining the S_C and n (or S_{100} and m), the volume or weight parameters, V_C and V_{100} can be determined through Eqn. 5-3, and n_v and m_v can be obtained by

$$n_v = 3\,n, \tag{5-8}$$

$$m_v = 3\,m. \tag{5-9}$$

The whole block size distribution of a blastpile in terms of block volumes can therefore be estimated.

The main advantages of the technique described above are that a reasonably accurate assessment of the BBSD of a blastpile can be obtained and that it is simple and does not need any image analysis software and sophisticated equipment.

However, just as with the image analysis technique, the following consideration should be taken into account when using the technique.

(1) Obtaining photographs is central to the application of this method. The quality of photographs taken will play an important role in its practical application. As a result, it is advised that photographs be taken as near as perpendicular to the blastpile as possible. The use of long focal length zoom lenses may help reduce distortion and the overlapping error to a minimum.

(2) The proper scaling is another key factor. It is recommended that at least one scaling square (board) or pair of perpendicular scaling bars should be placed on each blastpile prior to taking the photograph. One scaling reference should be ideally placed on the central part of a photograph.

(3) The eventual blasted block sizes are typically distributed in the range from 1.0 mm (and down to dust) to over 1.0 m. The size range of aggregates of the artificial blastpile used in the experiment varies from 1.0 mm to 150 mm. This range is comparatively small and may be representatives of only one part of the fine or coarse part of the actual block size range. This consideration may influence the applicability of Eqn. 5-4 to Eqn. 5-7 when used for the practical assessment of BBSD in full scale blastpiles.

(4) An actual blastpile might be different from an artificial one. The relationships expressed by Eqn. 5-4 to Eqn. 5-7 are derived from a set of artificial blastpiles consisting of crushed limestone and sand. These differences may effect the application of these equations.

(5) The representativeness of the surface blocks has been an important issue of the blast of employing image analyses technique. Using photographs taken from the back of dump trucks has not been mentioned. However, such photographs might have better representativeness than surfaces of blastpiles (Franklin & Maerz, 1988). Thus, it is suggested that both photographs taken from a blastpile surface and from the back of dump trucks should be used to improve the representativeness.

In Chapter 7 the technique developed in this chapter will be used for assessing the BBSD of actual blastpiles.

6. BLASTABILITY OF ROCK MASS AND ITS ASSESSMENT

In previous chapters, the estimations of both IBSD and BBSD were examined and new techniques introduced. This chapter will focus on characterising the blastability of a rock mass. It will also focus on the understanding of the relationship between the blastability and the properties and discontinuity structure of the rock mass. Here, blastability is considered to be a composite intrinsic property of the rock mass describing the ease, in energy terms, with which it can be blasted.

It was noted from the discussion in Chapter 2 on the blastability of a rock mass that in-situ rock mass properties are among the most important contributory factors in fragmentation, and that the characterisation of the blastability has become a pressing task for blasting operations. It was also found that a rigorous rock blastability system which incorporates the mechanical properties of a rock mass, in-situ block size, and the input energy, based on the current scientific understanding of fragmentation, has not yet been achieved. Consequently, an attempt to develop a blastability characterisation system will be made in this chapter, in order to help direct a blasting operation towards a more optimal result. The development of the blastability system will be on the basis of current understanding of the fragmentation process drawn from the literature findings. Firstly, the development will focus on the characterisation of blastability and its physical background. After that, the Rock Engineering Systems approaches will be used to establish a blastability system.

6.1 CHARACTERISATION OF THE BLASTABILITY AND THE ENERGY-BLOCK-TRANSITION MODEL

Two different rock masses, when subjected to identical blast geometry and energy input from explosives, will produce quite different degrees of fragmentation. This is because the rock masses have inherently different blastability.

The fragment size is a fundamental characteristic, and is governed by the geomechanical nature of the host rock mass and the distribution of explosive energy related to blast design (Singh et al, 1991). As shown in Fig. 6.1, blasting can be looked upon as a transformation from the state with IBSD to the state with BBSD. This transforming process is implemented by inputting a certain energy, i.e. a quantity of explosive.

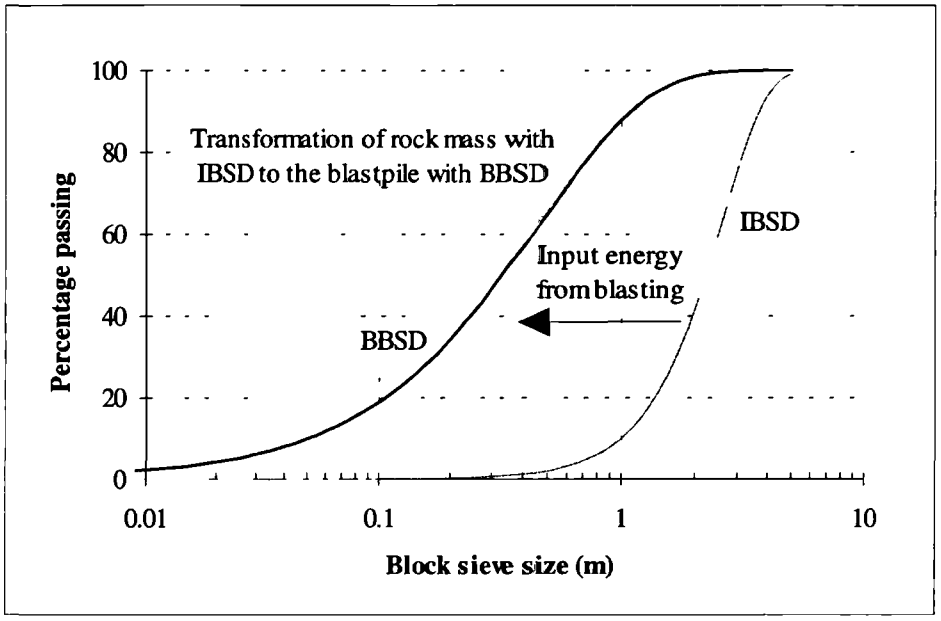

Fig. 6.1 Illustration of the transformation of rock from the in-situ state with IBSD into the blastpile state with BBSD by inputting a certain explosive energy

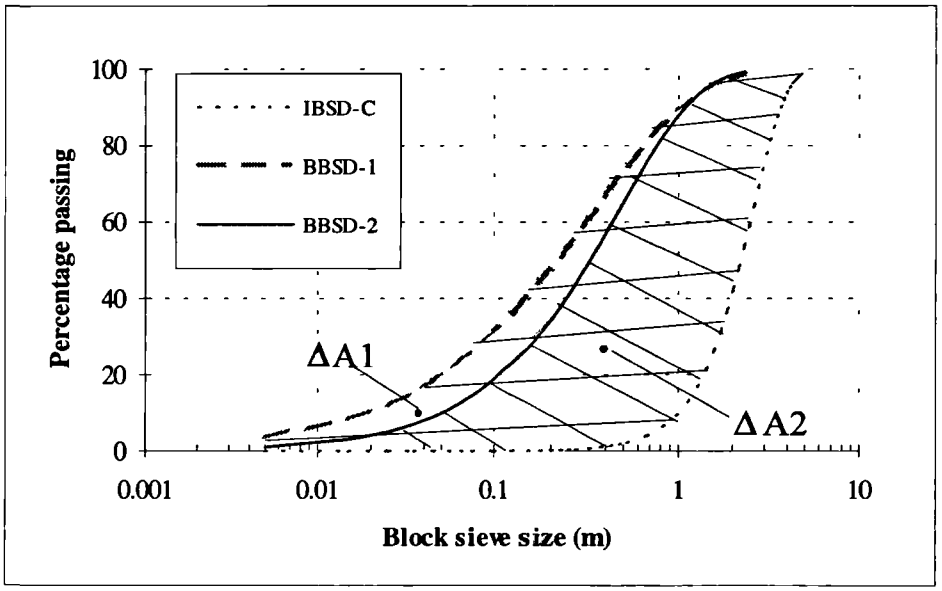

Fig. 6.2 The concept of blastability: two different rock masses with the same IBSD but with different blastability are transformed to two different BBSD curves

The transforming process might be very complicated, however, the transforming result can be indicated by the resultant blastpile. Suppose that E_S represents the explosive energy input per unit rock mass that is consumed in transforming the rock mass with a given IBSD into a blastpile with a given BBSD and that ΔA, a property of any fragmentation process is the area enclosed by the IBSD and BBSD curves and the 0 and 100% passing lines (see Fig. 6.2, for convenience, ΔA will be called the

transformation area), let us consider a possible relationship characterising the blastability of a rock mass.

In Fig. 6.2, two different rock masses with the same IBSD are noted *IBSD-C*. *BBSD-1* and *BBSD-2* are the BBSDs of the first and the second rock masses obtained by inputting an identical amount of explosive energy. The transformation areas for the two different rock masses subject to identical blast design are represented by ΔA_1 and ΔA_2. The second rock mass proves to be intrinsically more difficult to fragment by blasting than the first one although their IBSDs are identical, since the second blastpile contain many more large blocks than the first. For reasons that will become clear later, the area bounded by the IBSD and BBSD curves (and the 0 and 100% passing line), for a particular blasting operation, is considered to have special significance.

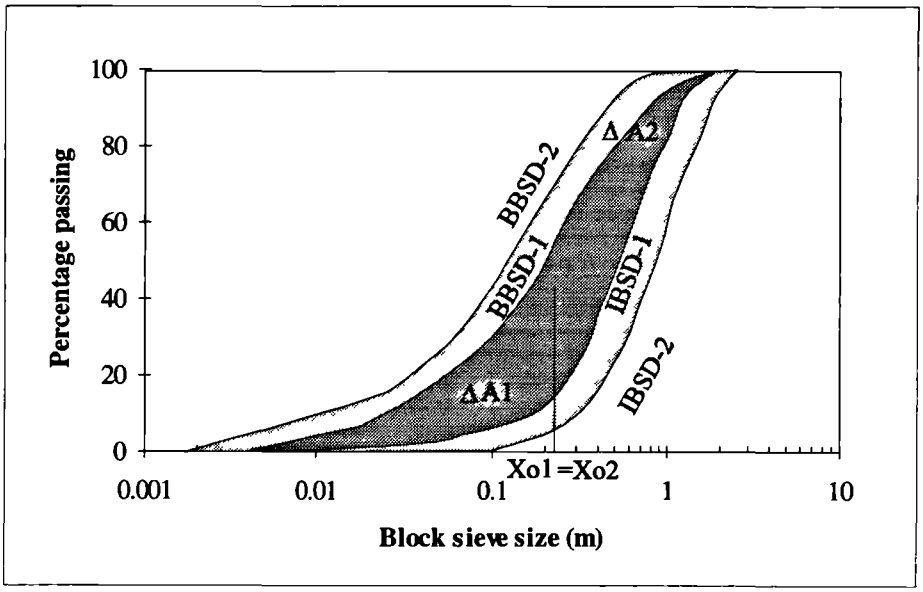

Fig. 6.3 Illustration of two different rock masses with different intrinsic resistance to fragmentation subject to the same input of explosive energy and blast design: two different rock masses with different IBSD curves (but with the same objective size X_O) are transformed to two blastpile with different BBSD curves. The difference between ΔA_1 and ΔA_2 indicates the difference in blastability between the two rock mass

Further, consider another case where the enclosed areas for the two different rock masses subject to identical input of explosive energy and blast design are as represented by Fig. 6.3. Now ΔA_2 represents the very effective transformation of relatively large in-situ blocks to a blastpile with a high fines content, whereas ΔA_1 is

the less effective transformation for comparatively smaller in-situ blocks to a blastpile with few fines. Notice that both transformations are with the same X_O, the gravitational centre of the geometric shape of ΔA; the significance of X_O will be discussed below. Obviously, the transformation indicated by ΔA_2 has to overcome more intrinsic resistance than the transformation indicated by ΔA_1. ΔA_1 is clearly much less than ΔA_2, and the possibility must exist that the different areas could be an indicator of the blastability of these two rock masses.

Actually, the points discussed above on the relationship of blastability with the energy, the in-situ block sizes of a rock mass and the blasted block sizes were addressed by a number of previous researchers who used theoretical and empirical equations to relate the input energy and the block sizes both before and after blasting, Possibly, the best known is Bond's Third Theory (Bond, 1952) in which Bond's work index, W_i is believed to provide a good representation of the resistance of rock mass to crushing, grinding, and breaking by blasting (Bond & Whitney, 1959).

In another case Schuhmann (1960) presented a relationship between energy input from the process of comminution and the size distribution of particles as follows:

$$E = C\frac{y}{100}x^{-\alpha}, \qquad (6\text{-}1)$$

where, E is energy input per unit volume of material; y is cumulative percent finer than x; x is particle size; α depends on the size distribution and C is a constant. Eqn. 6-1 states that the energy input is directly proportional to the cumulative percent finer than any given size x. Meanwhile, the equation also provides a simple measure of grindability ($1/C$) as the volume of comminuted material finer than unit size produced per unit of energy expended (Schuhmann, 1960)

The Kuznetsov equation (see Eqn. 2-11) also relates the resulting block size to the input energy and the in-situ rock properties. This equation appears to give a measure of blastability of a rock since the term V_b/Q and Q in the equation can be considered to be a measure of input energy; S_{b50} represents the block size after blasting and the rock factor A, to some extent, accounts for the influence of in-situ rock properties and discontinuity structures upon blasting.

Coming back to the blasting problem here, let us consider a possible relationship characterising the blastability of a rock mass. Based on the above discussion, a

working hypothesis, that $E_S \propto \Delta A$ is now introduced. In addition, it is clear that a given value of ΔA can be associated with any transformation. For example, the transformation may be for relatively large in-situ blocks to slightly smaller blocks in a blastpile or alternatively, a transformation with the same ΔA could be for relatively small in-situ blocks to a blastpile resembling powdery fines (see Fig. 6.4). But, because the latter case requires the generation of much more fracturing and surface area, it is logical that it would consume more energy. For each transformation with a certain value of ΔA, an effective size parameter, that can reflect this inverse size effect associated with an increase in energy consumption, could be, X_O, the gravitational centre of the geometric shape of ΔA. The empirical energy-size relation (Charles, 1957; Schuhmann, 1960, Nagahama & Yoshii, 1993) refers to an objective size parameter that has a similar significance to this effective size parameter and indicates that in general, the energy consumed in size reduction is inversely proportional to the objective size raised to some power. Combining the above working hypothesis with the definition of X_O, the following relationship is proposed,

$$E_s \propto \frac{\Delta A}{X_o^n}, \tag{6-2}$$

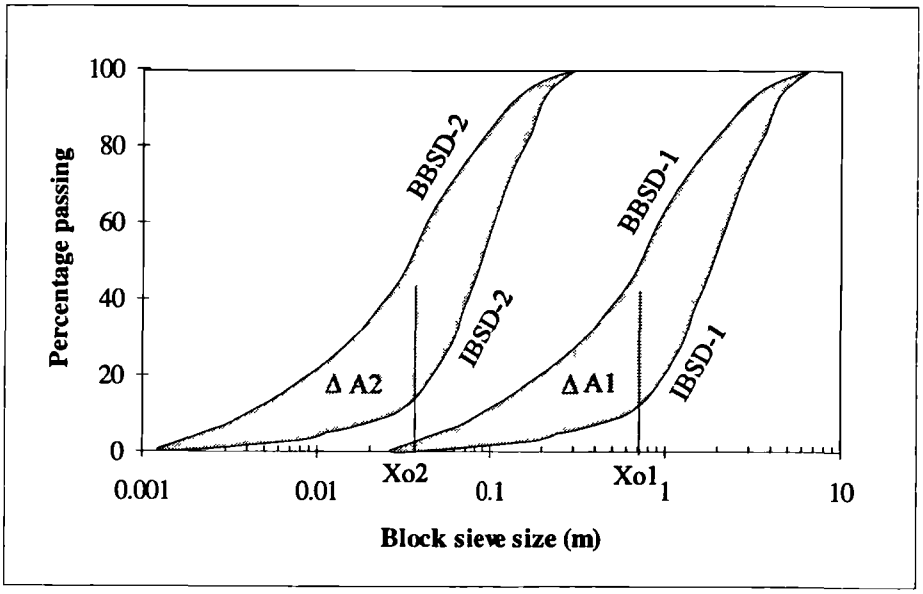

Fig. 6.4 Illustration of the dependence of energy E_S on an objective size X_O: two transformations of different rock masses with the same ΔA but different objective size X_O, $X_{O1} > X_{O2}$ and $E_{S1} < E_{S2}$, i.e. these two rock masses have a different blastability

By introducing a coefficient in the above relation, and substituting n=1/2 (the justification for which is given later), it can be written as

$$E_s = C_b \frac{\Delta A}{X_o^{1/2}}, \tag{6-3}$$

where C_b is a constant, relating the specific energy required to implement the transform process, or as

$$B_i = \frac{1}{C_b} = \frac{1}{E_s} \frac{\Delta A}{X_o^{1/2}}. \tag{6-4}$$

It can be seen that the value of B_i is an indicator of the ease with which the process of transforming the rock mass with IBSD into the blasted blocks with BBSD is implemented. The coefficient B_i is herewith referred to as the Energy-Block-Transition coefficient, and correspondingly, Eqn. 6-3 is hereafter referred to as the Energy-Block-Transition model. The following sections will explore the extent to which the model can describe the mechanism of fragmentation of a rock mass by blasting.

6.2 DETERMINATION OF PARAMETERS IN THE ENERGY-BLOCK-TRANSITION MODEL

6.2.1 Energy Input E_S

The energy in a blast is created by detonation of explosives. The energy released can be grouped into useful and wasteful parts (Konya & Walter, 1990). Useful energy is utilised in the fragmentation process in terms of both shock energy and gas energy. Wasteful energy does not in itself lead to fragmentation and does no useful work during a blasting process, and is finally expressed as acoustic energy, heat energy in the fragmented mass and released gases, light energy and seismic energy.

Strictly, the energy input E_S discussed in Section 6.1 should be the useful part of the energy released on detonation of explosives. The partition of the explosive energy in a blasting operation is a significant subject of current research, but a widely accepted process of energy utilisation in rock fragmentation by blasting seems still to be lacking. As a result, the precise description of the amount of explosive energy that is utilised as useful energy is limited. Thus, following Bond's model (Bond, 1952) and applications of Bond's model (Bond & Whitney, 1959; Da Gama, 1983; and CIRIA,

1991; Wang et al, 1992), E_S is broadly considered here to be the energy expended in the blasting divided by the total volume of rock mass, and is given by Eqn. 2-15, i.e.

$$E_s = \frac{0.00365 E_e P_f}{\rho}, \tag{6-5}$$

the notation for Eqn. 6-5 is the same as Eqn. 2-15.

6.2.2 Transformation Area, ΔA

A general expression for the transformation area that is applicable to any form of the in-situ or blasted block size distributions is derived and given in Appendix C1, where, an insight into the physical interpretation of transformation area, ΔA, is also given. The expression is:

$$\Delta A = S_{ai} - S_{ab}, \tag{6-6}$$

where, S_{ai} and S_{ab} are the mean sizes of both IBSD and BBSD respectively. They are given by the following mathematical definition for the mean of a size distribution:

$$S_a = \int_{S_l}^{S_u} S f(S) dS, \tag{6-7}$$

where, $f(S)$ represents the probability density function of block size; S_l represents the low boundary of block size, it may often be zero; and S_u is the upper boundary of block size.

It is instructive to compare S_c, S_{50} and S_a for a range of steepness in the cumulative size curves. Fig. 6.5 shows the relationships for a practical range of n-values in the Ros-Ram equation.

The ratio of S_a/S_{50} was derived (see Appendix C.2) by direct substitution of the Ros-Ram equation into Eqn. 6-7 as follows

$$\frac{S_a}{S_{50}} = \frac{\Gamma(1+\frac{1}{n})}{(\ln 2)^{\frac{1}{n}}}, \tag{6-8}$$

where, Γ is the Gamma function, and is defined by

$$\Gamma(\alpha) = \int_0^\infty x^{\alpha-1}e^{-x}dx, \qquad \alpha>0 \qquad (6\text{-}9)$$

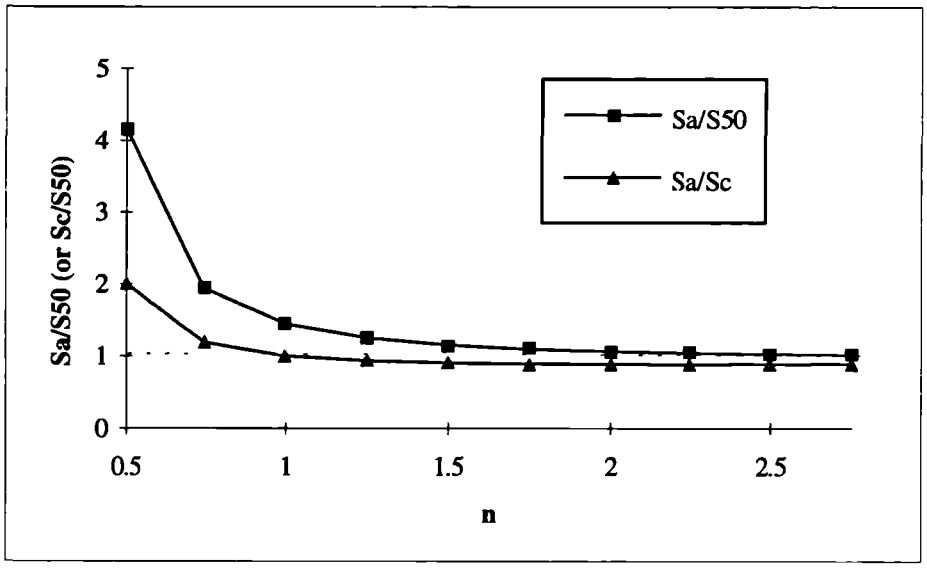

Fig. 6.5 Relationship between S_a/S_{50}, S_a/S_c and n for a practical range of n-values in the Ros-Ram equation

Thus, the mean blocks size S_a is different from the 50% passing size S_{50} although they approach each other at higher n-values (see Fig. 6.5). However, S_a might be approximated by S_{50} (or S_c) when n is comparatively large, (say, larger than 1.5). It is considered advisable to use S_{50} to approximate S_a when the block size distribution can be described using the Ros-Ram equation and n is larger than 1.5.

Suppose that both IBSD and BBSD have a theoretical distribution, say either the Schuhmann or the Ros-Ram distribution, let us look at the expression of ΔA.

Schuhmann Equation

Suppose that both the IBSD and the BBSD are the Schuhmann distributions, i.e. they both have the form represented by Eqn. 2-9 as follows

$$P_i = (\frac{S_i}{S_{100i}})^{m_{Si}}, \tag{6-10a}$$

$$P_b = (\frac{S_b}{S_{100b}})^{m_{Sb}}, \tag{6-10b}$$

The transformation area ΔA can then be derived according to Eqn. 6-6 (see Appendix C.1) as

$$\Delta A = \frac{m_{Si}}{m_{Si}+1} S_{100i} - \frac{m_{Sb}}{m_{Sb}+1} S_{100b}. \tag{6-11}$$

In practice, S_{100} is rarely determined with accuracy and precision. It is therefore advisable to make suitable substitution so that ΔA is derived from a more reliable size parameter, say S_{50} or S_{80}, located near the middle part of the distribution curve.

Ros-Ram distribution

If both the IBSD and the BBSD obey the Ros-Ram equation (see Eqn. 2-8), i.e. have the following distribution forms,

$$P_i = 1 - e^{-(\frac{S_i}{S_{ci}})^{n_{si}}}, \tag{6-12a}$$

$$P_b = 1 - e^{-(\frac{S}{S_{cb}})^{n_{sb}}}, \tag{6-12b}$$

According to Eqn. 6-6, the transformation area ΔA for the Ros-Ram distribution is as (see Appendix C.1)

$$\Delta A = S_{ci}\,\Gamma(1+\frac{1}{n_{si}}) - S_{cb}\,\Gamma(1+\frac{1}{n_{sb}}). \tag{6-13}$$

where, Γ is the Gamma function (see Eqn. 6-9).

It is worth noting that ΔA in both the Schuhmann and the Ros-Ram distributions is related to both a characteristic size and a steepness coefficient which jointly govern a block size distribution. This agrees with the commonly held view that it is not enough

to describe the influence of in-situ block size distribution of a rock mass on blasting using only one size parameter, say, S_{50} (or S_{100} in the Schuhmann equation or S_c in the Ros-Ram equation) Imagine that two rock masses with the same S_{i50} but different IBSDs have been fragmented by blasting and that they yield two different BBSDs but the same size S_{b50} (see Fig. 6.6). It is reasonable to suggest a single size parameter, whether for IBSD or BBSD or both, is not sufficient to express the important variations in the blasting process that can occur. The inclusion of ΔA in the proposed Energy-Block-Transition model accommodates this suggestion.

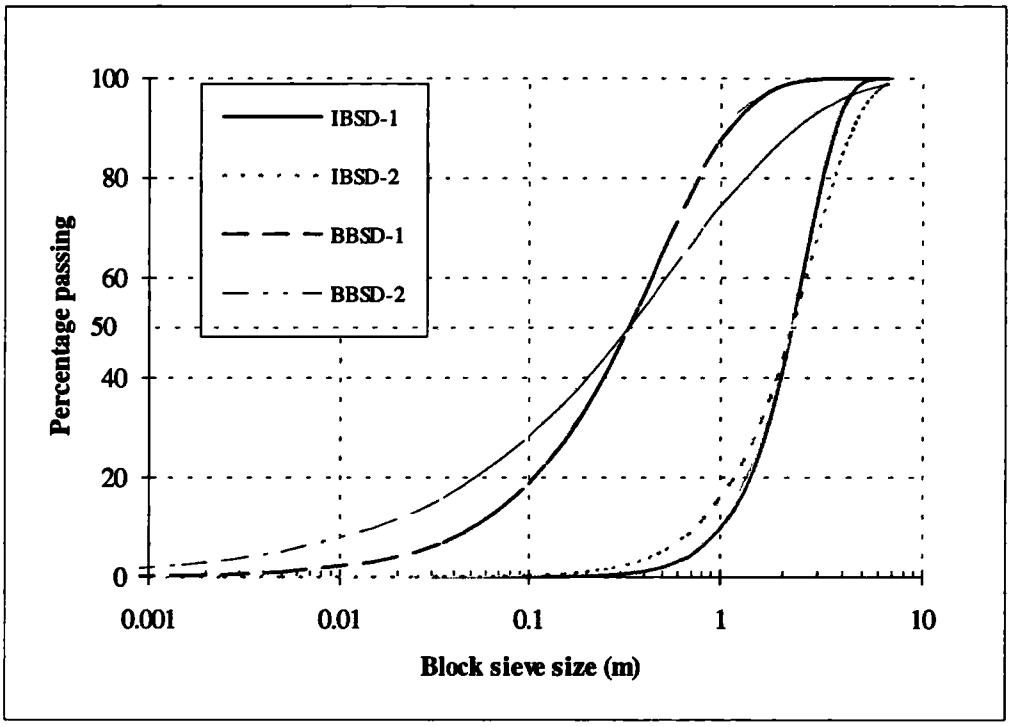

Fig. 6.6 Illustration of the insufficiency of using only one size parameter to describe blast process

6.2.3 Objective Size X_o

It was proposed in Section 6.1 (see Fig. 6.4) that X_o, the gravitation centre of a geometric shape ΔA could represent the inverse size effect associated with an increase in energy consumption in a blast process. The transformation area ΔA characterises a particular transformation of block sizes. This size location can be given the status of objective size of a blasting process and is given by the symbol X_o.

By definition of the gravitation centre of a geometric shape, X_g, as shown in Fig. 6.7, is as follows:

$$X_g = \frac{\int_{S_l}^{S_u} x[P_b(x) - P_i(x)]dx}{\int_{S_l}^{S_u} [P_b(x) - P_i(x)]dx}. \qquad (6\text{-}14)$$

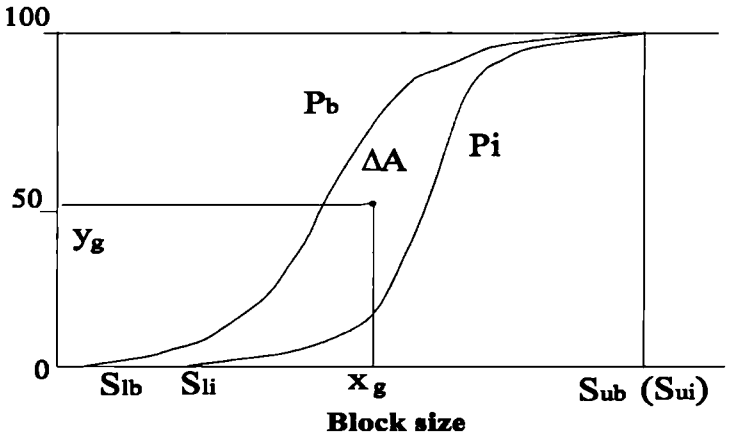

Fig. 6.7 Illustration of the gravitation centre of a geometric shape

Starting from Eqn. 6-14, we consider a simple case where both cumulative distribution curves of IBSD and BBSD are linear (shown in Fig. 6.8), which corresponds with the uniform probability density distribution. Now

$P_i = S/S_{ui}$, and $P_b = S/S_{ub}$.

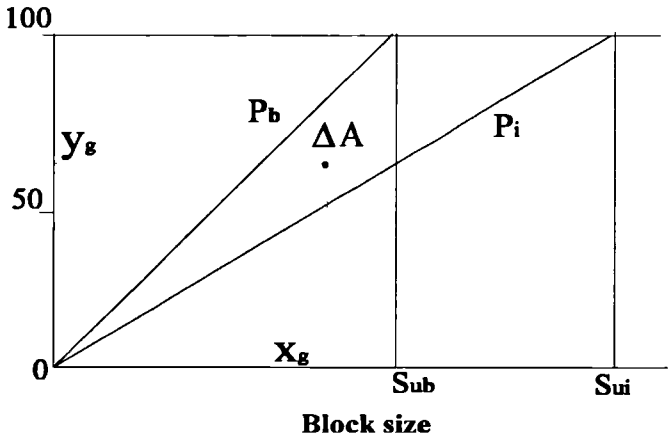

Fig. 6.8 Illustration of the gravitation centre of linear distributions of block sizes

It can be seen that the gravitation centre of ΔA, X_g in this case, is

$$X_g = \frac{4}{3}[\frac{1}{2}(S_{ai} + S_{ab})], \tag{6-15}$$

where, S_{ai} and S_{ab} are the mean sizes of both in-situ and blasted blocks.

If we consider another case where both cumulative distribution curves of IBSD and BBSD hold the Schuhmann distribution and assume that both m_i and m_b have the same value of m, it can be shown that the gravitation centre of ΔA, X_g is

$$X_g = \frac{1+m}{2+m}[\frac{1}{2}(S_{ai} + S_{ab})]. \tag{6-16a}$$

Taking into account that the value of m is usually in the range of 1 to 3, it follows that the value of X_g is

$$X_g = (\frac{2}{3} \sim \frac{4}{5})[\frac{1}{2}(S_{ai} + S_{ab})]. \tag{6-16b}$$

The location of X_g, the gravitation centre of ΔA is thus determined. The foregoing shows that X_O may therefore be represented by both the mean of in-situ block sizes and the mean of blasted block sizes where the mean size definition is given in Eqn. 6-7. Since it has now been shown that X_g is unlikely to vary above 4/3 or below 2/3 of $(S_{ai}+S_{ab})/2$, a reasonable choice of objective size is

$$X_o = \frac{S_{ai} + S_{ab}}{2}. \tag{6-17}$$

6.2.4 Physical Interpretation of the Energy-Block-Transition Model

From the foregoing sections, both the expression of the transformation area ΔA for the general case (Eqn. 6-6) and the approximation of the objective size X_O (Eqn. 6-17) have been obtained. Substituting Eqns. 6-6 and 6-17 into Eqn. 6-4, the Energy-Block-Transition model can be then represented as

$$E_s = \frac{S_{ai} - S_{ab}}{B_t(\frac{S_{ai} + S_{ab}}{2})^{0.5}}, \tag{6-18}$$

or

$$B_i = \frac{S_{ai} - S_{ab}}{E_s(\frac{S_{ai} + S_{ab}}{2})^{0.5}} \tag{6-19}$$

It can be seen that the Energy-Block-Transition model comprehensively relates the energy input, the characteristic sizes before and after blasting, and the size distributions of the in-situ and blasted blocks. The Energy-Block-Transition coefficient B_i represents the ease or resistance offered by the rock mass to the transformation from the in-situ to blasted blocks when applying a certain amount of explosive energy. To some extent, it reflects the effectiveness of the input energy in breaking up the rock. Expressed more precisely in terms of the formula's variables, the Energy-Block-Transition coefficient B_i is a measure of the intensity of the transformation of mean block size compared to the objective size X_O associated with the transformation process for a given input of energy. In the transformation process, the in-situ rock mass with large block sizes characterised by the mean block size S_{ai} is transformed into blasted blocks with small block sizes characterised by the mean block size S_{ab}. In other words, the ease with which a rock mass can be fragmented by blasting can be measured using the coefficient B_i.

The larger the Energy-Block-Transition coefficient of a rock mass, B_i, the easier it can be fragmented by a given energy input for blasting. Eqn. 6-19 reveals therefore that the rock mass with the larger B_i will be easier to break down to small blocks than the rock with lower B_i. In other words, the larger B_i means the lower resistance of a rock mass to blasting.

In his investigation of relationships between energy and size-reduction in comminution, Charles (1957) described an empirical energy-size reduction relationship which was expressed mathematically as

$$dE = -C\frac{dx}{x^n}, \tag{6-20}$$

where dE is infinitesimal energy change, C is a constant, x is an object size, and n is a constant. This relation is referred as to the Walker-Lewis relation (Nagahama & Yoshii, 1993). From Eqn. 6-20, Rittinger's first comminution theory (where, the index n is 2), Kick's second comminution theory (where, the index n is 1), and Bond's third comminution theory (where, the index n is 1.5) can be derived. Eqn. 6-20 is a

differential equation. It "stated that the energy required to make a small change in the size of an object is proportional to the size change and inversely proportional to the object size to some power n" (Charles, 1957). Since both Kick's and Rittinger's hypotheses are reported to be poor ones for practical blasting operations, and Bond's hypothesis, which is a compromise and an improvement on Kick's and Rittinger's hypotheses, appears not to be significantly more in accordance with blasting results. It is tentatively proposed to introduce a stipulation, n=0.5 on the value of the power n, in this research. Substituting n=0.5, and approximating Eqn. 6-20 for a blasting process using a difference form to the equation, we obtain

$$\Delta E = C^* \frac{\Delta x}{x_o^{0.5}}, \tag{6-21}$$

where ΔE is the energy consumed in the blasting process, C^* is a constant, x_O is the objective size summarising the block sizes before and after blasting, Δx is the size change during the blasting process. It can be seen that the underlying physical concepts in Eqn. 6-21 and Eqn. 6-3 are similar, if not identical, although Eqn. 6-3 is derived from a different approach which considered the importance of the whole IBSD and BBSD curves. In fact, an approximation to Eqn. 6-18 can be obtained from Eqn. 6-20 by integration and by substitution of the value n=0.5,

$$\int_0^E dE = \int_{S_i}^{S_b} -C \frac{dx}{x^{0.5}}, \tag{6-22}$$

hence

$$E = 2C(S_i^{0.5} - S_b^{0.5}), \tag{6-23}$$

or

$$E = C \frac{S_i - S_b}{\frac{(S_i^{0.5} + S_b^{0.5})}{2}}. \tag{6-24}$$

It may be noted that the relationship between $[(S_i^{0.5} + S_b^{0.5}) / 2]$ and $[(S_i + S_b)/2]^{0.5}$, when S_b/S_i <1, is nearly a linear one (see Fig. 6.9). Eqn. 6-24 can therefore be expressed approximately as

$$E = C' \frac{S_i - S_b}{(\frac{S_i + S_b}{2})^{0.5}}. \qquad (6\text{-}25)$$

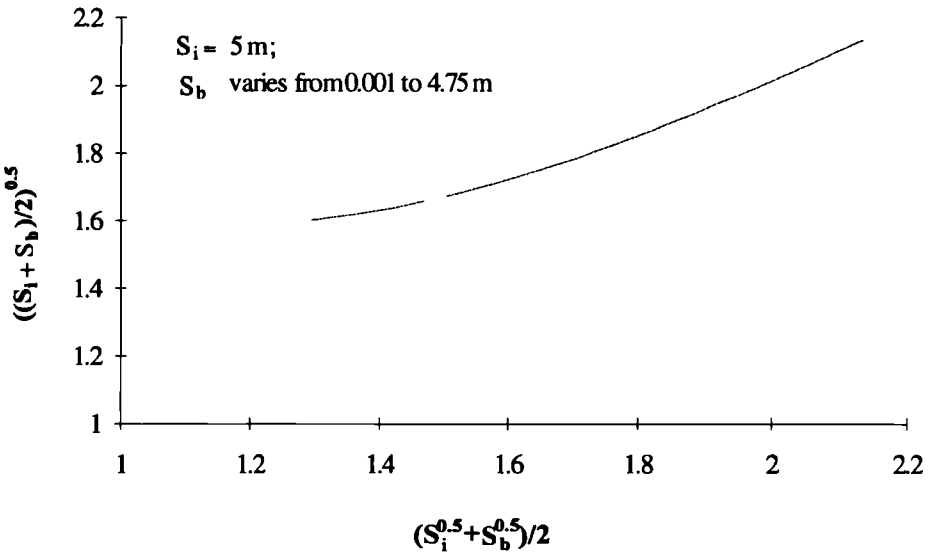

Fig. 6.9 The approximate linear relationship between $(S_i^{0.5} + S_b^{0.5}) / 2$ and $[(S_i + S_b) / 2]^{0.5}$, when $S_b/S_i < 1$

Replacing E with E_S, C' with $1/B_i$, and S with S_a, the approximate Eqn. 6-25 becomes identical to 6.19. Therefore Eqn. 6-19 appears to be a special case of the Walker-Lewis empirical relation between energy and size reduction, along with Rittinger's first comminution theory, Kick's second comminution theory, and Bond's third comminution theory.

6.3 VALIDATION OF THE ENERGY-BLOCK-TRANSITION MODEL

To determine whether the Energy-Block-Transition model proposed is an improvement on existing models requires an analysis of results from practical blasting operations. A set of model scale blasts, or preferably, a series of field blasts with constant and given in-situ conditions, but with differences in both blasting patterns and energy input, would be ideal for examination of the applicability of the model. Only two main sources of practical data which include information about IBSD,

BBSD and the energy input, were found in the literature. These are the case studies reported by Wang (1992) and Aler et al. (1996a, 1996b), and they have been considered in validating the model.

Case 1

The first case cited is the work reported by Wang (1992), in which five rounds of full scale blast trials were carried out at the Sandside Limestone Quarry located in Cumbria, Northern England. The information about IBSD, BBSD, explosive energy input, and blasting patterns were either given or can be derived.

Table 6.1 The percentage passing of in-situ block volumes (from Wang, 1992)

P (%)	10	20	30	40	50	60	70	80	90	100
Vi,p (m3)	0.146	0.297	0.448	0.650	0.891	1.218	1.674	2.367	3.689	10.642

Table 6.2 Grey correlation analysis to IBSD

Passing	V (m^3)			Correlation Coefficient	
(%)	Calculated	Ros-Ram	Schuhmann	Ros-Ram	Schuhmann
10	0.146	0.1323	0.0673	0.998	0.997
20	0.297	0.2903	0.2396	1.00	0.984
30	0.448	0.4745	0.5036	0.994	0.984
40	0.65	0.6912	0.8529	0.989	0.94
50	0.891	0.9516	1.2835	0.983	0.888
60	1.218	1.2748	1.7923	0.984	0.843
70	1.674	1.6968	2.377	0.995	0.814
80	2.367	2.2997	3.0355	0.981	0.822
90	3.689	3.3466	3.7664	0.901	0.997
100	10.642	10.577	4.5596	0.981	0.334
Total correlation coefficient				0.98	0.86

Table 6.1 gives the percentage passing in-situ block volumes of Face 1 in this quarry. A grey correlation analysis (see Section 3.5.3) was carried out to check the best-fitting theoretical distribution for the data. The grey correlation coefficient between the Ros-Ram equation and the results predicted is 0.980, and the correlation coefficient between the Schuhmann equation and the results is 0.86 (see Table 6.2). This result indicates that the IBSD can be fitted better by the Ros-Ram equation than the Schuhmann equation. It is interesting to note from Table 6.2, how the grey

correlation analysis can support a visual inspection of goodness-of-fit. In this example, it can be seen from the correlation coefficients at the ten measuring data that only at the tenth point, does the Schuhmann equation coefficient cause the significant loss in correlation measure.

The IBSD for this quarry can therefore be represented most effectively, by the Ros-Ram equation as

$$P = 1 - e^{-(\frac{V}{1.397})^{0.9547}}, \qquad (6\text{-}26a)$$

or in the form of a sieve size

$$P = 1 - e^{-(\frac{S}{1.32})^{2.8641}}. \qquad (6\text{-}26b)$$

Detailed blast design parameters used in four blast rounds out of the five rounds of trail blasts have been summarised in Table 6.3 and Table 6.4 (see Wang, 1992)

Table 6.3 Drilled geometry and the volume of rock masses blasted

Blast Round	Burden (m)	Spacing (m)	Hole depth (m)	Hole Dia. (mm)	Bench height (m)	V/hole (m^3)	Hole No.	Total V (m^3)
1	5.00	4.04	30.12	108	27.44	554.29	13	7205.7
2	5.02	4.35	30.12	108	27.44	599.21	13	7789.7
3	5.34	3.47	30.12	108	28.05	519.76	13	6756.9
4	4.30	4.21	30.12	108	28.35	513.22	14	7313.4

Table 6.4 Charging in four blasted rounds and related charge and stemming*

Blast round	ANFO	ED101 Eq. ANFO	ED103 Eq. ANFO	GRANEX Eq. ANFO	Total expl. Eq. ANFO	Specific Charge	Bottom Charge	Column charge		Stem-ming	Sub-drill	Back fill
								Height	Distribution			
	(kg)	(kg)	(kg)	(kg)	(kg)	(kg/m^3)	(m)	(m)	of expl.	(m)	(m)	(m)
1	1735	306.0	172.5	370	2583.5	0.359	2.74	23.17	no decking	3.66	2.13	0.61
2	837		448.5	481	1766.5	0.227	5.49	20.12	deck charge	3.66	1.83	0.91
3	553	280.5	69.0	481	1383.0	0.205	2.74	22.26	deck charge	4.57	1.52	0.91
4	885	137.5	172.5	333	1528.2	0.217	2.74	22.87	deck charge	3.96	0.91	0.91

* Detonation method was not included as a variable

The relative locations of five blast rounds are shown in Fig. 6.10. The BBSDs for these four rounds together with the IBSD are listed in Table 6.5. The data in the table was either taken directly or derived from results (Wang, 1992), the mean sizes are determined through Eqn. 6-7.

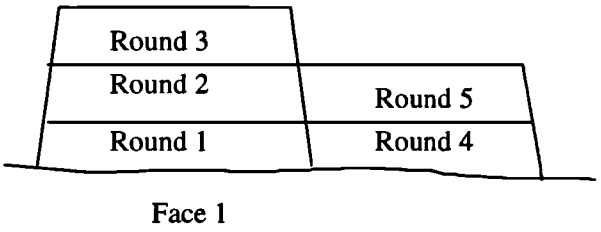

Fig. 6.10 A schematic illustration of the relative locations of the five blasts

Table 6.5 The characteristic size parameters for both IBSD and BBSD

Blast	IBSD					BBSD				
	n_s	S_c	S_{50}	S_{80}	S_a	n_s	S_c	S_{50}	S_{80}	S_a
Round		(m)	(m)	(m)	(m)		(m)	(m)	(m)	(m)
1	2.864	1.320	1.161	1.559	1.177	1.632	0.383	0.306	0.513	0.343
2						1.544	0.387	0.305	0.527	0.347
3						1.044	0.449	0.316	0.708	0.440
4						1.318	0.411	0.311	0.590	0.377

It can be seen from Table 6.3, Table 6.4 and Fig. 6.10 that the four blast rounds provide a data set of full scale blasting parameters with approximately the same geological in-situ conditions, but with differences in both blasting patterns and energy input. In fact, as reported (Wang, 1992), these four blasts had the following common features (Wang, 1992): similar bench heights of 27 to 28 m; the diameter of blastholes were all 108 mm with an inclination of 5°; each round had one row of blastholes except the fourth round blast which had a front of 10 holes and a back row of 4 holes; four types of explosives had been used, with the same stemming material; the type of primers were all Trojan of 140 g. Except for the above common features, each round had its specific blast design characteristics. Firstly the drill geometry was quite different since the ratio of burden to spacing varied from 1.02 to 1.54; secondly the specific charge varied significantly from 0.205 to 0.359 kg/m^3; thirdly there was a difference between their stemming length, decking and the distribution of explosives in the blastpile. In addition, there were differences in the bottom charge, the delay sequence and the delay time.

Clearly, in practical terms this is a good case for examining the applicability of the Energy-Block-Transition model but it is far from ideal for drawing conclusions. If the relationship between energy input, the block size before and after blasting within a blasting process obeys Eqn. 6-18, the Energy-Block-Transition coefficient, B_i for a rock mass should be a constant.

Table 6.6 Energy-block-transition coefficient, B_i and Bond's Work Index, W_i for four blast rounds with analysis of spread of the four results* (Case 1)

Blast round	Specific charge P_f (kg/m^3)	Input energy E_s (kwh/t)	B_i ($m^{0.5}$/kwh/t)	Bond' work index W_i (kwh/t)
1	0.359	0.0492	19.449	8.269
2	0.227	0.0312	30.513	5.398
3	0.205	0.0281	29.142	7.263
4	0.217	0.0298	30.497	5.940
Average (X_a)			27.390	6.717
$\Delta max/X_a$ (%)			40.38	42.73
σ/X_a (%)			16.88	16.72

* $\Delta_{max}=X_{max}-X_{min}$; and, $\sigma=\sqrt{\sum_{j}^{N}\frac{(X_j-X_a)^2}{N}}$

Table 6.7 Energy-block-transition coefficient, B_i and Bond's Work Index, W_i for three blast rounds with analysis of spread of the three results (excluding the first round of blast, Case 1)

Blast round	Specific charge P_f (kg/m^3)	Input energy E_s (kwh/t)	B_i ($m^{0.5}$/kwh/t)	Bond' work index W_i (kwh/t)
2	0.227	0.0312	30.51	5.40
3	0.205	0.0281	29.14	7.26
4	0.217	0.0298	30.50	5.94
Average (X_a)			30.05	6.20
$\Delta max/X_a$ (%)			4.56	30.08
σ/X_a (%)			2.14	12.63

Although there are only four blast rounds of data, and the other factors such as detonation might have had a significant effect on the fragmentation, it appears that the value of $\Delta max/X_a$ for B_i is lower than for W_i while σ/X_a, sample coefficient of

variation, for B_i is approximately identical for W_i (see Table 6.6). It is interesting to look at σ/X_a and $\Delta max/X_a$ when excluding the first blast round. In this case both σ/X_a and $\Delta max/X_a$ appears much lower than for W_i (see Table 6.7). This suggests that the Energy-Block-Transition model gives a closer fit to the blast data than the alternative Bond's model.

Case 2

The second case cited is the work reported by Aler et al. (1996a, 1996b), in which the data of IBSD, BBSD and explosive energy input from production blasts carried out in several mines were provided.

Two groups of data, one from Bench 4 in ENUSA mine and another from BENCH 3 in Reocin Open Pit, are used for checking the validity of the Energy-Block-Transition model. The characteristic size parameters of both IBSD and BBSD are summarised in Table 6.8, in which the S_{50}, S_{80} and S_a are derived from S_c and n_s given by Aler et al. (1996a, 1996b).

Once again, whether the Energy-Block-Transition coefficient, B_i for the rock mass in the two sites keeps at constant is examined using the data available.

Table 6.8 The characteristic size parameters for both IBSD and BBSD (from Aler et al. 1996a, 1996b)

Blast No.	IBSD					BBSD				
	n_s	S_c (m)	S_{50} (m)	S_{80} (m)	S_a (m)	n_s	S_c (m)	S_{50} (m)	S_{80} (m)	S_a (m)
	Site 1: ENUSA Mine, Bench 4									
E3	2.680	1.081	0.943	1.291	0.961	2.870	0.377	0.332	0.445	0.336
E5						2.260	0.542	0.461	0.669	0.480
E7						2.260	0.438	0.373	0.541	0.388
E8						2.560	0.737	0.639	0.888	0.654
E11						2.650	0.487	0.424	0.583	0.433
	Site 2, Reocin Open Pit Mine, Bench 3									
C9	2.680	1.800	1.570	2.150	1.600	2.280	0.617	0.525	0.760	0.547
C10						2.110	0.670	0.563	0.840	0.593
C11						2.280	0.870	0.741	1.072	0.771
C12						2.300	0.580	0.495	0.713	0.514

Table 6.9 Energy-block-transition coefficient, B_i and Bond's Work Index, W_i for the two sites with spread analysis Case 2)

Blast No.	Specific charge P_f (kg/m^3)	Input energy E_s (kwh/t)	B_i ($m^{0.5}$/kwh/t)	Bond' work index W_i (kwh/t)
	Site 1: ENUSA Mine, Bench 4			
E3	0.48	0.066	11.744	8.827
E5	0.48	0.066	8.570	13.828
E7	0.27	0.037	18.771	5.894
E8	0.331	0.046	7.492	15.997
E11	0.364	0.05	12.623	9.069
Average (X_a)			13.028	9.516
$\Delta max/X_a$ (%)			86.568	106.180
σ/X_a (%)			32.715	47.062
	Site 2, Reocin Open Pit Mine, Bench 3			
C9	0.308	0.042	23.987	9.119
C10	0.299	0.041	23.320	10.070
C11	0.323	0.044	17.138	15.664
C12	0.35	0.048	21.932	9.598
Average (X_a)			21.594	11.113
$\Delta max/X_a$ (%)			31.718	58.895
σ/X_a (%)			12.40	23.849

The Energy-Block-Transition coefficients B_i and the Bond work indices W_i are calculated and the relative dispersions are analysed and summarised in Table 6.9. It is seen from Table 6.9 that the value of $\Delta max/X_a$ for B_i is significantly lower than for W_i, which also suggests that the Energy-Block-Transition model gives a closer fit to the blast data than Bond's model.

Thus, although further examinations of the applicability of the Energy-Block-Transition model to practical blasting operations are desirable, the attempted validation of the model using the above two cases does encourage us to use the model for characterising a blasting process.

6.4 RELATIONSHIP BETWEEN FRACTAL DIMENSION AND THE BLASTABILITY

6.4.1 Introduction

Geological situations where fracture concentration alternates from high to low in adjacent regions is relatively common. Taken together, these fracture distributions are

inhomogeneous and are often found to have a fractal from of spacing (Boadu & Long, 1994). Fractal concepts were introduced extensively in previous chapters. However, this section opens another application of the fractal concept and this is with respect to the mechanical property of a rock mass best described as its fragility. Poulton et al (1990) argued that if scale invariance could be applied to rock breakage, then fracture frequency and block size should all show similar fractal dimensions for a given rock mass. They believed that the fractal dimension was potentially a key rock mechanics index, and that it might be possible to define the characteristics of a rock mass with much greater precision using fractal dimensions than using existing indices. Turcotte (1986) also argued that fragmentation would, in many cases, result in a fractal distribution of block sizes. Using a "renormalisation group" approach to fragmentation, Turcotte suggested that the fractal dimension should be a measure of the fragility of the fragmented materials, i.e. a measure of the fracture resistance of a rock mass relative to the process causing fragmentation. He also predicted the trend would be for a more fragile material to be associated with a block size distribution described by a smaller fractal dimension.

In the section below, the rationale for the supposed relation between mechanical fragility and fractal dimension is explored. The key work of Allegre et al. (1982) and Turcotte (1986) is reconsidered so that the Energy-Block-Transition coefficient, B_i, can be considered in the light of fragility based on fractal concepts.

6.4.2 Relation between the Energy-Block-Transition Coefficient and the Fractal Dimension of the IBSD

Either IBSD or BBSD is related to the distribution of pre-existing planes of weakness in the rock and it was established earlier that these may exhibit fractal characteristics. Turcotte (1986, 1989) showed that the fragmented rocks can often be described, with a good measure of fit, by a power-law distribution which is equivalent to the fractal distribution given in the follow equation:

$$N(s) = CS^{-D}, \qquad (6\text{-}27)$$

where $N(s)$ is the number of fragments with a linear dimension larger than S. Eqn. 6-27 describes a fractal relationship where D is the fractal dimension describing block sizes. The values of the fractal dimensions vary considerably but most lie in the range of 2 to

3 for fragmented geological materials such as jointed rock masses and blasted blocks (Turcotte, 1986).

A relationship between the fractal dimension and the blastability based on the Energy-Block-Transition model will be developed. Suppose that both IBSD and BBSD hold the Schuhmann distributions, then the mean size of blocks (see Eqns. 6-7 and 6-10) is given as:

$$S_a = \frac{m_s}{m_s + 1} S_{100}. \tag{6-28}$$

Turcotte (1986) has shown that the distribution index m_S governing the steepness of the commutative curve can be related to the fractal dimension D as:

$$D = 3\text{-}m_S. \tag{6-29}$$

Applying Eqn. 6.29 to both IBSD and BBSD yields:

$$D_i = 3\text{-}m_{Si}, \tag{6-30a}$$

$$D_b = 3\text{-}m_{Sb}. \tag{6-30b}$$

Substituting Eqns. 6-28 and 6-30 into Eqn. 6-19 gives the relationship between the fractal dimensions of in-situ rock blocks and blasted blocks and the Energy-Block-Transition coefficient B_i as

$$B_i = \frac{\sqrt{2}[(3 - D_i)(4 - D_b)S_{100i} - (3 - D_b)(4 - D_i)S_{100b}]}{E_s\sqrt{(4 - D_i)(4 - D_b)[(3 - D_i)(4 - D_b)S_{100i} + (3 - D_b)(4 - D_i)S_{100b}]}}. \tag{6-31}$$

Consider now the relationship between the fractal dimension of in-situ rock blocks and the blastability of a rock mass. It can be deduced from Eqn. 6-31 that B_i increases with decreasing D_i of in-situ rock blocks when other parameters in Eqn. 6-31 remaining constant, a case of which is illustrated in Fig. 6.11. This indicates that a rock with lower D and hence greater m_{Si} will be more easily fragmented by blasting than a rock with higher D hence lower m_{Si}.

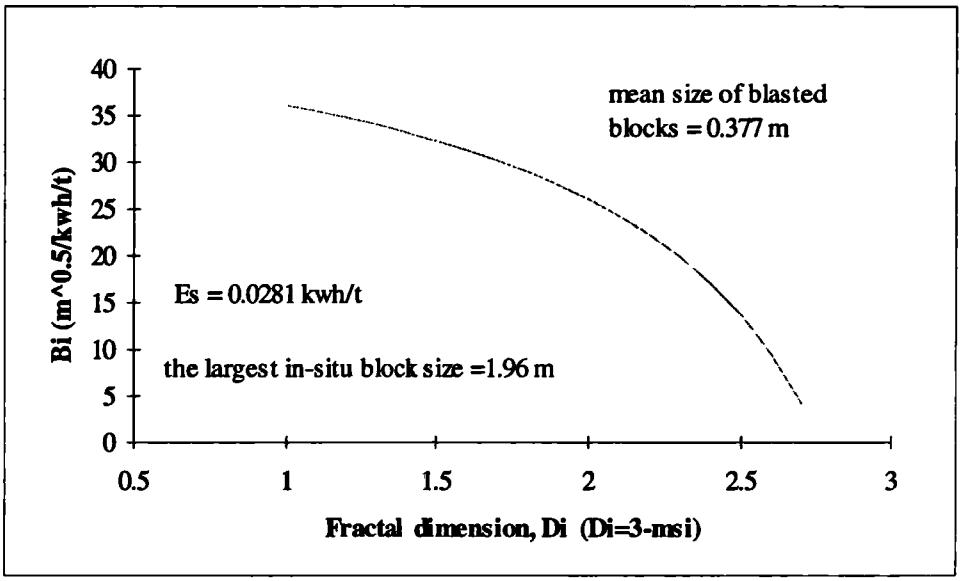

Fig. 6.11 A case to illustrate the relationship between the Energy-Block-Transition coefficient B_i and the fractal dimension of in-situ blocks, D_i

6.4.3 Extension of Renormalisation Group Methods to the Relation between Blastability and the Fractal Dimension of IBSD

Fragmentation is a catastrophic phenomenon which exhibits sudden or catastrophic change, much as a system undergoing a phase change. The feature of a phase change is a catastrophic change of macroscopic parameters of a system under a continuous change of the state variables in a system. A renormalisation group method (see Appendix C3) has been used to study scale invariant processes that exhibit catastrophic change (Allegre et al. 1982; Turcotte, 1986, 1992). The renormalisation group method often produces fractal statistics and explicitly uses scale invariance.

The discussion below follows closely the work of Allegre et al. (1982) and Turcotte (1986) and leads to the application of the significance of the relationship between breakage processes and fractal dimensions.

As shown in Appendix C3, using different specifications of the condition for the fragile or soundness of a cell, different numbers of fragile cells can be obtained. The criteria given in Appendix C3 described as "pillar of strength" (Allegre et al., 1982) and "plane of weakness" (Turcotte, 1986) give an indication of how different fractal dimension values can be related to rock masses with differing strength criteria, rock masses that have different degrees of fragility. Using the "pillar of strength" criterion, Allegre et al. concluded that the critical probability (the threshold for crack percolation) that leads to a catastrophic fragmentation p_c is 0.896 and that the related

fractal dimension D is 2.84. Using the "plane of weakness" criterion, Turcotte obtained that the probability p_c is 0.49 and that the related fractal dimension D is 1.97.

Following along the same lines and using the renormalisation group concepts outlined in Appendix C3, a "number of fragile elements" criterion is proposed by the author as a further step of investigation into how different fractal dimension values describing in-situ blocks of rock masses can be related to the rock masses that have different degrees of blastability. Also, the renormalisation group model illustrated in Fig. C.3 (hence the configurations for fragile or sound elements illustrated in Fig. C.4) is adopted in this investigation. In terms of the "number of fragile elements" criterion, a cell is considered as fragile if the number of fragile elements in the cell is greater than a certain critical value.

(1) A cell is assumed to be fragile if the number of fragile elements in a cell is three or greater. Using this criterion, the configurations numbered as from *3a* to *8* in Fig. C.4 will be considered as fragile. Thus, the probability p_n, that a cell at order n is fragile as a function of p_{n+1}, that a cell at order $n+1$ is fragile is given by (see Appendix C.3)

$$p_n = (p_{n+1})^8+8(p_{n+1})^7[1-(p_{n+1})]+28(p_{n+1})^6[1-(p_{n+1})]^2+56(p_{n+1})^5[1-(p_{n+1})]^3 +70(p_{n+1})^4[1-(p_{n+1})]^4+56(p_{n+1})^3[1-(p_{n+1})]^5. \quad (6\text{-}32)$$

By similarly applying catastrophic theory (see Appendix C.3) to the expression of Eqn. 6-32, it can be deduced that the critical probability that leads to a catastrophic fragmentation in this case, p_c is 0.197 and the related fractal dimension D is 0.70.

(2) If the number of fragile elements in a cell is four or greater, the cell is considered to be fragile. In which case the configurations numbered as from *4a* to *8* in Fig. C.4 will be fragile. In this case, the relation of p_n and p_{n+1} is deduced as

$$p_n = (p_{n+1})^8+8(p_{n+1})^7[1-(p_{n+1})]+28(p_{n+1})^6[1-(p_{n+1})]^2 +56(p_{n+1})^5[1-(p_{n+1})]^3+70(p_{n+1})^4[1-(p_{n+1})]^4. \quad (6\text{-}33)$$

Similarly, the critical probability that leads to a catastrophic fragmentation in this case, p_c is found to be 0.396, and the related fractal dimension D to be 1.662.

(3) A cell is assumed to be fragile if the number of fragile elements in a cell is five or grater. Based on this stipulation of fragility, the configurations from *5a* to *8* in Fig. C.4 are fragile. It follows that the relationship between p_n and p_{n+1} can be deduced as

$$p_n = (p_{n+1})^8+8(p_{n+1})^7[1-(p_{n+1})]+28(p_{n+1})^6[1-(p_{n+1})]^2+56(p_{n+1})^5[1-(p_{n+1})]^3$$
$$= (p_{n+1})^5[56-140(p_{n+1})+120(p_{n+1})^2-35(p_{n+1})^3]. \quad (6\text{-}34)$$

In this case, p_c is found to be 0.605 and the related fractal dimension D is 2.274.

Table 6.10 The relationship between fractal dimension and blastability (and fragility) of a rock mass

	1	2	3	4	5
Criterion for the fragility of a cell	No. of fragile elements ≥ 3	No. of fragile elements ≥ 4	Plane of weak-ness criterion	No. of fragile elements ≥ 5	Pillar of strength criterion
No. of fragile elements' configurations of cells	219	163	131	93	35
Critical probability, p_c	0.197	0.396	0.490	0.605	0.896
Fractal dimension, D	0.700	1.662	1.970	2.274	2.840
Fragility of rock mass	more fragile ----------→ less fragile				
Blastability of rock mass	more easily blasted ----------→ less easily blasted				

The above crude renormalisation group model, allows us to consider the relationship between fractal dimension and the blastability of a rock mass. When examining the above five fractal dimensions from the five different criteria that specify whether a cell is in a fragile or sound state, it can be seen that the greater number of fragile configurations corresponds to a lower fractal dimension. A rock mass with a lower fractal dimension can therefore be expected to be more easily fragmented by blasting. This is summarised in Table 6.10.

Comparing the results in Table 6.10 to Fig. 6.11, it can be seen that blastability as described by B_i and fragility both increase monotonically as D increases. That is, a lower fractal dimensions is always related to a rock mass which can be more easily fragmented by blasting. The fragility criteria used above are of course simple. However, they do reveal that there is an inherent relationship between fractal dimension and the blastability of the rock, that is based on a reasonable mechanical principle.

6.4.4 Insight into the Relation between Blastability, and the Fractal Dimension of Blasted Rock Blocks

The above development referred to the fractal dimension of the IBSD. Next, the relationship between the blastability and the fractal dimension of blasted blocks will be considered. It can be deduced from Eqn. 6-31 that B_i goes down with the rise of the index m_{sb} of BBSD, so that the required input energy goes down with a decrease in the fractal dimension of the BBSD, assuming other parameters are fixed. In other words, for a given in-situ rock mass, it is more difficult to obtain the BBSD with smaller m_{sb} (gentle curve) and thus a greater fractal dimension than that with a greater m_{sb} (steeper curve) thus a lower fractal dimension. That is, more explosive energy is needed to obtain the blasted rock blocks with greater fractal dimension.

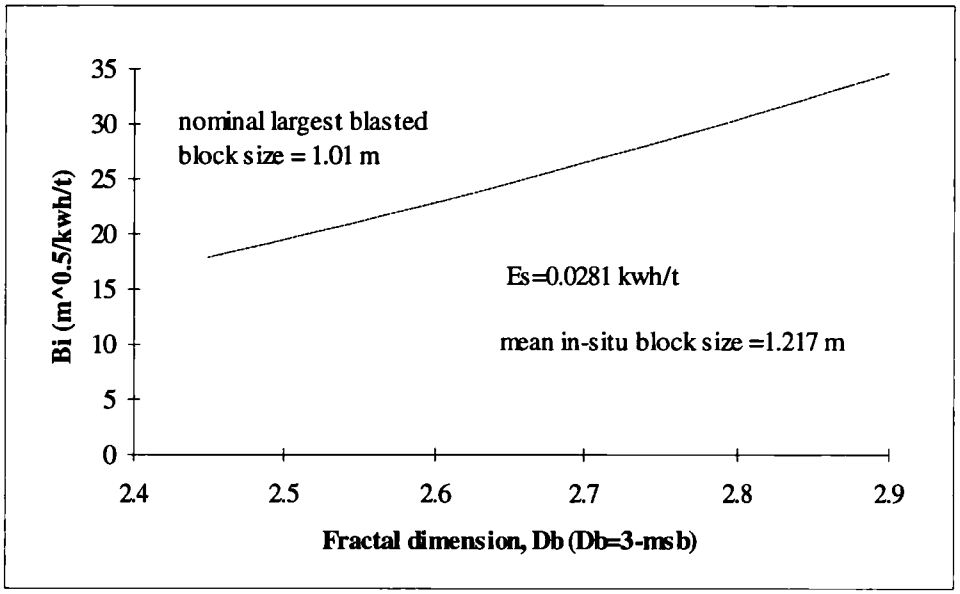

Fig. 6.12 A case to illustrate the relationship between the Energy-Block-Transition coefficient B_i and the fractal dimension, D_b, of blasted blocks

Furthermore, a key concept in fracture mechanics is that the extension of a fracture will occur once a critical crack extension force, G_C, has been reached or is exceeded. In the terms of Irwin's fracture criterion, this proposition can be expressed as (Atkinson, 1987; Xie, 1990)

$$G_C = 2\,\omega_s, \tag{6-35}$$

where ω_s represents fracture surface energy per unit of apparent macroarea, and the extension of fracture is deemed to be along a flat route which is not strictly what is observed. A zig-zag path is more common. The fractal concept has been introduced to obtain a better understanding of fracture extension when the dimension of particle and

crack length is considered at the micro-scale. In this case, Eqn. 6-35 was formulated to take more realistic crack path into account (Xie, 1990)

$$G_c = 2\,\omega_s \left(\frac{1}{r}\right)^{D_b-1} \quad , \tag{6-36}$$

where, r is the similarity ratio (see Section 3.3.2) and D_b is the fractal dimension of fractured products (e.g. blasted rock blocks). It is seen from Eqn. 6-36 that the higher is D_b, the higher is G_c, i.e. more energy has to be dissipated to produce blasted rock blocks with a greater fractal dimension than those that were a small fractal dimension. It can be deduced from Eqn. 6-18 that the Energy-Block-Transition coefficient, B_i, decreases with the rise of the index m_{sb}, thus decreases with the decrease of the fractal dimension, D_b, of blasted rock blocks (see Eqn. 6-31), a case of which is illustrated in Fig. 6.12. Thus, the classical approach of fracture mechanics leading to Eqn. 6-36 is compatible with the trend revealed in Fig. 6.12.

6.4.5 Summary of the Relation between Blastability and Fractal Dimensions

The aforementioned discussion has shown that coefficients m_{si} and m_{sb} which describe both IBSD and BBSD, and thus the fractal dimensions of both in-situ and blasted blocks, could be useful indicators of blastability.

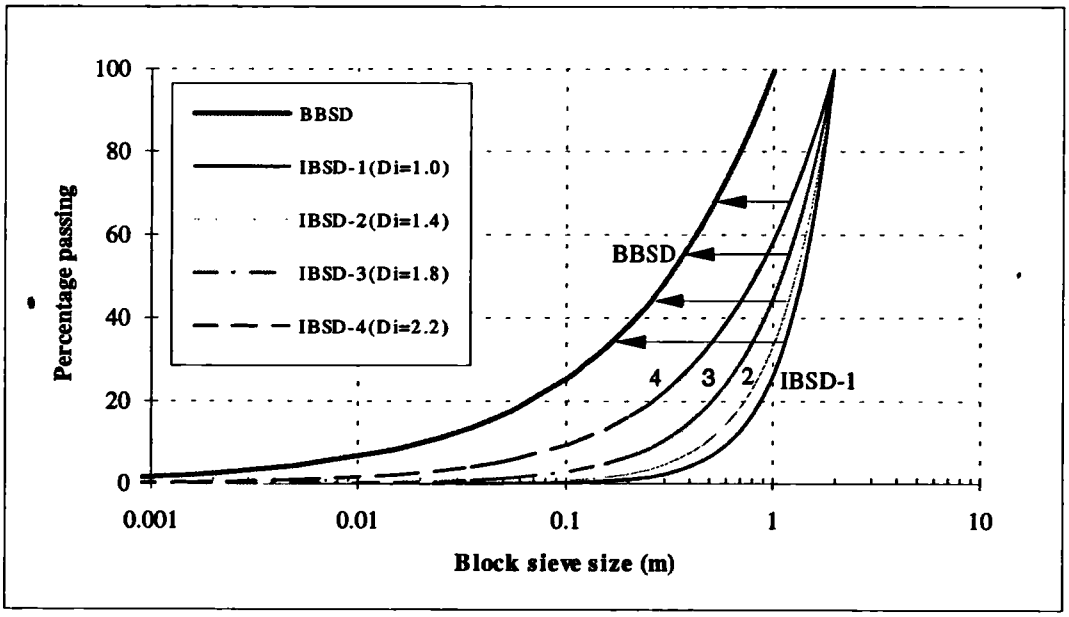

Fig. 6.13 Influence of fractal dimension, D_i, on the transformation of a rock mass from its in-situ state into a blastpile. All four cases have the same energy input but different B_i values

Recall that from Fig. 6.11 a rock mass with a lower fractal dimension of IBSD is easier to be blasted than a rock mass with a greater fractal dimension whereas Fig. 6.12 shows that a smaller fractal dimension in the blastpile is associated with a greater energy consumption and more difficult blasting than a higher fractal dimension.

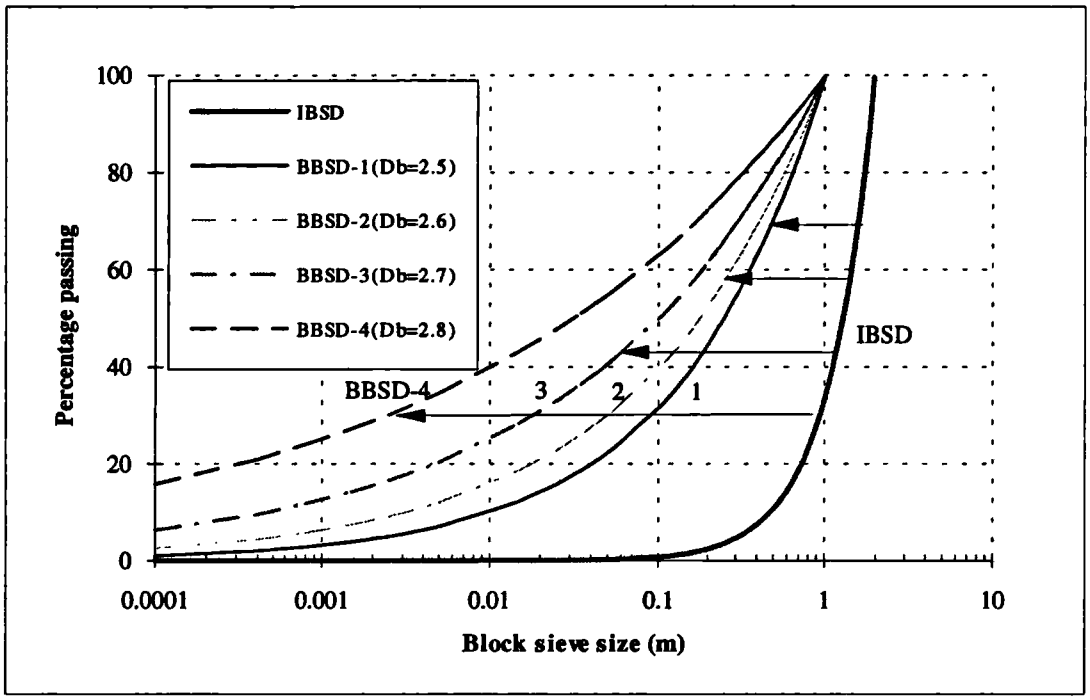

Fig. 6.14 Illustration of the fractal dimension, D_b, on the transformation of a rock mass from its in-situ state into a blastpile. All four cases have the same energy input but different B_i values

A further insight into the mechanism revealed in Fig. 6.10 is illustrated in Fig. 6.13, which might not be encountered in practice but simply as an illustration of the influence of D_i on the transformation. Four rock masses with the same largest in-situ block sizes but with different D_i are assumed to be fragmented to blastpiles with the same BBSD under the same energy input as shown in Fig. 6.13. It can be seen that a rock with lower D_i (relatively larger in-situ blocks) will be more easily fragmented by blasting than a rock with higher D_i, since the former consists of relatively larger in-situ blocks whereas the latter consists of relatively smaller in-situ blocks. That is, the rock masses are different in their degrees of blastability. The mechanism revealed in Fig. 6.12 that the fractal dimension, D_b, is the indication of blastability of a rock mass can be further analysed by means of Fig. 6.14. Four blastpiles with the same largest blasted block sizes but with different D_b are assumed to be formed from four rock masses that have the same IBSD. The blastpile with the highest values of D_b is associated with the rock mass that is blasted with greatest ease.

The above discussion supports Turcotte's proposition (1986) that an in-situ rock mass with a smaller fractal dimension can be expected to be more fragile. Furthermore, this has been inclined to reinforce the argument that the Energy-Block-Transition model is compatible with mechanical considerations of the blasting process and that the fractal dimension of in-situ rock blocks can be a significant characteristic of blastability.

The above arguments were developed under the assumption that both IBSD and BBSD hold the Schuhmann equations. It has been shown, on occasions, that the Ros-Ram distribution can be approximated by the Schuhmann distribution (Gilvarry, 1961; Brown et al., 1983; Turcotte, 1986; Grady & Kipp, 1987; Crum, 1990). Consequently, the discussion based on m_{si} and m_{sb} given above can be extended to n_{si} and n_{sb} and their respective fractal dimensions for cases where both IBSD and BBSD exhibit a good statistical fit to the Ros-Ram equation.

6.5 ASSESSMENT OF BLASTABILITY

The previous studies in this chapter have shown that the Energy-Block-Transition coefficient B_i, is a quantitative measure of the blastability of a rock mass. Applying the Energy-Block-Transition model to a practical blasting operation requires that the B_i coefficient for the rock mass of interest has been obtained. It will therefore be most advantageous for the coefficient B_i to be determined before rather than after blasting in order to help with the blast design of an excavation operation. The development of an assessment system for the blastability of rock masses is therefore of great significance and is the purpose of the following sections of this chapter.

6.5.1 Factors Influencing Blastability

In reviewing the blasting practices and literature published (Franklin et al., 1971; Just, 1973; Kuznetsov, 1973; Hagan & Just, 1974; Da Gama, 1983; Rustan et al., 1983; Lilly, 1986; Bellairs, 1986; Cunningham, 1987; Roke, 1988; JKMRC, 1991; Wang et al. 1991b; Stagg et al., 1992; Scott et al., 1993; Lizotte & Scobe, 1994; Matheson, 1995), it is obvious that many factors will affect the blastability of rock masses. These factors include intact rock properties such as strength, hardness, elasticity, deformability, density of rock etc., and discontinuity structure features such

as orientations and spacings of discontinuities and the in-situ block sizes. In addition, interactions between these factors will make the problem more complicated. This indicates that blastability probably involves several coupled variables that ultimately describe this intrinsic property of the rock mass. Therefore, it is inappropriate to characterise the blastability using only a single or a few separate rock parameters. Whereas one parameter, such as uniaxial compression strength, might be an important indicator of the blastability of rock, several others are perhaps even more important, such as sonic velocity or joint spacing. The question then arises, of the many different parameters thought to be important, how can duplication of similar parameters and the over-influence of minor parameters be avoided.

6.5.2 Methodology of Blastability Assessment

6.5.2.1 Introduction to Rock Engineering Systems

In spite of the long-history of rock blasting (Atlas Powder Company, 1987) and the advent of rock mass classification systems (Bieniawski, 1973; Barton, 1974), a generic methodology for the appraisal of the blastability of a rock mass encountering a standard blasting operation remains lacking. One of the reasons has been both the diversity of factors influencing the blastability of rock and the complexity of the associated representation of all the influences of the various factors and the interactive mechanisms between them.

Rock Engineering Systems (RES), is a systems methodology developed by Hudson (1992) in response to the need for an "all-encompassing" procedural technique to approach increasingly complex rock engineering problems. This new methodology aims at providing a useful checklist for a rock engineering project. More importantly, it also provides a framework from which the complete design procedure can be evaluated, leading a rock engineering project to an optimal result. It is proposed therefore that an RES description of the overall interactive mechanisms in rock blasting operations may be promising for the development of an approach to solving the complex blastability assessment problems.

The RES approach (Hudson, 1992) contains a very useful procedure for devising a rock mass classification scheme for any rock engineering project. In a rock mass classification scheme, a single parameter is required to comprehensively characterise the quality of any rock mass for a given engineering project that is to take place within

the rock mass. According to the RES approach, all possible rock mass classification schemes can be characterised simply as a function of the leading diagonal parameter values of an interaction matrix. The selection of the parameters and the definition of the weighting of each parameter in a classification system can be made through the coding of the interaction matrix. This coding is crucial to the applicability of the equation in the classification scheme. The RES approach has been applied to many rock engineering fields, for example, the assessment of stability of underground excavations (Lu & Hudson, 1993). The approach forms one key stage in establishing a blastability system.

6.5.2.2 The Interaction Matrix and its Coding

In the RES approach to rock engineering, the interaction matrix device is both the basic analytical tool and a presentational technique for characterising the important parameters and the interaction mechanisms in a rock engineering system. In the interaction matrix for a rock engineering system (e.g. a blastability system), all factors (or parameters) influencing the system are arranged along the leading diagonal of the matrix, called the diagonal terms. The influence of each individual factor (or parameter) on any another factor (or parameter) is accounted for at the corresponding off-diagonal position, and these are named the off-diagonal terms. The off-diagonal terms, are assigned values which describes the degree of the influence of one factor (or parameter) on the other factor (or parameter). Assigning these values is called coding the matrix. A problem containing only two factors is the simplest example of the interaction matrix, as shown in Fig. 6.15.

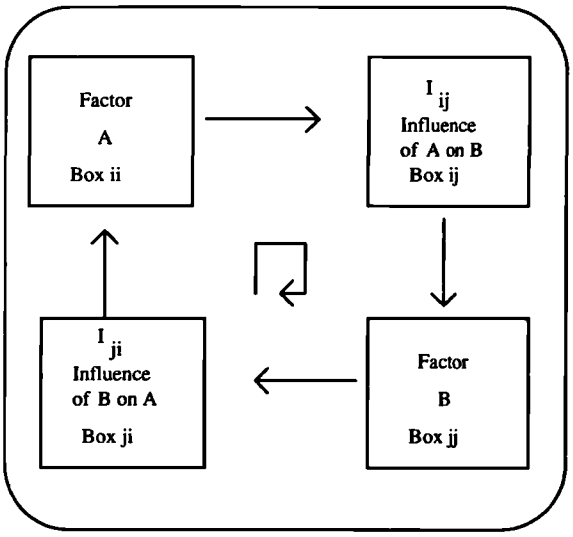

Fig. 6.15 Illustration of interaction matrix in RES (after Hudson, 1992)

In principal, there is no limit to the number of factors (or parameters) that may be included in an interaction matrix, although the number of factors (or parameters) needed to solve a practical engineering problem are finite. A problem which includes n factors (or parameters) will have an interaction matrix with n rows and n columns, as shown in Fig. 6.16.

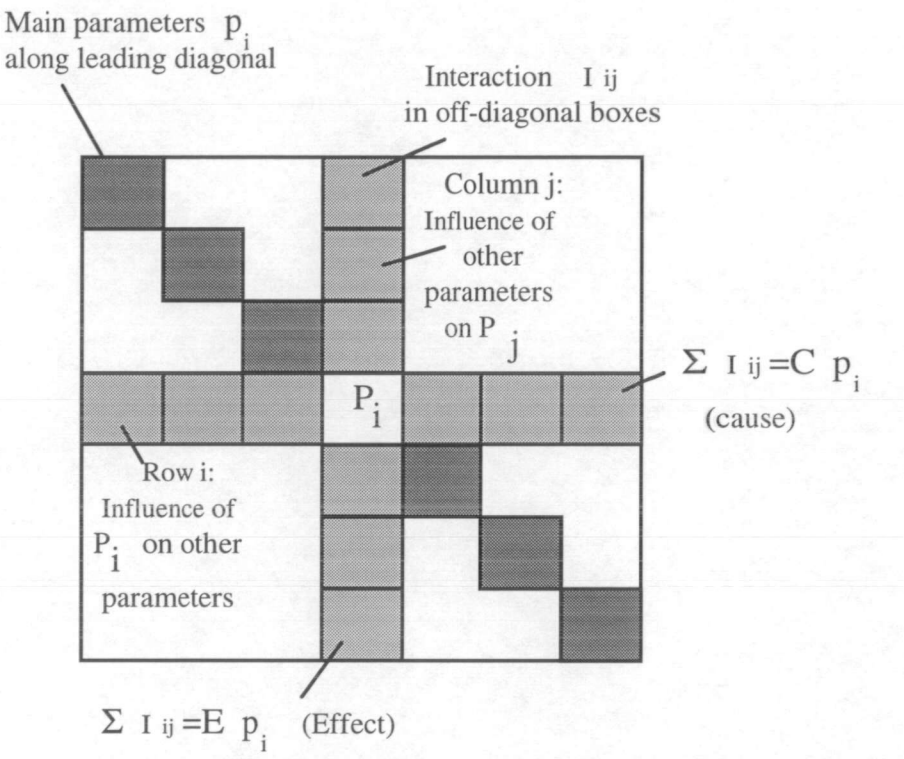

Fig. 6.16 General illustration of the coding of interaction matrix and the set-up of the cause and effect co-ordinates (after Hudson, 1992)

The row passing through P_i represents the influence of P_i on all the other factors in the system, while the column through P_i represents the influence of the other factors, or the rest of the system, on the P_i. Several procedures have been proposed for numerically coding this matrix, for example, the 0-1 binary and the expert semi-quantitative (ESQ) method (Hudson, 1992), and the continuous quantitative coding (CQC) method (Lu & Latham, 1994). After coding the matrix by inserting the appropriate values for each cell of the matrix, the sum of each row and of each column can be calculated. The sum of a row is termed the "cause" value and the sum of a column is the "effect" value, designated as co-ordinates (C, E) for a particular factor. C represents the way in which P_i affects the rest of the system; and E represents the

effect that the rest of the system has on P_i. The co-ordinate values for each factor can be plotted in cause and effect space, forming a so-called *C-E* Plot (Hudson, 1992). After obtaining the *C-E* plot for a system, an equation defining a classification index that takes into account key contribution factors can be developed. These stages are shown in Figs. 6.17 and 6.18.

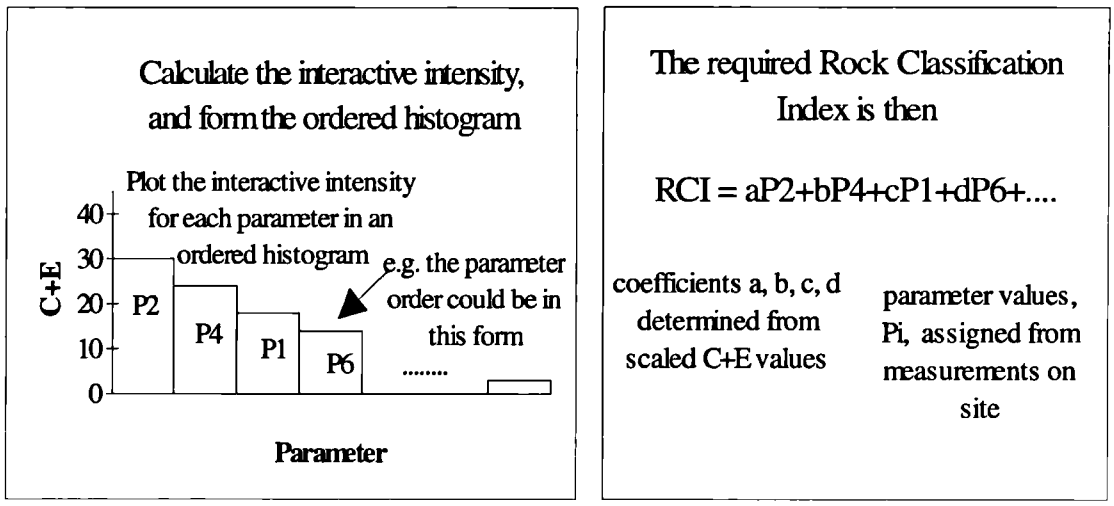

(a) (b)

Fig. 6.17 Developing a rock engineering classification system by means of the interaction matrix (after Hudson, 1992). (a) forming the ordered histogram; (b) formulating the Rock Classification Index

6.5.2.3 Formulating the blastability assessment

We now return to the development of a blastability system. Firstly, we select the factors influencing the blastability. Identification of relevant factors can be obtained from an extensive review of literature on blasting (e.g. references as listed in Section 6.5.1) combined with the author's experience. The following 12 factors (see the "Factors affecting blastability" column in Table 6.11) were chosen as the basic ones to be considered in establishing a blastability classification system for a general site, i.e. these 12 factors were chosen as the diagonal terms in the interaction matrix used to establish the blastability system. The matrix might be coded by means of subjective judgement and experience or objective measurements, or both. However, relating to each of these 12 factors, one (or two) measurable parameter(s) that can, to some extent, depict the factor's influence at a given site, has been used as the diagonal term to represent this factor in the interaction matrix (see the "depicting parameter" column in Table 6.11). The factors and their depicting parameters are listed below:

P1	0.65	0.7	0.85	0.65	0.55	0.4	0.75	0.5	0.55	0.3	0.4
0.75	**P2**	0.4	0.45	0.65	0.5	0.4	0.65	0.6	0.45	0.5	0.5
0.9	0.75	**P3**	0.8	0.7	0.8	0.45	0.5	0.25	0.25	0.2	0.2
0.8	0.5	0.7	**P4**	0.6	0.6	0.55	0.25	0.25	0.3	0.45	0.15
0.45	0.65	0.7	0.45	**P5**	0.5	0.25	0.45	0.45	0.4	0.25	0.45
0.7	0.5	0.75	0.4	0.5	**P6**	0.25	0.45	0.35	0.35	0.45	0.4
0.4	0.2	0.4	0.65	0.25	0.45	**P7**	0.5	0.2	0.25	0.25	0.15
0.5	0.7	0.2	0.2	0.15	0.5	0.35	**P8**	0.4	0.25	0.2	0.3
0.25	0.3	0.25	0.5	0.35	0.25	0.3	0.4	**P9**	0.8	0.65	0.45
0.65	0.6	0.3	0.35	0.25	0.35	0.4	0.55	0.65	**P10**	0.8	0.2
0.45	0.45	0.2	0.6	0.6	0.45	0.2	0.15	0.5	0.55	**P11**	0.25
0.25	0.65	0.1	0.3	0.45	0.25	0.15	0.5	0.55	0.25	0.3	**P12**

(a)

P_1- Strength;
P_2 - Resistance to fracturing;
P_3 - Sturdiness;
P_4 - Elasticity;
P_5 - Resistance to dynamic loading;
P_6 - Hardness of rock;
P_7 - Deformability;
P_8 - Resistance to breaking;
P_9 - *IBSD* or *PMS*;
P_{10} - Fragility of rock mass;
P_{11}- Integrity of rock mass;
P_{12}- Discontinuity plane's strength.

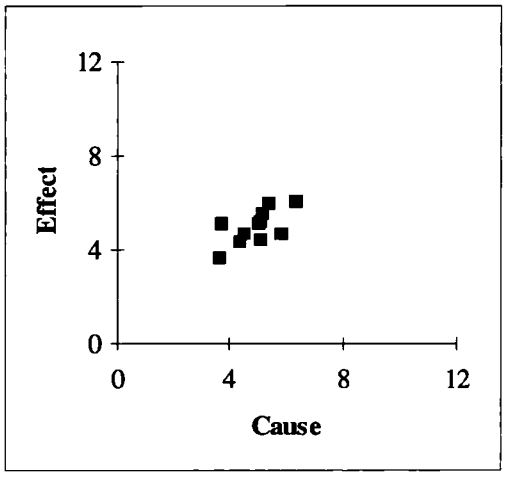

(b)

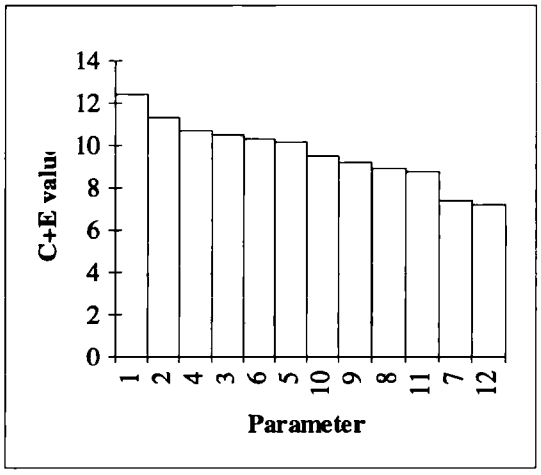

(c)

Fig. 6.18 Illustration of the interaction matrix coding results. (a) coding values, (b) the C-E plot and (c) the ordered histogram (Case Study 1, see Chapter 7).

P_1- Strength, represented by uniaxial compression strength (*UCS*) of intact rock or point-load strength index (*PLI*);
P_2 - Resistance to fracturing, represented by the uniaxial tensile strength (*UTS*);
P_3 - Sturdiness, represented by density of rock (ρ);
P_4 - Elasticity, represented by static or dynamic modulus of rock (*E*);
P_5 - Resistance of rock to dynamic loading, represented by P-wave velocity (V_p);
P_6 - Hardness of rock, represented by Schmidt hammer rebound value (*SHV*);
P_7 - Deformability, represented by Possion's ratio (μ);

P_8 - Resistance of rock to breaking, represented by fracture toughness of rock (K_{Ic});

P_9 - In-situ block size of rock mass, represented by mean in-situ block size (*MIBS*) or principal mean spacing (*PMS*);

P_{10} - Fragility of rock mass, represented by fractal dimension of in-situ block sizes (D);

P_{11}- Integrity of rock mass, represented by the elasticity wave velocity ratio, R_v (the ratio of velocity of P-wave in field to that in laboratory), or by *RQD;*

P_{12}- Discontinuity plane's strength, represented by cohesion, C or friction angle, ϕ of discontinuity plane.

Naturally, one can include more, such as the discontinuity orientation, water content in the rock mass, etc. Having chosen the various factors to be included, it may not be possible to find measurable parameters that fully quantify each factor. However, to simplify the system to manageable and relatively easily obtained field parameters, the set of depicting parameters above were chosen.

Using either the ESQ or the CQC coding method, the coding values, the *C-E* plot and the ordered histogram, all of which reflect the interaction intensity for each of the factors, can be obtained (see Fig. 6.18, which is the result of a case study that is described in Chapter 7). It is important to bear in mind that the coding values would probably vary according to different opinions from different researchers and ideally several experts' opinion should be involved in the factor selection and coding process. Then, the parameters with greatest interaction intensity and contribution to the blastability of a rock mass can be calibrated, based on the geological information before blasting.

Making use of the findings of blasting theory and practice, a quantitative list of classes of blastability connected to individual factors and their depicting parameters is suggested in Table 6.11. This table is the basis for both rating the influence of each parameter on the blastability and obtaining the rating value used in Eqn. 6-37. With reference to the above table, continuous rating charts corresponding to each single factor can be created. They are helpful for borderline cases and also remove an impression that abrupt changes in ratings occur between classes. Continuous rating charts for uniaxial compressive strength and mean in-situ block size are illustrated in Fig. 6.19, and the others are listed in Appendix D.

Table 6.11 Suggested quantitative indications for the classification of blastability of rock mass connected to individual factor

P_i	Description of ease of blasting / Blastability Class / Factors affecting blastability / Depicting parameter		Very Easy 1	Easy 2	Moderate 3	Difficult 4	Very difficult 5
P_1	Strength	Uniaxial compressive strength (UCS) (MPa)	<25	25-60	60-100	100-180	>180
		Point-load strength index (MPa)	<1	1-2.5	2.5-4	4-9	>9
P_2	Resistance to fracturing	Uniaxial tensile strength (UTS) (MPa)	<1.5	1.5-3	3-6	6-12	>12
P_3	Sturdiness of rock	Density, ρ (t/m^3)	<2.0	2.0-2.4	2.4-2.75	2.75-3.0	>3.0
P_4	Elasticity of rock	E(GPa)	<25	25-50	50-100	100-150	>150
P_5	Resistance to dynamic loading	P-wave velocity (km/s)	<1.5	1.5-2.5	2.5-3.0	3.0-4.0	4.0
P_6	Hardness of rock	Schmidt Hardness Value	<15	15-30	30-40	40-50	>50
P_7	Deformability	Possion's ratio	>0.35	0.3-0.35	0.25-0.30	0.25-0.20	<0.20
P_8	Resistance to breaking	Fracture toughness of rock ($MPa.m^{1/2}$)	<0.5	0.5-1.5	1.5-2.5	2.5-3.5	>3.5
P_9	In-situ block sizes mass	Mean IBSD (m)	<0.25	0.25-0.75	0.75-1.5	1.5-2.5	>2.50
		Mean spacing (m)	<0.1	0.1-0.5	0.5-1.5	1.5-2.5	2.5.3
P_{10}	Fragility of rock mass	Fractal dimension of in-situ rock mass, D	<1.50	1.50-2.00	2.00-2.50	2.50-2.75	>2.75
P_{11}	Integrity of rock mass	Ratio of P-wave in field to that in lab, R_v	<0.35	0.35-0.55	0.55-0.75	0.75-0.9	>0.90
		RQD (%)	<40	40-60	60-75	75-90	>90
P_{12}	Discontinuity planes' strength	Cohesion C (MPa)	<0.05	0.05-0.15	0.15-0.25	0.25-0.50	>0.50
		Fraction angle φ (°)	<7.5	7.5-15	15-20	20-30	>30

It is possible to include as many factors as might conceivably the blastability. However, only factors which make major contributions to the blastability system will be selected for the practical applications considered in this thesis, as this can probably give a relatively good approximation and reduces the burden of collecting data. Based on the associated *C-E* plot (for the significance of C-E plot in selecting the final contributory factors, see Fig. 9.6b in Hudson's book, 1992) and the ordered histogram

of the blastability system obtained, those factors contributing to most of the system, say larger than 70% of the Σ(C+E) total in the ordered histogram, can be selected as the factors to be used in assessing the blastability of the rock mass.

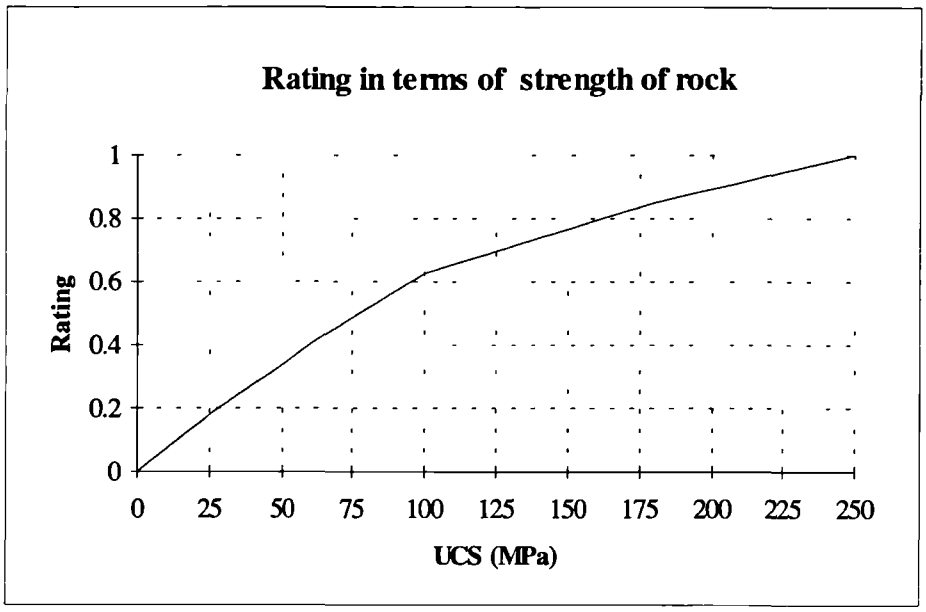

(a)

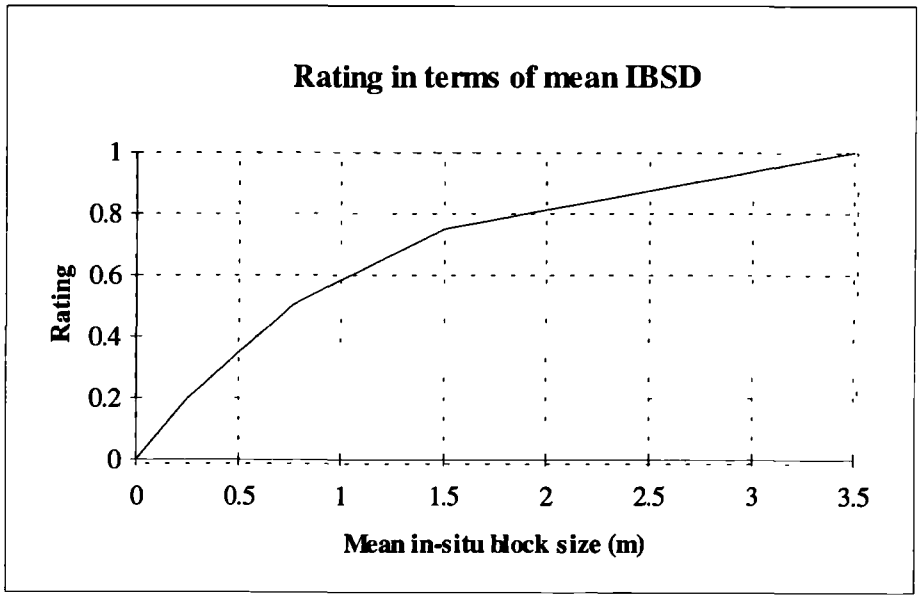

(b)

Fig. 6.19 The rating charts (a)for uniaxial compression strength; (b) for mean in-situ block size of rock mass

The assessment of blastability of the rock mass can then be made according to the following formula

$$BD = \sum_{j=1}^{n} W_j R_j, \qquad (6\text{-}37)$$

where *BD* is hereafter named Blastability Designation. *BD* is a designation which comprehensively reflects the ease or otherwise with which a rock mass can be fragmented by blasting. R_j is the rating value of the *jth* factor obtained from either Table 6.11 or the corresponding continuous rating charts as shown in Fig 6.19 and Appendix D according to values indirectly derived or measured from a site. W_j is the weighting coefficient determined from the *jth* factor according to its contribution to the system, which can be calibrated from the ordered histogram. It is obvious that the value of *BD* is in the range 0 to 1, and that the greater the *BD* is, the more difficult the rock is to be blasted.

Table 6.12 Suggested relationship between *BD* and blastability description

Description of ease of blasting	Very Easy	Easy	Moderate	Difficult	Very difficult
Blastability Class	1	2	3	4	5
BD	<0.25	0.25-0.50	0.50-0.70	0.70-0.85	>0.85

Descriptive terms for the blastability classes and their respective range of *BD* values are tentatively suggested in Table 6.12.

6.6 RELATIONSHIP BETWEEN *BD*, B_i, AND KUZNETSOV'S ROCK FACTOR *'A'*

6.6.1 Relationship between *BD* and B_i

As discussed above, *BD* is designed to give a comprehensive measure of the blastability of a rock mass. The value of *BD* is in the range of 0 and 1, and the greater is *BD*, the more difficult the rock is to be blasted. This contrasts with B_i which is lower for a rock that is more difficult to blast. However, both *BD* and B_i have the same physical significance. To progress with the application of the Energy-Block-Transition model a relationship between them is required. Unfortunately, a database of blasting operations with parameters from Table 6.11 is not available at present. However, an examination of the possible range of the values of both B_i and *BD* does provide a hint of the preliminary relationship.

The values of specific charge are usually in the range 0.15-0.7 kg/m^3, the ratio of S_{ai}/S_{ab} is usually in the range 2-10 and the range of *BD* is usually 0.2-0.9, thus the range of B_i is estimated to be from 5 to 60 (m$^{1/2}$/kwh/t). Combining these ranges with

the experience and results from case studies (see Chapter 7), the following empirical equation relating *BD* and B_i is suggested, which is illustrated in Fig. 6.20.

$$B_i = \frac{10}{BD}. \qquad (6\text{-}38)$$

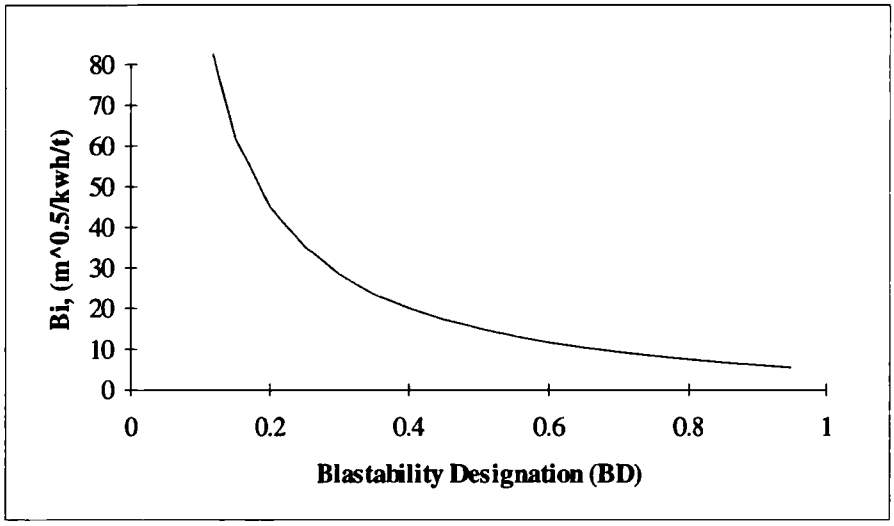

Fig. 6.20 Suggested empirical relationship of *BD* and B_i

6.6.2 Relationship between *BD* and the Rock Factor '*A*' in the Kuz-Ram Equation

The Kuz-Ram equation (Cunningham, 1983) has been widely used to predict block sizes of blastpiles for a given blast design. One of the main challenges to improve the method is to define the Rock Factor, *A* which is often roughly selected by rules of thumb or marginal improvements using empirical formulae. Based on Lilly's work (1986), Cunningham (1987) proposed an algorithm for calculating the values of *A*. This algorithm took 4 factors into consideration and improved the application of the Kuz-Ram equation. The Blastability Designation *BD* is developed using systems approach and is based on a more comprehensive range of both intact rock properties and discontinuity structures than Cunningham's algorithm. Thus, the use of the *BD* methodology in determining a value for *A*, could provide an improvement upon Cunningham's algorithm for use with the Kuz-Ram equation. A tentatively empirical equation relating *BD* and *A* is suggested as follows

$$A = 13 \times BD. \qquad (6\text{-}39)$$

The examination of Eqn. 6-39 will be described in the next chapter.

7. APPLICATIONS OF METHODOLOGY AND TECHNIQUES DEVELOPED: TWO CASE STUDIES

This chapter presents two case study examples from excavation sites showing the application of methodologies and techniques developed in the previous chapters. One concerns the blastability assessment of a rock mass for a road improvement scheme on the A5 at Glyn Bends. The other is the prediction of the BBSD of the "Overseas Quarry", a quarry that was opened in order to supply rock, including armourstone, for Beirut Airport, Lebanon.

7.1 APPLICATION 1: ASSESSMENT OF THE BLASTABILITY OF THE ROCK MASS FOR A NEW HIGHWAY CUTTING AT GLYN BENDS ON THE A5, NORTH WALES

7.1.1 Background

The assessment of the blastability of the rock mass at Glyn Bends was the principal aim of a wider study. These broader aims were to identify the reasons for the current problems encountered by the blasting contractor which included: a high proportion of blasting was producing unsatisfactory fragmentation (i.e. excess oversize), uneven toes and tight blastpiles.

Two site visits were made (May 1995, and July - August 1995). The first visit was a reconnaissance walk-over survey which enabled the author to become familiar with the layout of the site and to plan the second visit from which site investigation and data acquisition for blastability assessment was to follow. Data obtained from the author's site investigation, together with data available from previous site investigations made by others, was analysed. Reported below is the author's assessment of the blastability of the excavated rock mass at the A5 Glyn Bends site. The analysis presented incorporates the methodologies and techniques developed in the previous chapters.

7.1.2 Site Geology

7.1.2.1 The Site

The site is located at National Grid reference SH 933444 (Ordance Survey, 1986), as shown on the Fig. 7.1. It lies on the existing London-Holyhead A5 trunk road, which passes through a gorge in a series of tight bends supported by masonry retaining walls, at Glyn Bends, between the villages of Dinmael and Ty-Nant near Corwen, Clwyd. The new route under construction, at the west end, leaves the existing road at a garage and passes onto the edges of the river plain before recrossing the trunk road south of the Ty-Nant. The new route then passes into a deep cutting through the high ground to the north of the Afon Ceirw gorge. At the Tyn-y-Glyn the route emerges from the cutting and again recrosses the trunk road on its southern side, rejoining it in Dinmael.

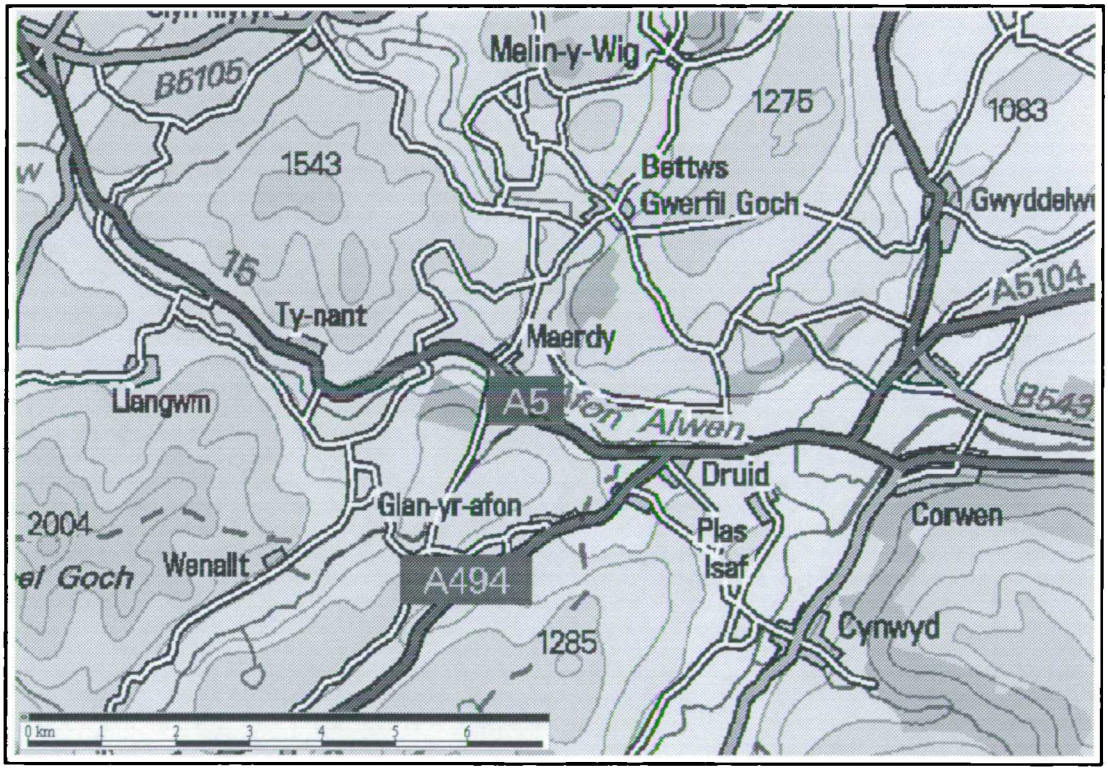

Fig. 7.1 Location of the A5 Glyn Bends Improvement Site , North Wales

The total length of the route that was under construction is approximately 2000 metres, nearly 600 metres of which are in a deep cutting. At the time of the study, the cutting was in the process of being excavated by blasting. The rock mass that was blasted was the subject of this case study. The road cutting was divided into benches, the height of a bench is generally 4-6 metres (see Fig. 7.2).

7.1.2.2 Site Geology Revealed by Previous Geological Investigations

Fig. 7.2 A view of the new rock cutting known as the A5 Glyn Bends Improvement site

According to the published British Geological Survey sheet No. 120 (BGS, 1993), the site geology consists of Allt Ddu Formation, Gelli-grin Calcareous Ash Formation, and Maerdy Mudstone Formation, and the rock materials were described as including siltstones, sandstones, tuffites, tuffs, and limestones.

Table 7.1 Geological data summarised from the previous site investigation (Mander, Raikes & Mashall (MRM), 1985)*

Borehole	Chainage	Depth	Density	UCS	Shearing strength		Discontinuity	
No.		(m)	(t/m^3)	(MPa)	C (MPa)	ϕ (°)	RQD	Spacing (m)
B60	Ch550	16.4	2.72	73.10				
B63	Ch650	23.8	2.68	48.59				
B66	Ch730	24.5	2.72	83.21	0.06	41.5	24	0.25
B70	Ch880	16.9	2.70	70.84	0.24	50.0	50	0.32
B83	Ch780	17.0	2.71	59.28	0.05	48.0	60	0.56
B85	Ch800	19.6	2.74	78.03			41	0.75

* The value of UCS given is the maximum among all test pieces; other property values are the average of all test results.

The main early ground investigations were carried out by MRM (1985) through trial pitting and trenching, which showed the site geology to consist of alluvium, glacial deposits, and Ordovician strata. The alluvium is seen in trial pits and encountered south of the Ty-Nant while the exploration holes passed through glacial deposits of varying depth. The Ordovician strata are seen to mainly consist of a siltstone with subsidiary sandstone, claystone and possibly volcanic horizons. The siltstone is faintly calcareous in places. The geological data and the mechanical properties of rock masses from laboratory tests presented by MRM in 1985 are summarised in Table 7.1.

7.1.2.3 Geological investigation and results of this study

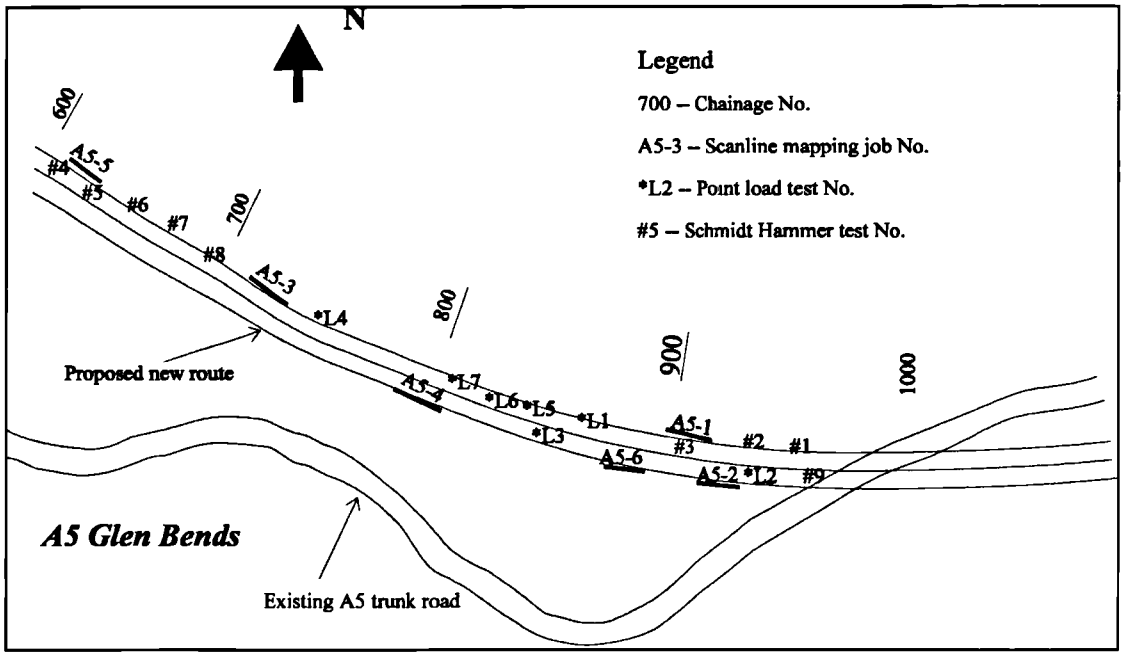

Fig. 7.3 A sketch plan for the geological investigation at the A5 site showing locations of scanline mapping and intact rock samples

The available geological data from the previous geological investigations, are limited by the poor exposures available, and appear to be an inadequate data set upon which to provide a satisfactory explanation for the blasting problems (a high proportion of blasts failed to give: satisfactory fragmentation, flat toes and loose blastpiles). During the author's site visit, the blasting was being carried out in the second bench. To provide a directly applicable set of geological data to assess the blasting problems at the A5 Glyn Bends site, further geological data acquisition was

undertaken by the author. The investigation involved: mapping discontinuities at various locations within the rock cutting; taking photos of blasting results immediately after blasting; performing point load tests and Schmidt Hammer tests in the field; collecting other associated geological data at each location and recording the blast design data.

A sketch plan for the investigation, together with the positions of the scanline mapping, the point load and Schmidt Hammer test samples, is illustrated in Fig. 7.3. The geological investigation that has carried out and the corresponding results are summarised as follows.

Discontinuities

Detailed discontinuity mapping was performed at 6 places including both the south and north cutting faces with the objective of deriving data for the in-situ block size and other mechanical parameters known to be important in predicting the outcome of blasting. The results of these six discontinuity surveys are summarised in Table 7.2. and the detailed discontinuity data mapped is listed in Appendix E.1.

Table 7.2 Summary data of detail scanline mapping

Mapping job No.	Scanline No.	Mapping place		Tape layout		Number of Discontinuity	Scanline Length (m)
		Chainage	Location	Azimuth (°)	Plunge (°)		
A5-1	SL-1-1	Ch910-940	North, the second bench bottom	125	0	16	11.0
	SL-1-2			100	0	23	17.0
A5-2	SL-2-1	Ch925-950	South, the second bench bottom	293	0	20	10.5
	SL-2-2			300	0	16	14.5
A5-3	SL-3	Ch730-750	North, the first bench bottom	140	0	33	16.0
A5-4	SL-4	Ch810-830	South, the first bench bottom	290	-8	42	17.0
A5-5	SL-5	Ch620-650	North , the first bench bottom	140	0	50	25.0
A5-6	SL-6	Ch890-910	South, the second bench bottom	145	0	44	20.0

For each of these 6 surveys, three sets of discontinuities can be isolated. Fig. 7.4 illustrates a typical output from an analysis of the mapped data. The spatial occurrence of discontinuities in the selected mapping areas are summarised in Table 7.3.

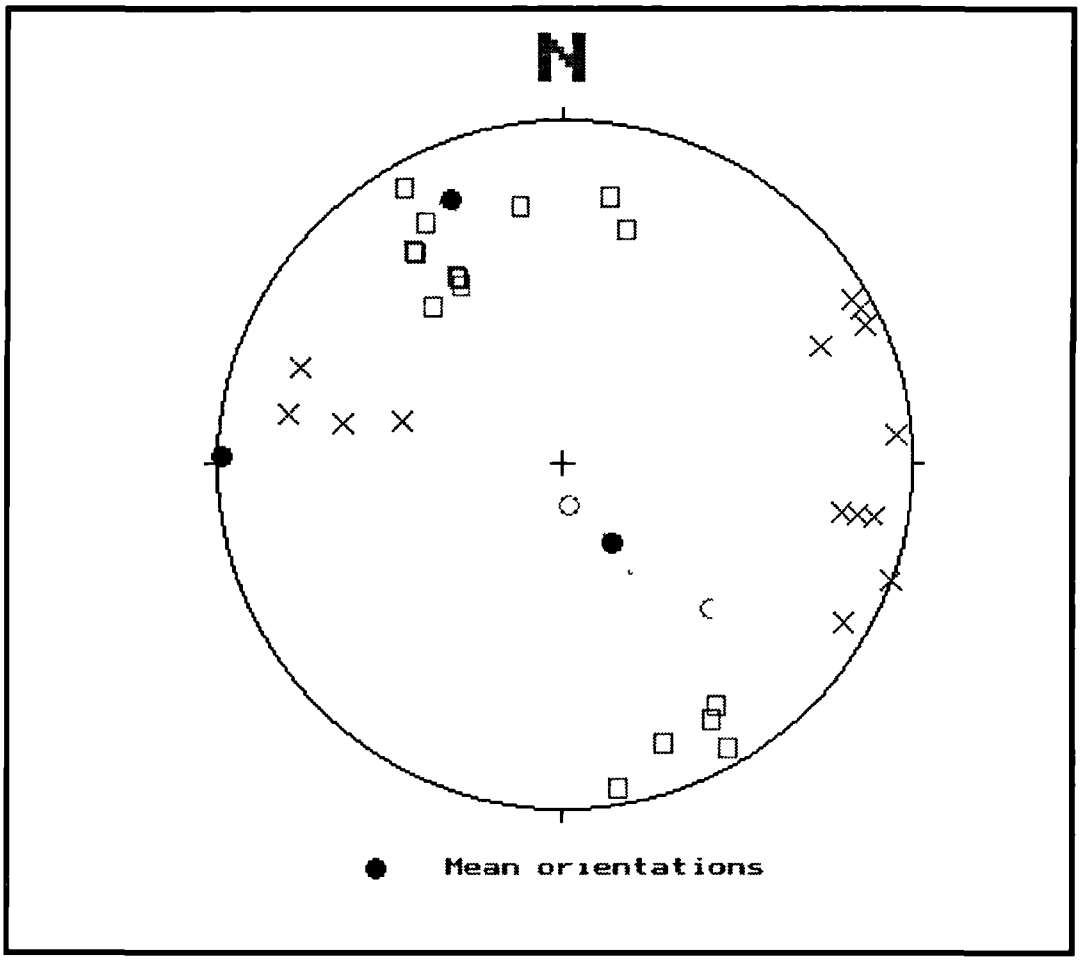

Fig. 7.4 The pole plot of discontinuities mapped in Mapping site A5-1

Table 7.3 Discontinuity occurrence

Mapping job No	Set 1			Set 2			Set 3		
	Dip dir. (°)	Dip (°)	M.S. (m)	Dip dir. (°)	Dip (°)	M.S. (m)	Dip dir. (°)	Dip (°)	M.S. (m)
A5-1	330.0	22.1	1.40	91.0	88.5	2.28	155.8	79.9	0.97
A5-2	352.3	37.8	1.19	83.1	85.6	0.72	167.8	64.4	1.20
A5-3	22.9	29.9	0.83	116.9	60.2	1.24	186.6	61.0	0.62
A5-4	209.5	24.2	0.04	90.6	78.3	0.61	142.4	70.8	1.15
A5-5	47.1	22.2	1.52	291.5	86.0	1.48	190.3	76.2	0.81
A5-6	170.7	35.4	0.49	289.4	83.2	1.98	194.5	69.1	0.33

It can be seen from the results of the six mapped regions that the discontinuities can be divided into three sets. The first is sub-horizontal and the mean dip varies between 22 to 40° with a near east-west strike. This set of discontinuities consists mainly of highly persistent bedding planes. The second and third sets of discontinuities are steeply dipping, with near south-north and east-west strikes respectively. These two sets of dipping discontinuities consist mainly of fractures, joints and cleavage planes, and often exhibit impersistence.

Intact rock properties

Point load strength index tests (ISRM, 1985) were performed on samples obtained from seven locations. The samples are taken either from the just finishing as-blasted piles or from the resident muckpiles. The details are shown in Table 7.4 (for the raw data, see Appendix .

Table 7.4 Details of point load tests and test results

Sample	Sampling place		Rock	Is(50)*	No.s of	σ
No.	Chainage	Location	description	(MPa)	Samples	
LPT-1	Ch890-903	31/07/95 blasting site	Dark, fine-grained siltstone, natural state	5.05	13	0.293
LPT-2	Ch945-955	South, Bench 1 bottom	Dark, fine-grained calcareous siltstone, natural state, air-dried 2-3 weeks	4.42	10	0.180
LPT-3	Ch877-890	01/08/95 blasting site	Very dark, fine-grained limestone and siltstone, natural state	5.92	10	0.413
LPT-4	Ch745-755	North, Bench 1 bottom	Very dark, fine-grained calcareous siltstone, natural state, about air-dried 2 months	6.51	12	0.308
LPT-5	Ch870-882	02/08/95 blasting site	Dark, very fine-grained siltstone, natural state, air-dried 1 day	4.70	11	0.235
LPT-6	Ch867-882	03/08/95 blasting site	Grey, fine-grained siltstone, natural state.	4.41	11	0.410
LPT-7	Ch850-860	04/08/95 blasting site	Grey, fine-grained siltstone, natural state.	4.52	9	0.268

* The top and bottom outlier results are rejected in the calculation

Schmidt Hammer test (ISRM, 1978) results were obtained from 14 locations and were as listed in Table 7.5.

Table 7.5 Details of Schmidt Hammer test and results

Sample No.	Sampling place		Rock description	Type	SHV	Incline (°)	UCS * (MPa)	UCS# (MPa)
	Chainage	Location						
Sch-1	Ch950	North, Bench 1 cutting face	Grey to dark, fine-grained calcareous siltstone, natural state	In-situ	47.8	40	150	137.5
Sch-2	Ch935	North, Bench 2 cutting face	Grey to dark, fine-grained calcareous siltstone, natural state	In-situ	48.8	10	155	141.8
Sch-3	Ch915	North, Bench 2 cutting face	Grey to dark, fine-grained siltstone, natural state	In-situ	43.6	15	120	119.5
Sch-4	Ch600	North, Bench 1 cutting face	Dark, fine-grained siltstone, natural state with weathering	In-situ	43.7	10	120	120
Sch-5	Ch625	North, Bench 1 cutting face	Very dark, fine-grained siltstone, natural state	In-situ	47.8	10	155	137.5
Sch-6	Ch650	North, Bench 1 cutting face	Dark, fine-grained limestone/siltstone, natural state	In-situ	46.7	10	135	132.8
Sch-7	Ch675	North, Bench 1 cutting face	Dark, fine-grained siltstone, natural state with weathering	In-situ	47	10	135	134.1
Sch-8	Ch700	North, Bench 1 bottom	Dark, fine-grained siltstone, natural state	In-situ	43.7	10	120	120
Sch-9	Ch950	South, Bench 2 cutting face	Grey to dark, fine-grained siltstone, natural state	In-situ	41.2	15	98	109.2
Sch-10	Ch820	South, Bench 2 cutting face	White to grey fine-grained limestone, natural state	In-situ	46.8	5	150	133.3
Sch-11	Ch820	South, Bench 1 cutting face	White to grey fine-grained limestone, natural state	In-situ	41.9	5	105	112.2
Sch-12	Ch880	South, Bench 2 cutting face	White to grey, fine-grained limestone, natural state	In-situ	39.7	15	88	102.8
Sch-13	Ch875	South, Bench 2 cutting face	Dark, fine-grained siltstone, natural state	In-situ	44.6	10	118	123.8
Sch-14	Ch868	South, Bench 2 cutting face	Dark, fine-grained siltstone, natural state	Block	45.1	20	120	126

* UCS is estimated according to Hoek & Bray (1981); #UCS is estimated according to Sachpazis (1990)

Other data collected

The photographs of 4 blastpiles, resulting from the blasting carried out from July 31 to August 3, 1995 were taken. In addition, the photographs of cutting faces were taken, and other data, including blasting parameters, were collected.

Summary

The rock mass data revealed from this geological investigation indicates that both the geological structures and the mechanical properties of rock materials vary from one place to another. The significance of the conclusion was apparently noted in previous geological investigations, which might explain why the blasting results had proven unpredictable and unsatisfactory. It would appear that blast designs were based on previous geological data that did not highlight this variability.

7.1.3 Predictions of IBSD

7.1.3.1 Preliminary predictions using the dissection method

It was found from the analysis of discontinuity spacings that some sets could not be fitted satisfactorily by a theoretical distribution and this was often because there were too few data (see Fig. 7.5). When theoretical distribution could be fitted at a site, there were no examples where the negative exponential or fractal distribution fitted all of the discontinuity sets.

Table 7.6 Results of in-situ block size distributions based on the dissection

Map-ping job	In-situ block size distribution parameters												
	Raw data output from Dissection				Ros-Ram equation				Schuhmann equation				Fractal Dimen.
	V_{50}	V_{632}	V_{80}	V_{100}	n_v	V_{632}	n_s	S_{632}	m_v	V_{100}	m_s	S_{100}	D_f
No.	(m^3)	(m^3)	(m^3)	(m^3)		(m3)		(m)		(m^3)		(m)	
A5-1	5.47	8.04	13.30	39.27	0.948	8.05	2.845	2.37	0.505	19.64	1.515	3.19	1.486
A5-2	18.10	26.00	41.70	151.90	1.008	26.01	3.024	3.50	0.534	60.19	1.602	4.63	1.397
A5-3	11.70	19.45	37.50	147.00	0.725	19.45	2.174	3.18	0.384	62.51	1.152	4.69	1.848
A5-4	1.10	2.15	5.02	22.27	0.554	2.14	1.663	1.52	0.296	9.85	0.888	2.53	2.113
A5-5	3.24	4.77	7.90	79.61	0.945	4.77	2.836	2.00	0.500	11.68	1.500	2.68	1.499
A5-6	5.05	10.6	14.5	112.90	0.938	8.93	2.813	2.45	0.602	22.81	1.806	3.35	1.194

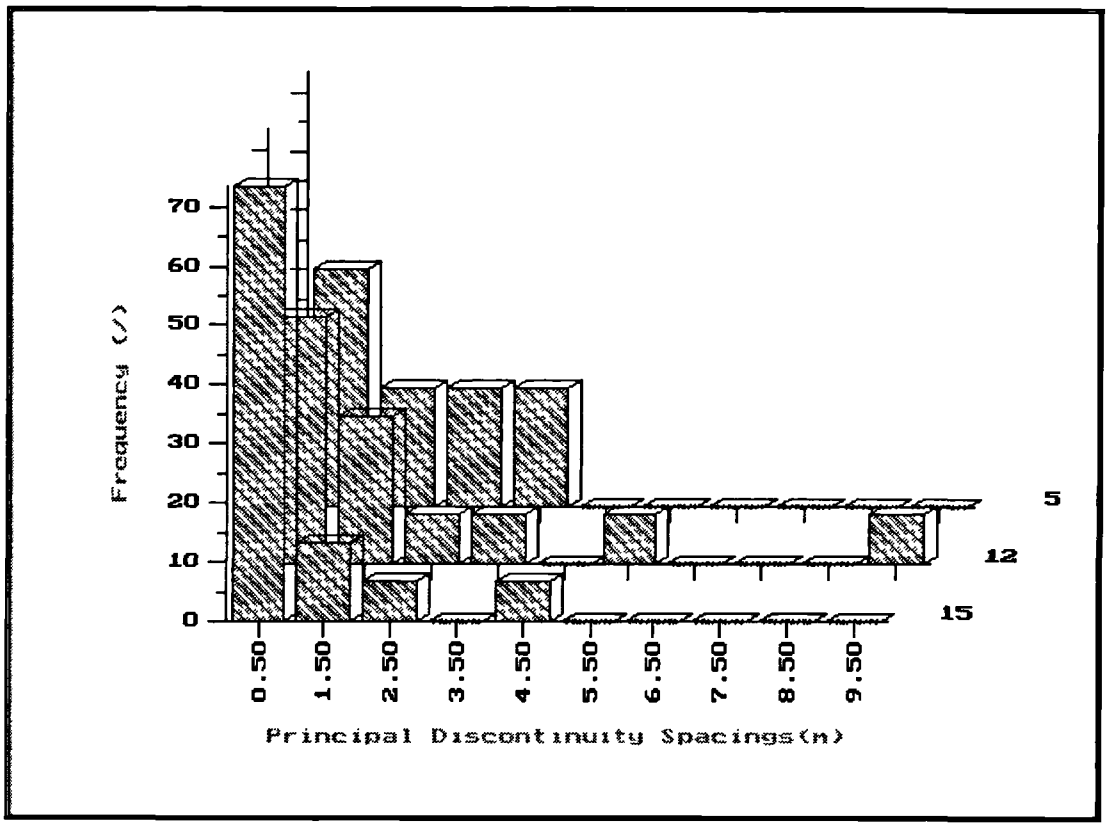

Fig. 7.5 Distribution of principle discontinuity spacings (A5-1 Mapping site)

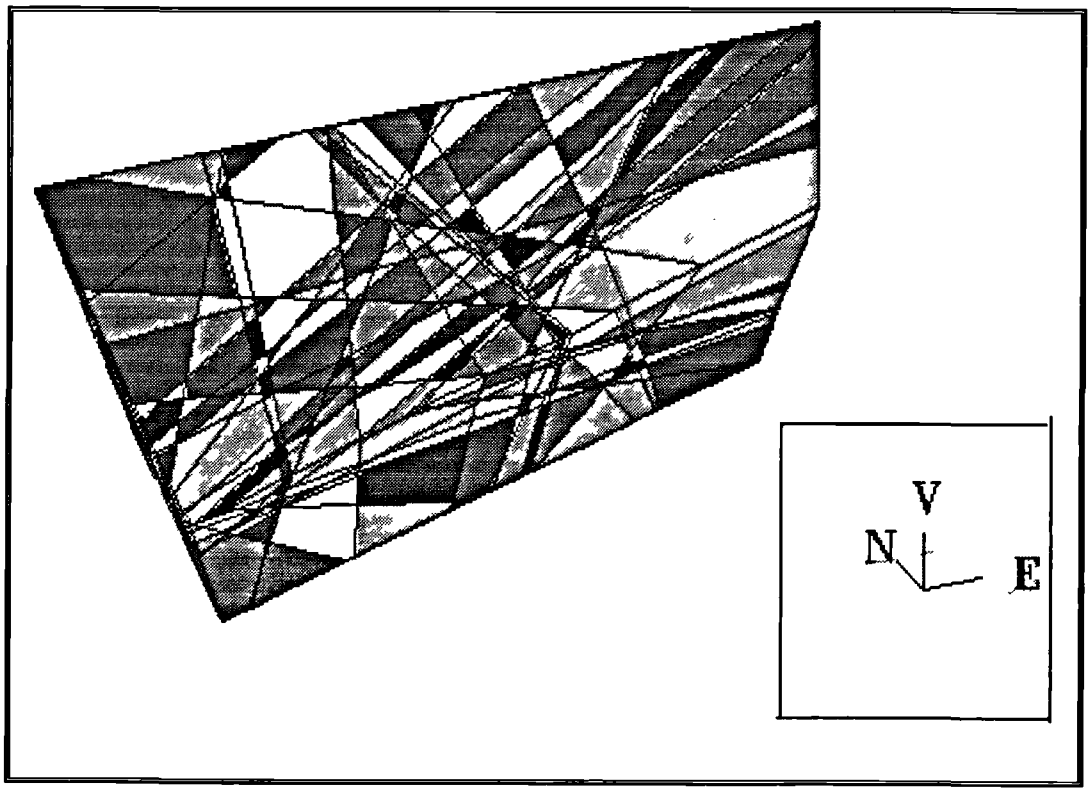

Fig. 7.6 Three dimensional view of discontinuity structure (A5-1 Mapping site)

Consequently, the IBSDs of these 6 mapping sites were derived using the dissection technique which makes no assumption about the spacing distribution, in preference to the equation method (Wang, 1992). The results of IBSDs are summarised in Table 7.6. The fractal dimension of IBSD has been calculated using a best fit for the Schuhmann equation.

In Table 7.6, V_{50}, $V_{63.2}$, V_{80} and V_{100} represent 50%, 63.2%, 80% and 100% passing volume respectively; $S_{63.2}$ and S_{100} represent 63.2% and 100% passing size respectively; n_s (n_v) is the index of uniformity in the Ros-Ram equation in terms of size (volume), m_s (m_v) is the index of uniformity in the Schuhmann equation in terms of size (volume), and the fractal dimension is obtained according to Eqn. 6.52.

The three-dimensional views of boundary block volumes intersected by discontinuities for each of the 6 mapping sites were constructed, assuming that all discontinuities mapped are persistent. Fig. 7.6 is the three-dimension view corresponding to the A5-1 Mapping site obtained using the program BLOCKS (Wang, 1992), and Fig. 7.7 is the photograph taken from the location near A5-1 Mapping site.

Fig. 7.7 Discontinuity structure of a cutting exposure at the A5 site.

7.1.3.2 Prediction from the equation methods

Although the poor fit of the data to the theoretical distribution was noted in Fig. 7.5, it is instructive to compare results obtained from the equation method with the dissect method results. One proposition arising from work in Chapter 3 was that the best estimate of the IBSD is likely to fall between that for the two extreme theoretical distributions which are the uniform spacing and the fractal spacing. This can be examined with results from the A5 site investigation.

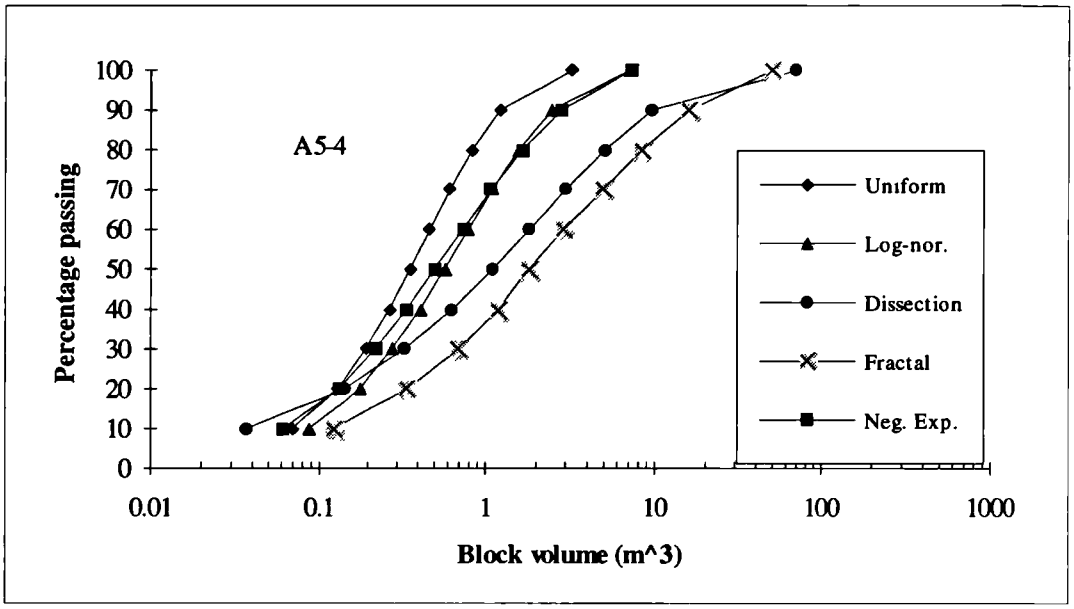

(a)

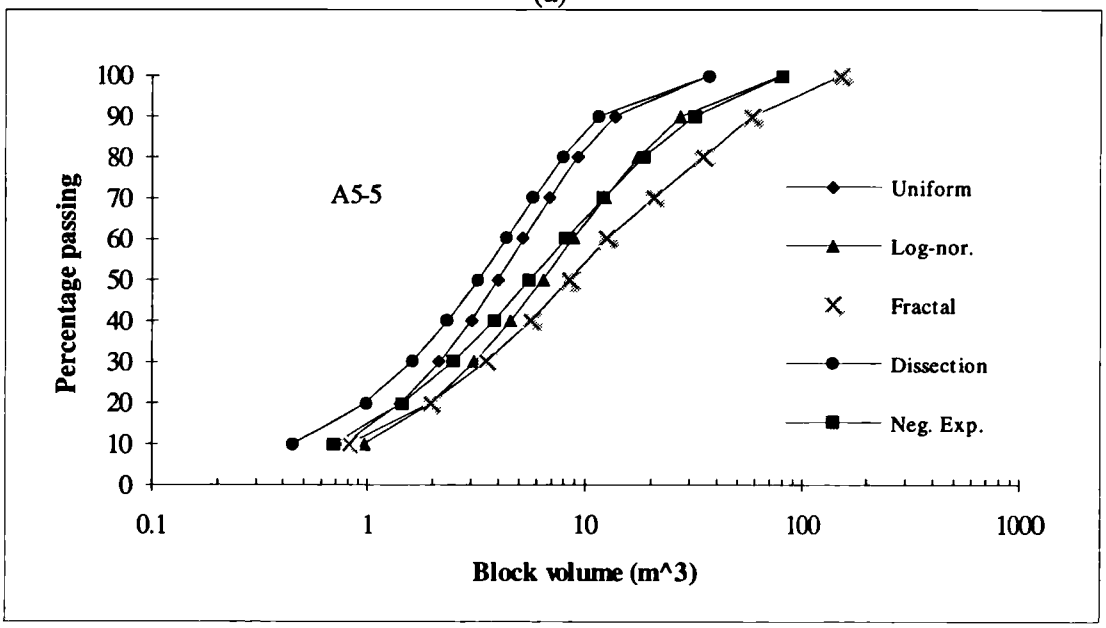

(b)

Fig. 7.8 Comparison of IBSD predictions between the dissection and the equation methods, (a) A5-4 site; (b) A5-5 site

For each site, the principal mean spacing of each set of discontinuities, S_{pm}, is weighted using the number of the discontinuity set, and then this weighted S_{pm} is used for the input to both Eqn. 2-10 and Eqn. 3-32 to get the approximate predictions of the IBSDs. The prediction results are listed in Table 7.7.

Fig. 7.8 shows a comparison between the predicted results using both the equation method and the dissection method. The comparison indicates clear discrepancy between the results from both the equation and the dissect methods although for site A5-4, the results obtained from the two methods are closed. The reason might be that discontinuity spacing could be not well described by one of three proposed theoretical distributions. In addition, the mean spacing subjectively weighted by the number of each discontinuity set can also contribute to the discrepancy. These suggest that the further investigation should be carried out to reveal the IBSD of a rock mass with combinations of different spacing distribution types although the assumption of there being only one distribution type for all sets can be used at present.

Table 7.7 The IBSD prediction results from the equation methods

Site	Mean Spacing (m)							V_{50} (m^3)				
	Set 1		Set 2		Set 3		Weighted	Equation method				Dissec-
	Value	No.	Value	No.	Value	No.		Uni.	Neg.exp	log-nor	Frac.	tion
A5-1	1.40	5	2.28	12	0.97	15	1.528	6.92	9.66	11 06	12.06	5.47
A5-2	1.19	5	1.20	14	0.72	10	1.033	2.14	2.99	3.42	5.66	18.08
A5-3	0.83	2	1.24	4	0.62	21	0.727	0.75	1.04	1.19	2.87	11.73
A5-4	0.04	10	1.15	8	0.61	16	0.569	0.36	0.50	0.57	1.79	1.10
A5-5	1.52	19	1.48	6	0.81	13	1.271	3.98	5.56	6.36	8.45	3.24
A5-6	0.49	11	1.98	9	0.33	15	0.805	1.01	1.41	1.62	3.50	5.00

7.1.3.3 Correction of the IBSD considering the impersistence of discontinuities

In Chapter 4, it has been pointed out that the impersistence of discontinuities should be taken into consideration when predicting IBSD. Using the technique developed in Chapter 4, the IBSDs at the A5 sites listed in Table 7.7 have been corrected as set out below. The trace length field measurements form the basic data from which the mean trace length and mean diameter of discontinuities were estimated.

As described above, the discontinuities in bedding plane sets are extremely persistent whereas the discontinuities in joint sets usually exhibit impersistence at outcrop scale. Thus the mean trace lengths of the joint sets were estimated using the techniques developed in Chapter 4 while the bedding sets retain their original mean trace length values. The mean diameters of discontinuity sets were then estimated using Eqns. 4-39 and 4-40. A weighted mean diameter for each site was worked out. Taking the scale of the road cutting and blasting operation into consideration, the scale dimension of the rock mass of interest, S_r, was set at 4 metre. The impersistence influence factors for the six sites were derived and the corrected IBSDs were determined. The estimates of mean trace lengths and mean diameters of discontinuities, the weighted mean diameters, and the impersistence influence factors are summarised in Table 7.8.

Table 7.8 Impersistence influence factor

Job No.	Joint set			Bedding set			Weighted	F_{imp}
	Mean T. L. (m)	Assumed Distribution	Mean Dia. (m)	Mean T. L. (m)	Assumed Distribution	Mean Dia (m)	Dia.* (m)	
A5-1	2.35	Log-nor.	1.732	5.59	Neg. exp.	4.355	2.606	0.652
A5-2	3.10	Neg. exp.	2.415	9.00	Neg. exp.	7.011	3.947	0.987
A5-3	1.30	Log-nor.	0.958	8.10	Neg. exp.	6.310	2.742	0.686
A5-4	1.40	Log-nor.	1.032	6.00	Neg. exp.	4.674	2.246	0.561
A5-5	2.30	Log-nor.	1.695	9.08	Neg. exp.	7.073	3.488	0.872
A5-6	1.25	Log-nor.	0.921	4.64	Neg. exp.	3.615	1.819	0.455

*Weighted diameter =(2/3)× mean diameter of joint set + (1/3)× mean diameter of bedding set

Table 7.9 Corrected IBSD considering influence of impersistent discontinuities

Map-ping job No.	In-situ block size distribution parameters												
	Dissection				Ros-Ram equation				Schuhmann equation				Fractal Dimen.
	V_{50} (m^3)	V_{632} (m^3)	V_{80} (m^3)	V_{100} (m^3)	n_v	V_{632} (m3)	n_s	S_{632} (m)	m_v	V_{100} (m^3)	m_s	S_{100} (m)	D_f
A5-1	6.31	9.27	15.34	45.30	0.948	9.28	2.844	2.48	0.505	22.65	1.514	3.34	1.486
A5-2	18.16	26.12	41.89	152.62	1.008	26.12	3.024	3.50	0.534	60.46	1.603	4.63	1.397
A5-3	13.30	22.06	42.53	166.67	0.725	22.06	2.175	3.31	0.384	70.89	1.152	4.89	1.848
A5-4	1.33	2.61	6.09	26.99	0.554	2.59	1.662	1.62	0.296	11.93	0.887	2.70	2.113
A5-5	3.39	4.99	8.27	83.33	0.945	5 00	2.835	2.02	0.501	12.23	1.501	2.72	1.499
A5-6	6.57	13.78	18.86	146.80	0.938	11.62	2.814	2.67	0.602	29.66	1.806	3.65	1.194

After selecting the index q in Eqn. 4-73 to be 1/3, the IBSDs of the rock mass at the A5 site determined by the dissection method were corrected as listed in Table 7.9.

7.1.4 Blastability Assessment

The methodology described in Chapter 6 has been employed to assess the blastability of the rock mass at the A5 Glyn Bends Improvement site. The blastability assessment has been made using both field data obtained by the author and previously available site data, and a comparison has been made.

7.1.4.1 Blastability assessment based on new field data

Six sites have been selected, the details of these sites are listed in Table 7.10. Based mainly on the information obtained from the site investigation carried out by the author, the blastability assessments of the above six sites at the A5 Glyn Bends Improvement have been made. Using the CQC approach (Lu & Latham, 1994) to coding the interaction matrix described, the coding results were obtained as described in Chapter 6 (see Fig. 6.17).

Table 7.10 Locations and details of the sites subjected blastability assessment

Site No.	Mapping place	
	Chainage	Location
S1	Ch910-940	North cutting face, Bench 1 bottom, near 03/03/95 blasting site
S2	Ch925-950	South cutting face, Bench 2 bottom, near 24/07/95 blasting site
S3	Ch730-750	North cutting face, Bench 1 bottom, still existing ridge there
S4	Ch810-830	South cutting face, Bench 1 bottom, near 03/08/95 blasting site
S5	Ch620-650	North cutting face, Bench 1 bottom
S6	Ch890-910	South cutting face, Bench 2 bottom, near 31/07/95

It is seen from Fig. 6.18 that the range in parameter interaction intensity is quite wide (cf. Fig. 9.6b in Hudson, 1992). Thus, only those factors contributing to a total of 72.5% of the Σ(C+E) in the ordered histogram, that is, the eight parameters, P_1, P_2, P_3, P_4, P_5, P_6, P_9, P_{10} have been chosen as the main contributory factors of the blastability of the rock masses at the A5 site. The corresponding weights of the eight factors were derived using the method illustrated in Fig. 6.17, and they are listed in

Table 7.11. Having completed the first stage, which is concerned with the matrix coding and thus the parameter weighting, the second stage is to obtain the actual results for each parameter using field samples, tests, and experience.

The assessment results of blastability are shown in Table 7.11. Due to a lack of a complete sets of test results, a number of empirical formulae based on published correlation studies have been used to derive missing parameters and these correlation equations are briefly explained below.

Where possible, a check on the validity of the correlation equations have been made since there is a considerable interdependence of test parameters. In Table 7.11, the densities of rock are the values obtained in the site investigation carried out by MRM (1985). The *UTS* values are estimated from the *PLI* values (or estimated from *UCS* values) according to the following empirical formula suggested by ISRM (1985).

$$UTS = 1.25\,PLI, \tag{7-1}$$

where, both *PLI* and *UTS* are in MPa.

The values of P-wave velocity, V_p, are estimated from the average obtained from the following two empirical formulae suggested by Karpuz et al. (1990).

$$V_p = 1549.9 UTS^{0.227}, \tag{7-2}$$

$$V_p = 993.4 + 1467\rho, \tag{7-3}$$

where *UTS* is in MPa, ρ in t/m^3, and V_p is in m/s. The results from the above two formulae examined using an empirical equation (Soedibjo, 1990) as follows.

$$V_p = 1.12\,PLI + 0.237, \tag{7-4}$$

where V_p is in km/s, and *PLI* is in MPa.

The values of elasticity modulus, E, are estimated according to the following formulae suggested by Beverly et al (1979, see Xu et al., 1990).

$$E = 0.192(SHV \times \rho^2) - 12.71, \tag{7-5}$$

where E is in GPa and ρ is in t/m^3. The estimates of E are also examined using the following empirical equations suggested by Sachpazis (1990).

$$SHV = 0.5155E + 17.488, \tag{7-6}$$

$$E = 0.3752UCS + 4.479, \tag{7-7}$$

where E is in GPa and UCS is in MPa.

Table 7.11 Blastability assessment of rock masses at the A5 Glyn Bends Improvement

Parameter			Weight	Blastability assessment								
No.	Description		Wi	S1			S2			S3		
P_i		Unit		Value	Rating	Wi*Ri	Value	Rating	Wi*Ri	Value	Rating	Wi*Ri
1	Is(50)	MPa	0.1475				4.42	0.65	0.096	6.51	0.8	0.118
	UCS	MPa		120	0.680	0.100						
2	UTS	MPa	0.1344	6.82	0.670	0.090	5.53	0.580	0.078	8.14	0.700	0.094
4	E	GPa	0.1273	48.80	0.495	0.050	45.13	0.380	0.048	52.39	0.410	0.052
3	ρ	t/m^3	0.1249	2.710	0.675	0.084	2.704	0.680	0.085	2.715	0.720	0.09
6	SHV		0.1225	43.6	0.710	0.087	41.2	0.660	0.081	46	0.750	0.092
5	V_p	m/s	0.1208	4901	0.920	0.111	4784	0.900	0.109	4996	0.930	0.112
10	D	m	0.1131	1.486	0.440	0.05	1.397	0.420	0.048	1.848	0.590	0.067
9	MBSD	m	0.1095	2.18	0.830	0.091	3.10	0.935	0.102	2.80	0.915	0.100
Blastability Designation						0.664			0.647			0.725
Parameter			Weight	Blastability assessment								
No.	Description		Wi	S4			S5			S6		
P_i		Unit		Value	Rating	Wi*Ri	Value	Rating	Wi*Ri	Value	Rating	Wi*Ri
1	Is(50)	MPa	0.1475	4.45	0.65	0.096				5.05	0.69	0.102
	UCS	MPa					135	0.730	0.108			
2	UTS	MPa	0.1344	5.563	0.590	0.079	7.67	0.710	0.095	6.31	0.680	0.091
4	E	GPa	0.1273	50.07	0.400	0.051	48 47	0.400	0.050	42.9	0.330	0.042
3	ρ	t/m^3	0.1249	2.70	0.675	0.084	2 63	0.610	0.076	2.70	0.680	0.084
6	SHV		0.1225	44.85	0.725	0.089	46.07	0.740	0.091	39.7	0.550	0.067
5	V_p	m/s	0.1208	4785	0.900	0.109	4908	0.920	0.111	4852	0.910	0.110
10	D	m	0.1131	2.113	0.690	0.078	1.499	0.450	0.051	1.194	0.370	0.042
9	MBSD	m	0.1095	1.31	0.690	0.076	1.78	0.790	0.087	2.22	0.830	0.091
Blastability Designation						0.662			0.669			0.631

The data taken from the author's site investigation and sampling based on 6 field locations along the cutting, when subjected to the blastability analysis, yielded value of the Blastability Designation from 0.631 to is 0.725, as shown in Table 7.11. That is, the rock masses in the highway cutting area belong basically to the border range between Class 4 (difficult blasting) and Class 3 (moderate blasting) (see Table 6.12). Applying the description terms to the *BD* results, this means that the rock masses are, in general, difficult or moderate to blast.

7.1.4.2 Blastability assessment based on previously available site data

The blastability of the rock masses at the site are assessed at three places based on the previous geological information presented in Table 7.1, and is shown in Table 7.12. The locations of Site OS1, Site OS2 and Site OS3 correspond roughly to the location of Site S3, Site S6 and Site S4 in Table 7.11 respectively. From the three field locations, where the previous geological information was available, the values of the Blastability Designation were from 0.498 to 0.569 (see Table 7.12). This indicates that the rock masses would belong to the border range between Class 2 (easy blasting) and Class 3 (see Table 6.12). That is, the rock masses would be assessed as easy or moderate to blast.

Table 7.12 Blastability assessment of rock masses at A5 Glyn Bends Improvement based on the previous geological information*

Parameter			Weight	OS1			OS2			OS3		
No.	Description		Wi	Value	Rating	Wi*Ri	Value	Rating	Wi*Ri	Value	Rating	Wi*Ri
P_i		Unit										
	UCS	MPa	0.1475	83.21	0.540	0.08	70.84	0.480	0.071	78.03	0 520	0.077
2	UTS	MPa	0.1344	4.728	0.520	0.07	4.025	0.500	0.067	4.434	0 510	0.069
4	E	GPa	0.1273	37.15	0.290	0.04	32.39	0.250	0.032	35.10	0.270	0.034
3	ρ	t/m^3	0.1249	2.72	0.750	0.09	2.70	0.740	0.092	2.71	0.745	0.093
6	SHV		0.1225	35.10	0.550	0.07	32.22	0.450	0.055	33.89	0.470	0.058
5	V_p	m/s	0.1208	4716	0.890	0.11	4621	0 880	0.106	4676	0.880	0.106
10	D	m	0.1131	1.848	0.590	0.07	1.194	0 370	0.042	2.113	0 690	0.078
9	PMS	m	0.1095	0.25	0.250	0.03	0.32	0.310	0.033	0.75	0.505	0.055
Blastability Designation						0.549			0.498			0.569

* *PMS* from logs of the report (MRM, 1985); the values of fractal dimension *D* are the same as those listed in Table 7.11.

7.1.5 Estimation of BBSD

Blastability assessment results obtained above should reflect in the blasting results which can be indicated by the BBSD. To examine the BBSD at the site, four approaches will be used and compared. These are (i) direct assessment of the BBSD by the photo-scanline method as described in Chapter 5; (ii) estimation using the previously published blast design Kuz-Ram model with no IBSD information needed; (iii) estimation using the previously published Bond-Ram model which can take advantage of the new IBSD estimation procedure and (iv) estimation using the new Energy-Block-Transition model and blastability assessment (see Chapter 6) .

In addition, a prediction of the BBSD primarily based on the Kuz-Ram model but with a correction such that the rock factor in the Kuz-Ram model, *A*, is determined not by Eqn. 2-13 but by Eqn. 6-39 which is based on the blastability assessment. The Kuz-Ram model with the corrected *A* based on the blastability assessment will be called the corrected Kuz-Ram model.

Table 7.13 Parameters associated with the predictions of BBSD

Blasting pattern parameters			Rock mass parameters		
Blasting site	31/07/95	03/08/95	Blasting site	31/07/95	03/08/95
Q (kg)	1430	605	Is(50) (MPa)	5.05	4.45
q (kg/m^3)	0.65	0.62	UCS (MPa)	111.10	97.90
Bench Height (m)	7		UTS (MPa)	6.31	5.56
Hole depth (m)	8		E (GPa)	46.10	50.10
Subdrill (m)	1		SHV	39.70	44.85
Hole No.s	55	22	Mean IBSD (m)	2.20	1.30
Hole Dia. (mm)	105		ρ (t/m^3)	2.70	2.70
Explosive	PG800/900		V_{50} (m^3)	6.57	1.33
Burden (m)	2.5		$V_{63.2}$ (m^3)	13.78	2.61
Spacing (m)	2.5		n_v	0.938	0.554
Bottom Charge (m)	1		S_{50} (m)	2.21	1.30
Column Charge (m)	3		$S_{63.2}$ (m)	2.83	1.63
Stemming (m)	3		n_s	2.813	1.663

The blast pattern data, the borehole parameters, and the explosive details are summarised in Table 7.13, where the data has been obtained from the site investigations and a number of blast designs carried out on site, as provided by CAB. The BBSD results were estimated using the photo-scanline technique and have been listed in Table 7.14. Fig. 7.9 is one of several typical blastpile photographs.

Fig. 7.9 A typical blastpile photograph, B1-1 taken from the A5 site (scale bar: 50 cm division; note, the scale bars form a right angle and this enable a correction to be applied to the photographic data)

Table 7.14 The BBSDs estimated using the photo-scanline technique

Photo	Ros-Ram		Schuhmann		Blasting
No.	S_c (m)	n_s	S_{100} (m)	m_s	site
B1-1	0.354	0.769	0.746	0.641	31/07/95
-2	0.325	1.079	0.653	0.83	
-3	0.419	1.275	0.67	1.148	
-4	0.476	1.004	1.076	0.681	
Average	0.394	1.032	0.786	0.825	
B2-1	0.541	1.0863	1.029	0.861	01/08/95
-2	0.572	1.123	1.071	0.641	
-3	0.527	0.73	1.174	0.594	
Average	0.547	0.980	1.091	0.699	
B3-1	0.221	1.2625	0.4111	0.9498	02/08/95
-3	0.5548	1.088	1.528	0.9462	
-4	0.6875	0.7107	1.555	0.575	
Average	0.488	1.020	1.165	0.824	
B4-1	0.2633	0.7869	0.5894	0.6063	03/08/95
B4-4	0.4149	1.0556	0.8373	0.7803	
Average	0.339	0.921	0.713	0.693	

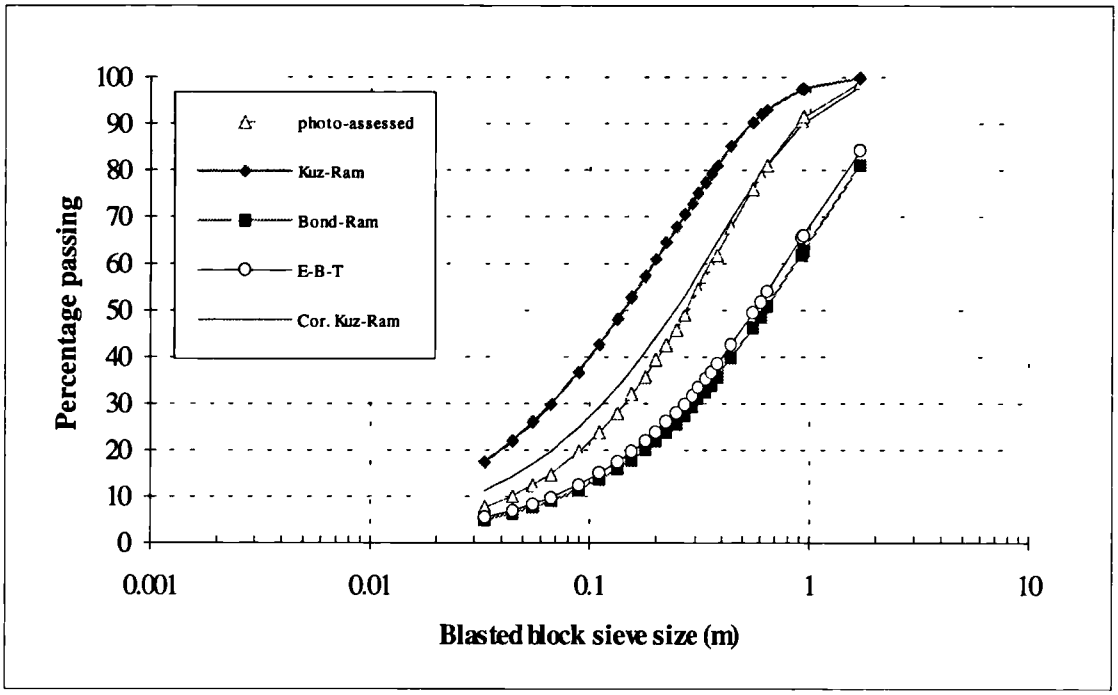

Fig. 7.10 Comparison of BBSDs from different prediction models and from the photo-scanline technique (31/07/95 blast)

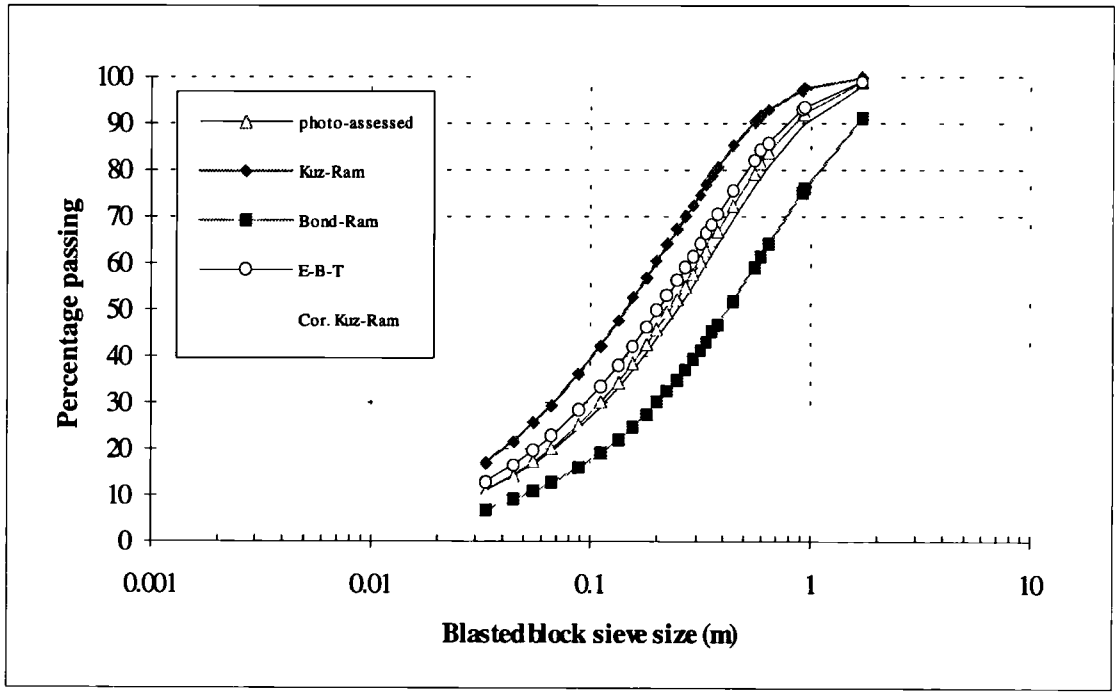

Fig. 7.11 Comparison of BBSDs from different prediction models and from the photo-scanline technique (03/08/95 blast)

A comparison of the BBSD results of two blasts, one carried out on July 31 and another on August 3, 1995, which also consider the different prediction models and the

photo-assessments is illustrated in Figs. 7.10 and 7.11. The comparison of the characteristic BBSD size parameters are shown in Table 7.15.

Table 7.15 Characteristic BBSD size parameters from different predictions

Blasting site	BBSD parameters									
	31/07/1995					03/08/1995				
	n_s	S_{50}	$S_{63.2}$	S_{80}	S_{90}	n_s	S_{50}	$S_{63.2}$	S_{80}	S_{90}
Model		(m)					(m)			
Kuz-Ram	0.892	0.142	0.214	0.365	0.545	0.892	0.144	0.217	0.370	0.553
Photo	1.032	0.276	0.394	0.625	0.884	0.921	0.228	0.339	0.568	0.838
Corrected Kuz-Ram	0.892	0.234	0.353	0.601	0.899	0.892	0.237	0.357	0.609	0.910
EBT	0.892	0.569	0.858	1.463	2.186	0.892	0.202	0.304	0.518	0.774
Bond-Ram	0.892	0.677	0.949	1.619	2.417	0.892	0.393	0.631	1.076	1.607

From Figs. 7.10, 7.11, and Table 7.15 the following important observations can be made. First, for each of the two blasts, the estimate of the blastpile's BBSD from the photo-scanline technique appears to lie near the average of the predictions from the Kuz-Ram, the Bond-Ram, the Energy-Block-Transition model and the corrected Kuz-Ram model. This suggests that the photo-scanline technique could provide a reasonable tool, although further research and direct sieving of blastpiles may be required to examine the technique and establish whether it can compete with other analysis methods.

Second, the BBSD predictions from the Kuz-Ram and Bond-Ram models form the far upper and far lower boundaries while that from either the newly developed Energy-Block-Transition model or the corrected Kuz-Ram model based on the blastability assessment is approximately in the middle of the range formed by BBSDs from the Kuz-Ram and the Bond-Ram models. The BBSD result from either the Energy-Block-Transition model or the corrected Kuz-Ram model appears to be a refinement and improvement on the Bond-Ram and the Kuz-Ram models.

Third, the BBSD from the Energy-Block-Transition model and the corrected Kuz-Ram model are close to the BBSD assessed using the photo-scanline technique.

7.1.6 Discussion

The results from the site investigation carried out by the author show the degree to which both mechanical properties and discontinuity structures change from one place to another. As a result, the blastability of rock masses will exhibit these differences. Different fragmentation would be expected if no modification of blasting pattern is undertaken to tailor it to variations in the different blastability of an area. Not taking account of this variability could be one reason why the previous blasting results were unsatisfactory in various places.

It seems reasonable to assume that early blasting operations at the site began by taking account of the historical geological data. This study has shown that a more representative and comprehensive data set suggests, from the above comprehensive analysis, that the resistance to blasting would be greater than that likely to be estimated from the initial data set. Furthermore, the variability of resistance to blasting was not previously recognised, since the difference between Blastability Designation of 0.631 (Site S6) and 0.725 (Site S3) (see Table 7.11) represents a clear increase in specific charge required (cf. Eqns. 6.18 and 6.38).

At Site S3, for example, there remained a hard ridge of more than 1 metre in height. This site is located near Chainage 740 and the blasting happened in February. The specific charge (or powder factor) is around 0.4 kg/m^3. Based on the previous geological data where in particular, the intact strength sampled seemed to be rather lower than representative, its value of Blastability Designation is assessed to be 0.569 (see Site OS3 in Table 7.12). This means that the rock material should be 'moderately blasted' (see Table 6.12), whereas the remaining hard ridge is evidence to the contrary. Based on the geological data obtained by the author, the value of Blastability Designation was 0.725 (Table 7.11), which indicates that the rock material at this site location is difficult to blast.

It is therefore suggested that some adjustment to blasting design should be made according to the geological data as revealed in the new site investigation in order to achieve a satisfactory blasting result - one that could reduce oversize and by implication, improve the loosening of the blastpile.

Although outside the scope of this study, in practice, the blast design was constrained by environmental factors and a limitation on maximum instantaneous charge was imposed. Since the powder factor was up to 0.6 kg/m^3, it seems unlikely that a decrease in burden and spacing would have eliminated the rough toes and minimised big boulders. However, it was suggested that increasing the length of

subdrilling a little, say from the present 1.0 metre to 1.2 metres, could have helped in producing better fragmentation and a looser blastpile. It is reasonable to expect that where subhorizontal discontinuities are widely spaced, the chance location of such discontinuities near the base of the boreholes can have a strong influence on the position and evenness of the toe.

7.2 APPLICATION 2: PREDICTION OF BBSD OF AN OVERSEAS QUARRY SUPPLYING ARMOURSTONE

7.2.1 Background

The opportunity for the second case study arose from an investigation into the future potential of a quarry that had just been opened. This quarry was to provide the rock materials for a massive reclamation structure upon which a new overseas airport was to be built. In the early development of this quarry which was to be dedicated to the supply of rock fill and armourstone, some doubts were raised as to whether the overseas quarry would be able to produce sufficient volumes of rock blocks in the armourstone size range. The case study reported here did not involve a field site visit by the author (although the author suggested the procedure of field discontinuity mapping survey on the site), but is based on a detailed analysis of geological and geotechnical data including results of a blast obtained from the engineers involved in developing the overseas quarry site. The analysis tools employed were those described in this thesis and the aim was to provide an analysis that would help in decision making regarding the need for further site investigation to target areas of greater armourstone potential and the need to consider alternative quarry sources of armourstone for the airport project.

It will be clear from the foregoing chapters that the prediction of quarry BBSD curves, i.e. fragmentation curves, is notoriously difficult, but of extremely high economic significance. Therefore all reasonable researched and commercially available prediction methodologies, including the Energy-Block-Transition model developed in Chapter 6, and their results should be considered carefully and evaluated. Measurements of block sizes from trial blasts can be used as the input of back-analysis to fine-tune the coefficients used in the prediction methodology and thereby to improve accuracy of initial estimates of quarry yields at a given site. Confidence in a prediction methodology can be gained once its relative success in predicting the

outcome of blasting in different geological conditions (over which the blast engineer has no control) have been demonstrated. However, it is not often that a calibrated methodology is the applied and checked with photo-assessments of BBSDs from different areas and unfortunately this was also not possible in the case history reported here.

It was suggested in the first road cutting case study that the Energy-Block-Transition model makes an improvement on both the Kuz-Ram and the Bond-Ram model. However, this model has also not yet been extensively calibrated and therefore it is of interest to adopt the common development procedure often used in quarries and mines which is to rely on the fine-tuning of predictive models from back analysis of trial blasts in areas of differing IBSD. Thus, this case study aims to further examine the Energy-Block-Transition model through comparing the model to the Kuz-Ram and the Bond-Ram models while providing predictions of the BBSD.

7.2.2. Geological Data

7.2.2.1 Physical and Mechanical Property Test Data

Reports of the early quarry site investigation work containing logs of the variation with depth of physical and mechanical properties have been examined briefly for all the boreholes (OVERSEAS QUARRY Item-1, Item-2, via. J. Simm in H. R. Wallingford). A general location diagram of boreholes on a contoured base map of the overseas quarry site was also available (OVERSEAS QUARRY Item-3, Item-9, via. J. Simm), as shown in Fig 7.12. The information accumulated from the above data suggests that this sedimentary sequence of limestone is difficult to cross-correlate between boreholes and that variations in degree of cementation, weathering and alteration both laterally and with depth occur over relatively short distances. Of greater significance with respect to predicting armourstone yields are the data relating to discontinuity spacings between joints and bedding planes.

7.2.2.2 Discontinuity Spacing and Other Relevant Data

Available discontinuity and other relevant data includes:

(i) General photographic record of surface exposures (OVERSEAS QUARRY Item-4);

(ii) Detailed logs of discontinuity spacings from retrieved cores of sub-vertical boreholes (OVERSEAS QUARRY Item-5);

(iii) Discontinuity spacings from sub-horizontal scanlines within surface exposures, set up on three different elevations (OVERSEAS QUARRY Item-6)

(iv) Approximate position of scanlines were recorded with respect to the base map;

(v) Results of sieve analysis of the blast-pile from the trial blast near BH4 (OVERSEAS QUARRY Item-7).

The details of discontinuity spacings from retrieved cores of sub-vertical boreholes and the sub-horizontal scanline mapping are listed in Appendix E.2.

7.2.3 Prediction Methodologies

As described previously, the IBSD of the rock mass imposes a critical influence on the blast outcome. Thus the IBSD of rock mass at the overseas quarry should be firstly estimated. It will be apparent that there is a great significance to be attached to the average in-situ block size distribution, IBSD and how it varies from place to place in the quarry. It is the quick scanline technique used on rock exposures with horizontally stretched scanlines and on recovered borehole cores that have been exploited in the case study. As such only the equation method has been applied to the available data, as the quick scanline data seemed appropriate for early analysis when considering the types of discontinuities found in the quarry.

A brief analysis of the initial borehole investigations of the rock quality and spacing between bedding planes and fractures have shown very little systematic variation. Not only is there no easily discernible increase of discontinuity spacing with depth below the weathered surface topography, there is also little borehole evidence that specific more thickly bedded series of sub-horizontal horizons can be traced laterally to any great extent and this is apparently not untypical of reef limestones of the type described in the site investigation report. However, photographs of outcrops do indicate certain locations with bedding that appears substantially more favourable for armourstone production than others. There therefore seems to be some potential for sampling the spatial variation of that one factor (i.e. the in-situ block sizes) which exerts most control over the BBSD. The average IBSD of the whole area to be exploited could then be predicted down to a moderate depth of some 15 metres. More important perhaps, those specific areas and depths that have higher armourstone potential could be identified and perhaps quarried with special techniques to enhance large block production (e.g. see Wang et al, 1991b).

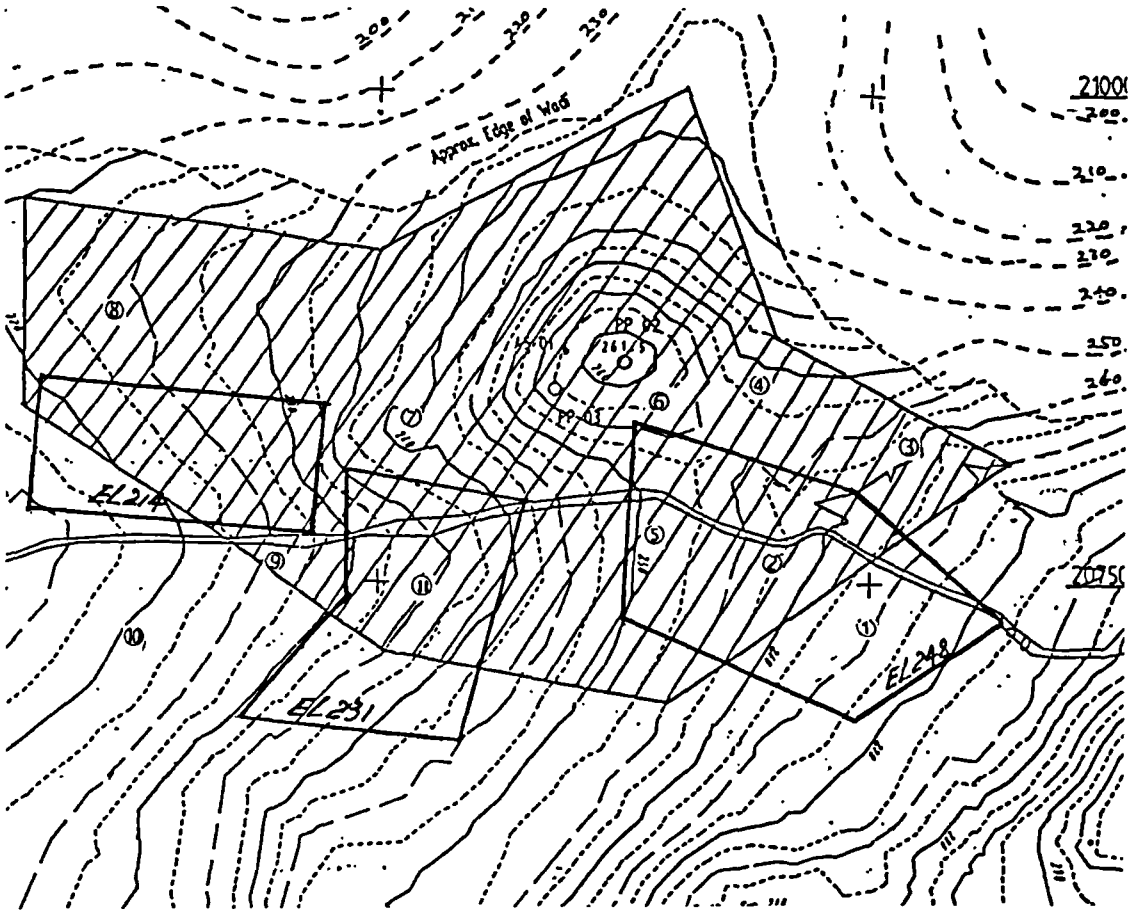

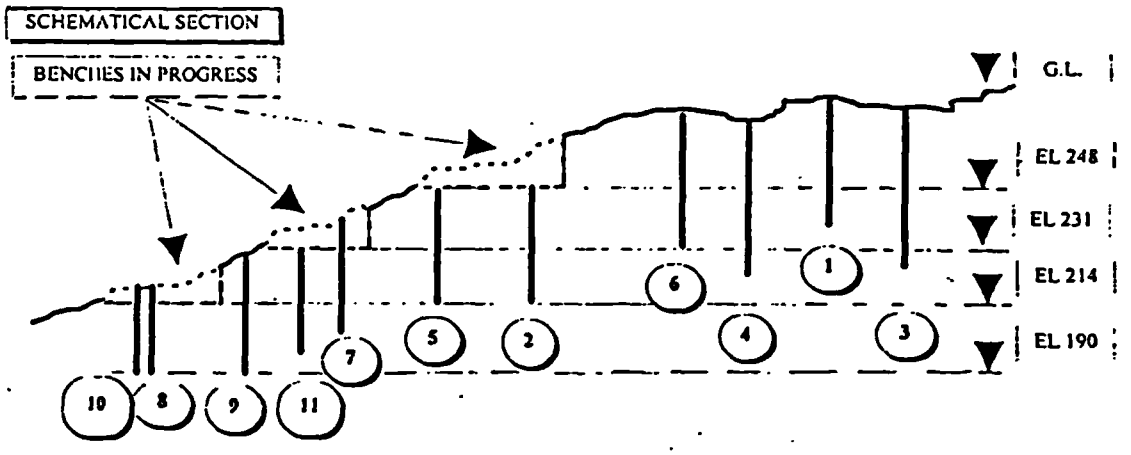

Fig. 7.12 Illustration of both the elevations and boreholes at the overseas quarry

There are three different types of available data: (i) Good quality data is available from 10 boreholes in many areas and all elevations. These assess the spacing of sub-horizontal joints and bedding planes. (ii) Moderately good quality data is available from scanlines on elevations in areas including BH4 which can be combined with the nearest borehole data at the same elevation. Taken together (i) and (ii), these data assess the spacing of sub-horizontal and sub-vertical discontinuities in three dimensions. (iii) Excellent blastpile sieve size results from Elevation 248 in the area near BH4 are also available.

Methodologies for predicting the yield curves can utilise several blast design models if they incorporate IBSD information from fracture spacings along horizontal scanlines as well from the borehole data. They are likely to give better estimates than methodologies based on borehole data without scanlines in the other two directions provided the scanline data quality is satisfactory when compared with good quality core recovery data, which seems be a reasonable condition in this case.

The methodologies presented below will utilise the discontinuity spacings in 3-D in such a way that the prediction methods are first presented and then fine tuned using coefficients which fit the trial blast data. The fine-tuned methods are then set for further predictions and are used to present the final BBSD prediction at all three elevations for which scanlines and borehole data were obtained.

7.2.4 Prediction of IBSD for three Elevations at the Overseas Quarry

At the time of gathering field data from scanlines, there were three benches in the quarry, which were at Elevation 248, Elevation 231 and Elevation 214 (see Fig. 7.10). For each bench, two scanlines were set out for discontinuity mapping measurements. When using the equation method to derive the IBSD, discontinuity data input is usually from a combination of at least three scanlines and borehole logging. For the quarry, the data input is from a combination of both horizontal scanlines (mainly sub-vertical joints and planes) and the borehole logs. Note that only the spacings from the top 12 metres of each borehole are considered when deriving data sets for a given elevation, as shown in Fig. 7.10.

When applying the equation method to the quick scanline data for the IBSD estimation, it is always assumed that the mean orientations of three discontinuity sets

are already known. The appropriate estimates of the mean orientations of the three sets of discontinuities, according to the information available, were obtained as follows:

Discontinuity Set	Dip	Dip direction
1	10-15	80
2	85-90	35-55
3	85-90	115-175

7.2.4.1 IBSD Prediction Result

In the analysis of the IBSD of the rock masses at the quarry, the measurements from two scanlines and one borehole log were first combined to form a group of input data for the IBSD analysis. The IBSD curves for the rock masses at the quarry are illustrated in Fig. 7.13. In the figure, the IBSD curve for Elevation 248 was obtained using the average values of IBSD of B1, B3, B4 and B5, where the data input for B1 was from the combination of Borehole 1 and the quick scanline measurements carried out on Elevation 248, and the data input for B3, B4 and B5 were combined in an equivalent manner. The IBSD curve for Elevation 231 was obtained using the average values of IBSD of B7, B9 and B11, where the data input for B7 was from the combination of Borehole 7 and the quick scanline measurements carried out on Elevation 231, and likewise for B9 and B11. The IBSD curve for Elevation 214 was obtained using the average values of IBSD of B8, B9 and B10, where the data input for B8 was from the combination of Borehole 8 and the quick scanline measurements carried out on Elevation 214, and likewise for B9 and B10.

As a comparison, another kind of input data which is only based on the data from vertical borehole logging, i.e. sub-horizontal joints and bedding planes was also taken into consideration. In the case where only the borehole logging is used, the other two sets of discontinuities were assumed to have the same principal mean spacings as that of the sub-horizontal discontinuity set taken from the borehole logs.

The IBSD results of three elevations from the data only supplied by borehole surveying are illustrated in Fig. 7.14. Comparison of Fig. 7.13 and Fig. 7.14 indicates that the in-situ block sizes resulting from the combination of scanline measurement and borehole logging is larger than that using borehole logging data alone. This is because the sub-horizontal discontinuity spacings formed in the recovered cores are quite significantly smaller than the sub-vertical discontinuity spacing indicated by

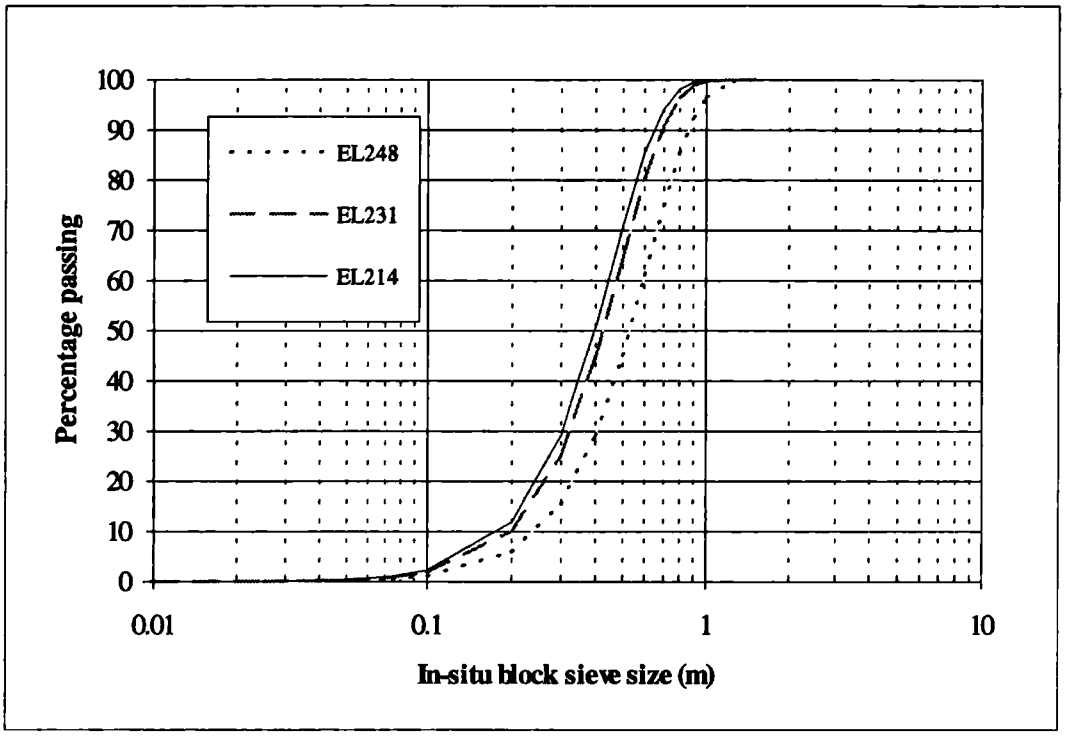

Fig. 7.13 IBSD curves of the Quarry

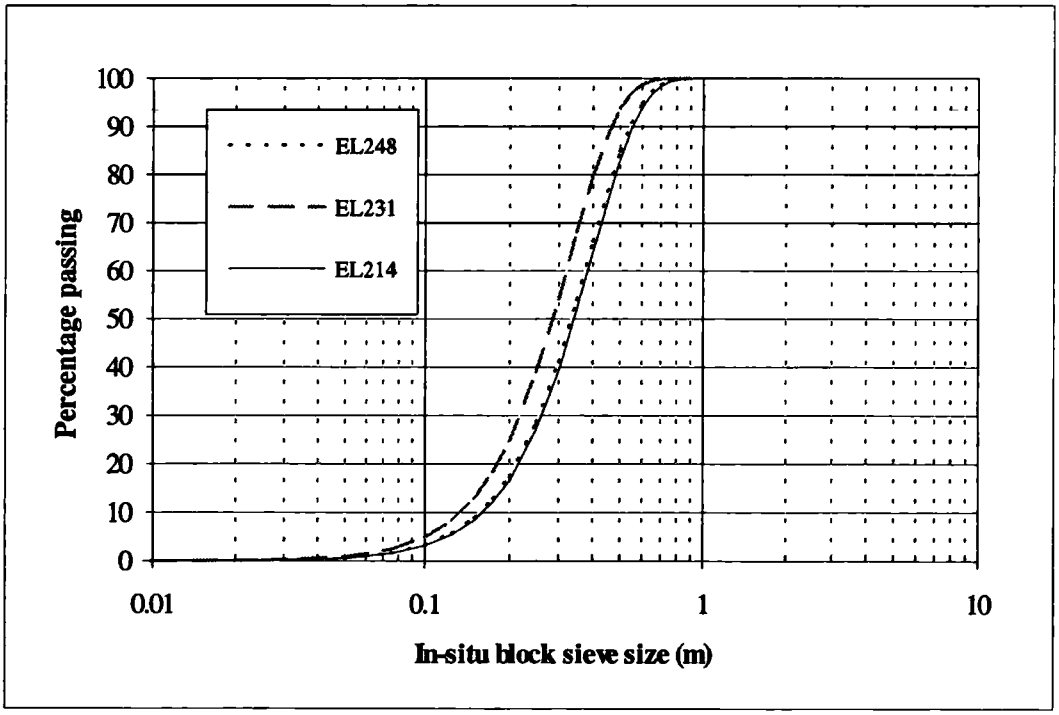

Fig. 7.14 IBSD curves of the Quarry, using data only from borehole logging (the top 12 metres only)

scanline data (with the possible exception of Elevation 214). When the principal mean spacings of the two sets of sub-vertical discontinuities are assumed to have the same values as that of the sub-horizontal discontinuity set taken from the borehole logs, the concluding results seem to command less confidence than those derived from the scanline measurements, thus the analysis hereafter will only be based on the IBSD information predicted from the combination of both scanline measurements and borehole logging.

Because of the lack of discontinuity trace length information, the correction of the influence of impersistent discontinuities could not be included.

7.2.5 Prediction of BBSD for Elevation 248 at the Overseas Quarry

7.2.5.1 Input Parameters

Since only one trial blast near Borehole 4 has been made, the blast design information was rather limited. However, an estimation of the BBSD in the locality of this trial blast could be based on available and partly assumed data on the rock mechanical properties, discontinuity geometry and the blasting conditions (OVERSEAS QUARRY Item-1, Item-2, Item-3, Item-8) as follows:

Discontinuity Structures and Rock Properties	
1) Rock mass description	Powdery/Friable
2) Density of rock (kg/m^3):	2.59
3) UCS of rock material (MPa)	71.43
6) Point Load Index ((MPa)	5.49
4) Young's Modulus (GPa)	30.67 (estimated)
5) Schmidt Hammer Value	33.2
Geometrical Pattern	
1) Bench height (m):	4.5
2) Burden (m):	3.0
3) Spacing (m):	3.0
4) No.s of holes in a row:	10
5) No.s of rows in a blast:	1
6) Diameter of blasthole (mm):	64
7) Subdrill (m):	0.3

8) Drilling accuracy (m):	0.1
Explosive and charge structure	
1) Explosive type:	ANFO
3) Relative strength (%):	100
4) Specific charge (kg/m^3):	0.29
5) Bottom charge (m):	0.5
6) Column charge height (m):	3.5
7) Stemming length (m) :	0.8

Kuz-Ram model

Using the above data, the model yields $A = 2.1$, $n_S = 1.305$, and the equation for the BBSD is given by

$$P = 1 - e^{-(\frac{S}{0.123})^{1.305}}, \qquad (7\text{-}8)$$

Bond-Ram Model

Using the above rock mechanical properties, discontinuity geometry and blasting conditions, the following results were obtained: $E_C = 20.25$, $S_{b80} = 0.5393$ m, and the equation for the BBSD is as follows.

$$P = 1 - e^{-(\frac{S}{0.3745})^{1.305}}, \qquad (7\text{-}9)$$

Energy-block transition model

Using the above information about rock mechanical properties, discontinuity structures and blasting conditions, the blastability was assessed for the rock mass at the quarry using the methodology presented in Chapter 6. Because of only based on the author's experience but not a couple of experts' judgement, the Expert Semi-quantitative (ESQ) coding method was therefore used to code the blastability interaction matrix. The coding values, the cause vs. effect plot and the ordered histogram, all of which reflect the interaction intensity for each factor, are illustrated in Fig. 7.15. It is worth pointing that these coding values can be altered according to different experts' judgement.

Similar to the first case study, the parameters P_1, P_2, P_3, P_4, P_5, P_6, P_9, P_{11} (see Fig. 7.15), are finally chosen as the factors in assessing the blastability of rock masses. W_i (i =1, 2, ..., 8), the weighting coefficients in Eqn. 6.-64, correspond to the weighting coefficients of eight parameters of P_1, P_2, P_3, P_4, P_5, P_6, P_9 and P_{11}, are determined from scaled $C+E$ values (Fig. 7.15) and are respectively 0.144, 0.133, 0.112, 0.124, 0.131, 0.122, 0.116, and 0.118.

P1	2	3	3	3	3	1	3	2	2	1	2
3	**P2**	2	2	2	2	2	3	3	2	1	2
4	3	**P3**	3	2	3	2	2	1	1	1	1
4	1	2	**P4**	3	3	2	1	1	1	2	1
2	3	4	2	**P5**	2	1	2	3	2	2	2
3	2	2	2	2	**P6**	1	2	2	1	2	2
1	1	2	3	1	2	**P7**	2	1	0	1	0
2	3	1	1	1	2	1	**P8**	2	1	1	2
1	1	0	2	1	1	1	0	**P9**	4	4	2
3	3	0	1	1	1	0	1	3	**P10**	3	1
2	3	1	3	3	2	1	1	3	2	**P11**	1
1	3	0	1	2	1	1	2	3	2	2	**P12**

(a)

P_1- Strength;
P_2 - Resistance to fracturing;
P_3 - Sturdiness;
P_4 - Elasticity;
P_5 - Resistance to dynamic loading;
P_6 - Hardness of rock;
P_7 - Deformability;
P_8 - Resistance to breaking;
P_9 - *IBSD* or *PMS*;
P_{10} - Fragility of rock mass;
P_{11}- Integrity of rock mass;
P_{12}- Discontinuity plane's strength.

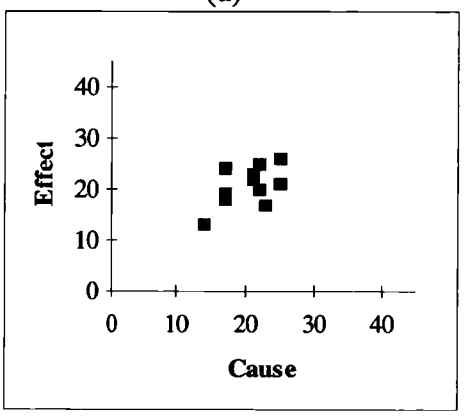

(b)

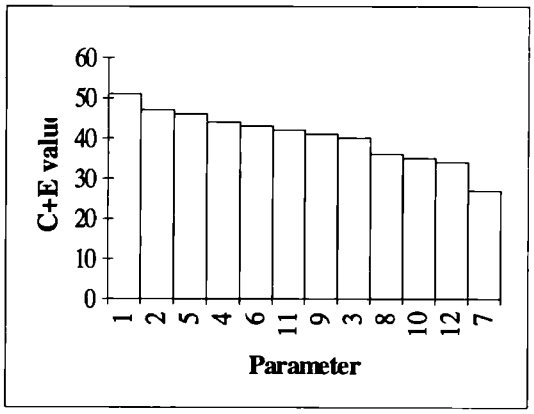

(c)

Fig. 7.15 Coding the interaction matrix of the blastability system of the quarry. (a) Coding values, (b) The associated C-E plot, and (c) The ordered histogram

The following results were derived: Blastability Designation BD = 0.576, Energy-block-transition coefficient B_i=17.36 ($m^{0.5}$/ kwh/t), and the equation for the BBSD is as follows.

$$P = 1 - e^{-(\frac{S}{0.164})^{1.305}}, \qquad (7\text{-}10)$$

The characteristic size parameters for the BBSD from the three models are listed in Table 7.16, and the corresponding BBSD curves are illustrated in Fig. 7.16.

Table 7.16 Characteristic size parameters for the BBSD predicted

Model	Kuz-Ram	Bond-Ram	E-B-T	Direct Sieving
n_s	1.305			0.672
S_{b50} (m)	0.093	0.285	0.124	0.153
$S_{b63.2}$ (m)	0.123	0.375	0.165	0.277
S_{b80}(m)	0.177	0.539	0.237	0.539

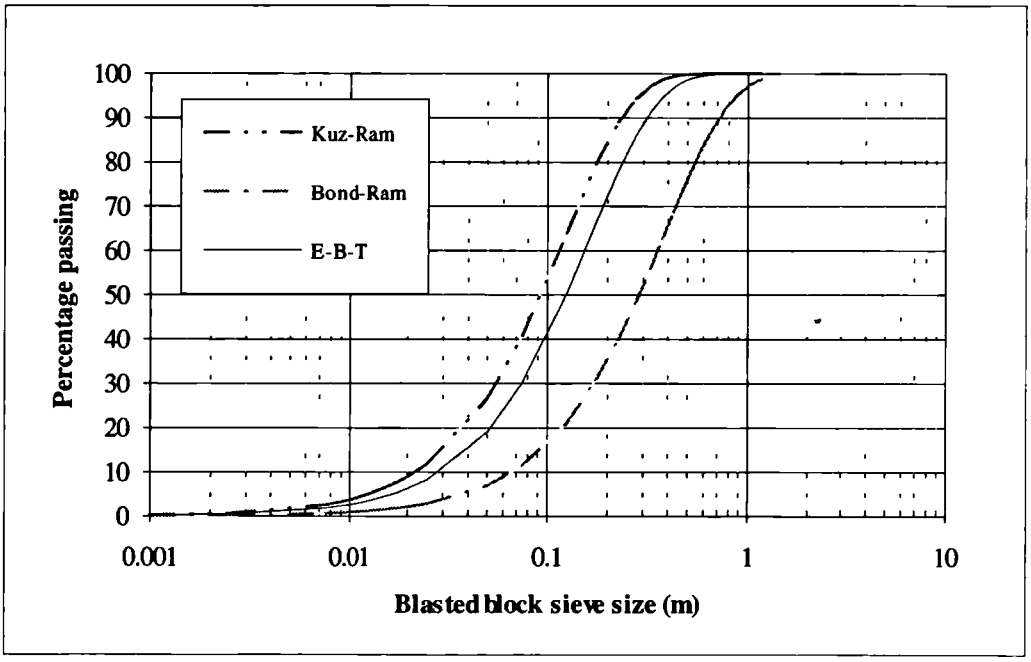

Fig. 7.16 Comparison of predicted BBSD from Kuz-Ram, Bond-Ram and Energy-block transition models respectively

7.2.6 Actual BBSD from Full Scale Sieving Analysis of Trial Blast near Borehole 4

The BBSD result of the trial blast carried out near borehole 4 has been directly sieved, and a sample of 1340 tonnes was obtained from the blastpile (OVERSEAS QUARRY Item-7). The sieve size distribution resulting from sieving was fitted with the two most widely used equations: the Ros-Ram and the Schuhmann equations, and the fitted results are illustrated in Fig. 7.17. The figure indicates in terms of goodness-of-fit, there may be little to choose between them. The fitted equations are as follows:

For the Ros-Ram equation:

$$P = 1 - e^{-(\frac{S}{0.1971})^{0.6714}}, \qquad (7\text{-}11)$$

and for the Schuhmann equation

$$P = (\frac{S}{1.2052})^{0.3767}. \qquad (7\text{-}12)$$

It should be noted just how well the Ros-Ram equation fits the raw data for the largest 10% of blocks but how it slightly underestimate the 50% passing size.

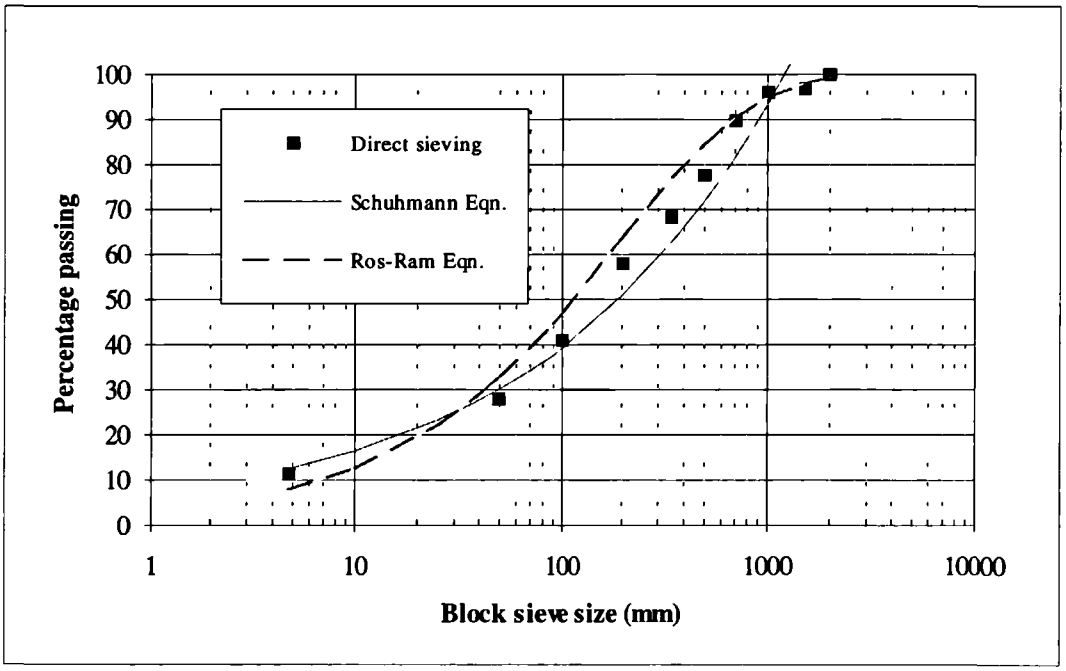

Fig. 7.17 Raw sieving data and best fit analysis of the block size distribution after blasting for the area around Borehole 4, using two widely used empirical equations: Ros-Ram and Schuhmann models.

7.2.7 Calibration of BBSD Prediction Models Using the Sieving Result

Using the data from direct sieving of the trial blastpile, a calibration of the prediction models can be made. The comparison between the BBSD result from the direct sieving data supplied from Borehole 4 and the results predicted from the above

three prediction models, using the IBSD information derived, is illustrated in Fig. 7.18.

It can be seen from Fig. 7.18 that the result from the Energy-Block-Transition model is closest to the direct sieving result for the important characteristic size parameter S_{b50}, whereas the Bond-Ram Model is closest to the direct sieving result in terms of the large sizes and the Kuz-Ram Model is closest to the direct sieving result in terms of smaller sizes. To examine the goodness of fit to the sieve sizes of each of the three model predictions, a grey correlation analysis (see Section 3.5) was performed. The grey correlation measures were 0.806, 0.786 and 0.755 for the Bond-Ram, the Energy-Block-Transition model and the Kuz-Ram models respectively, suggesting that the Bond-Ram model may be the best one if a whole curve prediction is required.

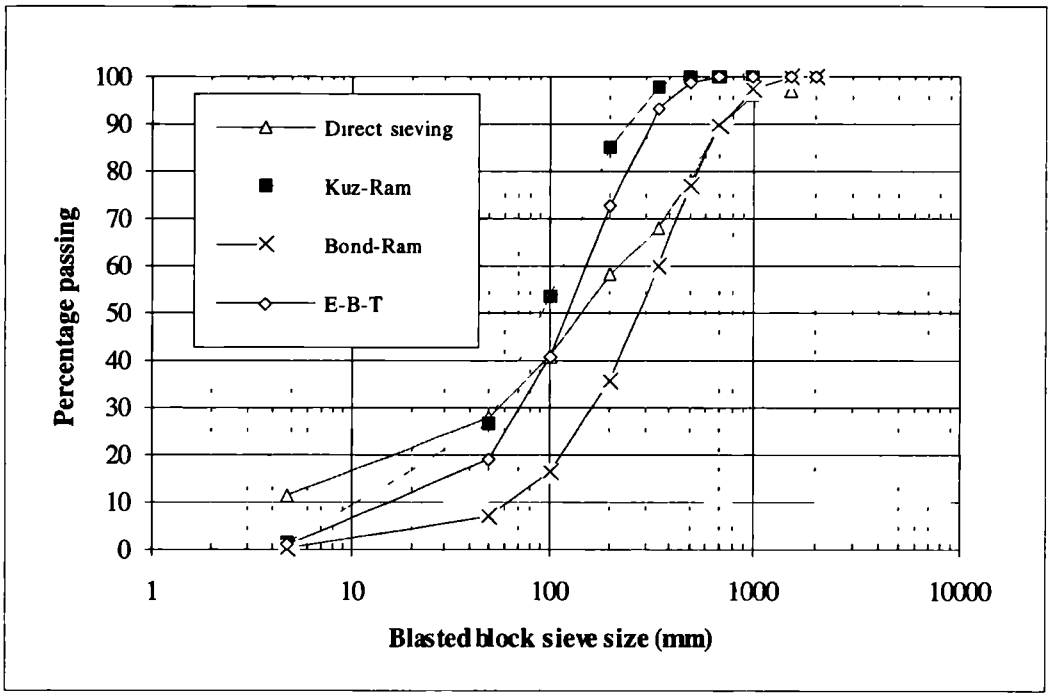

Fig. 7.18 Comparison between the BBSD result from the direct sieving data supplied from Borehole 4 and that from the three prediction models

Further consideration of Fig. 7.18 suggests that the difference between the predicted BBSD and direct sieving could be caused by the deviation of the n_S value, determined by the algorithm devised by Cunningham (1987), from that determined by the direct sieving result. It appears that Cunningham's algorithm needs to be further calibrated perhaps because it includes only geometric parameters of blast design pattern. Note, also that Yang and Rustan (1983), Aler et al. (1996b) showed that a

rock mass and its structures would influence n_S. This suggests that it is appropriate at this stage to take the n_S value determined from the direct sieving result as the nominal value of n_S for the quarry.

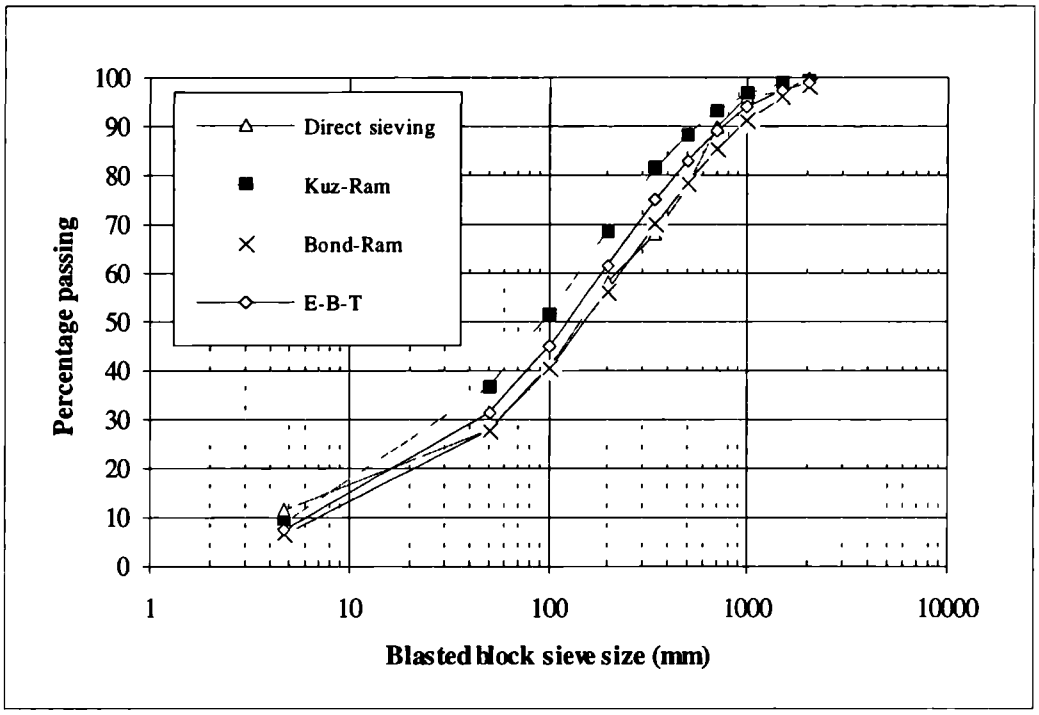

Fig. 7.19 Comparison between the BBSD result from the direct sieving data supplied from Borehole 4 and that from the three calibrated prediction models

After replacing n_S based on the Cunningham's algorithm with n_S from the sieve analysis and thereby calibrating the value of n_S to be fixed for this part of quarry, we can compare the BBSDs from the above three prediction models in a more meaningful way. The BBSD predictions based on this calibration were derived and a comparison between these calibrated BBSD results and the direct sieving results is illustrated in Fig. 7.19 and in Table 7.17.

It can be seen that the prediction of the BBSD curve from the Bond-Ram model appears the best one among the three models in terms of the overall size range. However, Fig. 7.19 does suggest that this approach is capable of overestimating the amount of large blocks, giving greatest accuracy below the 500 mm sizes and that the Energy-Block-Transition model appears nearly as good as the Bond-Ram, particularly in the range of larger than 80% passing block sizes. This is supported by the grey correlation analysis, in which the grey correlation measures comparing direct sieving with the results from the Bond-Ram, the energy-block-transition and the Kuz-Ram models are 0.867, 0.820 and 0.722 respectively. With such little data available, it

seems reasonable to take n_S from the direct sieving of the blastpile near Borehole 4 rather than n_S from the Cunningham's algorithm as the average value of n_S for the quarry. Without further research, it is suggested that the BBSD from different domains of the quarry can best be predicted using the sieve analysis n_S throughout the quarry and applying the Bond-Ram model with the Energy-Block-Transition model as a back-up prediction for comparison.

Table 7.17 Calibrated characteristic sizes of blasted blocks

Model	Kuz-Ram	Bond-Ram	Transition	Direct Sieving
n_S	0.6714			
S_{b50} (m)	0.093	0.154	0.124	0.153
$S_{b63.2}$ (m)	0.161	0.266	0.215	0.277
S_{b80}(m)	0.326	0.539	0.436	0.539
S_{b90}(m)	0.556	0.919	0.742	0.705
S_{b95}(m)	0.823	1.361	1.098	0.951

7.2.8 Preliminary Prediction of BBSD for Three Different Areas and Elevations from the Overseas Quarry

From the above calibration, it was argued that the both the Bond-Ram and the Energy-Block-Transition models might be suitable and that an average n_S for the overseas quarry can be taken as 0.6714. Thus we can now make predictions of the BBSD at the three elevations of the overseas quarry.

Using the IBSD information from the combination of scanline measurement and borehole logging and the blasting conditions applied and assumed for the trial blasting carried out near Borehole 4, the values of E_C (see Eqn. 2-16) obtained for Elevations 248, 231, 214 are 20.25, 19.30, 19.04. The BBSD curves for these three elevations are illustrated in Fig. 7.20.

Table 7.18 Characteristic size for the BBSD

Parameter	EL248	EL231	EL214	Direct sieving
n_S	0.6714			
S_{b50} (m)	0.1538	0.1257	0.118	0.153
$S_{b63.2}$ (m)	0.2655	0.2170	0.2036	0.277
S_{b80} (m)	0.5393	0.4408	0.4137	0.539
S_{b95} (m)	1.3607	1.1121	1.0436	0.950

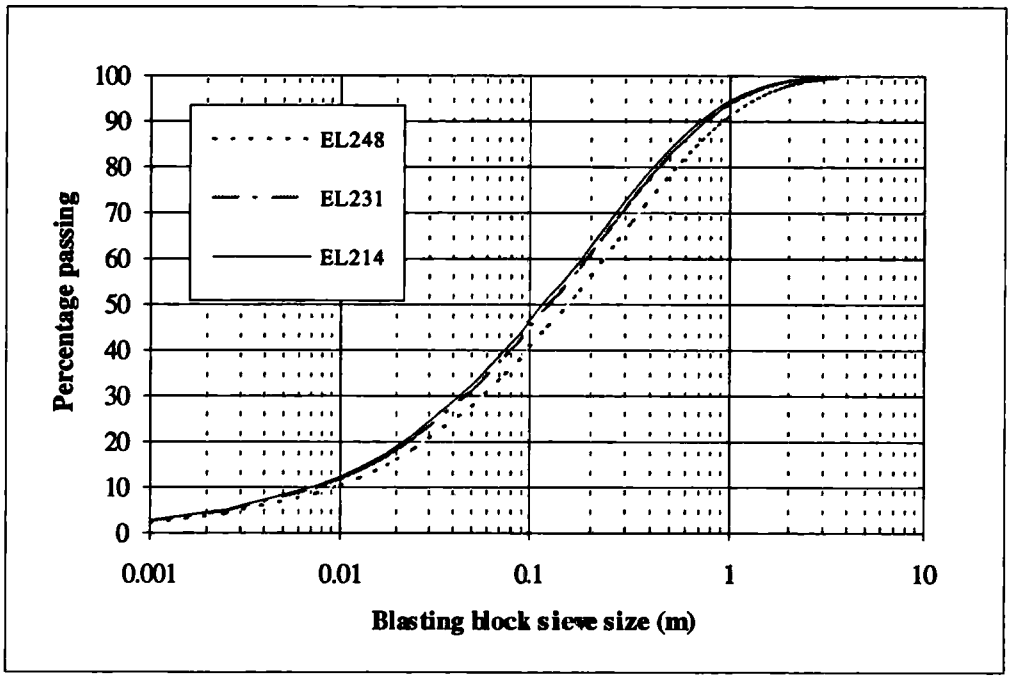

Fig. 7.20 Prediction of the BBSD curves of the overseas quarry using the Bond-Ram model

The characteristic sizes for the BBSDs for the three elevations are summarised in Table 7.18, but recall that the 95% size is likely to be an overestimate (see Fig. 7.19).

The distribution of block masses corresponding to the BBSD curve can be obtained using the following formula, where 0.847 is an empirically derived shape factor that relates sieve size to the size of the equivalent cube (CIRIA, 1991; Wang, 1992).

$$W_t = \rho(0.847S)^3, \qquad (7\text{-}13)$$

where, W_t is the weight of a block with sieve size S, and ρ is the density of rock. For instance, the S_{b95} for EL 248 in Table 7.18 is 1.3607 and ρ is 2.59 t/m^3, so the 95% passing rock weight is as follows

$$W_{95} = 2.59 \times (0.847 \times 1.3607)^3 = 3.965\,(t)$$

7.2.9 Discussion

The lack of data relating to the exact orientation of the sets of discontinuities, however unsystematic they may at first appear, might restrict accuracy of analysis predictions. Since the back analysis of the blast results is only based on the single trial blast near borehole 4, this might significantly reduce the potential improvements in accuracy offered by the analysis .

Table 7.19 Expected percentage yields based on the trial blast alone

Block mass (Tonnes)	Block sieve size (m)	Trial blast percentage exceeding (%)
0.5	0.682	10.00
1	0.860	6.80
2	1.083	4.33
3	1.240	3.21
4	1.365	2.56
5	1.470	2.12

If the sieve analysis of the trial blast near BH4 was to be typical of the whole quarry area, examination of Fig. 7.17 for the largest blocks suggests that the percentage yields would be roughly as given in Table 7.19. These have been worked out using the best-fit Eqn. 7-11 and Eqn. 7-13. The table suggests that approximately 2% would be greater than 5 tonnes and 4.3% greater than 2 tonnes, with about 10% greater than 500 kg.

However, the RQD value, which is an indicator of sub-horizontal bedding fracture spacing, found in Borehole 4 at around Elevation 248 (to 12 metres depth) where the blast was carried out equalled 71% and is greater than that for the quarry's average RQD value from all borehole logs taken to considerable depth which was 40%. An average yield curve for the whole quarry would on this basis give a less favourable proportion of armour-sized blocks.

The best prediction of block yields can be discussed with reference to Table 7.20. Once the variation in spacings of sub-vertical fractures are taking into account, further confirmation that the direct results of the trial blast will over-estimate the proportion of large blocks is given. For a best prediction up to the 90% passing size, reference should be made to curves in Fig. 7.18. However, as pointed out in the previous discussion, with respect to armourstone-sized blocks, the Energy-Block-Transition model has appeared nearly as good as the Bond-Ram, particularly in the range of largest blocks and this Energy-Block-Transition model will therefore be considered

here. The Energy-Block-Transition model has predicted the 95% blasted block size result to be slightly less than that from the Bond-Ram model (see Fig. 7.19) which is also reflected by the BBSD using the Bond-Ram model and the IBSD information only based on the borehole logging. Thus, the overall prediction for the upper elevation of the overseas quarry is as highlighted in bold figures in Table 7.20.

Table 7.20 Summary of block weight yields based on the Bond-Ram model shown in Fig. 7.18 and two alternative results

W_i	EL248	EL231	EL214	Average	Direct sieving
	BH1, 3 , 4, 5	BH7, 9, 11	BH8, 9, 10		EL248, BH4
W_{50} (kg)	5.73	3.13	2.59	**3.81**	5.64
W_{80} (kg)	246.90	134.80	111.40	**164.44**	246.40
W_{95} (tonnes)	3.965	2.165	1.789	2.639	1.349
W_{95}* (tonnes)	1.118	0.731	1.194	**1.014**	
W_{95}** (tonnes)	2.083	0.401	0.270	**0.918**	

*assuming BBSD based on the IBSD information acquired from the borehole logging;
**based on the Energy-Block-Transition model.

Evidence that the block sizes yielded from depth in the overseas quarry will be greater was considered to be far from conclusive at the stage reached during this investigation.

7.2.10 Conclusion and Recommendation

The best initial estimate for yields in the whole quarry was:

50% less than 4 kg
80% less than 164 kg
95% less than 1 tonne

The analysis results together with the analysis tools and methodology have been elaborated upon. The results indicate that the Energy-Block-Transition model has exhibited a prediction capability worthy of equal status with previous models. The suite of methodologies were able to provide operators of the quarry with valuable information about the block yields. Quarry operators were advised that further work and detailed surveying of discontinuities within specific areas of interest should be carried out in order to greatly improve the confidence in the initial predictions

reported to them. One striking conclusion was that the curve fitting criteria need to be geared towards the part of the curve that has most influence on the economic objective. For example, if it is crucial to establish the capability of producing armourstone, the emphasis should be given to matching trail blast results with functions that fit this upper part of the curve and possibly at the expense of a less good fit for most of the smaller part of the curve. In mining, other criteria would apply.

8. CONCLUSIONS AND SUGGESTIONS FOR FURTHER RESEARCH

8.1 TECHNIQUES AND METHODOLOGIES - CONCLUSIONS

8.1.1 Discontinuity Spacing and Trace Length Distributions

A systematic study of research data reported in the literature leads to the conclusion that discontinuity spacing distributions, measured from scanlines from a wide range of rock masses can be described adequately by a great many mathematical distributions. The best distribution model will usually be one of the following: negative exponential, lognormal or fractal. A similar systematic study of the literature for trace lengths measured along scanline suggests the best distribution model will usually be one of the above three distributions.

The goodness-of-fit of any theoretical distribution compared with real discontinuity spacing or trace length data can be assessed using classic statistical methods, but grey correlation analysis technique provides a powerful additional tool for selecting the best theoretical distribution out of a number of proposed alternatives. An analytical procedure for applying the grey correlation analysis to this problem has been presented.

The study of fractal spacing distributions using simulation techniques requires the numerical generation of spacings with a fractal distribution. Such a random generator was developed in this research study.

8.1.2 In-situ Block Size Distribution of Rock Masses with Fractal Discontinuity Spacing Distributions

For this investigation into the IBSD, discontinuities with a fractal spacing distribution are investigated using a computer simulation of randomly produced artificial discontinuities. The investigation indicates that the IBSDs of rock masses with fractal spacing distributions are quite different from those with negative exponential, lognormal and uniform spacing distributions when identical mean spacings are considered. The relationship between the product of three principal mean

spacing values and the IBSD for a rock mass with a fractal discontinuity spacing distribution is not linear, which is in contrast to the result of Wang (1992) obtained for a rock mass with negative exponential, uniform and lognormal spacing distributions. To distinguish the types of spacing distribution of discontinuities has important implications for predicting the IBSD, and its numerous applications concerning quarry production of aggregates, armourstone and building stone, not to mention mining.

Two sets of empirical equations, have been derived from Monte Carlo simulations of a dissected volume of rock, for predicting the IBSD of a rock mass with discontinuities of fractal spacing distributions. They are given by

$$V_{i,p} = C_{i,p} \times (D_1 \times D_2 \times D_3)^{-b_{i,p}}, \tag{8-1}$$

and

$$V_{i,p} = C_{i,p} \times (S_{pm1} \times S_{pm2} \times S_{pm3})^{b_{i,p}}. \tag{8-2}$$

where $V_{i,p}$ (i=*10, 20,...,100*) are block volumes of percentage passing (in m^3), and, $C_{i,p}$ and $b_{i,p}$ are empirical coefficients; i are percentages; D_1, D_2 and D_3 are the fractal dimensions of the three sets of discontinuity spacing values, and S_{pm1}, S_{pm2} and S_{pm3} are the principal mean spacing values of three sets of discontinuities.

These two equations, together with the coefficients given in Tables 3.3 and 3.4 provide us with a tool for predicting the IBSD of a rock mass for which the three sets of discontinuities have fractal spacing distributions.

This study indicates that for a given mean spacing the IBSD curve, derived from the assumption that all three sets of discontinuities have a fractal spacing distribution, will give an IBSD with the largest block sizes. Furthermore, the real IBSD should fall within the envelope formed by the lower boundary IBSD curve created with the uniform spacing distribution assumption and the upper boundary IBSD curve created from the fractal spacing distribution assumption. In the case study carried out at the A5 Glyn Bends Improvement site, only one of the three sets was best described by a fractal spacing distribution and the direct assessment of IBSD using the dissect method showed the IBSD to fall within the envelope defined by upper and lower boundaries based on the equation method and described above.

8.1.3 The Influence of Impersistent Discontinuities on the Prediction of IBSD

From a simple counting survey of an exposure with discontinuities censored at different given levels, initial estimates of mean trace length of discontinuities with fractal and lognormal distributions have been established. They have been expressed in the form of sets of charts.

Based on the theoretical relationship between trace length and size of discontinuity derived by Warburton, a numerical algorithm for estimating the discontinuity size distribution, has been developed. The procedure handles discontinuities with negative exponential, lognormal and fractal trace length distributions, i.e. those most often encountered in practice. A set of equations for the estimation of discontinuity size distributions corresponding to the above three trace length distributions has been derived.

A "relative impersistence factor" is proposed for describing the influence of the impersistence of discontinuities. It compares the mean size of discontinuities and the dimension of the rock mass of interest. This factor can then be incorporated into the estimation of IBSD, an improvement on the pre-existing approaches to prediction of the IBSD which neglect the influence of impersistence of discontinuities. A preliminary application of the proposed new technique for improving the estimate of natural block size distributions of a rock mass has been presented in a case history in Chapter 7.

8.1.4 Assessment of Block Size Distributions in Blastpiles and the Energy-Block-Transition Model

A "photo-scanline" technique of assessing the BBSD of a blastpile directly from photographs has been devised in Chapter 5. The technique assumes that the BBSD of a blastpile can be represented by either the Ros-Ram or the Schuhmann equation which are the two most widely used equations for representing the BBSD. The calibrated relationship between the size distribution obtained from the photograph of a blastpile surface and the true underlying distribution has been derived by an analysis of fully quantified artificial blastpiles prepared in laboratory. The calibration has then be used to derive the governing distribution parameters S_c and n for the Ros-Ram equation (or S_{100} and m for the Schuhmann equation) of the blastpile. Data acquisition from photographs is based on information of lengths of visible blocks

exposed on the surface and intersected by survey lines on properly scaled photographs of the blastpile. The application of the technique to actual blastpiles has been illustrated in the highway cutting case study presented in Chapter 7. The technique appears to be reasonably accurate, simple and user-friendly, but field results using the technique have not yet been compared with results from other direct assessment techniques.

A blast design model called the Energy-Block-Transition model developed from the concept of blastability has been proposed in Chapter 6. The model characterises the ease with which a rock mass can be transformed by blasting from the state with IBSD into that with BBSD and is represented by the following relationship:

$$E_s = \frac{S_{ai} - S_{ab}}{B_i \left(\frac{S_{ai} + S_{ab}}{2}\right)^{0.5}}. \qquad (8\text{-}3)$$

where, E_s represents the explosive energy input per unit rock mass that is used in transforming the rock mass with a given IBSD into a blastpile with a given BBSD; B_i is the Energy-Block-Transition coefficient; and S_{ai} and S_{ab} are the mean sizes of both IBSD and BBSD respectively.

The Rock Factor A in the Kuz-Ram equation developed by Cunningham can also be calculated using an assessment of blastability of rock masses proposed in this research. The calculation of A is based on a more comprehensive range of in-situ rock properties and discontinuity structures than Cunningham's algorithm. Using A based on blastability assessment instead of Cunningham's A appears to give an improvement in the accuracy of the Kuz-Ram equation when applied to case study BBSD analysis of blastpiles assessed with direct sieving and the photo-scanline methods.

The Energy-Block-Transition model, the corrected Kuz-Ram equation, together with the Kuz-Ram and the Bond-Ram models can all be used for estimating the BBSD of a rock mass provided that the discontinuity structure, intact rock properties and blast conditions are all given. Applications of these equations to both the A5 Glyn Bends Improvement site and the Overseas Quarry have been described in Chapter 7. The upper and lower borders for the envelope defining the range of model predictions of BBSD for the two case studies were found to be the Bond-Ram and the Kuz-Ram models respectively. For these case studies, the new models give BBSD

predictions within this envelope such that the blastability corrected Kuz-Ram model and the Energy-Block-Transition model give a decrease in sizes from those predicted by the Bond-Ram model. This apparent narrowing of the uncertainty envelope for the predicted BBSD may not be a general result since both the new models are very sensitive to the determination of the Blastability Designation.

8.1.5 Characterisation and Assessment of Blastability of Rock Masses

Looking upon blasting as a transformation from the in-situ state to the as-blasted state, the blastability of a rock mass has been, in this research study, defined as the ease with which the rock mass can be fragmented by the blasting process causing the transformation. The proposed Energy-Block-Transition model is based on the consideration of the blastability of the rock mass.

The Energy-Block-Transition model and its associated coefficient B_i have been devised to characterise the blasting process and the rock mass blastability respectively. The coefficient B_i is defined by its role in the equation describing the Energy-Block-Transition model (Eqn. 8-3). It represents the explosive energy consumed per unit volume of rock mass with a given object size, required to transfer the in-situ rock mass with a mean block size S_{ai} into blasted blocks with a mean size S_{ab}. The Energy-Block-Transition model is a special case of the empirical energy-size reduction relationship known as the Walker-Lewis relation in comminution, although it evolved from the Energy-Block-Transition concept. A sample of available data sets from the literature suggest that the Energy-Block-Transition model will generally give an improvement in BBSD prediction compared with the Bond-Ram model. The case studies give further confidence to the potential value of the model.

The "renormalisation group" approach has been exploited to further investigate the relationship between the blastability and the fractal dimensions characterising both the IBSD and the BBSD. The "number of fragile elements" criterion was introduced into the discussion together with the pre-existing "plane of weakness" and "pillar of strength" criteria. An investigation based on developments of these three criteria using the renormalisation group approach indicates that the larger the fractal dimension characterising the IBSD, the more difficult it is to fragment the rock mass by blasting; and that the larger the fractal dimension characterising the BBSD, the easier it will have been to fragment the rock mass by blasting. It was agreed that these conclusions are in conformity with the process revealed by the Energy-Block-

Transition model while being supported by the concept of fracturing in fracture mechanics.

Taking into account that blastability is a complex property, a methodology for the assessment of blastability of rock masses using the Rock Engineering Systems method has been proposed in Chapter 6. The methodology has systematically taken into account twelve factors which a review suggested would give a comprehensive set of factors that influence the blastability of a rock mass. The contribution of each of these factors to the blastability of the rock mass is identified using interaction matrix analysis, which is implemented by deriving a weighting for each factor. Combining the results from the interaction matrix analysis and the rating charts proposed in this research, the blastability of the rock mass may be represented quantitatively using the Blastability Designation. A preliminary classification for blastability of rock masses according to the Energy-Block-Transition coefficient has therefore been suggested as follows.

Table 8.1 Blastability classification according to the Energy-Block-Transition coefficient B_i and BD

Description of ease of blasting	Very Easy	Easy	Moderate	Difficult	Very difficult
Blastability Class	1	2	3	4	5
B_i ($m^{0.5}$/kwh/t)	>40	20-40	13-20	8-13	<8
BD	<0.25	0.25-0.50	0.50-0.70	0.70-0.85	>0.85

The methodology has been successfully applied to the assessment of the blastability of rock materials at the A5 Glyn Bends Improvement site and to the prediction of armourstone production of the Overseas Quarry, both presented in Chapter 7.

8.1.6 Further Conclusions from Case Studies

The A5 Glyn Bends Improvement site:

Both the geological structures and the mechanical properties of rock materials vary significantly from one place to another. As a result, the blastability of the rock mass exhibits differences. These differences could be one reason that the blasting results prior to this study were on certain occasions unsatisfactory.

The new field data set obtained from this case study, when compared with a previous available geological data set, suggests that the resistance to blasting had previously been underestimated. This could be why the previous blasting results experienced tight blastpiles and a significant oversize fraction.

The variability of blastability of the rock materials at the site should ideally have been taken into account, since the increase between Blastability Designation of 0.631 (Site S4) and 0.725 (Site S3) may represent an obvious increase of specific charge required.

The Overseas Quarry.

It was concluded from the data available, that 95% of blasted blocks in the quarry would be less than 1 tonne. This result indicated that the quarry might not able to produce the sufficient quantity of large blocks that was needed for the armourstone contract. It was suggested that a further quarry site investigation and analysis should be carried out in order to improve the confidence of these initial predictions of the BBSD in the quarry.

It has found that Cunningham's algorithm for calculating the value n, representing the steepness of BBSD, should be further calibrated since there was an obvious large difference in the values of n between the sieving result and the derivation from Cunningham's algorithm.

8.2 TOPICS SUGGESTED FOR FURTHER RESEARCH

8.2.1 Investigations into IBSDs of Rock Masses with more than Two Spacing Distributions

So far, and with the exception of direct block dissection methods using raw data, all the investigations of the IBSD of rock masses have been limited to the prediction of IBSD with one type of spacing distribution for all discontinuity sets, although preliminary discussion of the possible outcome of IBSD from two or more types of discontinuity spacing distributions was included in this research. In practice, it is common for two or more kinds of discontinuity spacing distributions to be encountered. This research has deduced that the IBSD of a rock mass with two or more of the most common kinds of discontinuity spacing distributions would fall into the envelope formed by the lower

boundary IBSD curve from discontinuities with uniform spacing distributions and an upper boundary IBSD curve from discontinuities with fractal spacing distributions. Whilst this preliminary deduction was supported by the case study of the A5 Glyn Bends site, there is scope to explore combined distributions so as to narrow the IBSD range. This could be realised using similar procedures to those reported in Chapter 3 by including two or more different discontinuity spacing distributions. Through such an investigation, it might be possible to improve significantly our understanding of the influence of discontinuity pattern on engineering properties of rock masses.

8.2.2 Influence of Impersistent Discontinuities on Prediction of IBSD

In Chapter 4 the following equation

$$V_{i,p} = \frac{1}{(F_{imp})^q} (V_{i,p})_0 \qquad (8\text{-}4)$$

has been developed for adjusting the prediction of IBSD based on the assumption of all-persistent discontinuities, where $(V_{ip})_0$ represents the predicted result of IBSD from the all-persistent assumption, V_{ip} is the corrected result incorporating the influence of impersistent discontinuities on the result. F_{imp} is the relative impersistence factor. It has been suggested that the index q in Eqn. 8-4 should take the value of 1/5-1/2, which has been supported by the case studies. It is obvious that the adjusted result will be quite sensitive to the value of q. As such, its calibration from a much wider source of field case studies should be carried out.

8.2.3 Improvement on the Photo-scanline Technique for Estimating BBSDs of Blastpiles

The photo-scanline technique used for directly assessing the BBSD of a blastpile devised in this research has been developed from artificial blastpiles. The sizes of aggregates in the artificial blastpiles are not more than 150 mm, far from 1.0 m - a typical upper size of a real blastpile. This might affect the application of the equations although the BBSD blast design predictions from the A5 Glyn Bends' case study has given support to the validity of the direct photo-scanline BBSD technique. The errors related to the technique encountered require further investigation although a preliminary discussion of these has been given. Investigations of the influence of

the number and directions of surveying lines laid on a photographs and further case studies with direct sieving results of BBSD will be necessary to help improve the technique and to advance its applications along-side development in image analysis software for measurement of blast fragmentation.

8.2.4 Validation of the Energy-Block-Transition Model

The proposed Energy-Block-Transition model has been the subject of examination in the two case studies carried out in this research and the data cited from published literature. A well-developed model should, however, be exposed to a variety of case study examinations with different geological conditions in order to use it with sufficient confidence in practice. This could be most efficiently implemented by the setting up of a database with the full record of different in-situ geological conditions, blast patterns, explosive energy inputs and the directly assessed BBSD results, e.g. by sieving, photo-scanline, image analysis etc. Thus, a series of trial model or full-scale blasts could be necessary for this purpose.

In the present Energy-Block-Transition model, the energy input has only been related to uncontrollable factors consisting of in-situ rock mass properties and geological structures, represented by the Energy-Block-Transition coefficient. It is known that in a practical blast, the energy input will be partly affected by many factors controlled by the blast design, such as burden, spacing, timing, decoupling, etc. An improvement on the present Energy-Block-Transition model which includes such controllable factors could be expressed as follows:

$$E_s = \frac{f_c}{B_t} \frac{S_{ai} - S_{ab}}{(\frac{S_{ai} + S_{ab}}{2})^{0.5}}, \qquad (8\text{-}5)$$

where f_C represents a coefficient which includes the influence of the controllable factors on the energy input needed. A detailed investigation based on an examination of Eqn. 8-5, using a database of blasting results would be of great interest for blast design.

8.2.5 The Classification of Blastability

The classification of blastability presented in Chapter 6 and suggested in Table 8.1 has been based on the blastability assessment of rock masses. The assessment includes a significant account of subjective criteria through the matrix coding procedure that was undertaken by the author. Systems approaches such as the Rock Engineering Systems and the Grey Systems have been exploited in this research to reduce the subjectivity. Further investigations into how to more effectively select the key representative factors in the interaction matrix of the blastability system, how to more reasonably represent them by objectively measurable parameters and how to more accurately code the interaction mechanisms in the matrix are necessary questions to answer for improvement in the blastability assessment. The setting up of a research programme of purpose-designed blasts and the setting-up of a database collected from these blasts would be one of most important steps towards improvement in blasting models. The introduction of expert systems analysis and neural network analysis could provide assistance in the realisation of improvement in predicting the output of blasting.

In the Chapter 6, Eqn. 6-38 for the relationship between the Energy-Block-Transition coefficient and the Blastability Designation, and Eqn. 6-39 for estimating the Rock Factor A according to the Blastability Designation are both poorly constrained empirical equations with low confidence levels. They need to be re-calibrated using further blast results.

REFERENCE

Aler, J., Du Mouza, J. & Arnould, M. 1996a. Measurement of the fragmentation efficiency of rock mass blasting and its mining applications. Int. J. Rock Mech. Min. & Geomech. Abstr. 33(2), pp. 125-139

Aler, J., Du Mouza, J. & Arnould, M. 1996b. Evaluation of blast fragmentation efficiency and its prediction by multivariate analysis procedure. Int. J. Rock Mech. Min. & Geomech. Abstr. 33(2), pp. 189-196

Allegre, C. J. Le Mouel, J. L. & Provost, A. 1982. Scaling rules in rock fracture and possible implications for earthquake prediction. Nature, 297, (May), pp. 47-49

Atlas Powder Company. 1987. Explosives and Rock blasting. Texas: Atlas Powder Company. 662pp

AusIMM 1990. Proc. of Third Int. Symp. on Rock Fragmentation by Blasting. Brisbane, Australia

Aviles, C.A. & Scholz, C. H. 1987. Fractal analysis applied to characteristic segments of the San Andreas Fault. J. Geophys. Res. 92(B1), pp. 331-334

Baecher, G. B., Lanney, N. A. & Einstein, H. H. 1977. Statistical description of rock properties and samples. in: Proc. of 18th US Symp. on Rock Mech., Colorado: Johnson Pub., pp. 5C1_1- 5C1_8

Baecher, G. B. & Lanney. 1978. Trace length bias in joint surveys. Proc. of 19th US Symp. on Rock Mech., pp. 56-65

Baecher, G. B. 1983. Statistical analysis of rock mass fracturing. Math. Geol. (13), pp. 329-348

Bahat, D. 1988. Fractographic determination of joint length distribution in chalk. Rock Mech. Rock Engng. 21, pp. 79-94

Barnsley, M. 1988. Fractals everywhere. Boston: Academic Press, 394pp.

Barton, N., Lien, R. & Lunde, J. 1974. Engineering classification of rock masses for the design of tunnel support. Rock Mech. 6(4), pp. 189-236

Barton, C. A. & Zoback, M. D. 1992. Self-similar distribution and properties of microscopic fractures at depth in crystalline rock in the Cajon Pass scientific drill hole. J. Geophys. Res. 97(B4), pp. 5181-5200

Barton, C. C. & Larsen, E. 1985. Fractal geometry of two-dimensional fracture networks at Yucca Mountains, Southwestern Nevada. in: Fundamentals of Rock Joints (Stephansson ed.), Sweden: Centek Pub., pp. 77-84

Belland, J. M. 1966. Structure as a control in rock fragmentation. CIM. 59, pp. 323-328

Bellairs, P.G. 1986. Improved blast pattern design on Mt. Whaleback based on the pilbara iron ore classification. in: Large Open Pit Mining Conference (Davidson ed.), Victoria: AusIMM, pp. 89-92

Benjamin, J. R. & Cornell, C. A. 1970. Probability, statistics, and decision for civil engineers. New York: McGraw-Hill

Bhandari, S. & Vutukuri, V.S. 1974. Rock fragmentation with longitudinal explosives charges. in: Advances in Rock Mechanics, Proc. of 3rd Cong. of ISRM, Washington, D.C.: National Academy Sciences, 1(B), pp. 1337-1342.

Bieniawski, Z. T. 1973. Engineering classification of jointed rock mass. Trans. of South Afr. ICE, 15, pp. 335-344

Boadu, F. K. & Long, L.T. 1994. The fractal character of fracture spacing and RQD. Int. J. Rock Mech. Min. Sci. & Geomech. Abstr., 31(2), pp. 127-134

Bond, F. C. 1952. The third theory of comminution. Trans. AIMM 193, p.484

Bond, F. C. & Whittney, B. B. 1959. The work index in blasting. Quarterly of the Colorado School of Mines. 54(3), pp. 77-82

Bridges, M. C. 1975. Presentation of fracture data for rock mechanics. in: 2nd ANZ Conf. on Geomaterials. Brisbane, pp. 144-148

British Geological Survey, 1993. 1: 50000 Series, England and Wales Sheet 120, Corwen. Southampton: Ordance Survey & NERC

Brosch, F. J., Polsler, P. & Riedmuller G. 1992. The use of fractal dimension in engineering geology. Bull. of IAEG, 45, pp. 83-88

Brown, W. K., Karpp, E. R. & Grady, D. E. 1983. Fragmentation of the universe. Astrophys. Space Sci. 94, pp. 401-412

Cai, S. 1991. Investigation into the mechanical response characteristics of rock masses and fills in transverse cut-and-fill mining at Xin Chen Gold Mine. Ph.D Thesis, Univ. Sci. Tech. Beijing, China

Call, R. D., Savely, J. P., Nicholas, D. E. 1977. Estimation of joint set characteristics from surface mapping data. in: Monograph on Rock Mechanics Application in Mining (Brown, Green & Hustrulid eds.) New York: SME, AIME, pp. 65-73

Carlsson, O. & Nyberg, L. 1983. A method for estimation of fragment size distribution with automatic image procedures. in: Proc. 1st Int. Symp. on Rock Fragmentation by blasting, Lulea, Sweden, Aug. 1983, pp. 333-345

Carr, J. R., Warriner, J. B. 1987. Rock mass classification using fractal dimension. in: Proc. 28th US Symp. on Rock Mech. (Farmer ed.), Rotterdam: Balkema, pp. 73-80

Charles, R. J. 1957. Energy-size reduction relations in comminution. Trans. of AIME, 208, pp. 80-88

Cheung, C.C. & Ord, A. 1991. Use of stereo shape measurement in industrial applications: passive or active?. in: Proc. Workshop on Computer Vision-from Cognitive Science to Industrial Automation, Sydney, Australia. IJCAI-91, 12th Int. Joint Conf. on Artificial Intelligence. Aug., 1991 (Jarvis, ed)

CIRIA/CUR, UK & The Netherlands, 1991. Manual on the use of rock in coastal and shoreline engineering. CIRIA Special Pub. 83/ CUR Report 154

Clarke, G. B. 1987. Principles of rock fragmentation. New York: John Wiley, 610pp.

Costa, J .E. & Baker, V. R. 1981. Surfacial geology: Building with the earth. New York: John Wiley

Cotes, D. F. 1970. Rock mechanics principles. Dept. of Energy, Mines and Resources, Mines Branch Monograph 874

Crum, S. V. 1990. Fractal concepts applied to bench-blast fragmentation. in: Proc. 31th US Rock Mech. Symp. Rotterdam: Balkema, pp. 913-919

Cruden, D. M. 1977. Describing the size of discontinuities. Int. J. Rock Mech. Min. & Geomech. Abstr. 14, pp. 133-137

Cunningham, C. 1982. Rock fragmentation related to blasting. Quarry Management & Production. Dec. 1982. pp. 820-824

Cunningham, C. 1983. The Kuz-Ram model for prediction of fragmentation from blasting. in: 1st Int. Symp. on Rock Fragmentation by Blasting. Lulea, Sweden, pp. 439-453

Cunningham, C. 1987. Fragmentation estimation and the Kuz-Ram model --four years on. in: 2nd Int. Symp. on Rock Fragmentation by Blasting. Colorado, USA, pp. 475-487

Da Gama, C. D. 1977. Computer model for block size analysis of jointed rock masses. in: 15th APCOM Symp. Brisbane, Australia, 1977. pp. 305-315

Da Gama, C. D. 1983. Use of comminution theory to predict fragmentation of jointed rock mass subjected to blasting. in: 1st Int. Symp. On Rock. Fragmentation by Blasting. Lulea, Sweden, pp. 563-579

Davy, Ph., Sornette, A. & Sornette, D. 1990. Some consequences of proposal fractal nature of continental faulting. Nature, 348, pp. 56-58

Deere, D. U. 1964. Technical description of rock cores for engineering purposes. Rock Mech. Eng. Geol. 1, pp. 16-22

Den J. 1982. Control problem of grey system. System and Control Letters. 1(5), pp. 228-294

Den J. 1985. The Grey Control Systems. Wuhan (China): The Press of CCUT(in Chinese)

Den J. 1987. Fundamentals of Grey Systems Approaches. Wuhan (China): The Press of CCUT. (in Chinese)

Dershowitz, W. S. & Einstein, H. H. 1988. Characterising rock joint geometry with joint system models. Rock Mech. Rock Engng., 21, pp. 21-51

Dolgov, K. A. 1983. Regulations of the process of hard rocks fragmentation by blasting. in: Proc. 1st Int. Symp. on Rock Fragmentation by blasting, Lulea, Sweden, Aug. 1983, pp. 143-147

Einstein, H. H. & Baecher, G. B. 1983. Probabilistic and statistical methods in engineering geology, special methods and examples, part I: exploration. Rock Mech. Rock Engng. 16, pp. 39-72

Einstein, H. H., Veneziano, D., Baecher, G. B. & O'Reilly, K. J. The effect of discontinuity persistence on rock slope stability. Int. J. Rock Mech. Min. & Geomech. Abstr. 20 (5), pp. 227-236

Farmer, I. W., Kemeny, J. M. & McDoniel, C. 1991. Analysis of rock fragmentation in bench blasting using digital image processing. in: Proc. 7th ISRM Int. Cong. on Rock Mech., Rotterdam: Balkema, pp. 1037-1042

Feder, J. 1988. Fractals. New York: Plenum Press. 283pp.

Fourney, W. L., Barker, D. B. & Holloway, D. C. 1983. Fragmentation in jointed rock materials. in: 1st Int. Symp. on Rock Fragmentation by Blasting. Lulea, Sweden, pp. 505 -531

Fourney, W. L. & Dick R. D. (eds.) 1987. Proc. of Second Int. Symp. on Rock Fragmentation by Blasting. Soc. for Experimental Mechanics, Keystone, Colorada

Fox, C. G. 1989. Empirically derived relationships between fractal dimension and power law from frequency spectra. PAGEOPH, 131(1/2), pp. 211-239

Franklin, J. A., Broch, E. & Walton, G. 1971. Logging the mechanical character of rock. Trans. IMM, A1- A9

Franklin, J. A. 1974. Rock quality in relation to the quarrying and performance of rock construction materials. 2nd Int. Cong. IAEG, V1, IV-PC-2.1-2.12

Franklin, J. A. 1986. Size-strength system for rock characterisation. in: Application of Rock Characterisation Techniques in Mine Design (Karmis ed.), Littleton(USA): SME, pp. 11-16

Franklin, J. A. & Maerz, N. H. 1988. Photographic measurements of jointing and fragmentation. in: 2nd International Symp. on Field Measurements in Geomech. (Sakurai ed.), Rotterdam: Balkema, pp. 227-237

Genske, D. D., Herda, H. W. & Ohnishi, Y. 1992. Fracture and fractals. in: Rock Characterisation (Hudson ed.). London: Thomas Telford, pp. 19-24

Ghosh, A., Daemen, J. J. K. & van Zyl, D. 1990. Fractal concepts applied to bench-blast fragmentation. in: Proc. 31th US Rock Mech. Symp. Rotterdam: Balkema, pp. 905-912

Ghosh, A. & Daemen, J. J. K. 1993. Fractal characteristics of rock discontinuities. Engng. Geol., 34, pp. 1-9

Gillespie, P. A, Howard, H., Walsh, J.J & Watterson, J. 1993. Measurement and characterisation of spatial distributions of fracture. Tectonophysics, 226, pp113-141

Gilvarry, J. J. 1961. Fractures of brittle solids. I. Distribution functions for fragment size in single fracture (theoretical), J. Appl. Phys., 32(3), pp. 391-399

Goodman, R. E. & Shi, G. 1985. Block theory and its application to rock engineering. New Jersey: Prentice-Hall, 338pp

Gozen, J. S., Britton, R. R. Fodo, J. D. 1986. Predetermining average fragment size - A case study. in: Application of Rock Characterisation Techniques in Mine Design (Karmis ed.), Littleton(USA): SME, pp. 190-195

Grady, D. E. & Kipp, M. E. 1987. Dynamic rock fragmentation. in: Fracture mechanics of rock. London: Academic Press, pp. 429-459

Grainger, P., McCann, D. M. & Gallois, R. W. 1973. The application of the seismic refraction technique to the study of the fracturing of Middle Chalk at Mundford, Norfork. Geotechnique. 23, pp. 219-232

Grainger, K. M. & Paine, G. G. 1990. Development and application of a photographic sizing assessment technique for blast analysis. in: Proc. 3rd Int. Symp. on Rock fragmentation by Blasting, Brisbane, Parkville: AusIMM, pp. 255-258

Hagan, T. N. & Just, G. D. 1974. Rock breakage by explosives - theory, practice and optimisation. in: Proc. of 3rd Cong. of ISRM, Washington, D.C.: National Academy Sciences, 1(B), pp. 1349-1358

Haines, A. 1993 Mining geotechnical investigation in quarry design practice. Quarry Management, 1993(April), pp. 15-19

Harries, G. & Hengst, B. 1977. The use of a computer to describe blasting. in: 15th APCOM Symp., Brisbane, Australia, pp. 317-323

Harris, C., Franssen, R. & Loosveld, R. 1991. Fractal analysis of fractures in rocks: the Cantor's dust method--comment. Tectonophysics 198, pp. 107-111

Hartmann, W. K. 1969. Terrestrial , lunar, and Interplanetary rock fragmentation, ICARUS, 10, pp. 201-213

Hirata, T., Satoh, T. & Ito, K. 1987. Fractal structure of spatial distribution of microfracture in rock. Geophys. J. R. Astr. Soc. 90, pp. 369-374

Hirata, T. 1989. Fractal dimension of fault systems in Japan: fractal structure in rock fracture geometry at various scales. PAGEOPH, 131(1/2), pp. 157-170

Hobbs, B. E. 1993. The significance of structural geology in rock mechanics. in: Comprehensive Rock Engineering (Hudson et al. eds), Vol.1, pp. 25-62

Hoek, E. & Bray, J. W. 1981. Rock slope engineering. 3rd ed. London: IMM

Hoek, E., Wood, D & Shah S. 1992. A modified Hoek-Brown failure crterion for jointed rock masses. in: Rock Characterisation (Hudson ed.) London: Thomas Telford, pp. 209 - 214

Holmgerg, R. & Rustan A. (eds.) 1983. Proc. of 1st Int. Symp. on Rock Fragmentation by Blasting. Lulea, Sweden

Hudson, J. A. & Priest, S. D. 1979. Discontinuity and rock mass geometry. Int. J. Rock Mech. Min. & Geomech. Abstr. 16, pp. 339-362

Hudson, J. A. & Priest, S. D. 1983. Discontinuity frequency in rock mass. Int. J. Rock Mech. Min. & Geomech. Abstr. 20, pp. 73-89

Hudson J. A. & De Puy M. A 1990. Rock Characterisation according to Engineering Objectives. in: Proc. of 3rd Conf. on Rock Mech. & Engng.- Weak Rock. Torino, Italy

Hudson J. A. 1992. Rock Systems Engineering: theory and practice. Chichester: Ellis Horwood

Hudson J. A., Sheng J. & Arnold P.N. 1992. Rock engineering risk assessment through critical mechanism and parameters evaluation. in: Proc. of 6th Australia-New Zealand Conf. on Geomech. Christchurch: NZGS, pp. 442-447

Hunter, G. G., McDermott, C., Miles, N. J., Singh, A. & Scoble, M. J. 1990 Review of images analysis technique for measuring blast fragmentation. Min. Sci. Technol. 11(1) pp. 19-36

ISRM 1978. Suggested methods for description of discontinuities in rock mass. Int. J. Rock Mech. Min. & Geomech. Abstr. 15 (6), pp. 319-368

ISRM 1985. Suggested method for determining point load strength. Int. J. Rock Mech. Min. & Geomech. Abstr. 22(2), pp. 53-60

Jennings, J. E. 1968. A preliminary theory for the stability of rock slopes based on wedge theory and using results of joint surveys. Univ. of the Wutewatersrand, Internal Report.

JKMRC. 1991 Advanced Blasting Technology. AMIRA P93D (1987-1990), Final Report, JKMRC, Univ. of Queensland, Australia

Johansson, C. H. & Persson, P. A. 1974, Fragmentation systems. in: Proc. 3rd Cong. of ISRM, 2(B), pp. 1557-1566

Just, G. D. & Henderson D.S. 1971. Model studies of fragmentation of explosives. in: Proc. of the 1st Australia-New Zealand Conf. on Geomech., pp. 238-245

Just, G. D. 1973. The Application of size distribution equations to rock breakage by explosives. Rock Mech., 5(3), pp. 151-162

Just, G. D. 1979. Rock fragmentation in blasting. CIM Bull., March, 1979, pp. 143-148

Karpuz, C., Pasamehmetoglu, G., Bozdag, T. & Müftüoglu, Y. 1990 Rippability assessment in surface coal mining. in: Mine Planning and Equipment Selection (Singhal & Vavra eds.), Rotterdam: Balkema, pp. 315-322

Karzulovic, A. & Goodman, R. E. 1985. Determination of principal joint frequency. Int. J. Rock Mech. Min. & Geomech. Abstr. 22(6), pp. 471-473

Kazi, A. & Sen, Z. 1985. Volumetric RQD: an index of rock quality. in Fundamentals of rock joints (Stephansson ed.). Sweden: Centek Pub. pp. 95-101

Khanukayev, A. N. 1974 Some aspects on theory and practice of rock fragmentation by blasting. in: Proc. of 3rd Cong. of ISRM, Washington: National Academy Sciences, 2(B), pp. 1707-1711

Kikuchi, K., Mimuro, T., Kobayashi, T., Izumiya, Y. & Mito, Y. 1987. A joint survey and determination of joint distribution. in: 2nd Int. Symp. on Field Measurements in Geomech. (Sakurai ed.), Rotterdam: Balkema, pp. 239-248

Kikuchi, K, Kuroda, H. & Mito, Y. 1987. Stochastic estimation and modelling of rock joint distribution based on statistical sampling. in: Proc. 6th ISRM Cong. On Rock Mech. (Herget & Vongpaisal eds.) Rotterdam: Balkema, pp. 425-428

King, R. P. 1984. Measurement of particle size distribution by image analyser. Powder Technology. 39: 279-289

Kleine, T. H & Villaescusa, E. 1990. A rock joint model to estimate the *in-situ* block size distribution in natural joint rock. in: XXIII APCOM, Berlin, pp. 693-704

Kirstern, H.A.D. 1988. Cases histories of groundmass characterisation for excavatability. in: Rock classification systems for engineering purposes. ASTM STP 984 (Kirkalide ed.), Philadelphia: ASTM, pp. 102-120

Konya, C. J. & Walter, E. J. 1990. Surface blast design. New Jersey: Prentice Hall

Korvin, G. 1989. Fractured but not fractal: fragmentation of the Gulf of Suez Basement. PAGEOPH, 131(1/2), pp. 289-305

Kou, S.-Q. & Rustan, A. 1992. Burden related to blasthole diameter in rock blasting. Int J. Rock Mech. Min. Sci. & Geomech. Abstr., 29(6), pp. 543-553

Kulatilake, P. H. S. W. & Wu, T. H. 1984a. Estimation of mean trace length of discontinuities. Rock Mech. Rock Engng., 17, pp. 215-232

Kulatilake, P. H. S. W. & Wu, T. H. 1984b. Sampling bias on orientation of discontinuities. Rock Mech. Rock Engng., 17, pp. 243-253

Kulatilake, P. H. S. W.& Wu, T. H. 1986. Relation between discontinuity size and trace length. in: Proc. 27th US Symp. on Rock Mech., pp. 130-133

Kulatilake, P. H. S. W., Wathugala, D. N. & Stephansson, O. 1990. Three stochastic joint geometry modelling including a verification: a case study. in: Rock Joints (Barton & Stephansson eds.), Rotterdam: Balkema, pp. 67-74

Kulatilake, P. H. S. W., Wathugala D. N. & Stephansson, O. 1993. Joint network modelling with a validation exercise in Stripa Mine, Sweden. Int. J. Rock Mech. Min. & Geomech. Abstr. 30(5), pp. 503-526

Kuznetsov, V. M. 1973. The mean diameter of the fragments formed by blasting rock. Soviet Mining Science, 9(2), pp. 144-148

Langefors, U. & Kihlstrom, B. 1978. The modern technique of rock blasting (3rd Ed.) New York: John Willy, 405 pp.

La Pointe, P. & Hudson, J. A. 1985. Characterisation and interpretation of rock mass joint patterns. Boulder(USA): Geol. Soc. Am., Special Paper 199, 37pp

La Pointe, P. 1988. A method to characterise fracture density and connectivity through fractal geometry. Int J. Rock Mech. Min. Sci. & Geomech. Abstr., 25(6), pp. 421-429

La Pointe, P., Wallmann P. & Dershowitz. 1993. Stochastic estimation of fracture size from simulated sampling. Int. J. Rock Mech. Min. & Geomech. Abstr. 30(7), pp. 1611-1617

La Pointe, P. 1993. Modern developments in discontinuity analysis - the persistence - connectivity problem. in Comprehensive Rock Engineering (Hudson et al. eds), Vol.3, pp. 193-213

Latham, J.-P. (ed). 1992 Proc. on Armourstone: production, evaluation, specification, use. QMWC, London Uni.

Latham, J.-P., Wang, H. 1992. Constraints on armourstone production rates. in: Proc. on Armourstone: production, evaluation, specification, use (Latham ed.), London: QMWC, pp. 95-104

Latham, J. P., Wang, H. & Poole, A. 1994. Rock for maritime engineering. in Coastal, Estuarial and Harbour Engineeers' Reference Book, London: E & FN Spon, pp. 523-540

Lilly, P.A. 1986. An empirical method of assessing rock mass blastability. in: Large Open Pit Mining Conference (Davidson ed.), Victoria: AusIMM, pp. 89-92

Lizotte, Y. C. & Scoble, M. J. 1994. Geological control over blast fragmentation. CIM Bull., 87(983), pp. 57-71

Long, J. C. S.1993. Construction of equivalent discontinuum models for fracture hydrology. in: Comprehensive Rock Engineering (Hudson et al. eds), Vol.3, pp. 241-295

Lownds, C. M. 1983. Computer modelling of fragmentation from an array of shotholes. in: 1st Int. Symp. on Rock Fragmentation by Blasting. Lulea, Sweden, 1983. pp. 455-485

Lu, P. & Hudson, J. A. 1993. A fuzzy evaluation approach to the stability of underground excavations. in: ISRM Symposium: EUROCK'93 (Ribeiro e Sousa & Grossmann eds.), Rotterdam: Balkema, pp. 615-622

Lu, P. & Latham, J.-P. 1994. A continuous quantitative coding approach to the interaction matrix in rock engineering systems based on grey systems approaches. in: Proc. 7th Int. Cong. of IAEG, Rotterdam: Balkema, pp. 4761-4770

Mandelbrot, B. B. 1967. How long is the coast of Britain? statistical Self-similarity and fractional dimension. Science, 156, pp. 636-638

Mandelbrot, B. B. 1975. Stochastic models for the Earth's relief, the shape and the fractal dimension of the coastline, and the number-area rule for islands. Proc. Nat. Acad. Sci. USA, 72(10), pp. 3825-3828

Mandelbrot, B. B. 1983. The fractal geometry of nature. New York: Freeman

Mandelbrot, B. B. 1986. Self-affine fractal sets. in: Fractals in physicas (Pietronero & Tosattie eds.), Amersterdam: Freeman, pp. 3-28

Mandelbrot, B. B. 1990. Fractal geometry: what is it, and what dose it do? in: Fractals in the natural sciences. Princeton: Princeton Univ. Press, pp. 3-16

Mander, Raikes & Marshall (MRM), 1985. A5 London-Holyhead Trunk Road, Improvements at Glyn Bends, Clwyd, Factual Report on Site Investigation

Matheson, G. D. 1995. Aspects of highway rock engineering in the UK. in: Engineering Geology of Construction (Eddleston et al. eds.), London: Geol. Soc., pp. 169-187

Mathis, J. I. 1987. Discontinuity mapping -- A comparison between line and area mapping. in: Proc. 6th ISRM Cong. On Rock Mech. Rotterdam: Balkema, pp. 1111-1114

Mathis, J. I. 1989. RQD prediction using joint centre densities. in: Engineering Geology and Geotechnical Engineering (Watters ed.). Rotterdam: Balkema, pp. 313-318

Milne, D., Germain, P. & Potvin, Y. 1992. Measurements of rock mass properties for mine design. in: Rock Characterisation (Hudson ed.). London: Thomas Telford, pp. 245-250

Mojtabai, N, Farmer, I. W. & Savely, J. P. 1990. Optimisation of rock fragmentation in bench blasting. in: Proc. 31th US Rock Mech. Symp. Rotterdam: Balkema, pp. 897-905

Nagahama, H. & Yoshii, K. 1993. Fractal dimension and fracture of brittle rocks. Int J. Rock Mech. Min. Sci. & Geomech. Abstr., 30(2), pp. 173-175

Nie, S.-L. & Rustan, A. 1987. Techniques and procedures in analysing fragmentation after blasting by photographic methods. in: Proc. 2nd Int. Symp. Rock Fragmentation by blasting, Colorado, pp. 102-113

Noren, C. H. & Porter, S. D. 1974. A comparison of theoretical explosive energy and energy measured underwater with measured rock fragmentation. in: Proc. 3rd Cong. of ISRM, IIB, pp. 1371-1375

Numerical Algorithms Group. 1984. Nag FORTRAN Library Manual, Mark 11, V5. Computer Service, QMWC, London Univ.

Ord, A. & Cheung, C. C. 1991. Image analysis techniques for determining the fractal dimensions of rock joints and fragment size distribution. in: Proc. of 7th Conf. of IACMAG, Rotterdam: Balkema, pp. 87-91

Ordance Survey. 1986. 1:50000 Landranger series, Sheet 116, Denbugh & Colwyn Bay. Southampton: Ordance Survey

Owen, D. R. J., Munjiza, A. & Bicanic, N. 1992. A finite element-discrete element approach to the simulation of rock blasting problems. in: Proc. 11th Symp. on FE in Sfr., Cape Town: CRCAM, pp. 39 -58

The Overseas Quarry, 1995. Item-1 to Item 9: Geological and blasting data and information of the Sibline Quarry. Prepared by Touma Engineering and Research, F. Mauthe, J. D. Simm respectively

Palmstrom, A. 1985. Application of the volumetric joint count as a measure of rock mass jointing. in Fundamentals of rock joints (Stephansson ed.), Sweden: Centek Pub., pp. 103-109

Panek, L. A. 1985. Estimating fracture trace length from censor measurements on multiple scanlines. in: Fundamentals of rock joints (Stephansson ed.), Sweden: Centek Pub., pp. 13-23

Piteau, D. R. 1970. Geological factors significant to the stability of the slopes cut. in: Proc. of the Open Pit Mining Symp.. S. Afr. Inst. Min. Metall., pp. 33-53

Piteau, D. R. 1973. Characterising and extrapolating rock joint properties in engineering practice. Rock Mech. Suppl. 2, pp. 5-31

Pollard, D. D. & Yadin, A. 1988. Progress in undersdanding jointing over the past century. Geol. Soc. Amer. Bull. 100, pp. 1181-1204

Pollard, D. D., Zeller, S., Olson, J. & Thomas, A. 1990. Understanding the process of jointing in brittle rock masses. In: Proc. 31st US Symp. on Rock Mech. (Hustrulid & Johnson eds.), Rotterdam: Balkema, pp. 447-454

Poulton, M. M., Mojtabai, N. & Farmer, I. W. 1990. Scale invariant behaviour of massive and fragments rock. Int J. Rock Mech. Min. Sci. & Geomech. Abstr., 27(3), pp. 219-221

Priest, S. D. & Hudson, J. A. 1976. Discontinuity spacing in rock. Int. J. Rock Mech. Min. & Geomech. Abstr. 13, pp. 135-148

Priest, S. D. & Hudson, J. A. 1981. Estimation of discontinuity spacing and trace length using scanline surveys. Int. J. Rock Mech. Min. & Geomech. Abstr., 18, pp. 183-197

Priest S. D. 1993a. Discontinuity analysis for rock engineering. London: Chapman & Hall

Priest, S. D. 1993b. The collection and analysis of discontinuity orientation data for engineering design, with examples. in: Comprehensive Rock Engineering (Hudson et al. eds), Vol.3, pp. 167-192

Press, W. H., Flannery, B. P., Teukolsky, S. A. & Vetterling, W. T. 1986. Numerical Recipes. Cambridge: Cambridge Univ. Press

Ranalli, G. & Hardy, L. 1988. Statistical approach to brittle fracture in the earth's crust. in Statistical applications in the Earth science (Agterberg & Bonham-Carter eds.) Geol. Surv. Canada, Paper 89-9, pp 255-262

Rives, T., Razack, M., Petit, J.-P. & Rawnsley, D. 1992. Joint spacing: analogue and numerical simulations. J. Struc. Geol. 14(8/9) pp. 925-937

Robertson, A. 1970. Geological factors significant to the stability of slopes cut in rock. Proc. of the Open Pit Mining Symp. Johannesburg: S. Af. Inst. Min. Met., pp. 55-71

Rorke A. J. 1988. A scientific approach to blast design. Quarry management. 1988. Oct.

Rosin, P. & Rammler, E. 1933. The laws governing the fineness of powder ed coal. J. Inst. Fuel, 7, pp. 29-36

Rossmanith, H. P. (ed.) 1993. Proc. of Fourth Int. Symp.-FRAGBLAST-4. Rotterdam: Balkema, 534.pp

Rouleau, A. & Gale, J. E. 1985. Statistical characterisation of fracture system in the Stripa Granite, Sweden. Int. J. Rock Mech. Min. & Geomech. Abstr. 22(6), pp. 353-367

Rustan, A., Vutukuri, V. S. & Naarttijarvi, T. 1983. The influence from specific charge, geometric scale and physical properties of homogenous rock on fragmentation. in: Proc. 1st Int. Symp. on Rock Fragmentation by blasting, Lulea, Sweden, pp. 115-142

Rustan, A. 1992. Burden, spacing and borehole diameter at rock blasting. Int. J. Surf. Min., 6(3), pp. 141-149

Sachpazis, C. I. 1990. Correlating Schmidt hardness with comprehensive strength and Young's modulus of carbonate rocks. Bulletin IAEG, No.42, pp. 75-83

Sammis, C., King, G. & Biegel, R. 1987. The kinematics of gouge deformation. PAGEOPH, 125(5), pp. 777-812

Sammis, C. & Biegel, R. 1989. Fractals, fault-gouge, and friction. PAGEOPH, 131(1/2), pp. 255-271

Santalo, L. A. 1976. Integral Geometry and Geometric Probability. Massachusetts: Addison-Wesley, 404pp

Scholz, C. H. & Mandelbrot, B. B. 1989. Introduction to Fractals in Geophysics. PAGEOPH, 131(1/2), pp. 1-4

Schuhmann, Jr. R. 1940. Principles of comminunition, I - size distribution and surface calculations. AIME Tech. Pub. No.1189, Min. Engrs, AIME, New York

Schuhmann, Jr. R. 1960. Energy input and size distribution in comminution Trans. Am. Ist. Min. Metall. Petrol. Engrs. 217, pp. 22-25

Scoble, M. J. & Muftuoglu, Y.V. 1984. Derivation of a diggability index for surface mine equipment selection. Min. Sci. & Tech., 1, 305-322

Scott, A., Chitombo, G. & Kleine, T. 1993. The challenge of the prediction and control of fragmentation in mining. in: Proc. of 4th Int. Symp.-FRAGBLAST-4 (Rossmanith ed.), Rotterdam: Balkema, pp. 507-517

Segall, P. & Pollard, D. D. 1983. Joint formation in granitic rock of the Sierra Nevada. Geol. Soc. Amer. Bull. 94, pp. 563-575

Sen, Z. 1984. RQD models and fracture spacing. J. Geol. Eng. 110, pp. 203-216

Sen, Z. & Kazi, A. 1984. Discontinuity spacing and RQD estimates from finite length scanlines. Int. J. Rock Mech. Min. & Geomech. Abstr. 21, pp. 203-212

Sen, Z. & Eissa, E. A. 1992. Rock quality charts for log-normally distributed block sizes. Int. J. Rock Mech. Min. & Geomech. Abstr. 29, pp. 1-12

Sen, Z. 1993. RQD-fracture frequency chart based on a Weibull distribution. Int. J. Rock Mech. Min. & Geomech. Abstr. 30(5), pp. 555-557

Simm, J. D., Latham, J.-P. & Orbell-Durrant, C. 1992. Standardising the approach to specifying quarried rock in coastal structures and breakwaters. in: Coastal Structures and Breakwaters. London: Thomas Telford, pp. 267-283

Singh, D. P. & Sarma, K. S. 1983. Influence of joints on rock blasting -- a model scale study. in: 1st Int. Symp. on Rock Fragmentation by Blasting, Lulea, Sweden, pp. 533-554

Singh, D. P. & Sastry, V. R. 1987. An investigation into the effect of blast geometry on rock fragmentation. in: Proc. 6th ISRM Cong. On Rock Mech. (Herget & Vongpaisal eds.), Rotterdam: Balkema, pp. 721-725

Soedibjo 1990. Geotechnical classification and determination of the rock materials properties. in: Proc. of 6th Int. IAEG Cong. Rotterdam: Balkema, pp. 745-752.

Stewart, D. R. 1986. A review of techniques for predicting the natural fragmentation characteristics of block caving orebodies. in: Application of Rock Characterisation Techniques in Mine Design, Littleton(USA):SME, pp. 181-189

Sornette, A., Davy, Ph. & Sornette, D. 1990. Growth of fractal fault patterns. Phys. Rew. Lett., 65, pp. 2266-2269

Stagg, M. S., Otterness, R. E. & Siskind, D. E. 1992. Effects of blasting practice on fragmentation. in: Proc. of 33rd US Symp. on Rock Mech. Rotterdam: Balkema, pp. 313-322

Stephansson, O. Wang, W. X. & Dahlhielm, S. 1992. Automatic image analysis of aggregates. in: Rock Characterisation (Hudson ed.). London: Thomas Telford, pp. 31-35

Thomas, R.S. 1992. The pros and cons of rock armour in coastal works. in Armourstone - production, evaluation specification, use. (Latham ed.). Queen Mary and Westfield College, pp. 1-10

Turcotte, D. L. 1986. Fractals and Fragmentation. J. Geophy. Res., 91(B2), pp. 1921-1926

Turcotte, D. L. 1989. Fractals in geology and geophysics. PAGEOPH, 125(5), pp. 171-176

Turcotte, D. L. 1992 Fractals and chaos in geology and geophysics. Cambridge: Cambridge Univ. Press

Van Aswegen, H. & Cunningham, C. V. B. 1986. The estimation of fragmentation in blast buckpiles by standard photographs. J. S. Af. Inst. Metall., 86(12), pp. 469-474

Villaescusa, E. & Brown, E. T. 1990 Characterising joint spatial correlation using geostatistical methods. in Rock Joints (Barton & Stephansson eds.), Rotterdam: Balkema, pp. 115-122

Villaescusa, E. & Brown, E. T. 1992. Maximum likelihood estimation of joint size from trace length measurements. Rock Mech. & Rock Engng., 25, pp. 67-87

Walsh, J. J. & Watterson, J. 1993. Fractal analysis of fracture patterns using the standard box-counting technique: valid and invalid methodologies. J. Struc. Geol. 15(12), pp. 1509-1512

Wang, H. & Latham, J.-P. 1991. Prediction of block size distribution for highway rock excavation. Geomaterials Unit, Queen Mary and Westfield College, 65pp.

Wang, H. 1992. Predictions of in-situ and blastpile block size distributions of rock masses, with special reference to coastal requirements. Thesis of PhD, Queen Mary and Westfield College, London University

Wang, H., Latham, J.-P. & Poole, A. B. 1990. In-situ block size assessment from discontinuity spacing data. in: Proc. 6th Int. IAGE Cong. (Price ed.), Rotterdam: Balkema, pp. 117-127

Wang, H., Latham, J.-P. & Poole, A. B. 1991a. Prediction of block size for quarrying. Q. J. Engng. Geol., 24, pp. 91-99

Wang, H., Latham, J.-P. & Poole, A. B. 1991b. Blasting design for armourstone production. J. Quarry Management, Part I (July), pp. 17-21; Part II (Aug.), pp. 19-22

Wang, H., Latham, J.-P. & Matheson, G. D. 1992. Design of fragmentation blasting in surface excavation. in: Rock Characterisation (Hudson ed.). London: Thomas Telford, pp. 233-238

Warburton, P. M. 1980. A stereological interpretation of joint trace data. Int. J. Rock Mech. Min. & Geomech. Abstr. 17, pp. 181-190

Xie, H. 1990. Damage mechanics of rock and concrete. Xuzhou (China): The Press of China University of Min. Sci. & Tech. (in Chinese) (also see Xie, H. 1993. Fractals in rock mechanics, Rotterdam: Balkema)

Xu, J. & Cojean, R. 1990 Three dimensional simulation of natural rock granulometry (in French), Proc. of 6th Int. Cong. IAEG, Rotterdam: Balkema, pp. 797-802

Xu, S., Grasso, P. & Mahtab, A. 1990. Use of Schemidt hammer for estimating mechanical properties of weak rock. in: Proc. of 6th Int. IAEG Cong. (Price ed.) Rotterdam: Balkema, pp. 511-519.

Yang, Z.-G. & Rustan, A. 1983. The influence from primary structure on fragmentation. in 1st Int. Symp. on Rock Fragmentation by Blasting. Lulea, Sweden, pp. 581-603

Zhang, X. & Liao, G. 1990. Estimation of confidence bounds for mean trace length of discontinuities using scanline surveys. Int. J. Rock Mech. Min. & Geomech. Abstr. 27(3), pp. 207-212

APPENDIX A. PROGRAM LISTINGS FOR GCA AND DIATRACE

A.1 PROGRAM LISTIN FOR GREY CORRELATION ANALYSIS, GCA

```
C   ************************************************************************
C   * PROGRAM OF CALCULATING THE CORRELATION MEASURE
C   * COMPILED IN QMWC BY P. LU, IN MAY 1994
C   ************************************************************************
        DIMENSION X0(14),X(4,14),PSI(4,14),RM(4)
        DIMENSION SUBV(14),DMI(4),DMA(4),XX(14)
        OPEN(3,STATUS='OLD',FILE='GCA-d-I.DAT')
        OPEN(4,STATUS='NEW',FILE='GCA-D-O.DAT')
        READ(3,*) NI,NK,NC,COFP
        WRITE (4,129)NI,NK,NC,COFP
        READ(3,*) (X0(J),(X(I,J),I=1,NI),J=1,NK)
129     FORMAT(/1x,'*****Grey correlation analysis output**********',//
     +  '******Control data is****'//3x,3I5,F8.3)
        WRITE (4,109)
109     FORMAT(1X,'********Original data*******'//)
        WRITE (4,119) (J,X0(J),(X(I,J),I=1,NI),J=1,NK)
119     FORMAT(1X,I4,5F12.4)
C     **INITIALIZING DATA**
        IF (NC .EQ. 0) GOTO 55
        CALL INTI(X0,X,NI,NK)
        WRITE (4,429)
429     FORMAT(//1X,'********Initialized Data*******'/)
        WRITE (4,419) (J,X0(J),(X(I,J),I=1,NI),J=1,NK)
419     FORMAT(1X,I4,5F12.4)
C     **ENDING OF INITIALIZING DATA**
55      DO 210 I=1,NI
        DO 99 J=1,NK
        XX(J)=0.0
99       CONTINUE
        DO 230 J=1,NK
        XX(J)=X(I,J)
230     CONTINUE
        CALL VSUB(X0,XX,NK,SUBV)
        CALL COMPMI(SUBV,NK,DMI(I))
        CALL COMPMA(SUBV,NK,DMA(I))
210     CONTINUE
        DO 250 I=1,NI
        DO 299 J=1,NK
        XX(J)=0.0
299     CONTINUE
        CALL COMPMI(DMI,NI,DDMI)
        CALL COMPMA(DMA,NI,DDMA)
        DO 290 J=1,NK
        X0K=ABS(X0(J)-X(I,J))
        CALL COEFF(DDMI,DDMA,COFP,X0K,PPSI)
        PSI(I,J)=PPSI
        XX(J)=PSI(I,J)
290     CONTINUE
        CALL CORMEA(XX,NK,RR)
```

```
      RM(I)=RR
250   CONTINUE
      WRITE(4,149)
      WRITE (4,159) (J,(PSI(I,J),I=1,NI),J=1,NK)
159   FORMAT(1X,I4,4F12.4)
149   FORMAT(/1X,'****The correlation coefficients of Xi-X0 at time k ***'/)
      WRITE (4,179)
      WRITE (4,199) RM
179    FORMAT (//1X,'***The correlation measure of Xi--X0 ****')
199    FORMAT (/1X,4F12.4)
      STOP
      END
C
C
C
C     SUB-PROGRAM OF CALCULATING THE COEFF. OF CORRELATION AT POINT
      SUBROUTINE COEFF(DMIN,DMAX,P,DIK,EIK)
      EIK=(DMIN+P*DMAX)/(DIK+P*DMAX)
      RETURN
      END
C
C     SUB-PROGAMME OF CALCULATING THE MINUS VALUE
C
      SUBROUTINE VSUB(X0,X1,N,CAL)
      DIMENSION X0(N), X1(N),CAL(N)
      DO 110 I=1,N
      CAL(I)=ABS(X0(I)-X1(I))
110   CONTINUE
      RETURN
      END
C
c    SUB-PROGRAM FOR CALCULATING THE CORRELATION MEASURE
C
      SUBROUTINE CORMEA(COFI,N,R)
      DIMENSION COFI(N)
      SUM=0.0
      DO 120 I=1,N
      SUM=SUM+COFI(I)
120   CONTINUE
      R=1.0/N*SUM
      RETURN
      END
C
C
c     SUB-PROGRAM OF COMPARING THE Xk.
C     COMPARING THE Xk AND IDENTIFYING THE MINIMUM VALUE
C
      SUBROUTINE COMPMI(R,K,VMI)
      DIMENSION R(K)
      VMI=R(1)
      DO 100 I=2,K
      IF (VMI.LE. R(I))  GOTO 100
      VMI=R(I)
100   CONTINUE
      RETURN
      END

C     COMPARING THE Xk  AND IDENTIFYING THE MAXMUM VALUE
C
```

```
      SUBROUTINE COMPMA(R,K,VMA)
      DIMENSION R(K)
      VMA=R(1)
      DO 100 I=2,K
      IF (VMA.GE.R(I)) GOTO 100
      VMA=R(I)
100   CONTINUE
      RETURN
      END
C
C
C
C     SUB-PROGRAM FOR INITIALIZING THE DATA

      SUBROUTINE INTI(X0,X,NI,NK)
      DIMENSION X0(NK),X(NI,NK)
      DX01=X0(1)
      DO 510 I=1,NK
      X0(I)=X0(I)/DX01
510   CONTINUE
      DO 410 I=1,NI
      DX1=X(I,1)
      DO 430 J=1,NK
      X(I,J)=X(I,J)/DX1
430   CONTINUE
410   CONTINUE
      RETURN
      END
```

A.2 PROGRAM LISTING FOR ESTIMATION OF DISCONTINUITY DIAMETER, DIATRACE

```
C   DETERMINE THE MEAN DIAMETER FROM TRACE LENGTH DISTRIBUTION, USING
C   Warburton's EQUATION THROUGH NUMERICAL SOLUTION
    PARAMETER (N=21,NP=21)
    DIMENSION X0(N+1),DIA(N),PX(N),PD(N),A(N,N),B(N),INDX(N),VV(100)
    DIMENSION A1(N,N),B1(N),PFD(N),PDX(N),SSUM(500),CC(500)
        OPEN(9,FILE='POT.DAT',STATUS='NEW')
C   READ RUNNING-CONTROL ID
    WRITE(*,5)
5   FORMAT(/1X,'INPUT TRACE LENGTH DISTRIBUTION CONTROL ID: 0,1,2,3.',
   &1x,'ID=0, no assumption on distribution of trace length;',1x,
   &'ID=1,2,3 are respectively negative exponential, lognormal and',
   &1x,'fractal trace length distribution '/)
        READ (*,*)ID
C   READ RUNNING-CONTROL,IC
    WRITE(*,7)
7   FORMAT(/1X,'INPUT RUNNING-CONTROL NUMBER: 0/1. IC=1, LOOP-',
   & SEARCHING; IC=0, POINT-SEARCHING',/)
        READ (*,*)IC
        WRITE (9,9)
9   FORMAT (//1X,'NUMERICAL SOLUTION TO DIAMETER DISTRIBUTION WHEN',
   & ASSUMING OR DETERMINING THE TRACE LENGTH DISTRIBUTION'/)
C   READ THE VALUES ARRAY X0
```

```
C    READ (*,*)X0
C    FINDING THE VALUES OF DIA(N)
     DO 20 I=1,N
          DIA(I)=(X0(I)+X0(I+1))/2
20   CONTINUE
C    FINDING THE ACCUMULATIVE PROBABILITY OF TRACE LENGTH DISTRIBUTION
     IF (ID.EQ.0) THEN
          WRITE (*,22)
22    FORMAT (/1X,'no assumption on dis. trace length, INPUT ITS',1x,
    *' ACCUM. PROB. FOR ITS DISTRIBUTION & ITS MEAN TRACE LENGTH'/)
C     READ(8,*)AMEAN, PX
           GOTO 5555
          ELSE IF (ID.EQ.1) THEN
           GOTO 1111
          ELSE IF (ID.EQ.2) THEN
           GOTO 2222
          ELSE IF (ID.EQ.3) THEN
           GOTO 3333
          END IF
1111      WRITE(*,1112)
1112    FORMAT(1X,'EXP-NEG. DIS, INPUT MEAN ITS LENGTH VALUE',/)
     READ (*,*) AMEAN
          WRITE(9,1114)AMEAN
1114    FORMAT(1X,'MEAN TRACE LENGTH IS',F12.4)
          WRITE (*,1114)AMEAN
     DO 1117 I=1,N
          CALL FUNEXP(X0(I),X0(I+1),AMEAN,PXLU)
          PX(I)=PXLU
      PDX(I)=PX(I)/(X0(I+1)-X0(I))
1117    CONTINUE
          GOTO 5555
2222    WRITE(*,2212)
2212    FORMAT(1X,'INPUT CONTROL VALUES FOR MEAN LENGTH, u, Sigma',/)
     READ (*,*) XU,XSIGM
          AMEAN=EXP(XU+XSIGM*XSIGM/2.)
          WRITE(9,2214)XU,XSIGM,AMEAN
2214    FORMAT(1X,'XU=',F8.4,3X,'XSIGM=',F11.4,3X,'X(MEAN)=',F12.4)
          WRITE (*,2216)AMEAN
2216    FORMAT(/1X,'MEAN TRACE LENGTH FOR LOG-NOR. DIS. IS',F10.4/)
     DO 2218 I=1,N
          CALL FUNLN(X0(I),X0(I+1),40,XU,XSIGM,PXLU)
          PX(I)=PXLU
      PDX(I)=PX(I)/(X0(I+1)-X0(I))
2218    CONTINUE
          GOTO 5555
3333    WRITE(*,3312)
3312    FORMAT(1X,'INPUT CONTROL FOR FRACTAL MEAN LENGTH,L-X,U-x,D',/)
     READ (*,*) AD,BD,DD
          AMEAN=DD/(1.0-DD)*(BD-AD*(BD/AD)**DD)/((BD/AD)**DD-1.0)
          WRITE(9,3314)AD,BD,DD,AMEAN
3314    FORMAT(1X,'X(L)=',F8.4,3X,'X(U)=',F11.4,3X,'D(FRAC.)=',F8.3,3X,
    &'X(MEAN)=',F12.4)
          WRITE (*,3316)AMEAN
3316    FORMAT(/1X,'MEAN TRACE LENGTH FOR FRAC. DIS. IS ,F10.4/)
     DO 3318 I=1,N
          CALL FUNFRA(X0(I),X0(I+1),AD,BD,DD,PXLU)
          PX(I)=PXLU
      PDX(I)=PX(I)/(X0(I+1)-X0(I))
3318    CONTINUE
```

```
C   NORMOLISING PX(I)
5555    SSM=0.0
    DO 45 I=1,N
    SSM=SSM+PX(I)
45  CONTINUE
    WRITE (*,*) SSM
    DO 41 I=1,N
    PX(I)=PX(I)/SSM
41  CONTINUE
C
    WRITE (9,44)
    WRITE (9,33) (I,X0(I),DIA(I),PX(I),PDX(I),I=1,N)
44    FORMAT (/5X,'*I*',3X,'**X(I)**',2X,'**DIA.(I)*',2X,'*PDF(I)****
   &**PDX(I)***'/)
33    FORMAT (1X,I4,2F12.4,2F12.6)
        WRITE (9,55) N+1,X0(N+1)
55    FORMAT (1X,I4,F12.4)
C   ARRANGING THE ELEMENTS BELOW DIAGONAL AS 0
    DO 80 I=2,N
        DO 60 J=1,I-1
         A(I,J)=0.0
60    CONTINUE
80  CONTINUE
C   FINDING THE VALUES OF DIAGONAL ELEMENTS
    DO 120 I=1,N
    A(I,I)=SQRT(DIA(I)**2-X0(I)**2)
120 CONTINUE
C   FINDING THE VALUES OF ELEMENTS ABOVE DIAGONAL
    DO 160 I=1,N-1
        DO 140 J=I+1, N
         A(I,J)=SQRT(DIA(J)**2-X0(J-1)**2)-SQRT(DIA(J)**2-X0(J)**2)
140   CONTINUE
160 CONTINUE
C   COPY ORIGINAL A(N,N)
    DO 175 I=1,N
    DO 165 J=1,N
        A1(I,J)=A(I,J)
165   CONTINUE
175 CONTINUE
C    WRITE (*,199) ((A(I,J),J=1,N),I=1,N)
199 FORMAT(1X,14F5.3)
C   CALL LUDCMP TO GET THE BASIC MATRIX FOR
C     SOLVING THE LINEAR EQUATION SET
    CALL LUDCMP(A,N,NP,INDX,D)
C   INPUT OR ADJUSTED TO THE MEAN TRACE LENGTH
        IF (IC.NE.0) GOTO 222
200 WRITE(*,211)
211 FORMAT(1X,'INPUT A NEW VALUE OF THE JOINT DIAMETER',/)
    READ (*,*)C
        GOTO 244
222   IA1M=ANINT(0.25*AMEAN)
        IA2M=ANINT(0.9*AMEAN)
        IA3M=IA2M-IA1M
        DO 500 IA=1,4*IA3M
        C=0.25*IA+IA1M
244   IF (C.EQ.0.0) GOTO 999
    DO 220 I=1,N
    B(I)=PX(I)*C
C   COPY ORIGINAL B(I)
```

```
      B1(I)=PX(I)*C
220   CONTINUE
C     CALL SUB-ROUTINE to SOLVE THE LINEAR EQUATION SET
      CALL LUBKSB(A,N,NP,INDX,B)
c     examing if PD(i)> or =0
      do 230 i=1,n
      if (b(i).GE.0) goto 230
      write (*,232)
232   format (/1x,'there is some P(i)<0, please adjust X(i)'/)
      goto 999
230   continue
C     WRITE (*,*)B
C     CALL SUB-ROUTINE TO IMPROVE THE SOLUTION
C     DO 240 I=1,5
      CALL PROVE(A1,A,N,NP,INDX,B1,B)
C240  CONTINUE
      DO 260 I=1,N
      PD(I)=B(I)
260   CONTINUE
C     EXAMINING WHETHER SUM OF PD(I) EQUAL TO 1
      SUM=0.0
      DO 280 I=1,N
      SUM=SUM+PD(I)
280   CONTINUE
          IF(IC.EQ.0) GOTO 299
          CC(IA)=C
          SSUM(IA)=SUM
      IF (IC.NE.0) GOTO 290
299   IF (ABS(SUM-1).LE.0.005) GOTO 555
      write (*,*) B
          GOTO 200
290   IF (ABS(SUM-1).LE.0.005) GOTO 555
500     CONTINUE
          GOTO 666
555   WRITE (9,311)C,SUM
      WRITE(*,*) B
311   FORMAT(//1X,'MEAN DIAMETER=',F10.4,5X,'SUM OF ACCU. PROB.=',F10.5)
C     COMPUTING THE PROBABILITY DENSITY OF DIAMETER
      DO 300 I=1,N-1
      PFD(I)=PD(I)/(DIA(I+1)-DIA(I))
300   CONTINUE
C     PFD(1)=PD(1)/(DIA(1)/2+(DIA(2)-DIA(1))/2)
      PFD(N)=PD(N)/(DIA(N)-DIA(N-1))
      WRITE (9,355)
      WRITE(9,333)(I,DIA(I),PD(I),PFD(I),I=1,N)
355   FORMAT(/1X,'*I****DIA.(I)***ACCUM. P(D)*****PROB.DENS. g(d)****'/)
333   FORMAT (1X,I4,3F12.5)
          GOTO 999
666     WRITE(9,688)
          WRITE(*,*)B
          WRITE(*,*)C,SUM
          WRITE (9,677) (I,CC(I),SSUM(I),I=1,4*IA3M)
688     FORMAT(1X,'**I********C******SUM******'/)
677     FORMAT (1X,I4,2F12.5)
       DATA X0/0.5,75,130,195,265,335,435,525,635,750,875,1000,1140,1250,
     &1445,1675,1900,2200,2450,2675,3000,3400/
999   STOP
      END
C
```

```
C    MAIN PROGROMME END
C
C
C    FINDING THE ACCU. PROBABILITY OF NEG-EXP TRACE LENGHT DISTRIBUTION
C      NEGTIVE-EXPONENTIAL DISTRIBUTION
     SUBROUTINE FUNEXP(XL,XU,AM,PX)
     PX=(1-EXP(-XU/AM))-(1-EXP(-XL/AM))
     RETURN
     END
C
C
C    FINDING THE ACCU. PROBABILITY OF LOGNORMAL TRACE
C    LENGTH DISTRIBUTION USING MUNERICAL INTEGRATION
     SUBROUTINE FUNLN(XL,XU,NH,BU,BSIGM,PX)
     X=XL
     H=(XU-XL)/NH
      X1=(LOG(X)-BU)/BSIGM
      FX=1./(SQRT(2*3.142)*BSIGM*X)*EXP(-0.5*X1**2)
     S=0.0
     DO 10 I=1,NH
     SI=FX*H
     S=S+SI
     X=X+H
      X1=(LOG(X)-BU)/BSIGM
      FX=1./(SQRT(2*3.142)*BSIGM*X)*EXP(-0.5*X1**2)
10   CONTINUE
     PX=S
     RETURN
     END
C
C
C    FINDING THE ACCU. PROBABILITY OF FRACTAL TRACE LENGHT DISTRIBUTION
          SUBROUTINE FUNFRA(XL,XU,AD,BD,DD,PX)
C
C      FRACTAL DISTRIBUTION
          PX1=(1-(AD/XL)**DD)/(1-(AD/BD)**DD)
          PX2=(1-(AD/XU)**DD)/(1-(AD/BD)**DD)
          PX=PX2-PX1
          RETURN
          END
C
C
C
C    GIVEN AN N*N MATRIX A, WITH PHYSICAL DIMENSION NP, THIS SUBROUTINE
C  REPLACE IT BYTHE LU DECOMPOSITION OF A ROWWISE PERMUTATION OF ITSELF
          SUBROUTINE LUDCMP(A,N,NP,INDX,D)
          PARAMETER (NMAX=100,TINY=1.0E-20)
          DIMENSION A(NP,NP),INDX(N),VV(NMAX)
          D=1.
           DO 12 I=1,N
            AAMAX=0.
            DO 11 J=1,N
            IF (ABS(A(I,J)).GT.AAMAX) AAMAX=ABS(A(I,J))
11         CONTINUE
             IF (AAMAX.EQ.0 ) PAUSE 'Singular matix.'
             VV(I)=1./AAMAX
12       CONTINUE
     DO 19 J=1,N
          IF (J.GT.1) THEN
```

```
          DO 14 I=1,J-1
           SUM=A(I,J)
           IF (I.GT.1) THEN
             DO 13 K=1,I-1
                  SUM=SUM-A(I,K)*A(K,J)
13          CONTINUE
             A(I,J)=SUM
           ENDIF
14       CONTINUE
          ENDIF
          AAMAX=0.
          DO 16 I=J,N
           SUM=A(I,J)
           IF (J.GT.1) THEN
            DO 15 K=1,J-1
             SUM=SUM-A(I,K)*A(K,J)
15         CONTINUE
            A(I,J)=SUM
           ENDIF
          DUM=VV(I)*ABS(SUM)
          IF (DUM.GE.AAMAX) THEN
            IMAX=I
            AAMAX=DUM
          ENDIF
16      CONTINUE
          IF (J.NE.IMAX) THEN
           DO 17 K=1,N
            DUM=A(IMAX,K)
            A(IMAX,K)=A(J,K)
            A(J,K)=DUM
17        CONTINUE
           D=-D
           VV(IMAX)=VV(J)
          ENDIF
          INDX(J)=IMAX
          IF(J.NE.N) THEN
           IF (A(J,J).EQ.0.) A(J,J)=TINY
           DUM=1./A(J,J)
           DO 18 I=J+1,N
            A(I,J)=A(I,J)*DUM
18        CONTINUE
          ENDIF
19      CONTINUE
          IF(A(N,N).EQ.0.) A(N,N)=TINY
          RETURN
          END
C
C
C    SOLVES THE SET OF N LINEAR EQUATIONS A*X=B. HERE A IS THE MATRIX A
C    RATHER ASITS LU DECOMPOSITION , DETERMINED BY THE SUBROUTINE LUDCMP
      SUBROUTINE LUBKSB(A,N,NP,INDX,B)
      DIMENSION A(NP,NP),INDX(N),B(N)
      II=0
      DO 12 I=1,N
           LL=INDX(I)
           SUM=B(LL)
           B(LL)=B(I)
           IF (II.NE.O) THEN
            DO 11 J=II,I-1
```

```
            SUM=SUM-A(I,J)*B(J)
11        CONTINUE
          ELSE IF (SUM.NE.0.) THEN
            II=I
          ENDIF
          B(I)=SUM
12    CONTINUE
      DO 14 I=N,1,-1
          SUM=B(I)
          IF (I.LT.N) THEN
            DO 13 J=I+1, N
              SUM=SUM-A(I,J)*B(J)
13        CONTINUE
          ENDIF
          B(I)=SUM/A(I,I)
14    CONTINUE
      RETURN
      END
C
C
C     IMPROVE THE SOLUTION
      SUBROUTINE PROVE(A,ALUD,N,NP,INDX,B,X)
      PARAMETER (NMAX=100)
      DIMENSION A(NP,NP),ALUD(NP,NP),INDX(N),B(N),X(N),R(NMAX)
      REAL*8 SDP
      DO 12 I=1,N
          SDP=-B(I)
          DO 11 J=1,N
            SDP=SDP+DBLE(A(I,J)*DBLE(X(J)))
11      CONTINUE
          R(I)=SDP
12    CONTINUE
      CALL LUBKSB(ALUD,N,NP,INDX,R)
      DO 13 I=1,N
          X(I)=X(I)-R(I)
13    CONTINUE
      RETURN
      END
```

APPENDIX B GENERATING RANDOM NUMBERS AND COMPILING GROUPS OF INPUT DATA

B.1 GENERATION OF RANDOM NUMBERS WITH UNIFORM DISTRIBUTION

A random number generator, named G05CAF, for producing random numbers with uniform distribution is called by RANFRA. The program RANFRA (see Appendix B.2) is for generating the real numbers with fractal distribution for simulating natural discontinuities in rock masses. The generator G05CAF for producing random numbers with uniform distribution has also been used to generate the data files of dip direction and dip of discontinuities in the simulations. This generator is a standard NAG routine available on the mainframe at QMWC (Numerical Algorithms Group, 1984).

The routine G05CAF returns the next pseudo-random number from the basic uniform [0,1] generator. The basic generator uses a multiplicative congruential algorithm:

$$b_{i+1}=13^{13}\times b_i \bmod 2^{59}. \qquad \text{(B-1)}$$

The integer b_{i+1} is divided by 2^{59} to yield a real value y in the range of 0 and 1. The value of b_i is preserved internally in the code. The initial value of, is set by default to $123456789\times(2^{32}+1)$.

If a pseudo-random real number from a uniform distribution between a_{min} and a_{max} ($a_{min}<a_{max}$) rather than 0.0 and 1.0 is required, a call to Nag G05DAF has to be made, which returns a pseudo-random number s taken from a uniform distribution over the interval (a_{min}, a_{max})

$$s=a_{max}+(a_{max}-a_{min})y, \qquad \text{(B-2)}$$

where, y is a random number from a uniform distribution over (0,1), generated by G05CAF.

The following are two examples of them.

(1) Random numbers varying in the range of 170 and 190

185.9025
174.5143
177.4256
174.5007
187.5749

(2) Random numbers varying in the range of 80 and 110

87.4256
84.5007
97.5749
80.9495
83.6114

B.2 GENERATION OF ARTIFICIAL DISCONTINUITIES WITH FRACTAL SPACINGS AND THE PROGRAM RANFRA

To generate a uniform probability distribution (see Appendix B.1), we know the probability of generating a number between x and $x+dx$, denoted $p(x)dx$, is given by

$$p(x)dx = \begin{cases} dx & 0 < x < 1 \\ 0 & otherwise \end{cases}. \qquad \text{(B-3)}$$

The probability distribution $p(x)$ is normalised, so that

$$\int_0^1 p(x)dx = 1. \qquad \text{(B-4)}$$

Suppose that we generate a uniform variable x and then take some prescribed function of it, $y(x)$, the probability distribution of y, denoted $p(y)dy$, is defined by the following basic transformation law of probabilities, which is simply given by

$$|p(y)dy| = |p(x)dx)|, \qquad \text{(B-5)}$$

or

$$p(y) = p(x)\left|\frac{dx}{dy}\right|. \qquad \text{(B-6)}$$

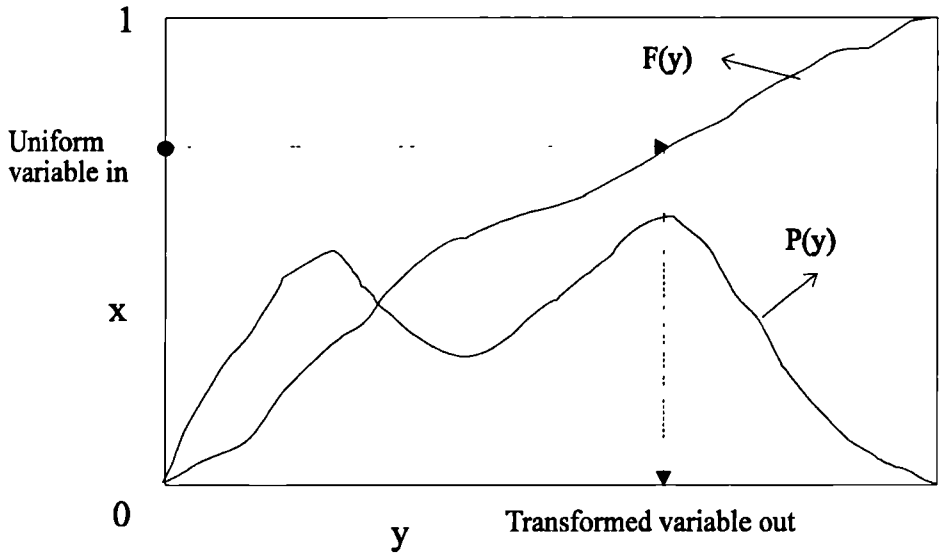

Fig. B.1 Generation of desired distribution from uniform variable using transformation (after Press et al., 1986)

Let us see what is involved in using the above transformation method to generate a desired distribution of y, say one with $p(y)=f(y)$ for a positive function whose integral is 1 (see Fig B.1).

According to Eqn. B-6, we need to solve the differential equation

$$\frac{dx}{dy} = f(y). \qquad \text{(B-7)}$$

The solution to Eqn. B-7 is just $x=F(y)$, where, $F(y)$ is the indefinite integral of $f(y)$. The desired transformation which takes a uniform variable into a distribution as $f(y)$ is therefore

$$y(x)=F^{-1}(x), \qquad \text{(B-8)}$$

where F^{-1} is the inverse function to F. Eqn. B-8 has an immediate geometric explanation (see Fig. B.1). Since $F(y)$ is the area under the probability curve to the left

of y, Eqn. B-8 is just the prescription: select a uniform random x, then find the value y that has that fraction x of probability area to its left, and return the value y. In other words, for a continuous random variable, if the cumulative distribution function is $F(x)$ then for a uniform (0, 1) random variable, u, y=$F^{-1}(u)$ will have the cumulative distribution function $F(x)$.

Whether the transform method will work is dependent upon whether it is feasible to compute the inverse function $F^{-1}(x)$. Sometimes, it is, and sometimes it is not. For a fractal distribution

$$F(x) = -\frac{A}{D}x^{-D}. \tag{B-9}$$

$F^{-1}(x)$, the inverse function to $F(x)$ is therefore as follows

$$F^{-1}(x) = (-\frac{D}{A}x)^{-(1/D)}. \tag{B-10}$$

We are therefore able to generate a value distributed fractally by firstly creating a pseudo-random real number y from a uniform distribution between 0 and 1, then changing y to the value u by $u = F^{-1}(y)$ defined by Eqn. B-10. A FORTRAN programme named RUNFRA for generating the pseudo-random real number with fractal distribution has been developed.

The random number generator, i.e. the programme RANFRA has been used to generate real numbers with fractal distribution for simulating natural discontinuities in rock masses. The generator has to be jointly used with the generator for producing real numbers with uniform distribution, which is a standard NAG routine available on the mainframe at QMWC.

Running the programme RANFRA in the mainframe, the real numbers with fractal distribution for simulating natural discontinuities in rock masses can be obtained. The program of this generator is listed below. The numbers obtained have been used to form the spacing data files of a fractal distribution with given fractal dimensions or principal mean spacings.

The program listing for RANFRA

```
************************************************************************
* Generator of random number distributed fractally (f(x)=Ax^-(1+D),
* where D is the fractal dimension defined by number-frequency relationship
* N(x)=Cx^-D, compiled by P. Lu, in QMWC, London Univ. in May, 1994
************************************************************************
*    RUNFRA Program Text
*    .. Parameters ..
     INTEGER        NOUT
     PARAMETER      (NOUT=6)
*    .. Local Scalars ..
     DOUBLE PRECISION X, Y(100), A, X0, BM,XMEAN, D
     INTEGER        I
*    .. External Functions ..
     DOUBLE PRECISION RUNFRA
     EXTERNAL       RUNFRA
*    .. External Subroutines ..
     EXTERNAL       G05CBF
*    .. Executable Statements ..
          WRITE (*,*) 'INPUT VALUES OF Xmin,Xmax,D'
          OPEN (NOUT, STATUS='NEW', FILE='of.dat')
     WRITE (NOUT,*) 'Fractal Rundom Generation Program Results'
          READ (*,*)X0,BM,D
c         X0=0.05
c         BM=10.0
c         D=0.50
          A=D*X0**D/(1-(X0/BM)**D)
          XMEAN=A/(1-D)*(BM**(1-D)-X0**(1-D))
          WRITE (NOUT,99) X0,BM,XMEAN,A,D
 99       FORMAT(//1X,'Low Cut-off X0=',F6.3, 2X,'Upper cut-off B=', F8.3,2X
    *'Average Spacing S=',F10.4,1X//'Coefficient A=',F12.6,5X,
    *'Fractal Dimension D=',F10.3)
          WRITE(NOUT,*)
          CALL G05CBF(0)
     DO 20 I = 1, 100
*
       X = RUNFRA(A,D,X0)
*
*         Y(I)=X
       WRITE (NOUT,99999) X
  20 CONTINUE
c         WRITE (NOUT,99999)Y
     STOP
*
99999 FORMAT (1x,F12.4)
     END

     FUNCTION RUNFRA(A,D,X0)
*    .. External Functions ..
     DOUBLE PRECISION A,D,G05CAF,X,X0
     EXTERNAL       G05CAF
     DOUBLE PRECISION RUNFRA
          RUNFRA=(X0**(-D)-G05CAF(X)*D/A)**(-(1/D))
     RETURN
     END
```

An example of random numbers with fractal distribution has been represented as follows, where the lower cut-off is 5 cm, upper cutoff is 10 m; the fractal dimension is 0.24, and the average spacing is 1.20 m; only the first 20 numbers have been listed.

1.720
0.105
0.183
0.104
3.234
0.058
0.089
0.237
0.056
0.463
6.318
0.600
0.651
0.863
0.096
3.294
0.166
0.312
0.139
0.069

B.3 GENERATING GROUPS OF DISCONTINUITIES AND COMPILING DATA

Using the generated random numbers described in B.1 and B.2, we can compile input data files for running the programme BLOCKS (Wang, 1992) according to the assumptions and simplifications made in Section 3.6. Among these data files, one kind is orientation data files which are formed by uniformly distributed random numbers, another is the spacing data files which are formed by random numbers with fractal distributions.

The mean orientations of three sets of discontinuities are assumed to be (1) north-south striking and vertical (N-S vertical set); (2) east-west striking and vertical (E-W vertical set); and (3) horizontal (H set). The ranges of the random variation of the dips and dip directions for them are illustrated in Table B.1

Table B.1 Orientation parameters in the three sets of discontinuities simulated

Set No.	Mean orientation description	Range of dip (°)	Range of dip direction (°)
1	Horizontal	0 - 10	0 - 360
2	E-W vertical	80 - 100	170 - 190
3	N-S vertical	80 - 100	80 - 100

Note the convention used to describe the dip. Dip is usually recorded as 0 - 90°. Here we used the convention out of this range. This is for expressing conveniently the direction sense of a plane. Using this convention, a discontinuity having a dip direction 170° and a dip 95° or -85° will be recorded to be 350°/85°.

In order to form a group of discontinuities, not less than nine data files are requested. Among them, three are the orientation data files for dips, three are the orientation data files for dip directions, and the last three are the spacing data files. More than sixty groups of such data files have been generated.

Table B.2 Sample of input data of simulated discontinuities for one set

Discontinuity No.	Intercepts (m)	Dip direction (°)	Dip (°)
1	1.720	185.9025	87.4256
2	1.824	174.5143	84.5007
3	2.007	177.4256	97.5749
4	2.111	174.5007	80.9495
5	5.345	187.5749	83.6114

To compile a group of data files of simulated discontinuities, the first discontinuity in a set is formed by selecting one data starting at any point from each of three selected data files (i.e. the intercept,dip direction and dip files). Selecting sequentially another three data from these three data files respectively generates the second discontinuity. Repeating this procedure until the needed number of discontinuities in

each set has been obtained, the input file for this group of discontinuities is compiled. For example, the combination of the two example data for orientation listed in B.1, and the first 5 data listed as the example data in B.2, gives five discontinuities. The spacing of these discontinuities is actually an example of one which holds a fractal statistical distribution with a fractal dimension of 0.24 (the mean principal spacing is about 1.2 m). Their orientations randomly distributed with the dip direction from 170° -190°, and the dip from 80 - 110°, as shown in Table B.2.

APPENDIX C DERIVATION OF THE TRANSFORMATION AREA ΔA, EXAMINATION OF THE MEAN/MEDIAN RELATION S_a/S_{50}, AND THE RENORMALISATION GROUP METHOD

C.1 DERIVATION OF THE TRANSFORMATION AREA ΔA

Generally, suppose that both IBSD and BBSD hold a theoretical distribution and their cumulative curves are respectively represented by both functions $P_i(s)$ and $P_b(s)$, as illustrated in Fig. C.1. It follows that ΔA can be obtained through the following equations.

$$\Delta A = \int_{S_{lb}}^{S_{ub}} P_b(S)dS + (S_{ui} - S_{ub}) - \int_{S_{li}}^{S_{ui}} P_i(S)dS, \qquad \text{(C-1)}$$

where, S_{ub} and S_{lb} are respectively the upper and lower boundaries of BBSD curve; S_{ui} and S_{li} are respectively the upper and lower boundaries of IBSD curve.

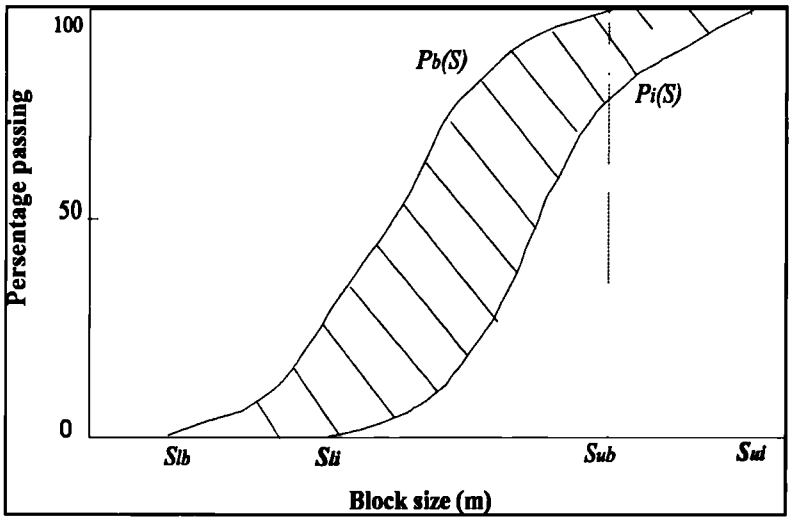

Fig. C.1 General illustration of determination of ΔA

Now let us consider the physical significance implied by the following integration.

$$I = \int_{x_b}^{x_p} P(x)dx. \qquad \text{(C-2)}$$

Suppose that $f(x)$ represents the distribution function of block size, i.e. the probability density function, and $P(x)$ is the cumulative probability. It follows that the corresponding cumulative distribution can be written as

$$P(x) = P(x \le X) = \int_{x_l}^{x} f(t)dt, \qquad \text{(C-3)}$$

where, x_l is the lower boundary of block size which may be zero. Hence

$$\int_{x_l}^{x_u} P(x)dx = \int_{x_l}^{x_u} \left(\int_{x_l}^{x} f(t)dt\right) dx, \qquad \text{(C-4)}$$

where, x_u is the upper boundary of block size. The laws governing definite integration allow for the integrating order to be exchanged provided the integration limits of variables are correspondingly changed (see Fig. C.2). Changing the integration order often turns intractable problems into solvable ones.

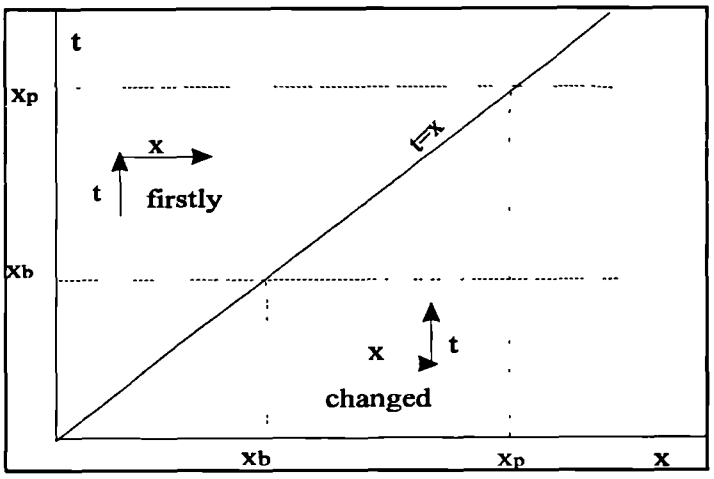

Fig. C.2 Illustration of change of integration order

As for the integration represented by Eqn. C-4, the definite integration of integrated $f(t)$ is over $[x_l, x]$, i.e. t varies between $[x_l, x]$; and the integration of integrated $\left(\int_{x_l}^{x} f(t)dt\right)$ is over $[x_l, x_u]$, i.e. x varies between $[x_l, x_u]$. The integration region is a triangle of the t-x co-ordinate plane, so that when the integration of variable x is advanced over t, the corresponding change of limits of integration has to be made, as illustrated in Fig. C.2. Thus, Eqn. C-4 is developed into:

$$\int_{x_l}^{x_u}\left(\int_{x_l}^{x} f(t)dt\right)dx = \int_{x_l}^{x_u}\left(\int_{x}^{x_u} f(t)\,dx\right)\,dt = \int_{x_l}^{x_u}\left(f(t)\int_{x}^{x_u} dx\right)\,dt$$
$$= \int_{x_l}^{x_u}(x_u - x)f(x)dx = \int_{x_l}^{x_u} x_u\, f(x)dx - \int_{x_l}^{x_u} x\, f(x)dx \qquad \text{(C-5)}$$

According to both definitions of the probability density function and the mean value X_a, we know that

$$X_a = \int_{x_l}^{x_u} x\, f(x)dx, \qquad \text{(C-6)}$$

and

$$\int_{x_l}^{x_u} f(x)dx = 1. \qquad \text{(C-7)}$$

Then, having

$$\int_{x_l}^{x_u} P(x)dx = x_u - X_a \qquad \text{(C-8)}$$

It is seen from the aforementioned derivation that integration of $I = \int_{x_l}^{x_u} P(x)dx$ is a kind of indicator of the mean size of the blocks. Substitution of Eqn. C-8 into Eqn. C-1 yields

$$\begin{aligned}\Delta A &= \int_{S_{lb}}^{S_{ub}} P_b(S)dS + (S_{ui} - S_{ub}) - \int_{S_{li}}^{S_{ui}} P_i(S)dS \\ &= (S_{ub} - S_{ab}) + (S_{ui} - S_{ub}) - (S_{ui} - S_{ai}) \\ &= S_{ai} - S_{ab}\end{aligned} \qquad \text{(C-9)}$$

Therefore, it becomes clear that the ΔA, in fact, represents the differencde of mean block sizes before and after blasting.

In the derivation to Eqn. C-9, there is no constraint on the form of either $P_i(S)$ or $P_b(S)$; it thus follows that the above derivation can be applicable to any form of the in-situ or blasted block size distributions.

The form of ΔA when both IBSD and BBSD hold either the Schuhmann or the Ros-Ram distribution can be derived as follows.

Schuhmann Equation

Suppose that both the IBSD and the BBSD hold the Schuhmann distribution, i.e. both have the forms as follows

$$P_i = \left(\frac{S_i}{S_{100i}}\right)^{m_{si}}, \tag{C-10a}$$

$$P_b = \left(\frac{S_b}{S_{100b}}\right)^{m_{sb}}. \tag{C-10b}$$

Now, the probability density function for the Schuhmann distribution is given by the following equations

$$p_i(S_i) = \frac{1}{(S_{100i})^{m_{si}}} S_i^{(m_{si}-1)}, \tag{C-11a}$$

$$p_i(S_b) = \frac{1}{(S_{100b})^{m_{sb}}} S_b^{(m_{sb}-1)}. \tag{C-11b}$$

According to Eqn. C-9, the ΔA is given by the following equation

$$\begin{aligned} \Delta A &= S_{ai} - S_{ab} \\ &= \int_0^{S_{100i}} S_i[p_i(S_i)]dS_i - \int_0^{S_{100b}} S_b[p_b(S_b)]dS_b \\ &= \int_0^{S_{100i}} S_i\left[\frac{1}{(S_{100i})^{m_{sb}}} S_i^{(m_{si}-1)}\right]dS_i - \int_0^{S_{100b}} S_b\left[\frac{1}{(S_{100b})^{m_{sb}}} S_b^{(m_{sb}-1)}\right]dS_b \end{aligned} \quad , \tag{C-12}$$

i.e.

$$\begin{aligned} \Delta A &= \int_0^{S_{100}} S_i\left[\frac{1}{(S_{100i})^{m_{sb}}} S_i^{(m_{si}-1)}\right]dS_i - \int_0^{S_{100b}} S_b\left[\frac{1}{(S_{100b})^{m_{sb}}} S_b^{(m_{sb}-1)}\right]dS_b \\ &= \frac{m_{si}}{m_{si}+1} S_{100i} - \frac{m_{sb}}{m_{sb}+1} S_{100b} \end{aligned} \tag{C-13}$$

Ros-Ram distribution

If both the IBSD and the BBSD exhibit a statistical dependence according to the Ros-Ram equation, i.e. having the following distribution forms,

$$P_i(S_i) = 1 - e^{-(\frac{S_i}{S_{ci}})^{n_{sb}}}, \qquad \text{(C-14a)}$$

$$P_b(S_b) = 1 - e^{-(\frac{S_b}{S_{cb}})^{n_{sb}}} \qquad \text{(C-14b)}$$

The probability density function for the Ros-Ram distribution is then given by

$$p_i(S_i) = \frac{n_{si}}{(S_{ci})^{n_{si}}} S_i^{(n_{si}-1)} e^{-(\frac{S_i}{S})^{n_{si}}}, \qquad \text{(C-15a)}$$

$$p_b(S_b) = \frac{n_{sb}}{(S_{cb})^{n_{sb}}} S_b^{(n_{sb}-1)} e^{-(\frac{S_b}{S_b})^{n_{sb}}}. \qquad \text{(C-15b)}$$

In contrast to the previous Schuhmann case, the upper and lower integration boundaries in Eqn. C-15 are the same, i.e. S_{li} and S_{lb} are zero and S_{ui} or S_{ub} are ∞. Thus, the ΔA is given by.

$$\begin{aligned} \Delta A &= S_{ai} - S_{ab} \\ &= \int_0^\infty S_i [p_i(S_i)] dS_i - \int_0^\infty S_b [p_b(S_b)] dS_b \\ &= \int_0^\infty S_i [\frac{n_{si}}{(S_{ci})^{n_{si}}} S_i^{(n_{si}-1)} e^{-(\frac{S}{S_{ci}})^{n_{si}}}] dS_i - \int_0^\infty S_b [\frac{n_{sb}}{(S_{cb})^{n_{sb}}} S_b^{(n_{sb}-1)} e^{-(\frac{S_b}{S_{cb}})^{n_{sb}}}] dS_b \end{aligned} \qquad \text{,(C-17)}$$

i.e.

$$\Delta A = \int_0^\infty \frac{n_{si}}{(S_{ci})^{n_{si}}} [S_i e^{-(\frac{S_i}{S_{ci}})^{n_{si}}}] dS_i - \int_0^\infty \frac{n_b}{(S_{cb})^{n_{sb}}} [S_b e^{-(\frac{S_b}{S_{cb}})^{n_{sb}}}] dS_b \qquad \text{(C-18)}$$

With making a substitution of the type $(\frac{S}{S_c})^{n_s} = t$, and following the definition of the Γ function (see Eqn. 6-9), it yields

$$\Delta A = S_{ci}\int_0^{\infty} t^{(\frac{1}{n_{si}}+1)}e^{-t}]dt - S_{cb}\int_0^{\infty} t^{(\frac{1}{n_{sb}}+1)}e^{-t}]dt$$
$$= S_{i}\ \Gamma(1+\frac{1}{n_{si}}) - S_{cb}\ \Gamma(1+\frac{1}{n_{sb}}) \qquad \text{(C-19)}$$

C.2 EXAMINATION OF THE MEAN/MEDIAN RELATION S_a/S_{50}

The transformation area ΔA, as illustrated in Appendix C.1 (see Eqns. C-13 and C-19), is related to both characteristic size and the steepness coefficient which jointly govern a block size distribution. This implies that only using a size parameter, say, S_{50} to describe the influence of in-situ block size distribution of a rock mass on blast result is insufficient.

The physical significance of the difference between the mean blocks size S_a and the 50% passing size S_{50} is given below despite their convergence in many cases.

The mean blocks size S_a is defined (see Eqn. 6-7) by

$$S_a = \int_{S_l}^{S_u} Sf(S)dS \qquad \text{(C-20)}$$

whereas the S_{50} is the 50% passing size corresponding to 50% passing size on a percentage passing-size curve. Taking block sizes with the Ros-Ram distribution as an example, their difference is examined as follows.

Now

$$P(S) = 1 - e^{-(\frac{S}{S_c})^{n_s}}, \qquad \text{(C-21)}$$

and the probability density function is then given by

$$p(S) = \frac{n_s}{(S_c)^{n_s}} S^{(n-1)} e^{-(\frac{S}{S_c})^{n_s}}, \qquad \text{(C-22)}$$

hence

$$S_a = \int_0^{\infty} S[\frac{n_s}{(S_c)^{n_s}} S^{(n_s-1)} e^{-(\frac{S}{S_c})^{n_s}}]dS = S_a\Gamma(1+\frac{1}{n_s}). \qquad \text{(C-23)}$$

For the Ros-Ram distribution, the 50% passing size is given by

$$S_{50} = s_c (ln2)^{1/n}, \tag{C-24}$$

hence for the Ros-Ram distribution case, the difference between the mean blocks size S_a and the 50% passing size S_{50} is given by

$$\frac{S_a}{S_{50}} = \frac{\Gamma(1+\frac{1}{n})}{(\ln 2)^{\frac{1}{n}}} \tag{C-25}$$

C.3 RENORMALISATION GROUP METHODS

Fragmentation is a catastrophic phenomenon which exhibits sudden or catastrophic change, much as a system undergoing a phase change. The feature of a phase change is a catastrophic change of macroscopic parameters of a system under a continuous change of the state variables in a system. A renormalisation group method has been used to study scale invariant processes that exhibit catastrophic change (Allegre et al. 1982; Turcotte, 1986, 1992). The renormalisation group method often produces fractal statistics and explicitly utilises scale invariance. The method is implemented in such a way that a relatively simple system is considered at the smallest order, the problem is then renormalised to utilise the same system at the next larger order; the process is iterated at larger and larger orders.

The rock mass is assumed to develop microfracturing under applied external force, i.e. explosive energy. For simplicity, a cube of rock mass with a linear length of h is considered, as shown in Fig. C.3. This cube is called a cell, which is divided into eight smaller cubic elements each with a linear length of $h/2$. Now the attention is paid to one of eight cubic elements. It becomes a cell of dimension $h/2$ at order 1, and then this cell is divided into eight first-order elements each with a length of $h/4$, and so on, as shown in Fig. C.3. This process is repeated at successively higher orders.

The essential assumption of the renormalisation group method is that the probability p_c that a cell will break into 8 elements is the same at all orders. p_c is

therefore referred to as the critical probability that leads to a catastrophic fragmentation. If we consider the *mth* stage of fragmentation, the total number of particles is

$$N_m = (1-p_c)[1+(8p_c)+(8p_c)^2+(8p_c)^3+\cdots+(8p_c)^m]. \qquad \text{(C-26)}$$

Similarly, the total number of particles with the $(m+1)th$ stage of fragmentation is

$$N_{m+1} = (1-p_c)[1+(8p_c)+(8p_c)^2+(8p_c)^3+\cdots+(8p_c)^m+(8p_c)^{m+1}]. \qquad \text{(C-27)}$$

From Eqns. 6-27, we can write

$$\frac{N_{m+1}}{N_m} = 2^D \quad . \qquad \text{(C-28)}$$

Combining Eqns. C-26, C-27 and C-28 and supposing $m >> 1$ and $8p_c>1$, we have approximately

$$D = \frac{Ln8\,p_c}{Ln2}. \qquad \text{(C-29)}$$

It can be seen that in order to define a fractal dimension, the range allowed for the probability of fragmentation is $1/8<p_c<1$. Once p_c for a fragment process is obtained, the correspond fractal dimension D can be determined.

The division into 8 cells is not unique, for example, a cubic cell with dimension h can also be divided into 64 cubic elements each with dimension $h/4$. However, it has been shown that the values of D are independent of the renormalisation configuration chosen (Turcotte, 1986).

Return now to the model illustrated in Fig. C.3. Following Allegre et al. (1982) and Turcotte (1986), each element in a cell is assumed to be either fragile if it is permeated with microfractures or sound if it is not. It is necessary to specify a condition for the fragility (or soundness) of the cell in terms of the fragility (or soundness) of the elements. In each cell, there can be zero to eight fragile elements and therefore there are $2^8=256$ possible combinations. Excluding multiplicities, there are 22 topologically different configurations, as illustrated in Fig. C.4. The fragile elements are indicated by the solid dots at the corners. Two states can be defined: when the local microfracture

density in a cell is greater than a certain critical value, it is considered as fragile; when it is less than that critical value, it is considered sound.

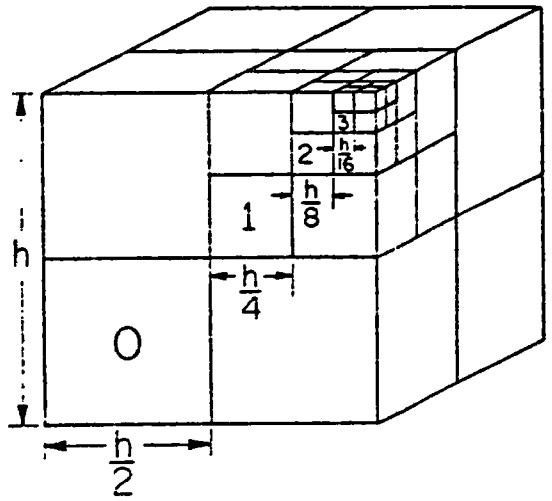

Fig. C.3 Illustration of the renormalisation group approach to fragmentation (from Turcotte, 1986)

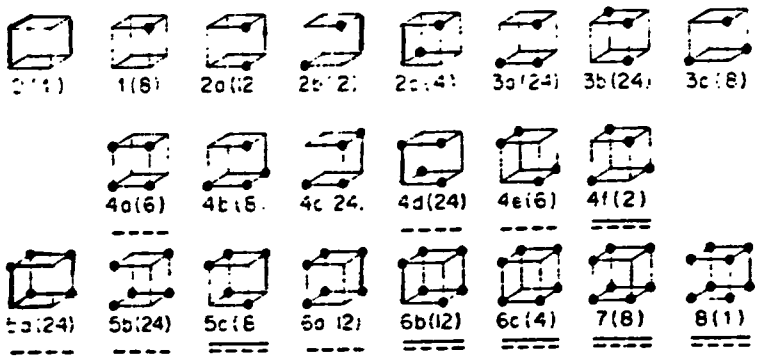

Fig C.4 Illustration of the topologically different configurations for fragile/sound elements (Using "pillar of strength" condition, the fragile cells are underlined with a solid line; using "plane of weakness" condition, the fragile cells are underlined with a dashed line) (from Turcotte, 1986)

Using different specifications of the condition for the fragility or soundness of a cell, we can obtain different numbers of fragile cells. Clearly, the greater the number of fragile configurations, the more fragile the rock mass, which in turn means the rock mass can be more easily fragmented by blasting. If p_n represents the probability that a cell at order n is fragile and p_{n+1} represents the probability that a cell at order $n+1$ is fragile. Then it can be shown (see Allegre et al., 1982; Turcotte, 1986) that the probability for a configuration with m fragile elements and k multiplicities is given by: $k(p_{n+1})^m (1-p_{n+1})^{8-m}$.

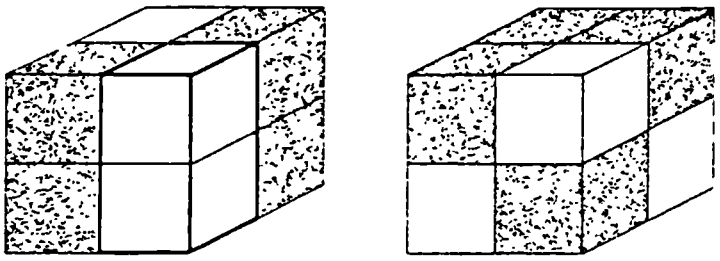

Fig C.5 Fragile and sound cell using the "pillar of strength" condition (Allegre et al., 1982)

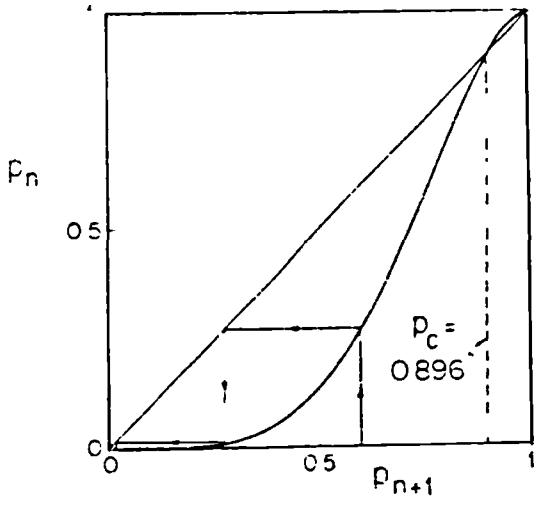

Fig C.6 Relationship between probability of fragility p_n at order n, and probability of fragility p_{n+1} at order $n+1$ (from Turcotte, 1986)

Allegre et al. (1982) considered the fragility at different scales and the related fractal dimension by means of a "pillar of strength" criterion proposed. Under the criterion of "pillar of strength", a cell will be considered as sound whenever there is a "pillar" of sound elements that links two opposite faces, otherwise, it is considered to be fragile. Examples of sound and fragile cells are shown in Fig. C.5 in which 5b is a sound cell and 5c is fragile. As such the cells configured by 4f, 5c, 6b, 7 and 8 are fragile and indicated by solid underlining in Fig. C.4.

In the above case, the probability, p_n, a cell at order n being fragile can be expressed as a function of the probability, p_{n+1}, a cell at order $n+1$ being fragile (Allegre et al., 1982; Turcotte, 1986) by

$$\begin{aligned} p_n &= (p_{n+1})^8+8(p_{n+1})^7[1-(p_{n+1})]+16(p_{n+1})^6[1-(p_{n+1})]^2 \\ &\quad +8(p_{n+1})^5[1-(p_{n+1})]^3+2(p_{n+1})^4[1-(p_{n+1})]^4 \\ &=(p_{n+1})^4(3(p_{n+1})^4-8(p_{n+1})^3+4(p_{n+1})^2+2) \end{aligned} \qquad \text{(C-30)}$$

Subsequent orders in the hierarchy of the renormalisation group method are obtained by considering elements of order n as cells of order $n+1$. The characteristic dimension of the nth-order cell is $h/2^n$, and the characteristic dimension of the $(n+1)th$-order element is $h/2^{n+1}$. On the basis of the assumption of self-similarity in the statistical distribution of microcracks, it follows that Eqn. C-30 will be valid at all orders. The relationship of p_n and p_{n+1} is illustrated in Fig. C.6. The critical probability that leads to a catastrophic fragmentation, p_c=0.896, can be derived according to catastrophic theory (Allegre et al., 1982; Turcotte, 1986). As shown in Fig. C.6, the points 0 and 1 are stable fixed points of the system; the iterative relation crosses the line $p_n = p_{n+1}$ at p_c=0.896, which is a bifurcation that separates the region of stable behaviour from the region of unstable behaviour. Substituting the value of p_c=0.896 into Eqn. C-29, it yields D=2.84 for the "pillar of strength" fragmentation model.

Turcotte (1986) proposed an alternative "plane of weakness" criterion and considered the fragility at different scales and the related fractal dimension. In the "plane of weakness" model, the sides of a fragile element are assumed to form planes of weakness. A cell is assumed as fragile if the sides of fragile elements from an internal plane through the cell, and a cell is considered as sound if there is no plane of weakness through the cell. As such the cells configured by 4a, 4d, 4e, 4f, 5a, 5b, 5c, 6a, 6b, 6c, 7 and 8 in Fig. C.4 are fragile and underlined by dashed lines (Turcotte,

1986). Examples of sound and fragile cells are shown in Fig. C.7 in which 4c is a sound cell and 4e is fragile.

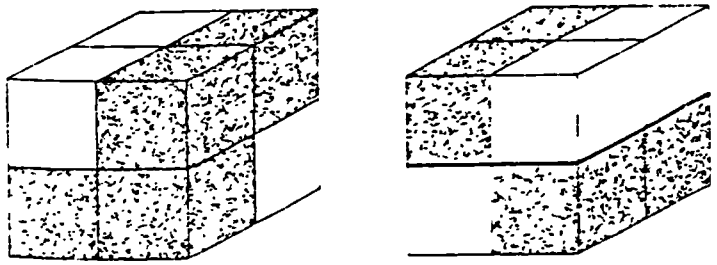

Fig C.7 Fragile and sound cell using the "weakness plane" criterion (Turcotte, 1986)

The "plane of weakness" fragmentation model is a more fragile one than the "pillar of strength" model, since there are more failure configurations in the former model than in the latter. This in turn means the rock represented by the plane of weakness fragmentation model will be more easily fragmented by blasting. Now let us consider the fragility at different scales and their fractal dimension. In this case, the probability of fragile cells of order n, p_n as a function of the probability of fragile cells of order $n+1$ p_{n+1} is given (Turcotte, 1986) by

$$\begin{aligned} p_n &= (p_{n+1})^8+8(p_{n+1})^7\,[1-(p_{n+1})]+28(p_{n+1})^6[1-(p_{n+1})]^2 \\ &\quad +56(p_{n+1})^5\,[1-(p_{n+1})]^3+38(p_{n+1})^4\,[1-(p_{n+1})]^4 \\ &= (p_{n+1})^4\,[3(p_{n+1})^4-32(p_{n+1})^3+88(p_{n+1})^2-96\,(p_{n+1})+38] \end{aligned} \qquad \text{(C-31)}$$

Similarly, it can be found that the critical probability that leads to a catastrophic fragmentation, p_C=0.49 and the related fractal dimension D is 1.97 (Turcotte, 1986). It can be seen that the difference in fragility, and by inference the difference in blastability, might be sensitive to the particular model of fragmentation that is hypothesised, which can be represented by the difference of fractal dimensions.

APPENDIX D CONTINUOUS RATING CHARTS FOR BLASTABILITY ASSESSMENT

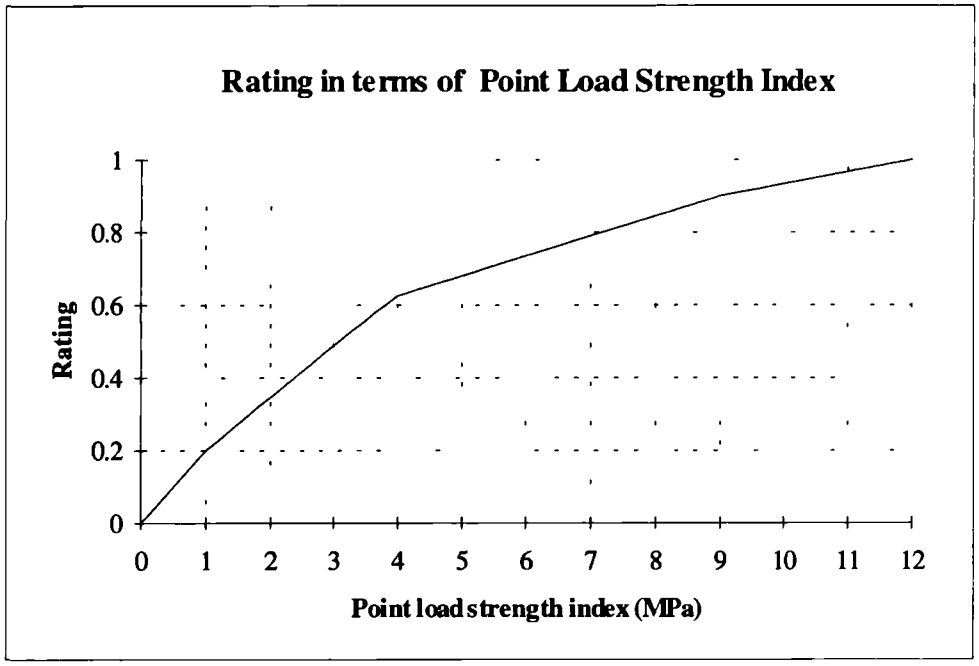

Fig. D.1 Rating chart of the point load strength index of rock

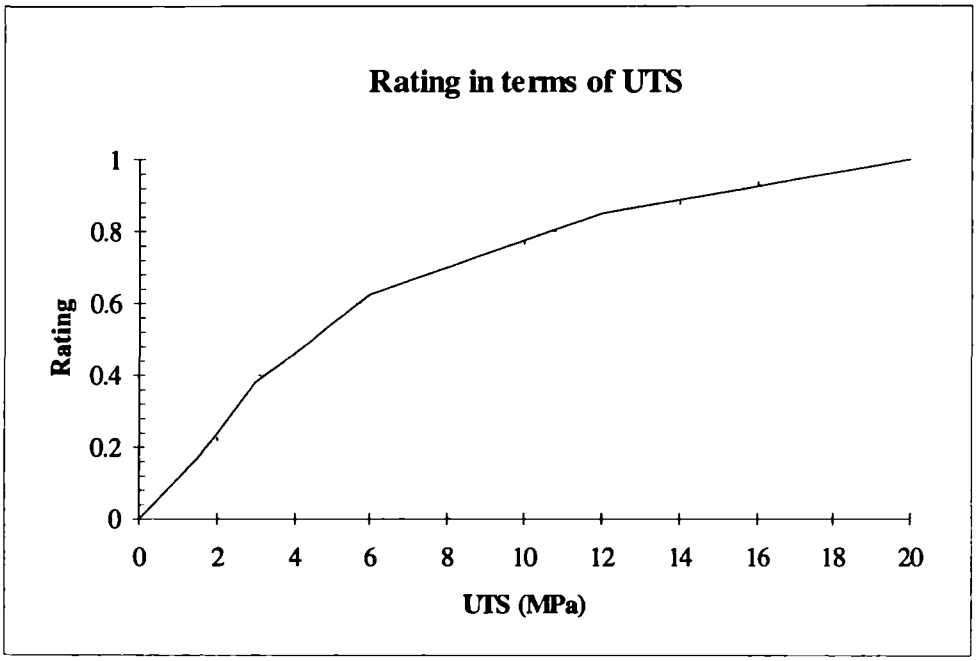

Fig. D.2 Rating chart of the uniaxial tensile strength of rock

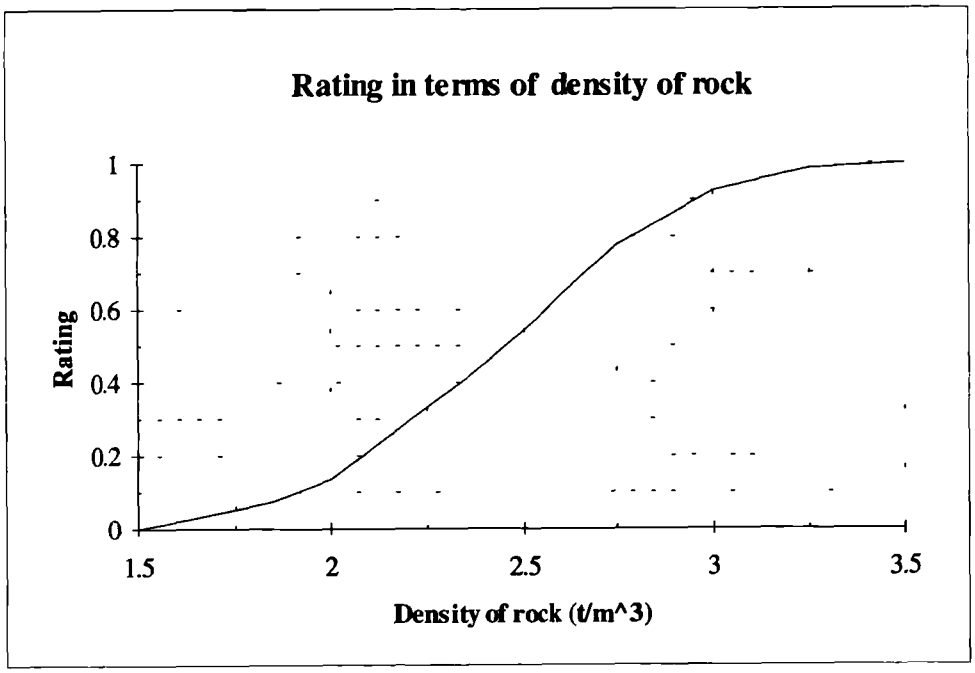

Fig. D.3 Rating chart of the density of rock

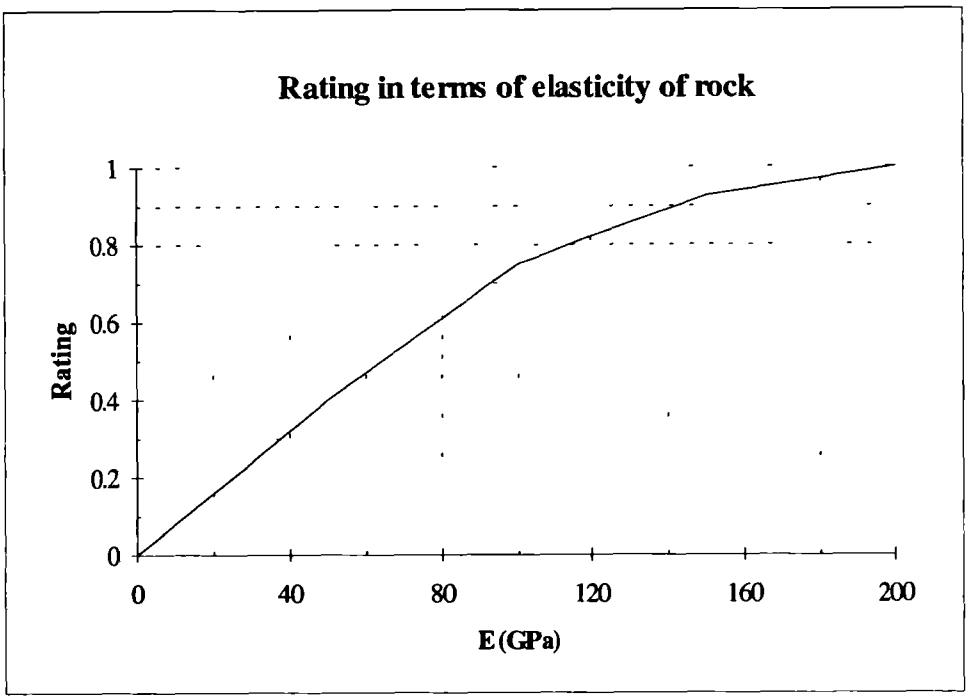

Fig. D.4 Rating chart of the elasticity of rock

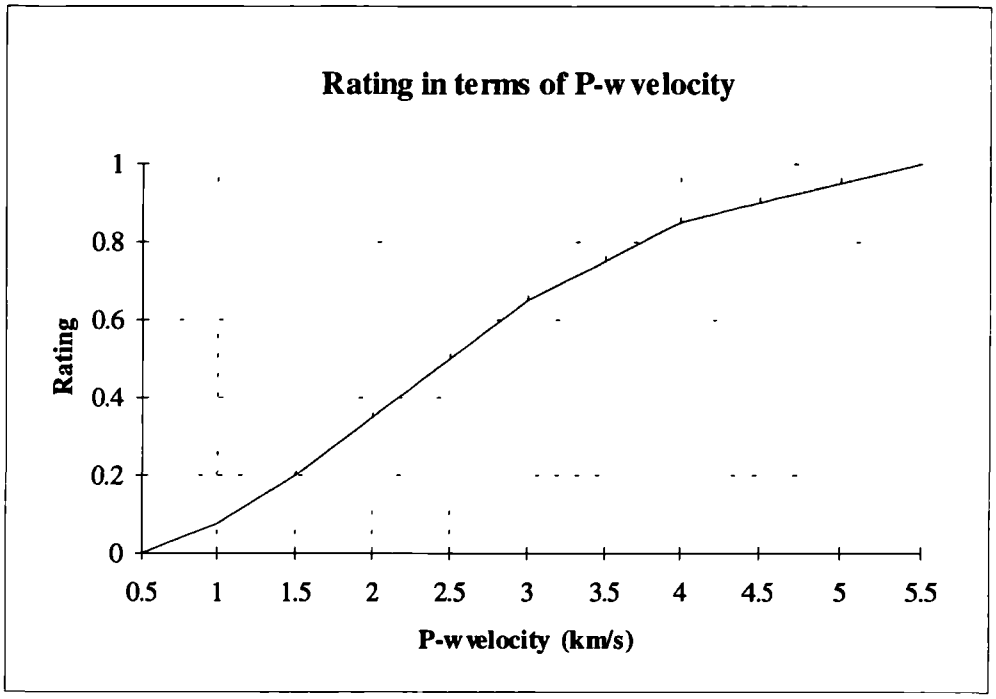

Fig. D.5 Rating chart of the P-w velocity of rock masses

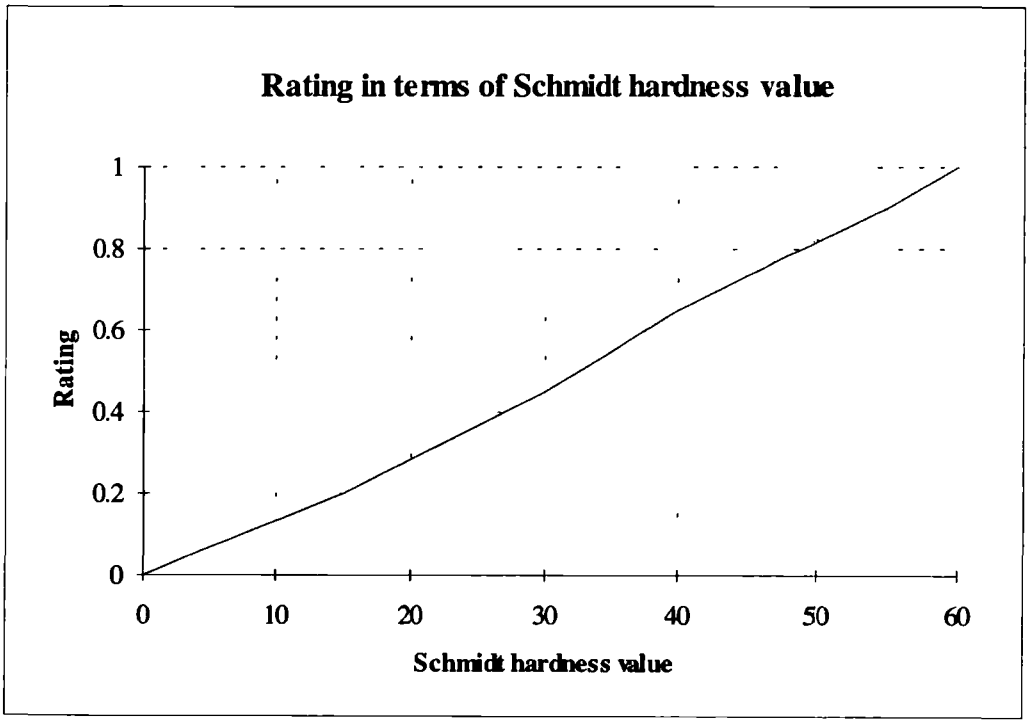

Fig. D.6 Rating chart of the Schmidt hammer value of rock masses

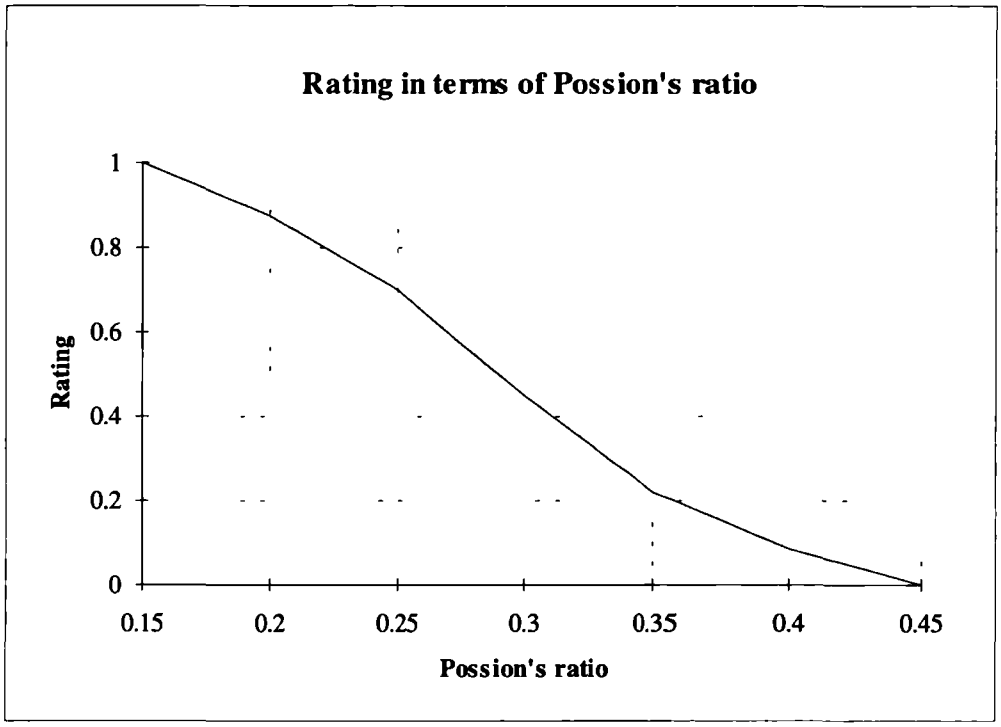

Fig. D.7 Rating chart of the Poission's ratio of rock

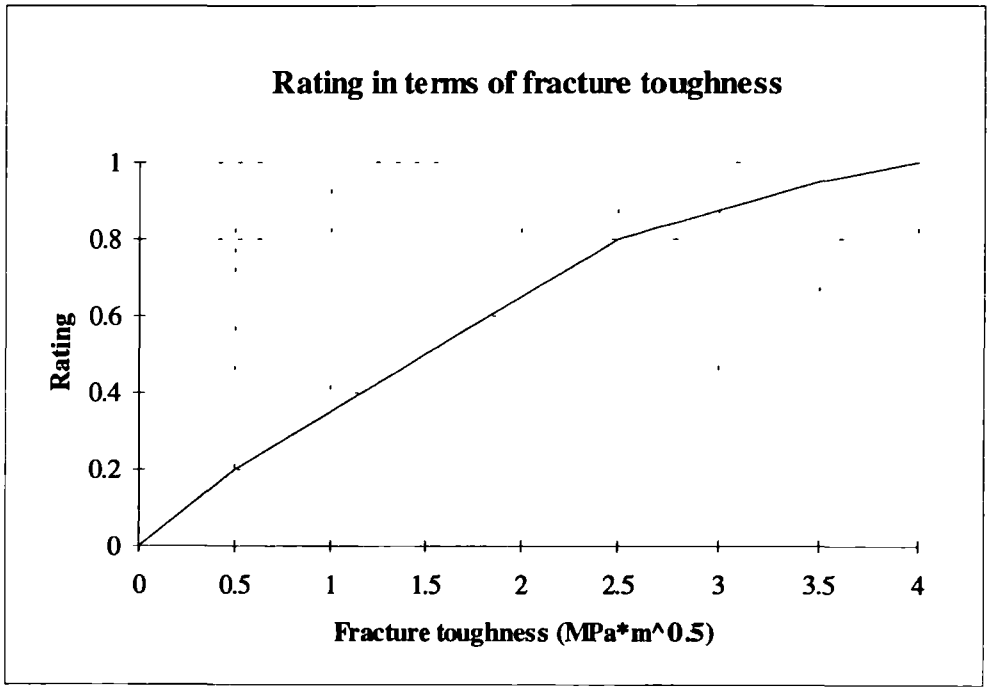

Fig. D.8 Rating chart of the fracture toughness of rock

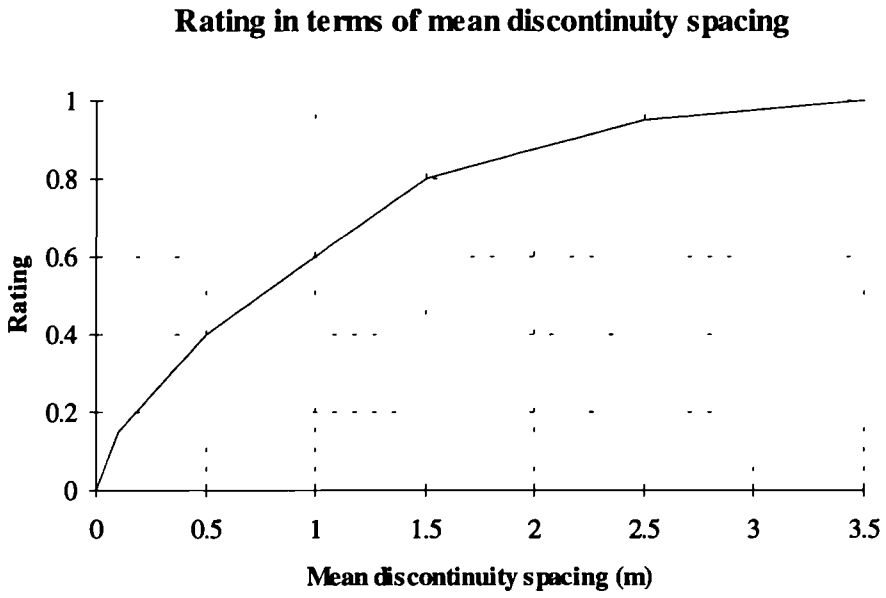

Fig. D.9 Rating chart of the mean discontinuity spacing of rock masses

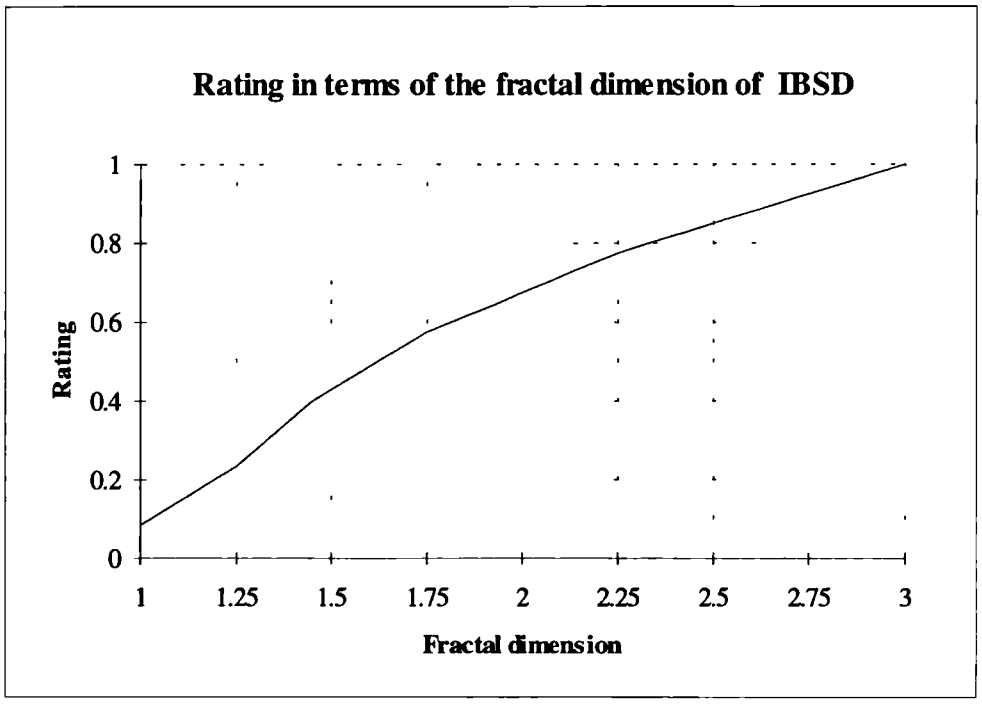

Fig. D.10 Rating chart of the fractal dimension of the IBSD of rock masses

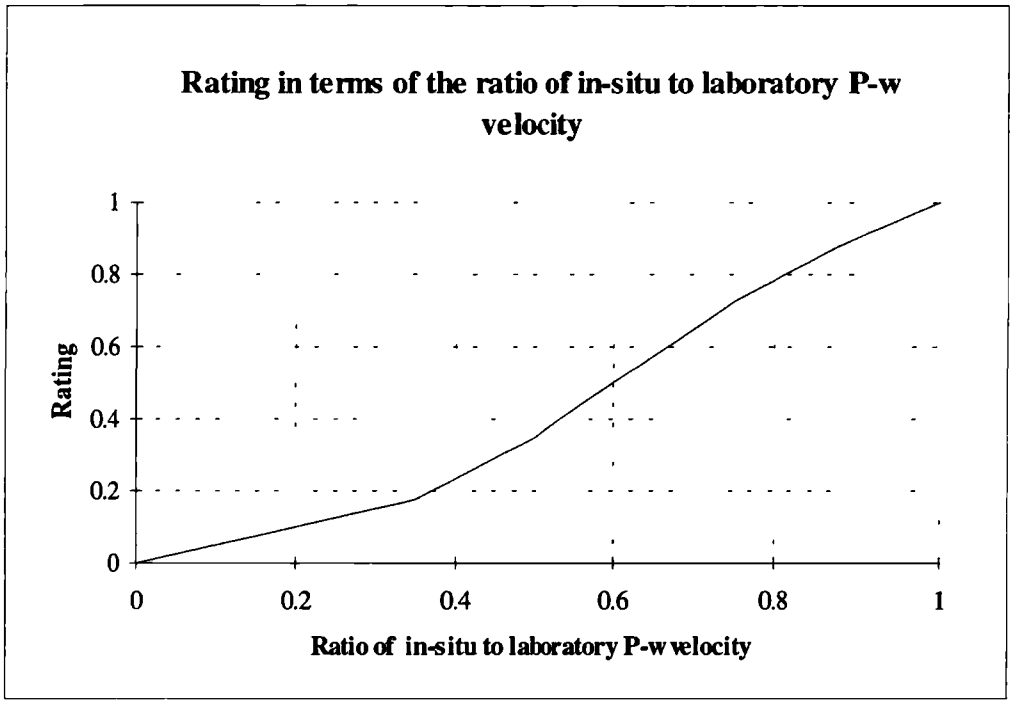

Fig. D.11 Rating chart of the ratio of P-w velocity of the in-situ rock mass to P-w velocity of rock sample in laboratory

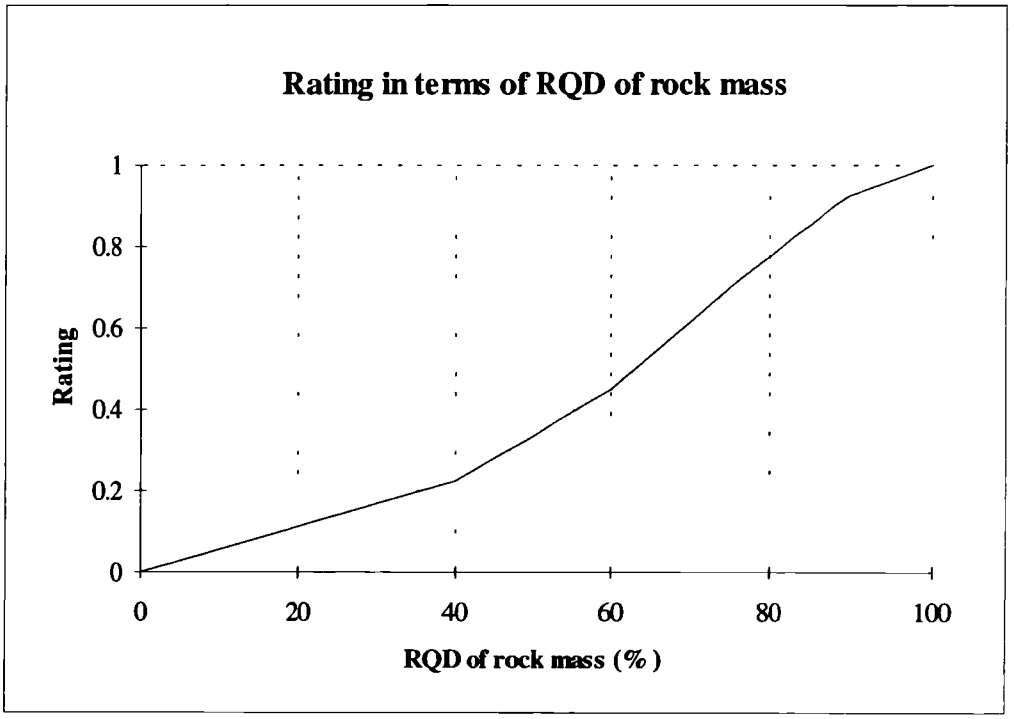

Fig. D.12 Rating chart of the RQD value of rock mass

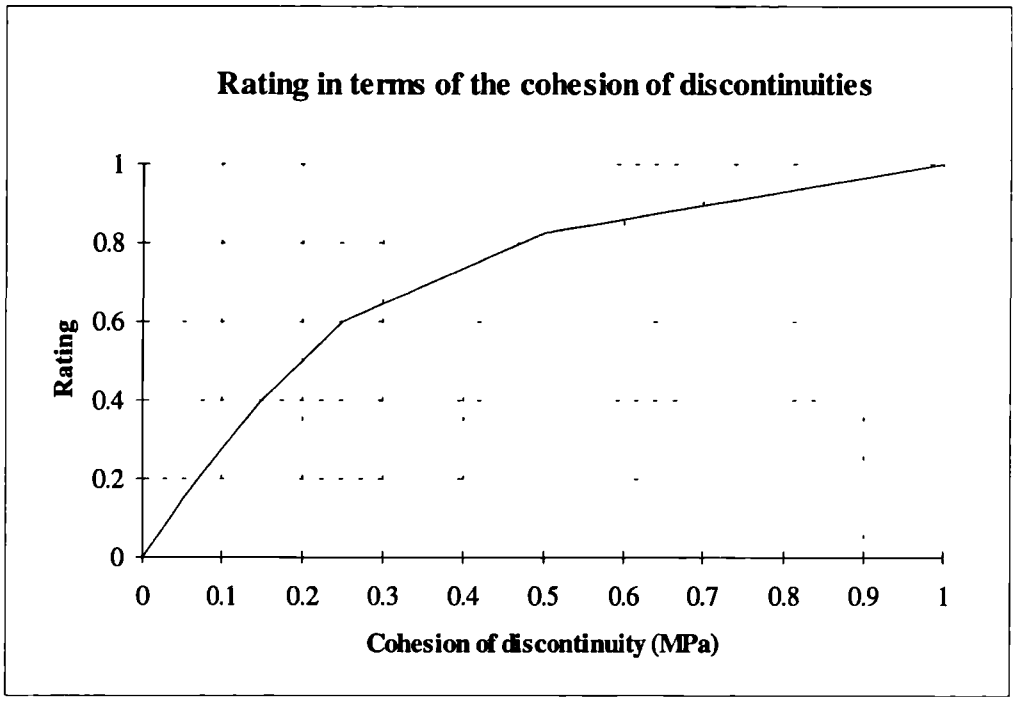

Fig. D.13 Rating chart of the cohesion of discontinuity of rock mass

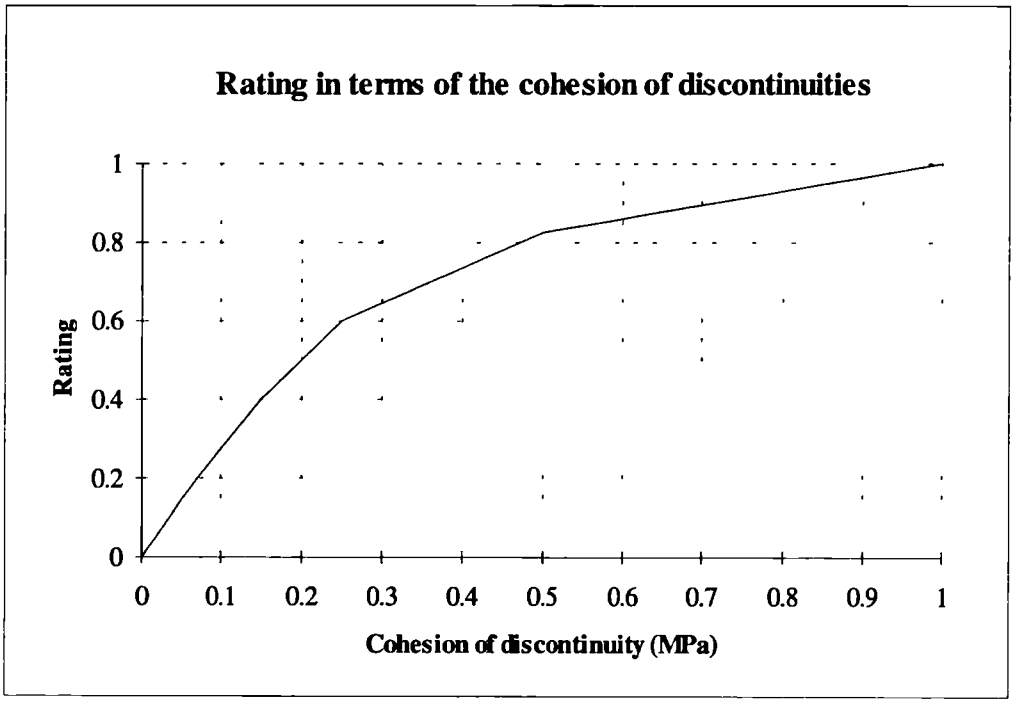

Fig. D.14 Rating chart of the friction angle for the shear strength of discontinuities of rock masses

APPENDIX E DISCONTINUITY DATA

E.1 DISCONTINUITY DATA FROM A5 GLEN BENDS IMPROVMENT SITE

Discontinuity Mapping Data Sheet

General Information

Job Number: / A5-1 / Site Name: / Glen Bends / Rock Type / Siltstone /
No. of Tape: / 1 / Tape Azimuth: / 125 / Tape Plunge(+/-) / 0 /
Sheet Number: / 1 / of / 1/ Operator(s) / P. LU / Date / 2/8/95 /

Discontinuity Data

No.	*Type*	*Intercept*	*Attitude*		*Semi-Trace length*	*Notes*
		(m)	*Dip Direction*	*Dip Angle*	*(m)*	
1	***2****	***3***	***4***	***5***	***6***	***7***
1		0.10	280	70	5.00	
2		1.15	330	18	3.00	
3		1.75	350	10	1.50	
4		2.30	40	14	2.00	
5	B	3.50	105	40	5.50	
6		4.40	280	80	5.00	
7		4.70	280	75	2.00	
8		4.90	290	24	1.80	
9		5.20	300	82	0.50	
10		7.20	350	65	5.00	
11	F	7.75	150	70	6.00	
12	B	8.00	315	50	6.00	
13		9.00	328	72	5.00	
14		9.60	190	68	2.00	
15		10.55	290	90	2.00	
16		11.00	330	85	5.00	
17	C	12.20	350	85	1.50	
18		12.40	330	75	2.00	
19		13.20	15	60	6.00	
20		14.35	265	85	3.50	
21		15.20	325	30	4.50	
22		15.60	245	85	4.80	
23		16.70	245	70	5.00	
24		17.00	240	85	1.50	
25	C	17.40	242	86	2.50	
26	B	17.70	150	82	6.50	
27	F	18.10	150	52	6.50	
28	F	18.70	150	50	6.00	
29		19.00	100	55	3.00	
30		19.40	145	65	3.50	
31		19.70	155	70	3.35	
32		20.80	150	53	5.00	
33		20.90	140	50	3.00	
34		21.70	100	70	1.00	
35		22.50	340	75	7.00	
36		23.40	340	18	1.50	
37		25.70	155	20	0.80	
38	B	27.40	145	64	4.00	
39	F	28.60	110	70	5.00	

** Blank - joint; C - cleavage; F - fault; B - bedding*

Discontinuity Mapping Data Sheet

General Information

Job Number:	/ A5-2 /	Site Name:	/ Glen Bends /	Rock Type	/ Siltstone /		
No. of Tape:	/ 1 /	Tape Azimuth:	/ 293 /	Tape Plunge(+/-)	/ 0 /		
Sheet Number:	/ 1 / of / 1 /	Operator(s)	/ P. LU /	Date	/ 2/8/95 /		

Discontinuity Data

No.	*Type*	*Intercept*	*Attitude*		*Semi-Trace length*	*Notes*
		(m)	*Dip Direction*	*Dip Angle*	*(m)*	
1	***2****	***3***	***4***	***5***	***6***	***7***
1	C	0.45	100	85	1.00	
2	B	1.45	50	75	5.00	
3		1.65	270	70	5.30	
4		1.70	270	80	4.00	
5	B	2.00	130	90	1.00	
6		2.40	230	60	2.50	
7		2.95	70	75	1.50	
8	B	3.10	340	65	7.00	
9		3.60	260	74	8.00	
10	F	4.10	60	80	6.00	
11	F	5.60	100	85	3.00	
12		5.90	110	70	6.00	
13		6.90	50	65	4.70	
14	C	7.00	270	70	1.50	
15		7.35	135	60	1.00	
16		8.25	90	85	2.50	
17	B	8.60	110	55	6.00	
18		10.30	320	60	4.50	
19	F	10.40	170	55	8.00	
20	F	11.50	30	45	5.50	
21	F	12.90	100	40	3.00	
22		14.55	190	70	1.50	
23		15.00	150	52	1.50	
24		16.10	160	58	1.50	
25	C	16.90	330	85	1.00	
26	F	17.60	190	80	10.00	
27		18.00	190	70	10.00	
28	F	18.60	190	70	10.00	
29		19.05	190	70	10.00	
30		19.40	185	22	3.50	
31		20.00	170	40	2.50	
32		21.40	140	60	2.50	
33		22.50	180	50	3.00	
34		23.40	170	52	5.00	
35		25.20	10	55	1.00	
36	C	25.80	310	55	2.20	

** Blank - joint; C - cleavage; F - fault; B - bedding*

Discontinuity Mapping Data Sheet

General Information

Job Number: / A5-3 / Site Name: / Glen Bends / Rock Type /Silt-/lime-stone/
No. of Tape: / 1 / Tape Azimuth: / 145 / Tape Plunge(+/-) / 0 /
Sheet Number: / 1 / of / 1 / Operator(s) / P. LU / Date / 2/8/95 /

Discontinuity Data

No.	*Type*	*Intercept*	*Attitude*		*Semi-Trace length*	*Notes*
		(m)	*Dip Direction*	*Dip Angle*	*(m)*	
1	*2**	*3*	*4*	*5*	*6*	*7*
1	F	0 40	180	85	6 00	
2	C	1.60	205	55	0.75	
3	C	1.70	200	55	0.75	
4	C	2.00	208	55	0 75	
5	C	2.10	208	50	0.75	
6		2.20	210	52	0 75	
7		2.30	200	55	0 75	
8		2.50	195	52	1.00	
9		2.70	195	55	1.00	
10		2.90	195	56	1.00	
11	B	3.10	270	25	1.50	
12		3.40	180	28	3.00	
13		3.70	175	50	6.00	
14		4.10	172	40	9 00	
15		4.40	170	70	2.00	
16		4.60	170	70	2 00	
17		4.70	190	72	2.00	
18		5.10	310	65	0 50	
19		5.40	145	80	0 80	
20		5 70	5	55	10.00	
21		5.90	5	54	1 50	
22		6.35	130	50	1 00	
23		6.80	280	52	8 00	
24		7.20	170	70	0.80	
25		8.30	140	56	8.00	
26		8.80	200	90	2.50	
27		10.65	160	70	5.00	
28		12.60	150	55	1.50	
29		12.70	170	65	3.00	
30		13.40	100	72	5 00	
31		14.00	160	82	6 00	
32		14.80	235	56	10.00	
33	B	15.80	235	56	10.00	

** Blank - joint; C - cleavage; F - fault; B - bedding*

Discontinuity Mapping Data Sheet

General Information

Job Number: / A5-4 / Site Name: / Glen Bends / Rock Type /Silt-/lime-stone /
No. of Tape: / 1 / Tape Azimuth: / 290 / Tape Plunge(+/-) / 8 /
Sheet Number: / 1 / of / 1 / Operator(s) / P. LU / Date / 2/8/95 /

Discontinuity Data

No.	*Type*	*Intercept*	*Attitude*		*Semi-Trace length*	*Notes*
		(m)	*Dip Direction*	*Dip Angle*	*(m)*	
1	*2**	*3*	*4*	*5*	*6*	*7*
1	C	2.30	135	80	2.00	
2	B	2.80	210	40	>6.00	
3	B	3.40	210	40	>6.00	
4	C	3.50	80	80	2.00	
5		3.90	340	80	2.00	
6	B	4.00	30	15	>6.00	
7	B	4.50	30	15	>6.00	
8		4.60	340	80	2.00	
9	B	4.90	30	15	>6.00	
10		5.30	110	65	1.50	
11	B	5.50	35	20	>6.00	
12		5.60	120	60	1.50	
13	B	5.80	210	22	>6.00	
14		5.95	120	60	2.50	
15	C	6.10	120	60	2.00	
16		6.50	120	60	1.50	
17		6 65	120	62	1 80	
18	B	7.00	210	22	>6.00	
19		7.10	125	55	2.00	
20		7.30	125	55	1.50	
21		7.55	125	55	1.50	
22		7.90	100	60	2.00	
23	B	8.00	210	22	>6.00	
24		8.20	100	60	2.00	
25		8.30	150	60	>6.00	
26	B	8.70	210	22	>6.00	
27		9.40	90	85	1.00	
28		9.65	90	85	1.00	
29		10.05	90	85	1.00	
30		10.15	90	85	1.00	
31		10.25	125	40	1.75	
32		10.45	120	42	1.00	
33	B	11.00	210	22	2.00	
34		11.30	120	42	>6.00	
35		11.80	95	80	2.00	
36	B	12.10	200	25	>6.00	
37		13.00	85	70	1.50	
38		13.75	90	70	1.00	
39		14.65	90	75	2.00	
40		15.50	100	75	2.00	
41		16.20	190	70	2.00	
42	C	16.45	70	80	1.00	

** Blank - joint; C - cleavage; F - fault; B - bedding*

Discontinuity Mapping Data Sheet

General Information

Job Number: / A5-5 / Site Name: / Glen Bends / Rock Type /Silt-/lime-stone /
No. of Tape: / 1 / Tape Azimuth: / 140 / Tape Plunge(+/-) / 0 /
Sheet Number: / 1 / of / 2 / Operator(s) / P. LU / Date / 2/8/95 /

Discontinuity Data

No.	*Type*	*Intercept*	*Attitude*		*Semi-Trace length*	*Notes*
		(m)	*Dip Direction*	*Dip Angle*	*(m)*	
1	*2**	*3*	*4*	*5*	*6*	*7*
1	B	1.50	40	35	10.00	
2		2.00	190	70	1.00	
3		2.90	190	55	10.00	
4	C	3.80	170	60	3.00	
5		4.60	170	60	2.00	
6		5.05	210	60	7.00	
7		5.40	180	75	3.00	
8		5.70	180	60	1.00	
9	B	6.00	195	60	10.00	
10		7.10	290	60	5.00	
11		7.25	190	80	1.50	
12		7.70	190	70	0.80	
13		7.85	205	80	1.20	
14	C	8.60	10	75	2.00	
15		9.25	300	75	6.00	
16		9.45	210	50	1.50	
17		10.20	150	52	1.00	
18		10.50	120	90	2.00	
19		11.20	190	55	3.00	
20		11.95	190	48	2.00	
21		12.40	200	90	2.00	
22		13.00	200	85	2.00	
23		13.30	200	85	2.00	
24	B	14.00	295	85	2.00	
25		14.20	315	65	5.00	
26	B	15.00	195	50	1.50	
27		15.20	315	55	3.00	
28		15.40	350	58	2.50	
29	B	16.30	340	50	7.00	
30		16.40	155	25	7.00	
31		16.55	140	60	5.00	
32	B	17.30	150	25	8.00	
33		18.20	155	68	4.00	
34		18.60	130	90	10.00	
35		18.70	140	90	2.00	
36		18.90	150	90	3.00	
37		18.95	150	90	1.00	
38		19.10	185	90	1.00	
39		19.40	285	90	10.00	
40	B	19.65	315	25	4.00	
41		19.75	170	90	3.00	
42		19.95	150	90	2.00	
43		20.10	190	70	10.00	

** Blank - joint; C - cleavage; F - fault; B - bedding*

continuous

-continued

Discontinuity Mapping Data Sheet

General Information

Job Number:	/ A5-5 /	Site Name:	/ Glen Bends /	Rock Type	/Silt-/lime-stone /
No. of Tape:	/ 1 /	Tape Azimuth:	/ 140 /	Tape Plunge(+/-)	/ 0 /
Sheet Number:	/ 2 / of / 2 /	Operator(s)	/ P. LU /	Date	/ 2/8/95 /

Discontinuity Data

No.	*Type*	*Intercept*	*Attitude*		*Semi-Trace length*	*Notes*
		(m)	*Dip Direction*	*Dip Angle*	*(m)*	
1	***2****	***3***	***4***	***5***	***6***	***7***
1	B	20.40	155	30	6 00	
2		21.50	300	80	2.00	
3		21.80	130	72	1.00	
4		22.20	185	80	0.80	
5	B	22.60	180	20	1.00	
6		22.70	270	75	1.00	
7		23.00	280	85	0.80	
8		23.20	320	80	5.00	
9		23.30	315	50	3.00	
10		24.10	130	65	4.00	
11		24.90	310	65	10.00	
12		25.50	135	60	3.00	
13		26.60	290	70	4.00	
14	B	26.90	300	28	10.00	
15		27.00	205	70	2.00	
16		27.05	205	70	2.00	
17		27.10	205	70	2.00	
18	C	27.20	205	70	2.00	
19		27.50	200	70	2.00	
20	C	27.85	200	70	2.00	
21		27.90	200	75	1.00	
22		28.15	285	75	1.50	

** Blank - joint; C - cleavage; F - fault; B - bedding*

Discontinuity Mapping Data Sheet

General Information

Job Number: / A5-6 / Site Name: / Glen Bends / Rock Type /Silt-/lime-stone /
No. of Tape: / 1 / Tape Azimuth: / 290 / Tape Plunge(+/-) / 0 /
Sheet Number: / 1 / of / 1 / Operator(s) / P. LU / Date / 2/8/95 /

Discontinuity Data

No.	*Type*	*Intercept*	*Attitude*		*Semi-Trace length*	*Notes*
		(m)	*Dip Direction*	*Dip Angle*	*(m)*	
1	*2**	*3*	*4*	*5*	*6*	*7*
1		0.20	290	80	3.50	
2		1.00	265	70	2.80	
3	B	1.30	350	35	5.00	
4	B	1.70	175	35	5.00	
5	B	2.40	170	36	4.50	
6		3.40	205	65	2.00	
7		3.90	210	55	0.80	
8		4.90	165	35	4.50	
9		5.40	30	65	3.00	
10		6.20	285	90	1.50	
11	B	6.80	170	35	4.00	
12	F	7.20	165	38	4.50	
13		7.70	105	75	0.80	
14	B	8.30	190	35	4.00	
15	B	8.80	175	38	4.00	
16		9.00	280	75	1.20	
17	C	9.60	205	68	1.00	
18	B	10.20	170	38	4.00	
19	B	10.50	160	38	4.00	
20		11.00	275	75	1.50	
21		11.70	200	72	3.00	
22	F	12.00	175	36	6.00	
23		12.40	295	80	4.00	
24		12.70	290	85	3.00	
25	C	13.00	185	70	0.65	
26	B	13.20	180	25	6.50	
27		13.50	195	65	2.00	
28		14.00	15	85	1.50	
29		14.20	305	80	1.50	
30		14.40	20	75	5.00	
31		15.20	190	80	1.50	
32	B	15.90	165	35	5.00	
33		16.10	315	85	0.80	
34		16.70	295	80	1.00	
35		17.10	10	85	1.50	
36		17.30	175	82	1.80	
37	B	17.60	160	40	4.00	
38		18.00	110	85	0.60	
39		18.80	10	60	0.40	
40		19.30	10	65	0.80	
41		19.50	20	40	4.50	
42		19.90	180	65	1.20	
43	B	20.40	175	35	5.00	

** Blank - joint; C - cleavage; F - fault; B - bedding*

E.2 DISCONTINUITY DATA FROM THE OVERSEAS QUARRY*

E2.1 Discontinuity Data from Scanline Mapping Survey

Discontinuity Mapping Data Sheet

General Information

Job Number: / E214-1 / Site Name: /Overseas Quarry/ Rock Type / Limetone /
No. of Tape: / 1 / Tape Azimuth: / 264 / Tape Plunge(+/-) / 0 /
Sheet Number: / 1 / of / 2 / Operator(s) / J. Simm / Date / 12/10/95 /

Discontinuity Data

No.	*Type*	*Intercept*	*Attitude*		*Semi-Trace length*	*Notes*
		(m)	*Dip Direction*	*Dip Angle*	*(m)*	
1	*2**	*3*	*4*	*5*	*6*	*7*
1		0.07				
2		0.19				
3		0.26				
4		0.42				
5		0.66				
6		0.80				
7		1.20				
8		1.33				
9		1.48				
10		1.57				
11		1.74				
12		1.89				
13		2.04				
14		2.15				
15		2.24				
16		2.46				
17		2.53				
18		2.75				
19		2.90				
20		3.10				
21		3.32				
22		4.23				
23		4.72				
24		5.05				
25		5.45				
26		5.56				
27		5.96				
28		6.02				
29		6.26				
30		6.44				
31		6.89				
32		7.09				
33		7.45				
34		7.65				
35		7.67				
36		8.05				

Continued

*The scanline mapping was done by Mr. J. Simm, and the borehole logging data was obtained via Mr. Simm from the quarry. Both types of data have been sorted out by the author.

-continued

Discontinuity Mapping Data Sheet

General Information

Job Number:	/ E214-1 /	Site Name:	/Overseas Quarry/	Rock Type	/ Limetone /
No. of Tape:	/ 1 /	Tape Azimuth:	/ 264 /	Tape Plunge(+/-)	/ 0 /
Sheet Number:	/ 2 / of / 2 /	Operator(s)	/ J. Simm /	Date	/ 12/10/95 /

Discontinuity Data

No.	*Type*	*Intercept*	*Attitude*		*Semi-Trace length*	*Notes*
		(m)	*Dip Direction*	*Dip Angle*	*(m)*	
1	***2****	***3***	***4***	***5***	***6***	***7***
1		8.10				
2		8.89				
3		9.13				
4		9.99				
5		10.10				
6		10.15				
7		10.46				
8		10.60				
9		10.70				

Discontinuity Mapping Data Sheet

General Information

Job Number:	/ E214-2 /	Site Name:	/Overseas Quarry/	Rock Type	/ Limetone /
No. of Tape:	/ 1 /	Tape Azimuth:	/ 238 /	Tape Plunge(+/-)	/ 0 /
Sheet Number:	/ 1 / of / 2 /	Operator(s)	/ J. Simm /	Date	/ 12/10/95 /

Discontinuity Data

No.	*Type*	*Intercept*	*Attitude*		*Semi-Trace length*	*Notes*
		(m)	*Dip Direction*	*Dip Angle*	*(m)*	
1	***2****	***3***	***4***	***5***	***6***	***7***
1		0.76				
2		0.85				
3		0.91				
4		1.08				
5		1.21				
6		1.28				
7		1.44				
8		1.75				
9		1.79				
10		2.05				
11		2.24				
12		2.36				
13		2.93				
14		3.03				
15		3.10				
16		3.20				
17		3.34				
18		3.73				
19		3.81				
20		4.15				
21		4.49				
22		4.61				
23		5.00				
24		5.28				
25		5.61				
26		5.66				
27		5.76				
28		5.84				
29		5.99				
30		6.05				
31		6.15				
32		6.25				
33		6.40				
34		6.50				
35		6.60				
36		6.74				
37		6.99				

Continued

-continued

Discontinuity Mapping Data Sheet

General Information

Job Number: / E214-2 / Site Name: /Overseas Quarry/ Rock Type / Limetone /
No. of Tape: / 1 / Tape Azimuth: / 238 / Tape Plunge(+/-) / 0 /
Sheet Number: / 2 / of / 2 / Operator(s) / J. Simm / Date / 12/10/95 /

Discontinuity Data

No.	*Type*	*Intercept*	*Attitude*		*Semi-Trace length*	*Notes*
		(m)	*Dip Direction*	*Dip Angle*	*(m)*	
1	***2****	***3***	***4***	***5***	***6***	***7***
1		7.04				
2		7.12				
3		7.25				
4		7.29				
5		7.53				
6		7.62				
7		7.71				
8		7.83				
9		8.00				
		8.08				
		8.38				
		8.45				
		8.54				
		8.74				

Discontinuity Mapping Data Sheet

General Information

Job Number:	/ E231-1 /	Site Name:	/Overseas Quarry/	Rock Type	/ Limetone /
No. of Tape:	/ 1 /	Tape Azimuth:	/ 216 /	Tape Plunge(+/-)	/ 6 /
Sheet Number:	/ 1 / of / 1 /	Operator(s)	/ J. Simm /	Date	/ 12/10/95 /

Discontinuity Data

No.	*Type*	*Intercept*	*Attitude*		*Semi-Trace length*	*Notes*
		(m)	*Dip Direction*	*Dip Angle*	*(m)*	
1	***2****	***3***	***4***	***5***	***6***	***7***
1		0.23				
2		0.48				
3		0.57				
4		0.72				
5		0.85				
6		1.00				
7		1.19				
8		1.25				
9		1.40				
10		1.61				
11		2.03				
12		2.18				
13		2.35				
14		3.13				
15		3.46				
16		3.80				
17		3.88				
18		3.98				
19		4.16				
20		4.30				
21		4.38				
22		4.43				
23		4.57				
24		5.07				
25		5.13				
26		5.45				

Discontinuity Mapping Data Sheet

General Information

Job Number:	/ E231-2 /	Site Name:	/Overseas Quarry/	Rock Type	/ Limetone /
No. of Tape:	/ 1 /	Tape Azimuth:	/ 216 /	Tape Plunge(+/-)	/ 8 /
Sheet Number:	/ 1 / of / 1 /	Operator(s)	/ J. Simm /	Date	/ 12/10/95 /

Discontinuity Data

No.	*Type*	*Intercept*	*Attitude*		*Semi-Trace length*	*Notes*
		(m)	*Dip Direction*	*Dip Angle*	*(m)*	
1	***2****	***3***	***4***	***5***	***6***	***7***
1		0.20				
2		0.37				
3		0.51				
4		0.59				
5		0.68				
6		0.71				
7		0.78				
8		0.89				
9		1.25				
10		1.31				
11		1.34				
12		1.45				
13		1.50				
14		1.72				
15		1.82				
16		2.03				
17		2.16				
18		2.23				
19		2.43				
20		2.48				
21		2.57				
22		2.85				
23		3.46				
24		3.75				
25		3.81				
26		4.56				
27		4.75				

Discontinuity Mapping Data Sheet

General Information

Job Number: / E248-1 / Site Name: /Overseas Quarry/ Rock Type / Limetone /
No. of Tape: / 1 / Tape Azimuth: / 348 / Tape Plunge(+/-) / 8 /
Sheet Number: / 1 / of / 2 / Operator(s) / J. Simm / Date / 12/10/95 /

Discontinuity Data

No.	*Type*	*Intercept*	*Attitude*		*Semi-Trace length*	*Notes*
		(m)	*Dip Direction*	*Dip Angle*	*(m)*	
1	*2**	*3*	*4*	*5*	*6*	*7*
1		0.10				
2		0.16				
3		0.22				
4		0.31				
5		0.41				
6		0.50				
7		0.69				
8		0.81				
9		0.98				
10		1.06				
11		1.17				
12		1.32				
13		1.53				
14		1.60				
15		1.70				
16		1.77				
17		1.96				
18		2.06				
19		2.58				
20		3.34				
21		3.42				
22		3.86				
23		3.96				
24		4.06				
25		4.19				
26		4.42				
27		4.52				
28		4.67				
29		4.80				
30		4.87				
31		4.92				
32		5.08				
33		5.13				
34		5.20				
35		5.24				
36						

Continued

-continued

Discontinuity Mapping Data Sheet

General Information

Job Number:	/ E248-1 /	Site Name:	/Overseas Quarry/	Rock Type	/ Limetone /
No. of Tape:	/ 1 /	Tape Azimuth:	/ 348 /	Tape Plunge(+/-)	/ 8 /
Sheet Number:	/ 2 / of / 2 /	Operator(s)	/ J. Simm /	Date	/ 12/10/95 /

Discontinuity Data

No.	*Type*	*Intercept*	*Attitude*		*Semi-Trace length*	*Notes*
		(m)	*Dip Direction*	*Dip Angle*	*(m)*	
1	***2****	***3***	***4***	***5***	***6***	***7***
1		5.57				
2		5.71				
3		5.83				
4		6.43				
5		6.55				
6		6.90				
7		6.95				
8		7.58				
9		8.40				
10		8.55				
11		9.00				
12		9.16				
13		9.60				

Discontinuity Mapping Data Sheet

General Information

Job Number: / E248-2 / Site Name: /Overseas Quarry/ Rock Type / Limetone /
No. of Tape: / 1 / Tape Azimuth: / 338 / Tape Plunge(+/-) / 0 /
Sheet Number: / 1 / of / 1 / Operator(s) / J. Simm / Date / 12/10/95 /

Discontinuity Data

No.	*Type*	*Intercept*	*Attitude*		*Semi-Trace length*	*Notes*
		(m)	*Dip Direction*	*Dip Angle*	*(m)*	
1	***2****	***3***	***4***	***5***	***6***	***7***
1		0.09				
2		0.15				
3		0.20				
4		0.58				
5		0.85				
6		0.93				
7		1.11				
8		1.26				
9		1.90				
10		2.08				
11		2.28				
12		2.45				
13		2.70				
14		2.83				
15		3.27				
16		3.66				
17		4.42				
18		4.67				
19		4.77				
20		4.93				
21		5.01				
22		5.24				
23		5.39				
24		5.50				
25		5.58				
26		5.81				
27		6.15				
28		6.36				
29		6.51				
30		6.60				
31		6.70				
32		6.80				
33		6.90				
34		7.06				
35		7.15				
36		7.46				
37		7.65				
38		7.86				
39		8.25				
40		8 30				
41		8.73				
42		8.96				
43		9.18				
44		9.38				

E.2.2 Discontinuity Data from Borehole Logging

Hole No.	BH1	BH3	BH4	BH5	BH7	BH8	BH9	BH10	BH11
Depth (m)	16.5-24	6.0-18	0-10.5	0-12	0-13 5	0-13.5	9-18	0-13.5	0-12
Elevation	251-241	252-240	252-242	248-236	242-229	224-211	216-207	221-209	231-219
No.	Discontinuity intercept (m)								
1	0.05	0.03	0.40	0.17	0.10	0.50	0.14	0.25	0.16
2	0.11	0.13	0.52	0.33	0.30	0.57	0.35	0.42	0.26
3	0.17	0.23	0.68	0.46	0.35	0.80	0.52	0.57	0.47
4	0.23	0.36	0.77	0.73	0.48	0.90	0.62	0.60	0.53
5	0.33	0.42	0.97	0.80	0.55	1.06	0.82	0.66	0.77
6	0.47	0.47	1.13	0.85	0.60	1.10	1.14	0.72	1.00
7	0.59	0.55	1.73	0.98	0.66	1.30	1.51	0.76	1.10
8	0.63	0.62	1.93	1.06	0.83	1.40	1.99	0.88	1.29
9	0.70	0.68	2.16	1.12	0.95	1.63	2.67	1.32	1.60
10	1.32	0.78	2.25	1.31	1.10	1.72	2.77	1.47	1.76
11	1.37	0.90	2.48	1.37	1.37	2.07	2.82	1.62	1.84
12	1.44	0.93	3.01	1.43	1.52	2.17	3.10	1.89	2.16
13	1.58	0.97	3.38	1.45	1.59	2.24	3.14	1.92	2.36
14	1.63	1.01	3.75	1.53	1.68	2.37	3.38	1.97	2.58
15	1.71	1.15	4.22	1.58	1.80	3.18	3.47	2.08	2.71
16	1.79	1.43	4.38	2.27	1.85	3.39	3.52	2.19	2.88
17	1.87	1.51	4.62	2.37	2.01	3.57	3.73	2.25	2.96
18	1.96	1.80	4.72	2.99	2.23	3.68	4.17	2.38	2.98
19	2.01	1.88	4.78	3.45	2.28	3.79	4.36	2.45	3.04
20	2.23	1.97	4.93	3.62	2.38	4.37	4.48	2.51	3.26
21	2.36	2.03	5.17	3.66	2.47	4.53	4.57	2.55	3.38
22	2.39	2.23	5.31	4.06	2.80	4.84	4.66	2.60	3.44
23	2.51	2.28	5.65	4.18	2.99	4.93	5.27	2.75	3.54
24	2.59	2.61	5.68	4.29	3.25	5.39	5.91	2.85	3.59
25	2.71	2.96	5.75	4.40	3.38	5.43	6.06	3.02	3.73
26	2.83	3.06	5.84	4.56	3.48	5.66	6.16	3.07	3.84
27	2.93	3.61	5.95	4.79	3.58	5.83	6.44	3.21	4.03
28	3.02	3.73	6.12	4.95	3.74	6.06	6.54	3.29	4.07
29	3.35	3.88	6.16	5.23	3.85	6.77	6.71	3.61	4.34
30	3.42	4.05	6.23	5.50	3.94	7.30		3.76	4.38
31	3.56	4.23	6.37	5.62	4.01	7.61		3.81	4.49
32	3.79	4.33	6.70	6.32	4.11	7.68		4.20	4.77
33	3.83	4.38	7.38	6.45	4.15	7.88		4.29	5.05
34	3.88	4.48	7.60	6.59	4.22	7.94		4.59	5.20
35	3.98	4.54	7.70	6.71	4.26	8.27		4.67	5.27
36	4.03	4.79	7.71	7.13	4.34	8.46		4.83	5.32
37	4.08	4.84	7.84	7.19	4.45	8.53		4.98	5.45
38	4.15	4.89	8.13	7.26	4.83	8.67		5.14	5.61
39	4.22	5.14	8.28	7.76	5.38	8.94		5.20	6.07
40	4.31	5.49	8.38	8.09	5.47	9.80		5.77	6.19
41	4.41	5.62	8.79	8.38	5.58	10.07		5.84	6.26
42	4.64	5.79	8.90	8.56	5.76	10.72		5.96	6.32

Continued

-continued

Hole No.	BH1	BH3	BH4	BH5	BH7	BH8	BH9	BH10	BH11
Depth (m)	16.5-24	6.0-18	0-10.5	0-12	0-13.5	0-13.5	9-18	0-13.5	0-12
Elevation	251-241	252-240	252-242	248-236	242-229	224-211	216-207	221-209	231-219
No.	Discontinuity intercept (m)								
43	4.68	5.86	9.20	8.70	5.80	11.11		6.20	6.40
44	4.90	5.99	9.39	8.85	6.00	11.22		6.34	6.43
45	4.93	6.11	9.40	9.28	6.28	11.33		6.48	6.48
46	5.16	6.25	9.53	10.52	6.68	11.93		6.60	6.60
47	5.43	6.34	9.79	11.97	6.76	12.35		6.69	6.81
48	5.66	6.64	9.85		6.81	12.51		6.93	6.91
49	5.74	7.07	10.02		7.00	12.66		7.08	6.98
50	5.86	7.22	10.10		7.11	12.79		7.20	7.17
51	5.96	7.49	10.15		7.32			7.95	7.33
52	6.13	7.61	10.36		7.43			8.05	7.46
53	6.80	7.80	10.55		7.64			8.19	7.62
54	6.86	7.86	10.62		7.76			8.55	7.72
55	6.93	8.16			7.82			8.69	8.05
56	6.96	8.59			8.07			9.01	8.27
57	7.06	8.74			8.26			9.15	8.50
58	7.12	9.01			8.61			9.23	
59	7.26	9.13			8.81			9.88	
60	7.54	9.32			9.01			10.12	
61	7.76	9.38			9.41			10.23	
62	7.84				9.67			10.41	
63	8.12				9.96			10.52	
64	8.28				10.09			10.94	
65	8.43				10.13			11.15	
66	9.10				10.34			11.52	
67	9.32				11.09			12.00	
68	9.43				11.17			12.32	
69	9.78				11.24				
70	9.88				11.34				
71	9.94				11.38				
72	10.01				11.45				
73	10.13				11.53				
74	10.30				11.58				
75	10.35				11.63				
76	10.40				11.69				
77	10.85								
78	11.07								
79	11.21								

APPENDIX F RAW DATA OF POINT LOAD STRENGTH TEST

Point Load Test Sheet (Highway cutting, A5 Glyn Bends Improvement.)									
Sheet No.	1	Data:	Aug. 1, 1995	Operator:	PL				
Place:	31/7 blasting site								
Rock description:									
Dark, fine-grained siltstone, fresh blasting blocks, taken from blasting site, natural state Air-dried one day, in-situ tested									
No.	Type	W(mm)	D(mm)	P(kN)	De (mm)	$De^2(mm^2)$	Is(MPa	F	Is(50)(MPa)
1	Block	65	44	18	60.341	3640.993	4.944	1.088	5.38
2	Block	55	51	18.2	59.758	3570.974	5.097	1.084	5.52
3	Block	85	50.5	22.5	73.923	5464.672	4.117	1.192	4.91
4	Block	72.5	52	15.2	69.278	4799.491	3.167	1.158	3.67
5	Block	62.5	45	6.5	59.837	3580.522	1.815	1.084	*1.97*
6	Block	55	46	9.5	56.753	3220.878	2.950	1.059	3.12
7	Block	73	64	25	77.122	5947.804	4.203	1.215	5.11
8	Block	60	49	23	61.179	3742.839	6.145	1.095	6.73
9	Block	67.5	55	21	68.748	4726.289	4.443	1.154	5.13
10	Block	55	45	14	56.133	3150.859	4.443	1.053	4.68
11	Block	60	42.5	18	56.977	3246.340	5.545	1.061	5.88
12	Block	57.5	41	15	54.784	3001.273	4.998	1.042	5.21
13	Block	50	25	9	39.892	1591.343	5.656	0.903	5.11
14	Block	80	48	22	69.919	4888.606	4.500	1.163	5.23
15	Block	40	28	13	37.760	1425.843	9.117	0.881	*8.04*
								Mean	5.05

Point Load Test Sheet (Highway cutting, A5 Glyn Bends Improvement.)									
Sheet No.	2	Data:	Aug. 3, 1995	Operator:	PL				
Place:	Ch950, the bottom of the first berm, south side face.								
Rock description:									
Dark, fine-grained siltstone (limestone?), natural state, air-dried 2-3 weeks, in-situ tested									
No.	Type	W(mm)	D(mm)	P(kN)	De (mm)	$De^2(mm^2)$	Is(MPa)	F	Is(50)(MPa)
1	Block	62	42	15.5	57.577	3315.086	4.676	1.066	4.98
2	Block	70	42	14.5	61.179	3742.839	3.874	1.095	4 24
3	Block	61	40	8.5	55.734	3106.302	2.736	1.050	*2.87*
4	Block	80	45	15.5	67.698	4583.068	3.382	1.146	3.88
5	Block	70	60	19.5	73.123	5346.913	3.647	1.187	4.33
6	Block	55	48	13.5	57.973	3360.917	4.017	1.069	4.29
7	Block	72	36	10	57.444	3299.809	3.030	1.064	3.23
8	Block	72	38	16.5	59.018	3483.132	4.737	1.077	5.10
9	Block	60	36	12	52.439	2749.841	4.364	1.022	4.46
10	Block	95	35	18.5	65.061	4232.973	4.370	1.126	4.92
11	Block	72	48	18.5	66.331	4399.745	4.205	1.136	4.78
12	Block	62	40	20	56.189	3157.225	6.335	1 054	*6 68*
								Mean	4.42

Point Load Test Sheet (Highway cutting, A5 Glyn Bends Improvement.)									
Sheet No.	3	Data:	Aug. 3, 1995	Operator:	PL				
Place:	Aug. 1st blasting site								
Rock description:									
Fine-grained siltstone , natural state, air-dried 2 days, in-situ tested									
No.	Type	W(mm)	D(mm)	P(kN)	De (mm)	$De^2(mm^2)$	Is(MPa)	F	Is(50)(MPa)
1	Block	60	45	26.2	58.629	3437.301	7.622	1.074	*8.19*
2	Block	65	43	16	59.651	3558.243	4.497	1.083	4.87
3	Block	62	40	10.5	56.189	3157.225	3.326	1.054	3.51
4	Block	72	40	14.5	60.551	3666.454	3.955	1.090	4.31
5	Block	65	45	23.5	61.022	3723.743	6.311	1.094	6.90
6	Block	63	38	18.2	55.206	3047.740	5.972	1.046	6.24
7	Block	65	50	24	64.323	4137.492	5.801	1.120	6.50
8	Block	80	42	11	65.403	4277.530	2.572	1.128	*2.90*
9	Block	60	36	19.5	52.439	2749.841	7.091	1.022	7.24
10	Block	56	40	19.5	53.401	2851.687	6.838	1.030	7.04
11	Block	75	45	21	65.549	4296.626	4 888	1 130	5 52
12	Block	55	42	20	54.229	2940.802	6.801	1.037	7.05
								Mean	5.92

Point Load Test Sheet (Highway cutting, A5 Glyn Bends Improvement.)									
Sheet No.	4	Data:	Aug. 3, 1995	Operator:	PL				
Place:	'Ch750, the bottom of first berm, north side face.								
Rock description:									
Very dark, fine-grained siltstone, natural state, about air-dried 2 months it is in the zone where existed a ridge, in-situ tested									
No.	Type	W(mm)	D(mm)	P(kN)	De (mm)	$De^2(mm^2)$	Is(MPa)	F	Is(50)(MPa)
1	Block	63	43	11	58.726	3448.759	3.190	1.075	3.43
2	Block	81	35.5	20	60.504	3660.726	5.463	1.090	5.95
3	Block	92	50	16	76 525	5856 143	2 732	1 211	*3.31*
4	Block	64	38	19.8	55.643	3096.117	6.395	1.049	6.71
5	Block	67	47.5	22.8	63.652	4051.560	5.627	1.115	6.27
6	Block	65	45	26	61.022	3723.743	6.982	1.094	7.64
7	Block	52	40	21.2	51 459	2647.995	8.006	1.013	*8.11*
8	Block	60	42	19.5	56.641	3208.148	6.078	1.058	6.43
9	Block	55	34	14	48.792	2380.649	5.881	0.989	5.82
10	Block	68.5	51	24.2	66.689	4447.486	5.441	1.138	6.19
11	Block	75	35	16.5	57.808	3341.820	4.937	1.067	5.27
12	Block	75	45	26.5	65.549	4296.626	6.168	1.130	6.97
13	Block	80	47	22	69.186	4786.760	4.596	1.157	5.32
14	Block	60	48	22.5	60.551	3666.454	6.137	1.090	6.69
								Mean	6.06

Point Load Test Sheet (Highway cutting, A5 Glyn Bends Improvement.)									
Sheet No.	5	Data:	Aug. 3, 1995	Operator:	PL				
Place:	Aug. 2nd blasting site								
Rock description:									
Dark,very fine-grained siltstone, natural state, air-dried 1 day Well-developed joints and clevage, in-situ tested									
No.	Type	W(mm)	D(mm)	P(kN)	De (mm)	$De^2(mm^2)$	Is(MPa)	F	Is(50)(MPa)
1	Block	58	35	9.5	50.836	2584.341	3.676	1.007	3 70
2	Block	64	46	16.5	61.220	3747.931	4.402	1.095	4.82
3	Block	68	52	15	67.094	4501.591	3.332	1.141	3.80
4	Block	70	47	9	64.718	4188.415	2.149	1.123	*2.41*
5	Block	72	57	22.5	72.282	5224.698	4.306	1.180	5.08
6	Block	58	38	20.5	52.970	2805.856	7.306	1.026	*7.50*
7	Block	52	42	13	52.729	2780.395	4.676	1.024	4.79
8	Block	75	52	25.5	70.463	4964.990	5.136	1.167	5.99
9	Block	85	36	14	62.415	3895.608	3.594	1.105	3.97
10	Block	70	45	13.5	63.326	4010.185	3.366	1.112	3.74
11	Block	80	70	28.5	84.435	7129.217	3.998	1.266	5.06
12	Block	75	62	26	76.940	5919.796	4.392	1.214	5.33
13	Block	90	75	35	92.700	8593.253	4.073	1.320	5.38
								Mean	4.70

Point Load Test Sheet (Highway cutting, A5 Glyn Bends Improvement.)									
Sheet No.	6	Data:	Aug. 3, 1995	Operator:	PL				
Place:	Aug. 3rd blasting site								
Rock description:									
Grey, fine-grained siltstone, natural state.									
No.	Type	W(mm)	D(mm)	P(kN)	De (mm)	$De^2(mm^2)$	Is(MPa)	F	Is(50)(MPa)
1	Block	59	34	14	50.535	2553.787	5.482	1.005	5.51
2	Block	59	35	16.5	51.273	2628.899	6.276	1.011	6.35
3	Block	75	37	22.5	59.437	3532.782	6.369	1.081	*6.88*
4	Block	85	54	12.5	76.442	5843.412	2.139	1.210	2.59
5	Block	74	38	13	59.832	3579.885	3.631	1.084	3.94
6	Block	75	50	17	69.094	4774.029	3.561	1.157	4.12
7	Block	62	39	14.2	55.482	3078.294	4.613	1.048	4.83
8	Block	85	40	7	65.791	4328.453	1.617	1.131	*1.83*
9	Block	75	45	10	65.549	4296.626	2.327	1.130	2.63
10	Block	90	28	17	56.641	3208.148	5.299	1.058	5.60
11	Block	55	33	14.5	48.069	2310.630	6.275	0.982	6 17
12	Block	72	55	14.2	71.003	5041.375	2.817	1.171	3.30
13	Block	55	45	10.5	56.133	3150.859	3.332	1.053	3.51
								Mean	4.41

Point Load Test Sheet (Highway cutting, A5 Glyn Bends Improvement.)									
Sheet No.	7	Data:	Aug. 3, 1995	Operator:	PL				
Place:	Ch850, the bottom of the first berm, near south side (Aug. 4th blasting site)								
Rock description:									
Dark, fine-grained siltstone, natural state, air-dried 2 days, in-situ test									
No.	Type	W(mm)	D(mm)	P(kN)	De (mm)	$De^2(mm^2)$	Is(MPa)	F	Is(50)(MPa)
1	Block	59	36	15.2	52.000	2704.010	5.621	1.018	5.72
2	Block	86	53	14.5	76.175	5802.673	2.499	1.209	3.02
3	Block	73	39	16	60.203	3624.443	4.414	1.087	4.80
4	Block	55	36	10.8	50.206	2520.687	4.285	1.002	4.29
5	Block	63	38	15.2	55.206	3047.740	4.987	1.046	5.21
6	Block	59	33	15.5	49.786	2478.676	6.253	0.998	*6.24*
7	Block	70	39	13.5	58.953	3475.493	3.884	1.077	4.18
8	Block	63	38	14.3	55.206	3047.740	4.692	1.046	4.91
9	Block	80	38	9	62.211	3870.146	2.325	1.103	*2.57*
10	Block	70	40	12.4	59.704	3564 609	3.479	1.083	3.77
11	Block	64	39.5	14.5	56.730	3218.332	4.505	1.058	4.77
								Mean	4.52